IntechOpen

Electrophoresis

Life Sciences Practical Applications

Edited by Oana-Maria Boldura and Cornel Baltă

ELECTROPHORESIS - LIFE SCIENCES PRACTICAL APPLICATIONS

Edited by **Oana-Maria Boldura** and **Cornel Baltă**

Electrophoresis - Life Sciences Practical Applications
http://dx.doi.org/10.5772/intechopen.71646
Edited by Oana-Maria Boldura and Cornel Baltă

Contributors

Stanislav Naryzhny, Thilakavathy Karuppiah, Tan Niu Jin, Amilia Afzan Mohd Jamil, Norhafizah Mohtarrudin, Leona Daniela Jeffery Daim, Paolo Iadarola, Simona Viglio, Maddalena Cagnone, Roberta Salvini, Laurent Chiarelli, Zuzana Kostecká, Dagmar Heinová, Eva Petrovova, Anouar Koubaa, Mansour Bargui, Gunnar Brunborg, Xianquan Zhan, Na Li, Shivam Pradeep Yadav, Raju Shrihari Shrihari Pawade, Ivan Vikhlyantsev, Zoya Podlubnaya

Notice

First published in London, United Kingdom, 2018 by IntechOpen
eBook (PDF) Published by IntechOpen, 2019
IntechOpen is the global imprint of INTECHOPEN LIMITED, registered in England and Wales, registration number: 11086078, The Shard, 25th floor, 32 London Bridge Street
London, SE19SG – United Kingdom
Printed in Croatia

British Library Cataloguing-in-Publication Data
A catalogue record for this book is available from the British Library

Additional hard and PDF copies can be obtained from orders@intechopen.com

Electrophoresis - Life Sciences Practical Applications
Edited by Oana-Maria Boldura and Cornel Baltă

p. cm.

Print ISBN 978-1-78923-552-4

Online ISBN 978-1-78923-553-1

eBook (PDF) ISBN 978-1-83881-596-7

Meet the editors

Oana-Maria Boldura graduated in Genetic Engineering with a specialization in Molecular Biology (2005), Master of Science degree in Genetic Manipulation (2007) and Pharmacy (2014), and PhD degree in Biotechnology (2010). From 2015, she is an assistant professor at the Banat University of Agricultural Sciences and Veterinary Medicine "King Michael I of Romania" Timisoara, Faculty of Veterinary Medicine, Department of Chemistry, Biochemistry, and Molecular Biology and a researcher at the "Horia Cernescu" Research Unit. Her main scientific interests are in the field of molecular biology, biotechnology, genomics, and biosecurity with technical aptitudes in manipulation and experimentation of nucleic acid and proteins (purification, sequencing, gene expression studies, SDS-PAGE analysis of proteins fractions, "Lab-on-chip" electrophoresis, and immunological testing). Her areas of interest are molecular forensic methods and apoptotic process pathways.

Cornel Baltă is licensed in Veterinary Medicine and Ph.D. in Veterinary Medicine (2011) he is researcher at the Institute of Life Sciences, at "Vasile Goldis" Western University Arad, Romania. The main scientific competencies are in the field of Laboratory Animals, Molecular Biology, Physiology, Histology and Clinical Laboratory with competences and technical aptitudes in nucleic acid examination by electrophoresis techniques, PCR and qPCR, qualitative and quantitative determination of proteins by Western Blot and microelectrophoresis. Area of interest - the study of molecular mechanisms involved in the evolution of liver and gastrointestinal diseases, study of molecular mechanisms involved in bone regeneration and remodeling using different types of polymers as the scaffold.

Contents

Preface

Electrophoresis is a widely used method in the field of life sciences, having multiple practical applications both in physical, chemical, biochemical, and molecular biology research and in industrial production.

Electrophoresis is defined as a physicochemical technique by which charged particles migrate and separate on a certain physical support under the influence of an electric field. An electrophoresis system is composed of two electrodes with the opposite chargecathode and anode—connected through a medium called electrolyte. The mobility of an ionic particle is determined by its shape, size, electrical charge, and chemical-physical factors of electrophoresis—temperature, electrical parameters, pH, viscosity, or pore size of the electrophoretic support.

Although the electrokinetic phenomenon was observed for the first time in the early 1800s, the method was developed in the 1930s, and since then, separation processes and chemical analysis techniques based on electrophoresis have continued to be developed, providing relevant data in the process of discovery of new non-bio-materials and research of biomolecules and their involvement in various biochemical processes that are studied, as well as to the clinical constant parameters already chosen as indicators of the health state of an organism.

This book contains 8 chapters describing various applications of this technique in biochemistry, molecular biology, and physical chemistry. The chapters describe the link between the exposed method and its applications in a very explicit manner and offer a wide range of practical examples. At the same time, the book aims to provide a vision of how future methods will evolve and their further development and the improvements that are needed to be made to the exposed techniques; therefore, a particular attention has been given to the described techniques as true guidelines in the fields where electrophoresis is recommended to be used, making it useful for not only the researchers but also the laboratory technicians.

Prof. Dr. Eng. Oana-Maria Boldura
Faculty of Veterinary Medicine
Department of Chemistry
Biochemistry and Molecular Biology
Banat University of Agricultural Sciences and
Veterinary Medicine "King Michael I of Romania"
Timisoara, Romania

Dr. DVM Cornel Baltă
"Vasile Goldis" Western University of Arad
Institute of Life Sciences
Arad, Romania

Chapter 1

Spontaneous Unexplained Preterm Labor with Intact Membrane: Finding Protein Biomarkers through Placenta Proteome

Niu J. Tan, Leona D.J. Daim, Amilia A.M. Jamil, Norhafizah Mohtarrudin and Karuppiah Thilakavathy

Additional information is available at the end of the chapter

http://dx.doi.org/10.5772/intechopen.74925

Abstract

Spontaneous unexplained preterm labor with intact membrane (sPTL-IM) remains as an unresolved challenge in obstetrics due to the complex syndromes involved during preterm birth. Two dimensional-gel electrophoresis (2D-GE) coupled with matrix-assisted laser desorption/ionization-time of flight/time of flight (MALDI TOF/TOF) mass spectrometry has become an alternative in screening for potential novel protein-based biomarkers and revealing the pathophysiology of sPTL-IM. To achieve this objective, protein extracted from fetal and maternal sides of the placenta obtained from sPTL-IM (n = 5) and the respective control (n = 10) groups were separated and compared using 2D-gel electrophoresis. MALDI-TOF/TOF mass spectrometry was utilized to identify the differentially expressed proteins between both groups, and the molecular functions of these proteins were studied. A total of 12 proteins were significantly differentiated in sPTL-IM over the control. Differentially expressed proteins were identified to have involved in structural/cytoskeletal components, immune responses, fetal and placenta development, and anticoagulation cascade. More proteins were found to be differentially expressed in the fetal side compared to the maternal side of the placenta. This postulates that the influence of sPTL-IM from fetus is greater than that of the mother. Ultimately, these results might lead to further investigations in elucidating the potential of these proteins as biomarkers and/or drug targets.

Keywords: comparative placenta proteomics, 2D-gel electrophoresis, MALDI-TOF/TOF, placenta tissues, proteomics, spontaneous unexplained preterm labor

1. Introduction

Spontaneous preterm labor (PTL) is one of the major causes of preterm birth (PTB), which accounts for 56% of the total PTB [1] and it possesses deteriorating effects, both long and short term, on the health of the mother and the offspring [2]. Moreover, statistics showed that 30% of pregnant women who experienced spontaneous PTL are often spontaneous with no known signs of PTL (herein termed as spontaneous unexplained PTL with intact membrane (sPTL-IM)) [3].

Current diagnosis for spontaneous PTL-IM was based on several predictors which include risk factors assessment, cervical measurement, and/or biochemical markers specifically fetal fibronectin and phosphorylated insulin-like growth factor-binding protein 1 [4]. These protein biomarkers possess a major limitation where they can only be detected 14 days prior to onset, providing a short time frame to plan for preventive care and treatment [5]. On the other hand, positive-predictive values of other newly found biomarkers including thioredoxin or interleukin 1 receptor antagonist had shown to be relatively poor [4, 5].

It has become evident that existing and newly found protein biomarkers often lack specificity and sensitivity to provide an effective prediction measure against sPTL-IM among pregnant women [6, 7]. Specific and sensitive predictive tool is important to allow the effective use of treatment or care for the risked mothers and avoid the use of unnecessary medical interventions, which further reduces medical costs. Furthermore, throughout every stages of pregnancy from conception to parturition, it is believed that levels of certain protein biomarkers fluctuate. Hence, the identification of these proteins that are associated with sPTL-IM is a sensational method to establish reliable novel biomarkers in assisting sPTL-IM prediction among pregnant women, as well as unwinding its underlying complex pathophysiologies [6, 7].

Since results from easily accessible biological fluids do not always reflect accurate localized information on the state of a pregnancy and impending labor, the use of gestational tissues can be advantageous. The placenta is an organ connecting developing fetus with the mother that plays roles during labor [8]. Interestingly, the study reported that protein expression in the fetally origin tissues (chorion) is different from the maternally origin tissues (decidua basalis) [9]. Thus, both the fetal and the maternal side of the placenta are a potential source of preliminary discovery of biomarker associated to the processes of sPTL-IM. Unfortunately, studies that applied proteomic approaches to discover protein alterations in the placenta mainly focused on pregnancies complicated with gestational diabetes mellitus and preeclampsia [10, 11] while little is known about the proteome from placenta in relation to sPTL-IM. Therefore, investigating protein levels in delivered placentas offers researchers not only to identify potential biomarker panels but also to study the delivery pathophysiology of sPTL-IM.

Given the clinical significance of sPTL-IM and the presence of proteomics technology, placenta has become a good source for proteome study associated with sPTL-IM. The purpose of this research was to discover protein biomarkers that could potentially be used to identify the risk of sPTL-IM among pregnant women. In addition, this will also allow us to understand any functional classes of proteins that are associated with sPTL-IM and disclose its

pathophysiological complications. For this, we have applied an existing proteomic approach (two dimensional-gel electrophoresis (2D-GE)-coupled matrix-assisted laser desorption/ionization-time of flight/time of flight mass spectrometry (MALDI-TOF/TOF MS)) to identify differentially expressed protein during sPTL-IM by comparing the fetal and maternal placenta proteome between the sPTL-IM and spontaneous term labor with intact membrane (sTL-IM) placentas, respectively, prior to the study of their functions.

2. Materials and methods

2.1. Sample population

The study was approved by the Medical Research and Ethics Committee (NMRR-13-1660-18742) and written informed consent was obtained from all subjects prior to placenta collection.

Placenta was taken from five asymptomatic pregnant women who experienced sPTL-IM (22 and 36 + 6 weeks of gestation). The control group comprised pregnant women who underwent spontaneous labor with ≥37 completed weeks of gestation (n = 10) and had at least one previous history of spontaneous PTB. Gestational age was determined from the last menstrual period and by ultrasound measurements up to the second trimester. Another ultrasound measurement was performed during the second trimester to rule out congenital malformations.

All subjects were patients who sought for prenatal care and delivered in Hospital Serdang, Malaysia, during 2014–2015 and represented the Malay population in Peninsula Malaysia who carried a singleton pregnancy. Risk factor was at least one prior spontaneous PTB of a singleton infant due to spontaneous PTL-IM (>20 to <37 weeks of gestation). Pregnant women with known obstetrical complications such as multiple gestations, chronic infective diseases, hypertension, preeclampsia, pregestational diabetes, severe anemia, placenta previa, known malignancy, known or suspected congenital malformation of the fetus, symptoms/signs of PTL, fetal loss in second trimester, intrauterine growth restriction (IUGR), had an immunodeficiency virus, cervical incompetence, planned cervical cerclage, uterine malformation, antepartum hemorrhage, and previous cervical surgery were excluded from the investigation. Subjects with uncertain gestation were also excluded from this study. Moreover, obstetric complications needing iatrogenic and preterm prerupture of membranes (PPROM) deliveries were also not recruited in the study. It is believed that PPROM did not share the same condition as spontaneous PTL [12]. Each patient was given an anonymized ID number. Demographic and clinical characteristics of these pregnant women from whom preterm and term samples utilized in this study were collected and are presented in **Table 1**.

2.2. Reagents

The chemicals used in this study include phosphate buffer saline (PBS, Sigma-Aldrich, USA, P4417), protease inhibitor mix (GE Healthcare, USA, 80-6501-23), β-mercaptoethanol (Invitrogen, US, 11528926), urea (GE Healthcare, USA, 17-1319-01), thiourea (GE Healthcare, USA, RPN6301), 3-[(3-cholamidopropyl)dimethylammonio]-1-propanesulfonate (CHAPS, GE

Characteristics	Case (n = 5)	Control (n = 10)	P value
Estimated gestational age (weeks)	35.4 ± 0.89	38.5 ± 0.53	–
Maternal age (years)	33.2 ± 5.89	32.7 ± 5.93	NS
Parity	3 (1–6)	4 (1–6)	NS
Fetus weight (kg)	2.32 ± 0.40	3.22 ± 0.25	0.02*
Placenta weight (g)	384 ± 20.74	488.5 ± 11.56	<0.002*

NS, not significant; data are presented as means ± SEM, except parity data are presented as median (range).*$P < 0.05$ when compared to the other group.

Table 1. Demographic and clinical details of women participated in this study.

Healthcare, USA, 17-1314-01), Tris (Bio-Rad, USA, 1610716), biolyte 3/10 ampholyte (Bio-Rad, USA, 1632094), dithiothreitol (DTT, GE Healthcare, USA, 17-1318-02), hydrochloric acid solution (HCl, Fisher Chemical, UK, SA48-500), ethylenediaminetetraacetic acid (EDTA, Sigma, USA, E9884), potassium chloride (KCl, Sigma-Aldrich, USA, P9541), sucrose (Fisher Reagent, USA, S25590), methanol (Fisher Reagent, USA, A4521), dichloromethane (DCM, Fisher Reagent, USA, AC326600025), lithium chloride (LiCl, Sigma-Aldrich, USA, 13013), 2D quant kit (GE Healthcare, USA, 80-6483-56), glycerol (Sigma-Aldrich, USA, G5516), sodium dodecyl sulfate (SDS, Bio-Rad, USA, 1610302), bromophenol blue (Bio-Rad, USA, 1610404), pre-stained BLUeye (Gene Direx, USA, PM007-0500), acrylamide/bis mixed solution (37.5:1) (Nacalai tecque, Japan, 06121), wide-range gel preparation buffer (Nacalai tecque, Japan, 07831-94), N,N,N′,N′-tetramethylethylenediamine (TEMED, GE Healthcare, USA, 17-1312-01), ammonium persulfate (APS, Sigma-Aldrich, USA, 09913), agarose NA (GE Healthcare, USA, 17-0554-01), glycine (Bio-rad, USA, 1610718), DNase I (New England Biolabs, UK, M0303 L), immobiline dry strip pH 3-10 non-linear, 13 cm (GE Healthcare, USA, 17-6001-15), dry strip cover fluid (GE Healthcare, USA, 17-1335-01), iodoacetamide (IAA, Bio-Rad, USA, 1632109), formaldehyde solution (Sigma-Aldrich, USA, F8775), silver nitrate (Sigma-Aldrich, USA, 209139), sodium carbonate (Sigma-Aldrich, USA, S7795), sodium thiosulfate pentahydrate (Sigma-Aldrich, USA, 217247), glacial acetic acid (Sigma-Aldrich, USA, 320099), ethanol (EtOH, Fisher Chemical, USA, A955-4), phosphoric acid (Fisher Chemical, USA, A260-500), ammonium sulfate (Fisher Chemical, USA, A702-500), Coomassie brilliant blue G-250 (Sigma, UK, 27815), acetonitrile (Fisher Chemical, UK, A998-212), acetic acid (Fisher Chemical, USA, A35-500), ammonium hydrogen citrate (Merck, UK, 101154), trifluoroacetic acid (TFA, Sigma-Aldrich, UK, 302031), and α-cyano-4-hydroxycinnamic acid (Sigma-Aldrich, UK, C8982).

Milli-q water (Milli-Q Integral 3 water purification system, Merck Millipore, USA) was used in preparing all the chemical solutions required.

2.3. Tissue collection, processing, and storage

To improve the homogeneity and comparability, placentas selected in this study were collected from pregnant women who were experiencing sPTL-IM or sTL-IM with prior history of spontaneous PTL-IM among Malay ethnicity only.

Placentas with attached fetal membranes and umbilical cords were collected within 10 min of delivery and thoroughly washed in ice-cold PBS to remove the blood. Placenta tissues were collected from six different locations from the side facing the basal plate (maternal side) as well as the side facing the chorionic plate (fetal side). Relative consistency was maintained during collection by selecting six closest locations between all collected placentas; a grid indicated with six locations was overlaid as a guide. Moreover, the site with calcium deposits, visible connective tissue, and blood clots were avoided. The chorion with adherent decidua was separated from the amnion using sterile forceps. All collected tissues were snapped frozen in liquid nitrogen and stored at −80°C until protein extraction.

Based on the histology evidence by a trained histologist, no evidence of histological infection in placenta parenchyma was reported in all samples.

2.4. Protein extraction by DNase/lithium chloride-dense sucrose homogenization-coupled dichloromethane-methanol precipitation

For each individual sample, a total of 500 mg placenta tissues were randomly chosen and pulverized in a mortar with pestle containing liquid nitrogen. Powdered placenta tissues were subjected to protein extraction using DNase/lithium chloride-dense sucrose, and then cleaned up with dichloromethane-methanol precipitation as described previously by Tan et al. [13].

These purified protein samples were stored at −80°C until 2D-GE was performed.

2.5. Protein quantification

The total placentas protein concentration of the purified placentas tissue lysates from both case and control (maternal and fetal sides) were quantified by 2D Quant kit (GE Healthcare) according to the manufacturer's instruction. Bovine serum albumin was used as a standard throughout all the independent experiments.

2.6. 2D gel electrophoresis

The 2D-placenta proteome of the fetal and maternal sides of sPTL-IM was compared to their term controls, respectively. The purified tissue lysates from both case and control placentas (maternal and fetal sides) were diluted in a rehydration buffer consisting of 7 M urea, 2 M thiourea, 4% CHAPS, 0.2% biolyte 3–10, 20 mM DTT, 40 mM Tris, 0.002% (w/v) bromophenol blue to a final concentration of 266 μg, and a total volume of 250 μL. The protein samples were passively rehydrated at room temperature onto the 13 cm, pH 3–10 nonlinear IPG strips (GE Healthcare) for 16 h. Strips were overlaid with a dry strip cover fluid and focused using IPGphor II IEF system (Ettan IPGphor 3 IEF, GE Healthcare, USA) at 20°C and 50 μA/strip of maximum current limit using the following program: step and hold at 500 V for 500 Vh, gradient at 1000 V for 750 Vh, gradient at 8000 V for 11,250 Vh, and step and hold at 8000 V for 7333 Vh.

After completion of the first dimension IEF, IPG strips were equilibrated for 15 min at room temperature in a buffer containing 6 M urea, 50 mM Tris/HCl pH 8.8, 40% (v/v) glycerol, 2% (w/v) SDS, 0.02% bromophenol blue, and 65 mM DTT, followed by a 15-min incubation at

room temperature in the same buffer containing 135 mM IAA in place of DTT. After equilibration, IPG strips were placed and sealed on top of a 1.0-mm thick 10% wide-range PAGE with 0.5% agarose containing 0.02% bromophenol blue dye for second dimension wide-range PAGE analysis. The gels were run using the SE 600 Ruby electrophoresis tank (GE Healthcare). Each gel was run at a constant current of 10 mA for 15 min at 15°C followed by 25 mA for the remainder of the run until the tracking dye migrated to within 1 cm of the bottom of the gel.

To minimize gel-to-gel variation, placenta tissue lysates from both sPTL-IM and control placentas were ran simultaneously in a quart gel electrophoresis system (Ruby, GE Healthcare) for the second dimension and stained.

2.7. Protein visualization, statistical analysis, and spot detection

Case and control 2D gels (maternal and fetal sides) were visualized by silver nitrate [14] or colloidal Coomassie blue staining [15]. After staining, silver-stained 2D gels were scanned using the Image Scanner III imager (Image scanner III, GE Healthcare, USA). Gels stained with colloidal Coomassie blue were kept in 1% (v/v) acetic acid at 4°C until spot picking for protein identification.

All gel images were imported, and the protein spots were quantified by using ImageMaster 2D platinum software, version 7 (GE Healthcare Amersham Biosciences) program for comparative analysis. Protein spots were quantified in terms of their relative volume where the individual spot volume is divided by the total volume of the whole set of gel spots.

2D-gel images of sPTL-IM (maternal and fetal sides) were compared with term controls (maternal and fetal sides), respectively. Automatic gel image alignment was applied first and adjusted manually. Every single spot detected by the software was reviewed, and artifacts were excluded. To avoid variation in analysis, the same parameters were used for each gel. Besides, a single master gel image with the best quality and containing all the spots was prepared in each group as the reference gel. Normalization of the spot intensities was conducted according to the total optical density of the gel. After determining the percentage of intensity for each spot, the mean intensity of each spot between the cases and controls was analyzed by Student's *t*-test. Only protein spots with complete reproducibility across the sample set, expression intensity more than twofold changes (increase or decrease) as well as the *P*-value less than 0.05 were considered statistically significant for protein identification.

2.8. In-gel tryptic digestion

The protein spots from colloidal Coomassie blue-stained wide-range PAGE selected for further protein identification were excised manually using a sterile surgical blade. These gel plugs were cut into smaller pieces and transferred to a microcentrifuge tube filled with gel plaque storage buffer (7% (v/v) acetic acid and 10% (v/v) methanol) and stored at 4°C until in-gel digestion.

Gel plugs were washed with 150 μL of 100 mM ammonium bicarbonate for 10 min, de-stained and dehydrated in 150 μL of 50% acetonitrile in 50 mM ammonium bicarbonate for five times (15 min each time), and rehydrated in 150 μL of 10 mM DTT in 100 mM ammonium bicarbonate at room temperature for 30 min. DTT solution was removed and the gel plugs were

alkylated in 150 μL of 55 mM iodoacetamide in 100 mM ammonium bicarbonate at room temperature for 20 min in the dark. The gel plugs were dehydrated twice in 150 μL of 50% acetonitrile (20 min each time), then 50 μL of 50% acetonitrile (15 min); following acetonitrile removal, the gel plugs were completely dried by vacuum centrifugation.

Each protein spot was "in-gel" digested in 25 μL of 7 ng/μL trypsin (Promega, cat# V5111) in 200 mM ammonium hydrogen citrate for overnight at 30°C; 25 μL of 50% acetonitrile was added to each protein spot, incubated for 15 min (room temperature), quick spin, trypsin digestion solutions were collected, and dried by vacuum centrifugation. The pellet was reconstituted with 10 μL of 0.1% TFA for their mass spectrometric analysis.

2.9. Mass spectrometry

The resulting tryptic peptides obtained after in-gel digestion were analyzed by using a Bruker Ultraflexreme MALDI-TOF/TOF MS (Ultraflexreme; Bruker Daltonics GmbH, Breman, Germany) to give a peptide mass fingerprint and peptide sequence information. A solution of α-cyano-4-hydroxycinnamic acid (0.7 mg/mL) in 85% acetonitrile, 15% water, and 0.1% TFA was used as the matrix. Equal volumes of the matrix solution were mixed with tryptic digest peptides in 1:1 and spotted onto the MALDI plate (Achorchip plate). By routine, a standard peptide calibration mix in the mass range of 800–3200 Dalton (Bruker Daltonics, Leipzig, Germany) was analyzed for external calibration of the mass spectrometer.

MALDI-TOF/TOF mass spectra were acquired with smartbeam laser at 355 nm and operated in a positive and reflectron mode with 25-kV accelerating voltage; TOF/TOF tandem MS fragmentation spectra were acquired for each sample, averaging 5000 laser shots per fragmentation spectrum on each of the seven to 10 most abundant ions present in each sample (excluding trypsin autolytic peptides and other known background ions). The collision energy was set to 1 kV, and nitrogen was used as the collision gas.

The resulting peptide mass fingerprints were submitted to a computer equipped with the MASCOT search program (Matrix Science Ltd., UK) (www.matrixcsience.com) for identification of the protein present in the gel spot. Searches were performed without constraining to the protein molecular weight or isoelectric point. MASCOT search parameters were set as follows: carbamidomethylation of cysteine as a fixed modification, oxidation of methionine as a variable modification, trypsin as a proteolytic enzyme, residues up to one missed cleavage site with trypsin, and mass tolerance as 200 ppm. MS/MS spectra were searched as above using a peptide mass tolerance of 100 ppm and a fragment mass tolerance of ±0.2 Dalton. The protein identification database used was the National Center for Biotechnology Information (NCBInr), and the species selected for analysis was *Homo sapiens*. Results were scored using probability-based MOWSE scores (protein score is $-10 \times \mathrm{Log}_{10}(P)$, where P is the probability that the observed match is a random event). Protein scores greater than 67 were considered significant ($P < 0.05$).

2.10. Data analysis

Student's *t*-test (SPSS version 19.0) was applied on 2D quantification data to compare and evaluate the statistical significance of targeted protein among the study groups. *P*-value less than 0.05 was considered to be significant in both cases.

3. Results

3.1. Characteristics of the research population and body weight of fetus

Five pregnant women who were experiencing sPTL-IM were recruited in the study group while 10 pregnant women experiencing sTL-IM were recruited as the control group. Clinical data of these pregnant women were compared between both groups. As shown in **Table 1**, there were no statistical significant differences between sPTL-IM and sTL-IM groups in maternal age and parity. Pregnant women resulted in a PTB due to sPTL-IM have significantly lighter babies (at birth) and placentas than their control ($P < 0.05$, **Table 1**).

3.2. Comparative two-dimensional protein profile analysis of placenta tissues obtained from spontaneous unexplained preterm labor with intact membrane and its corresponding control

To further investigate the proteomic alterations in the sPTL-IM, the spot intensities in placenta samples (maternal and fetal sides) from sPTL-IM and sTL-IM were compared using ImageMaster 2D platinum software program.

A normalized amount of protein extracted from placenta tissues of sPTL-IM and sTL-IM was fixed on 13-cm pH 3–10 IPG strips. Second dimension separation was performed on 10% wide-range PAGE, as described under "Materials and Methods" section. Silver-stained 2D gels representing sPTL-IM and sTL-IM (fetal and maternal sides) are shown in **Figure 1A** and **B**, respectively. A comparison of the fetal side of the placenta tissues obtained from both the sPTL-IM and sTL-IM proteomes revealed highly similar protein profiles (**Figure 1AI** and **BI**) despite important differences being observed in the relative levels of several proteins as illustrated by the closer view of differentially expressed protein profiles (**Figure 1C**). These results were in parallel for the maternal side of the placenta tissues (**Figure 1AII**, **BII**, and **C**).

Student's *t*-test analysis revealed 12 differentially expressed proteins that are significant (two spots with greater staining and 10 spots with decreased staining; dotted circles in **Figure 1** indicate upregulated proteins, whereas solid circles indicate downregulated proteins, AI and BI, $P < 0.05$) in the fetal side of sPTL-IM with 100% reproducibility across the sample set. Whereas on the maternal side, only two gel spots with decreased staining showed at least 2.0-fold changes (solid circle in **Figure 1AII** and **BII**, $P < 0.05$) for the same comparison.

3.3. Identification of differentially expressed proteins associated with spontaneous unexplained preterm labor with intact membrane by MALDI-TOF/TOF MS

Identified spots with significant protein scores are shown in **Tables 2** and **3**. The spot numbers in **Tables 2** and **3** corresponded to the numbers in **Figure 1C**.

As indicated in **Tables 2** and **3**, S100-A9 and Ig kappa chain C (IGKC) region were overexpressed (**Table 2**), while vimentin, calpain small subunit 1 (CAPNS1), protein PP4-X, ferritin light subunit (FTL), septin 2, peroxiredoxin 3 (Prdx 3), cytokeratin 8, cytokeratin 1, and tropomodulin 3 (Tmod-3) were underexpressed in the fetal side of the placenta obtained from sPTL-IM compared to the control (two different spots were identified as the same protein;

http://dx.doi.org/10.5772/intechopen.74925

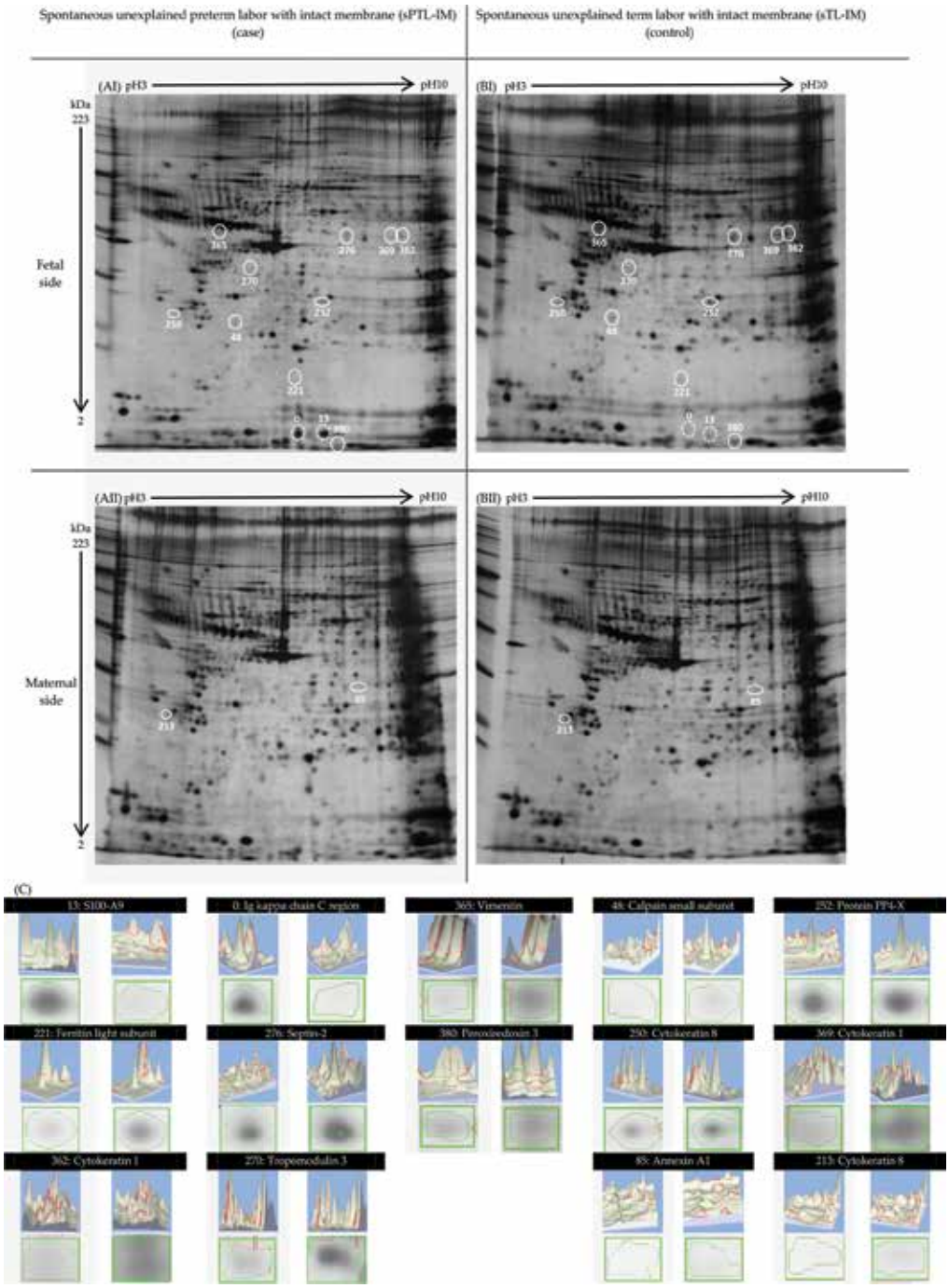

Figure 1. Representative 2D gels of placenta proteome. (AI and AII) Representative 2D gels of placenta tissue samples from sPTL-IM and (BI and BII) sTL-IM. The differentially expressed protein spots are circled on the gels and labeled with unique spot numbers. Dotted circles indicate overexpressed proteins in the gels analyzed using ImageMaster Software, while solid circles indicate underexpressed proteins. The spot number on the gels corresponds to the numbers in **Tables 2** and **3**. (C) A closer view of differentially expressed protein spots from 2D gels and their 3D images. The gray background boxes correspond to the sPTL-IM gels and the white background boxes correspond to the sTL-IM gels.

	Spot number[A]	NCBI accession #	Protein identified	Relative fold change[B]	Calculated pI/Mw (kDa)	P value	Mascot score[C]	Function	Sequence coverage (%)
Fetal side	13	NP_002956	Protein S100-A9	16.202	5.71/13.29	<0.001	70	Calcium binding protein	24
	0	P01834	Ig kappa chain C region	11.658	5.58/11.77	<0.001	120	Antigen binding agent	32

Accession #: accession numbers from SWISS-PROT database; A: arbitrary spot number supplied by Delta 2D. Numbers correspond to numbers in **Figure 1C**; B: fold change was calculated using ImageMaster 2D platinum software program; C: protein score generated by MS-MS identification platform, with a score higher than 67 being considered as statistically significant.

Table 2. Biochemical information of the overexpressed proteins in the placenta tissues of sPTL-IM.

	Spot number[A]	NCBI Accession #	Protein identified	Relative fold change[B]	Calculated pI/Mw (kDa)	P value	Mascot score[C]	Function	Sequence coverage (%)
Fetal side	365	AAA61279	Vimentin	−9.454	5.03/53.74	0.035	188	Stabilization of cytoskeletal interactions	9
	48	NP_001740	Calpain small subunit 1	−2.397	5.05/28.47	0.004	142	Stabilized calpain heterodimers	16
	252	AAC41689	Protein PP4-X	−2.356	5.65/36.26	0.022	150	Membrane fusion	9
	221	AAA52440	Ferritin light subunit	−2.494	5.65/16.44	0.080	227	Iron homeostasis and inflammatory response	30
	276	NP_004395	Septin-2	−2.311	6.15/41.69	0.015	70	Filament-forming cytoskeletal GTPase	7
	380	EAW49398	Peroxiredoxin 3	−2.025	6.06/11.16	<0.001	103	Mitochondrial dysfunction	13
	250	CAA31376	Cytokeratin 8	−2.104	4.91/30.84	0.026	162	Filament reorganization	12
	369	AFA52002	Cytokeratin 1	−6.141	8.15/66.18	0.011	207	Filament reorganization	13
	362	AFA52002	Cytokeratin 1	−2.759	8.15/66.18	132	Filament reorganization	13	
	270	AAF31670	Tropomodulin 3	−3.083	5.08/39.73	0.027	161	Maintaining cytoskeletal architecture	17

	Spot number[A]	NCBI Accession #	Protein identified	Relative fold change[B]	Calculated pI/Mw (kDa)	P value	Mascot score[C]	Function	Sequence coverage (%)
Maternal side	85	1AIN_A	Annexin A1	−2.003	7.77/35.25	0.005	95	Anti-inflammatory properties	7
	213	AAA35748	Cytokeratin 8	−2.896	5.30/53.66	0.005	118	Filament reorganization	9

Accession #: accession numbers from SWISS-PROT database; A: arbitrary spot number supplied by Delta 2D. Numbers correspond to numbers in **Figure 1C**; B: fold change was calculated using ImageMaster 2D platinum software program; C: protein score generated by MS-MS identification platform, with a score higher than 67 being considered as statistically significant.

Table 3. Biochemical information of the underexpressed proteins in the placenta tissues of sPTL-IM.

cytokeratin 1) (**Table 3**), whereas two proteins namely annexin A1 (ANXA1) and cytokeratin 8 were underexpressed (**Table 3**) in the maternal side of the placenta obtained from sPTL-IM compared to the control.

Interestingly, in both the fetal and maternal sides of the placentas, cytokeratin 8 was reduced in expression in relation to sPTL-IM (**Table 3**). There were no overexpressed proteins found in the maternal side of the placenta.

Of the total 12 proteins identified, four functional groupings emerge (**Figure 2**). Cytokeratin 8, cytokeratin 1, vimentin, Tmod-3, septin 2, and CAPNS1 are grouped under structural and cytoskeletal components (53.8%), S100-A9, IGKC, and ANXA1 are grouped under immunomodulatory proteins (23.1%), FTL and Prdx 3 are grouped under placenta-modulatory proteins (15.4%), and lastly, protein PP4-X is grouped under anticoagulation cascade (7.7%).

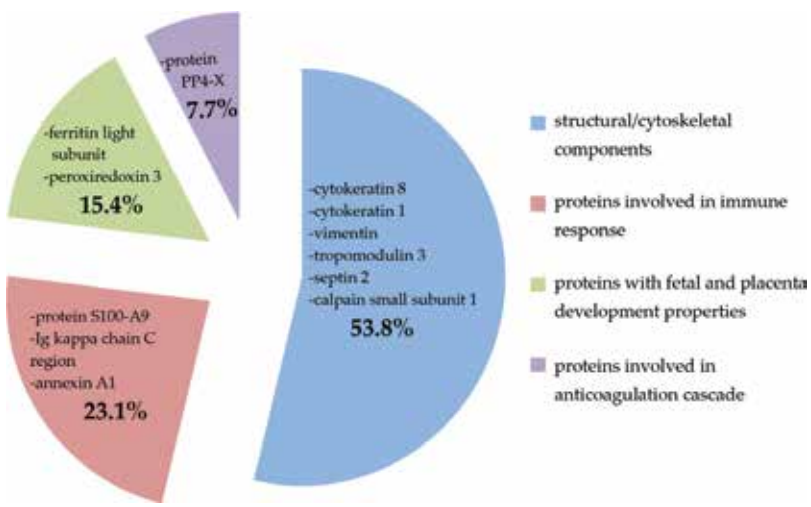

Figure 2. Functional grouping of differentially expressed proteins identified in the placentas obtained from pregnant women experiencing sPTL-IM.

4. Discussion

Current understanding of placenta association with sPTL-IM leading to PTB is strikingly limited, which further limits our ability to accurately predict the occurrence of this event. Despite great strides in neonatal care, infant survival rates remained low partly due to sPTL-IM nonetheless. This imparts a significant risk of various childhood diseases/disorders among premature infants. Thus, placenta proteome analyses of sPTL-IM allowed the identification of potential biomarkers and the exploration of the underlying molecular pathophysiology related to placenta insufficiency leading to this syndrome, where the study employing placenta proteome on this syndrome is still limited. As such, this report is designed to demonstrate the feasibility of using placenta proteome to study its association to sPTL-IM while making the initial findings widely available. In essence, we have identified 12 potentially important protein differences in the placenta of sPTL-IM.

It is possible that limitations exist in the 2D-GE technology. This is due to the presence of proteins that are extremely acidic and basic, hydrophobic, large molecular weights, and low copy numbers [16]. Furthermore, limitations were observed when identifying and quantifying proteins as the protein spots need to be excised out from the 2D gels and digested with proteases.

The differentially expressed proteins identified from sPTL-IM can be generally classified into four functional classes, which were (1) structural/cytoskeletal components, (2) proteins involved in immune response, (3) proteins with fetal and placenta development properties, and (4) proteins involved in anticoagulation cascade.

4.1. Structural or cytoskeletal components

A majority of the identified proteins were proteinaceous components of structural or cytoskeletons (**Figure 2**) which is not surprising since the cytoskeletal proteins are known as major regulators of the endothelial function and signaling processes [17]. A total of six proteins were grouped under this function. Half of the proteins that fall into this class were intermediate filaments namely cytokeratin 8, cytokeratin 1, and vimentin (**Figure 2**). Cytokeratin 8 was found to be differentially expressed in both the fetal and maternal sides from the sPTL-IM placenta while the expression of cytokeratin 1 and vimentin was observed only at the fetal side. Commonly, keratin types I and II copolymerize to form intermediate filaments in epithelia [18], and vimentin form type III filaments in endothelial cells [19]. As the placenta is a highly vascularized system of epithelial membranes, the presence of these components is expected.

Dysregulation of keratin expression has been reported in many pregnancy disorders. Studies had showed that dysregulation of keratins 7, 8, 18, and 19 expressions was associated with pregnancy disorder, with the results contradicting each other about up- or downregulation of these keratins [20, 21]. The reason for this discrepancy is still not certain, and it may be explained by the severity of cases, unhealthy women might be from different backgrounds, or there is a more complex effect of this pregnancy complication on placenta intermediate filaments. Most importantly, changes in keratin expression level might influence cell architectural properties such as cell polarity and shape.

Vimentin was presumed to play a vital role in anchoring and positioning organelles in the cytosol, maintenance of cell integrity, and stabilization of cytoskeletal interactions [22, 23]. Downregulation of vimentin was observed in the obese placenta as well as in human-aborted placenta tissues [24, 25]. A deficiency of this protein could result in the dramatic reorganization of vimentin filaments in the cytoplasm, leading to morphological changes and cellular fragmentation and ultimately destabilizes the overall cytoplasm architecture which might lead to PTL [23].

Meanwhile, the remaining half of the identified proteins that fell into this functional group includes cytoskeletal and cytoskeleton-associated proteins namely Tmod-3, septin 2, and CAPNS1 (the fetal side of placenta tissues) (**Figure 2**). Studies also demonstrated that pregnancy maintenance is regulated by various cytoskeletal and cytoskeleton-associated proteins [26, 27].

Tmod-3 is one of the components of membrane-associated tropomyosin-filamentous actin (TM-F-actin) networks, which is responsible for the polarization of plasma membranes of epithelial cell and sarcoplasmic reticulum membranes of skeletal muscle [28, 29]. This protein is also involved in endothelial cell migration, erythroblast enucleation and erythroblast-macrophage adhesion in erythropoiesis, and insulin-stimulated GLUT4 trafficking in adipocytes [30–32]. Moreover, Tmod-mediated stabilization of TM-F-actin is critical for membrane morphology, mechanics, and physiology [29]. It is thus conceivable that alteration in Tmod-3 levels may contribute to the deregulation of actin filaments of the placenta.

Septin is known to play roles in vesicle trafficking, cytoskeletal remodeling, and apoptosis through the organization of actin-myosin contractile ring [33]. It regulates ring contraction or the attachment of actin-myosin contractile ring to the plasma membrane [34]. Septin was also proposed to have additional functions in mammals such as cell surface organization and vesicle fusion processes [33, 34].

CAPNS1 is a regulatory subunit that is involved in calpain heterodimers (calpain-1 and calpain-2) stabilization and operation. CAPNS1 proteolytic activities had been reported to involve in various cellular functions including apoptosis, proliferation, migration, adhesion, and autophagy. *Capns1* deficiency was reported to be the factor of calpain-1 and -2 zero expression that resulted in embryonic lethality around embryonic day 10.5 due to possible cardiac defects and hemorrhages [35].

Collectively, alterations in the expression of proteins involved in the intermediate filaments and cytoskeletal network can lead to significant reorganization of the placenta cytoskeletal, as well as defects in placenta endothelial cell migration and tubule formation. Such cytoskeleton rearrangement and defects in endothelial cell signals transduction and function may be contributing factors to the characteristic disorganization of myofiber in placentas, where tissue structural capacity for stretch was altered, leading to sPTL-IM. This cause-and-effect interpretation is consistent with the higher incidence of PTL during multiple versus single gestations [36].

One possible justification for more proteins from this functional group was dysregulated in fetal compared to maternal which could be that the fetal involved significantly in the process of cytoskeleton reorganization. This observation is consistent with the findings by Tonami et al. [37], which have shown that microtuble-stabilizing protein is highly expressed in the fetal side of the placenta.

4.2. Proteins involved in immune response

Immunomodulatory proteins were also identified in placenta tissues from pregnant women with sPTL-IM. These include S100-A9, IGKC (fetal side of placenta tissues), and ANXA1 (maternal side of placenta tissues) (**Figure 1C**). Inflammation has been attributed to the occurrence of PTL in human [38]. This is possible because the presence of inflammatory cytokines cause cervical ripening and the maturation of the chorioamnion, leading to labor [38]. In addition, Pereira et al. also observed the presence of calgranulins and annexins in cervical-vaginal fluid from patients with spontaneous PTL [39].

S100-A9 (also known as calgranulin B) is a calcium-binding protein that regulates inflammatory and immune responses which function extracellularly as an antimicrobial agent [40, 41]. Various studies have reported significantly elevated levels of calgranulins A and B in amniotic fluid from intra-amniotic-infected women [41], as well as in vaginal fluid from 86% of patients who were presented with PTL without obvious evidence of genital tract infection or inflammation [42]. Women in labor secondary to intra-amniotic inflammation have also been found to have increased *S100-A8* and *S100-A9* in amniotic fluid and maternal blood [41, 43]. Moreover, calgranulin B can interact directly with β2 integrins in forming "activated receptor" epitopes and plays a role in cytoskeletal reorganization [44].

IGKC functions as an antigen-binding, immune regulation, and disposal of immune complexes [45]. Several lines of evidence suggested that during late pregnancy, recruitment of circulating maternal innate and adaptive leukocytes into the cervix and/or myometrium, and then to the decidua interface via chemotactic cascades induces a pro-inflammatory state which leads to labor [46].

ANXA1 is a calcium-dependent phospholipid-binding protein that is involved in cell proliferation, differentiation, mediating inflammation, apoptosis, and maintenance of pregnancy [42, 47, 48]. It has been reported that *ANXA1* deficiency leads to changes in the inflammatory response and the anti-inflammatory effects of glucocorticoids [48]. Moreover, anti-inflammatory effects by the potent inhibition of neutrophil trafficking were observed from mice that were administered with ANXA1 [49]. A decrease of ANXA1 expression can result in the liberation of phospholipase A2 activity, making more arachidonic acid (precursor of prostaglandins) available for prostaglandin generation [50], which is crucial in uterine contraction and cervical ripening.

Therefore, it remains possible that the premature activation of this inflammatory pathway can lead to a breakdown of feto-maternal tolerance and play a role in the induction of labor, which subsequently can result in spontaneous PTL.

4.3. Proteins with fetal and placenta development

Identified proteins that are associated to this function were Prdx 3 and FTL where both were identified from the fetal side of placenta tissues (**Figure 1C**).

Prdx 3 is a mitochondria antioxidant enzyme that was known to involve in apoptosis and response to oxidative stress [51]. Previous studies have shown that a lower expression of Prdx 3 in human placenta tissues triggered oxidative stress and caused dysfunction of mitochondria in trophoblast cells [52]. From our results, the downregulation of this protein in placentas of sPTL-IM patients suggested the stimulation of fatty acid cascade, such as arachidonic acid and cell cycle arrest by oxidative stress [53, 54]. Both processes are potentially synergistic mechanisms that contribute to preterm contractions, cervical dilatation, and PTL.

Ferritin is a multimeric protein that consisted of two subunits: ferritin heavy chain (FTH) and FTL, which share about 50% sequence homology and is mainly found in the villous stroma of the placenta [55]. FTL has been reported to play a critical role in iron storage as well as regulation of intracellular iron homeostasis and inflammatory response [56, 57]. Mutation in the *FTL* has also been demonstrated to cause neuroferritinopathy and neurodegeneration [58, 59]. On the other hand, anti-inflammatory activities were observed from FTL overexpression where Fan et al. [56] reported inhibition on lipopolysaccharide (LPS)-induced transcription of anti-inflammatory factor at the feto-maternal interface of the placenta leading to PTL [60]. Therefore, it is possible that the production of inflammatory mediators induced by LPS at feto-maternal interface of the placenta can contribute to FTL degradation and synergized to increase intracellular free iron. This leads to increased oxidative stress. Furthermore, elevated placenta oxidative stress was thought to play a key role in stimulating the release of factors, further leading to maternal endothelium activation [61].

4.4. Proteins involved in anticoagulation cascade

Only one identified protein was classified in this group. Protein PP4-X (also known as annexin IV (ANX4)) was downregulated in sPTL-IM placentas when compared to the control placentas at the fetal side (**Figure 1C**). This protein has been known to be involved in multiple cellular functions including endocytosis, exocytosis, ion fluxes, and apoptosis [62, 63]. This protein is also one of the important components of biological cascades regulating coagulation which makes it an important factor for the maintenance of pregnancy [63]. Placenta structural abnormality and dysfunction in IUGR fetuses were reported to be caused by reduction in two members of annexins (ANX4 and ANX8) [64]. Furthermore, coagulative disorder and antiphospholipid antibody syndrome have been associated with an increased incidence of pregnancy complications, including PTL [65]. Several cases of increased polymorphism rate in genes related to coagulation have also been associated with PTB [66]. Therefore, it is conceivable that alterations in ANX4 levels may contribute to a failure of placenta anticoagulation and structural abnormality, leading to impaired utero placenta development.

Interestingly, more proteins were differentially expressed in the fetal side than in the maternal side of the placenta tissues obtained from pregnant women who experienced sPTL-IM (**Tables 2** and **3**); this interpretation is consistent with the signals from the fetus where they are capable of initiating the onset of parturition process [67]. The work by Reinl and England [67] demonstrated a possible interplay between placenta corticotrophin-releasing hormone and fetal surfactant protein-A that drives parturition in human. Moreover, another study indicated that nuclear receptor coactivators 1 and 2 regulate the transcription of surfactant protein-A and consequently the induction of labor [68].

5. Conclusion

The underlying mechanisms leading to sPTL-IM are not fully understood. This leads to limited prediction and prevention of sPTL-IM due to its complex pathophysiological process. Placenta was an excellent biological tissue that might facilitate the discovery of potential biomarkers as well as to assess dysfunction in the framework of sPTL-IM. Moreover, sPTL-IM

may alter selected placenta functions that lead to PTL. For this, proteomic approaches have enabled the discovery of potential biomarkers in the placenta and unveiled the pathophysiological pathways associated to sPTL-IM. The identified proteins involved in four distinct functional classes include inflammation, oxidative stress, anticoagulation, and extracellular matrix remodeling leading to preterm parturition. These results can help in the future selection of more meaningful potential biomarkers for the early detection of sPTL-IM that might appear in easily accessible body fluid. Lastly, it is postulated that signals for the initiation of sPTL-IM are more likely to arise from the fetus and to a lesser extent from the mother due to more proteins differentially expressed in the fetal side of the placenta of sPTL-IM.

Acknowledgements

The authors would like to acknowledge the Fundamental Research Grant Scheme grant: FRGS/2/2013/SKK09/UPM/02/2 and My PhD fellowship by the Ministry of Higher Education, Malaysia. The authors would also like to thank Sime Darby Technology Centre Sdn. Bhd. for permission to use their proteomic facilities.

Conflict of interest

The authors reported no conflict of interest.

Author details

Niu J. Tan[1], Leona D.J. Daim[2], Amilia A.M. Jamil[3], Norhafizah Mohtarrudin[4] and Karuppiah Thilakavathy[1,5]*

*Address all correspondence to: thilathy@upm.edu.my

1 Medical Genetics Unit, Department of Biomedical Science, Faculty of Medicine and Health Sciences, Universiti Putra Malaysia, Serdang, Selangor, Malaysia

2 Sime Darby Technology Centre Sdn. Bhd., UPM-MTDC Technology Centre III, Lebuh Silikon, Universiti Putra Malaysia, Serdang, Selangor, Malaysia

3 Department of Obstetrics and Gynaecology, Faculty of Medicine and Health Sciences, Universiti Putra Malaysia, Serdang, Selangor, Malaysia

4 Department of Pathology, Faculty of Medicine and Health Sciences, Universiti Putra Malaysia, Serdang, Selangor, Malaysia

5 Genetics and Regenerative Medicine Research Centre, Faculty of Medicine and Health Sciences, Universiti Putra Malaysia, Serdang, Selangor, Malaysia

References

[1] Das A, Subrat P, Ahanthem SS, Sourabh GD, Bhanu Pratap SG. Preterm birth: Analysis of risk factors and neonatal outcome. Gynecology & Obstetrics Case Report. 2015;**1**:1-5

[2] Kugelman A, Colin AA. Late preterm infants: Near term but still in a critical developmental time period. Pediatrics. 2013;**132**:741-751

[3] Ahuja R, Sood A, Pal A, Mittal R. Role of micronized progesterone in prevention of preterm labour in women with previous history of one or more preterm births: A research study at a tertiary care hospital. International Journal of Reproduction, Contraception, Obstetrics and Gynecology. 2017;**4**:1176-1180

[4] Georgiou HM, Di Quinzio MK, Permezel M, Brennecke SP. Predicting preterm labour: Current status and future prospects. Disease Markers. 2015;**2015**:1-9

[5] Liong S, Di Quinzio MK, Fleming G, Permezel M, Rice GE, Georgiou HM. Prediction of spontaneous preterm labour in at-risk pregnant women. Reproduction. 2013;**146**:335-345

[6] Conde-Agudelo A, Papageorghiou AT, Kennedy SH, Villar J. Novel biomarkers for the prediction of the spontaneous preterm birth phenotype: A systematic review and meta-analysis. BJOG: An International Journal of Obstetrics & Gynaecology. 2011;**118**:1042-1054

[7] Shah J, Baxi B. Identification of biomarkers for prediction of preterm delivery. Journal of Medical Society. 2016;**30**:3

[8] Fox SI. Reproduction. In: Human Physiology. 9th ed. New York: McGraw-Hill Higher Education; 2006. pp. 700-730

[9] Takemura M, Kimura T, Nomura S, Makino Y, Inoue T, Kikuchi T, Kubota Y, Tokugawa Y, Nobunaga T, Kamiura S. Expression and localization of human oxytocin receptor mRNA and its protein in chorion and decidua during parturition. Journal of Clinical Investigation. 1994 Jun;**93**(6):2319

[10] Mine K, Katayama A, Matsumura T, Nishino T, Kuwabara Y, Ishikawa G, Murata T, Sawa R, Otsubo Y, Shin S, Takeshita T. Proteome analysis of human placentae: Preeclampsia versus normal pregnancy. Placenta. 2007;**28**:676-687

[11] Liu B, Xu Y, Voss C, Qiu FH, Zhao MZ, Liu YD, Nie J, Wang ZL. Altered protein expression in gestational diabetes mellitus placentas provides insight into insulin resistance and coagulation/fibrinolysis pathways. PLoS One. 2012;**7**:e44701

[12] Menon R, Taylor RN, Fortunato SJ. Chorioamnionitis—A complex pathophysiologic syndrome. Placenta. 2010;**31**:113-120

[13] Tan NJ, Daim LD, Jamil AA, Mohtarrudin N, Thilakavathy K. An effective placental cotyledons proteins extraction method for 2D gel electrophoresis. Electrophoresis. 2017;**38**:633-644

[14] Blum H, Beier H, Gross HJ. Improved silver staining of plant proteins, RNA and DNA in polyacrylamide gels. Electrophoresis. 1987;**8**:93-99

[15] Westermeier R. Sensitive, quantitative, and fast modifications for Coomassie Blue staining of polyacrylamide gels. Proteomics. 2006;**6**:61-64

[16] Lim SR, Gooi BH, Singh M, Gam LH. Analysis of differentially expressed proteins in colorectal cancer using hydroxyapatite column and SDS-PAGE. Applied Biochemistry and Biotechnology. 2011;**165**:1211-1124

[17] Kerem A, Yin J, Kaestle SM, Hoffmann J, Schoene AM, Singh B, Kuppe H, Borst MM, Kuebler WM. Lung endothelial dysfunction in congestive heart failure. Circulation Research. 2010;**106**:1103-1116

[18] Oriolo AS, Wald FA, Ramsauer VP, Salas PJ. Intermediate filaments: A role in epithelial polarity. Experimental Cell Research. 2007;**313**:2255-2264

[19] Strelkov SV, Herrmann H, Geisler N, Lustig A, Ivaninskii S, Zimbelmann R, Burkhard P, Aebi U. Divide-and-conquer crystallographic approach towards an atomic structure of intermediate filaments. Journal of Molecular Biology. 2001;**306**:773-781

[20] Ahenkorah J, Hottor B, Byrne S, Bosio P, Ockleford CD. Immunofluorescence confocal laser scanning microscopy and immuno-electron microscopic identification of keratins in human materno-foetal interaction zone. Journal of Cellular and Molecular Medicine. 2009;**13**:735-748

[21] Hefler LA, Tempfer CB, Bancher-Todesca D, Schatten C, Husslein P, Heinze G, Gregg AR. Placental expression and serum levels of cytokeratin-18 are increased in women with preeclampsia. Journal of the Society for Gynecologic Investigation. 2001;**8**:169-173

[22] Goldman RD, Khuon S, Chou YH, Opal P, Steinert PM. The function of intermediate filaments in cell shape and cytoskeletal integrity. The Journal of Cell Biology. 1996;**134**:971-983

[23] Morishima N. Changes in nuclear morphology during apoptosis correlate with vimentin cleavage by different caspases located either upstream or downstream of Bcl-2 action. Genes to Cells. 1999;**4**:401-414

[24] Higgins L, Greenwood SL, Wareing M, Jones RL, Cowley EJ, Sibley CP, Mills TA. Maternal obesity: Does placental cell turnover hold clues to the aetiology of aberrant fetal growth? Reproductive Sciences. 2010;**17**:194A

[25] Potdar PD, Chaugule S. Development and molecular characterization of human placental mesenchymal stem cells from human aborted fetal tissue as a model to study mechanism of spontaneous abortion. Advances in Stem Cells. 2014;**2014**:1-7

[26] Miehe U, Neumaier-Wagner P, Kadyrov M, Goyal P, Alfer J, Rath W, Huppertz B. Concerted upregulation of CLP36 and smooth muscle actin protein expression in human endometrium during decidualization. Cells, Tissues, Organs. 2005;**179**:109-114

[27] Flamini MI, Sanchez AM, Goglia L, Tosi V, Genazzani AR, Simoncini T. Differential actions of estrogen and SERMs in regulation of the actin cytoskeleton of endometrial cells. Molecular Human Reproduction. 2009;**15**:675-685

[28] Weber KL, Fischer RS, Fowler VM. Tmod3 regulates polarized epithelial cell morphology. Journal of Cell Science. 2007;**120**:3625-3632

[29] Moyer JD, Nowak RB, Kim NE, Larkin SK, Peters LL, Hartwig J, Kuypers FA, Fowler VM. Tropomodulin 1-null mice have a mild spherocytic elliptocytosis with appearance of tropomodulin 3 in red blood cells and disruption of the membrane skeleton. Blood. 2010;**116**:2590-2599

[30] Fischer RS, Fritz-Six KL, Fowler VM. Pointed-end capping by tropomodulin3 negatively regulates endothelial cell motility. The Journal of Cell Biology. 2003;**161**:371-380

[31] Sui Z, Nowak RB, Bacconi A, Kim NE, Liu H, Li J, Wickrema A, An XL, Fowler VM. Tropomodulin3-null mice are embryonic lethal with anemia due to impaired erythroid terminal differentiation in the fetal liver. Blood. 2014;**123**:758-767

[32] Lim CY, Bi X, Wu D, Kim JB, Gunning PW, Hong W, Han W. Tropomodulin3 is a novel Akt2 effector regulating insulin-stimulated GLUT4 exocytosis through cortical actin remodeling. Nature Communications. 2015;**6**:1-15

[33] Ahuja P, Perriard E, Trimble W, Perriard JC, Ehler E. Probing the role of septins in cardiomyocytes. Experimental Cell Research. 2006;**312**:1598-1609

[34] McQuilken M, Jentzsch MS, Verma A, Mehta SB, Oldenbourg R, Gladfelter AS. Analysis of septin reorganization at cytokinesis using polarized fluorescence microscopy. Frontiers in Cell and Developmental Biology. 2017;**42**:1-14

[35] Arthur JS, Elce JS, Hegadorn C, Williams K, Greer PA. Disruption of the murine calpain small subunit gene, Capn4: Calpain is essential for embryonic development but not for cell growth and division. Molecular and Cellular Biology. 2000;**20**:4474-4481

[36] Oliveira TA, Carvalho CM, Souza ED, Mariani-Neto C, Camano L. Detection of fetal fibronectin in twin pregnancies in relation to gestational age. Sao Paulo Medical Journal. 1999;**117**:121-124

[37] Tonami K, Kurihara Y, Aburatani H, Uchijima Y, Asano T, Kurihara H. Calpain 6 is involved in microtubule stabilization and cytoskeletal organization. Molecular and Cellular Biology. 2007;**27**(7):2548-2561

[38] Ekman-Ordeberg G, Dubicke A. Preterm cervical ripening in humans. Facts, Views & Vision in ObGyn. 2012;**4**:245

[39] Pereira L, Reddy AP, Jacob T, Thomas A, Schneider KA, Dasari S, Lapidus JA, Lu X, Rodland M, Roberts CT, Gravett MG. Identification of novel protein biomarkers of preterm birth in human cervical-vaginal fluid. Journal of Proteome Research. 2007;**6**: 1269-1276

[40] Roth J, Goebeler M, Sorg C. S100A8 and S100A9 in inflammatory diseases. The Lancet. 2001;**357**:1041

[41] Rüetschi U, Rosén Å, Karlsson G, Zetterberg H, Rymo L, Hagberg H, Jacobsson B. Proteomic analysis using protein chips to detect biomarkers in cervical and amniotic fluid in women with intra-amniotic inflammation. Journal of Proteome Research. 2005;**4**:2236-2242

[42] Klein LL, Jonscher KR, Heerwagen MJ, Gibbs RS, McManaman JL. Shotgun proteomic analysis of vaginal fluid from women in late pregnancy. Reproductive Sciences. 2008;**15**:263-273

[43] Buhimschi IA, Christner R, Buhimschi CS. Proteomic biomarker analysis of amniotic fluid for identification of intra-amniotic inflammation. BJOG: An International Journal of Obstetrics & Gynaecology. 2005;**112**:173-181

[44] Manitz MP, Horst B, Seeliger S, Strey A, Skryabin BV, Gunzer M, Frings W, Schönlau F, Roth J, Sorg C, Nacken W. Loss of S100A9 (MRP14) results in reduced interleukin-8-induced CD11b surface expression, a polarized microfilament system, and diminished responsiveness to chemoattractants in vitro. Molecular and Cellular Biology. 2003; **23**:1034-1043

[45] Gottlieb PD, Cunningham BA, Rutishauser US, Edelman GM. Covalent structure of a human γG-immunoglobulin. VI. Amino acid sequence of the light chain. Biochemistry. 1970;**9**:3155-3161

[46] Gomez-Lopez N, Tanaka S, Zaeem Z, Metz GA, Olson DM. Maternal circulating leukocytes display early chemotactic responsiveness during late gestation. BMC Pregnancy and Childbirth. 2013;**13**:S8

[47] Scannell M, Flanagan MB, Wynne KJ, Cagney G, Godson C, Maderna P. Annexin-1 and peptide derivatives are released by apoptotic cells and stimulate phagocytosis of apoptotic neutrophils by macrophages. The Journal of Immunology. 2007;**178**:4595-4605

[48] Hannon R, Croxtall JD, Getting SJ, Roviezzo F, Yona S, Paul-Clark MJ, Gavins FN, Perretti M, Morris JF, Buckingham JC, Flower RJ. Aberrant inflammation and resistance to glucocorticoids in annexin 1−/− mouse. The FASEB Journal. 2003;**17**:253-255

[49] Lim LH, Pervaiz S. Annexin 1: The new face of an old molecule. The FASEB Journal. 2007; **21**:968-975

[50] Herbert SP, Odell AF, Ponnambalam S, Walker JH. The confluence-dependent interaction of cytosolic phospholipase A2-α with annexin A1 regulates endothelial cell prostaglandin E2 generation. Journal of Biological Chemistry. 2007;**282**:34468-34478

[51] Li L, Yu AQ. The functional role of peroxiredoxin 3 in reactive oxygen species, apoptosis, and chemoresistance of cancer cells. Journal of Cancer Research and Clinical Oncology. 2015;**141**:2071-2077

[52] Wu WB, Menon R, Xu YY, Zhao JR, Wang YL, Liu Y, Zhang HJ. Downregulation of peroxiredoxin-3 by hydrophobic bile acid induces mitochondrial dysfunction and cellular senescence in human trophoblasts. Scientific Reports. 2016;**6**:1-14

[53] Joshi SR, Mehendale SS, Dangat KD, Kilari AS, Yadav HR, Taralekar VS. High maternal plasma antioxidant concentrations associated with preterm delivery. Annals of Nutrition and Metabolism. 2008;**53**:276-282

[54] Zurgil U, Ben-Ari A, Atias K, Isakov N, Apte R, Livneh E. PKCη promotes senescence induced by oxidative stress and chemotherapy. Cell Death & Disease. 2014;**5**:e1531

[55] Yang A, Zhao J, Lu M, Gu Y, Zhu Y, Chen D, Fu J. Expression of hepcidin and ferroportin in the placenta, and ferritin and transferrin receptor 1 levels in maternal and umbilical cord blood in pregnant women with and without gestational diabetes. International Journal of Environmental Research and Public Health. 2016;**13**:766

[56] Fan Y, Zhang J, Cai L, Wang S, Liu C, Zhang Y, You L, Fu Y, Shi Z, Yin Z, Luo L. The effect of anti-inflammatory properties of ferritin light chain on lipopolysaccharide-induced inflammatory response in murine macrophages. Biochimica et Biophysica Acta (BBA)-Molecular Cell Research. 2014;**1843**:2775-2783

[57] Mackenzie EL, Iwasaki K, Tsuji Y. Intracellular iron transport and storage: From molecular mechanisms to health implications. Antioxidants & Redox Signaling. 2008;**10**:997-1030

[58] Muhoberac BB, Baraibar MA, Vidal R. Iron loading-induced aggregation and reduction of iron incorporation in heteropolymeric ferritin containing a mutant light chain that causes neurodegeneration. Biochimica et Biophysica Acta (BBA)-Molecular Basis of Disease. 2011;**1812**:544-548

[59] Keogh MJ, Jonas P, Coulthard A, Chinnery PF, Burn J. Neuroferritinopathy: A new inborn error of iron metabolism. Neurogenetics. 2012;**13**:93-96

[60] Paintlia MK, Paintlia AS, Singh AK, Singh I. Attenuation of lipopolysaccharide induced inflammatory response and phospholipids metabolism at the feto-maternal interface by N-acetyl-cysteine. Pediatric Research. 2008;**64**:334

[61] Redman CW, Sargent IL. Latest advances in understanding preeclampsia. Science. 2005; **308**:1592-1594

[62] Gerke V, Moss SE. Annexins: From structure to function. Physiological Reviews. 2002; **82**:331-371

[63] Masuda J, Takayama E, Satoh A, Ida M, Shinohara T, Kojima-Aikawa K, Ohsuzu F, Nakanishi K, Kuroda K, Murakami M, Suzuki K. Levels of annexin IV and V in the plasma of pregnant and postpartum women. Thrombosis and Haemostasis. 2004;**91**:1129-1136

[64] Chen F, Wang T, Feng C, Lin G, Zhu Y, Wu G, Johnson G, Wang J. Proteome differences in placenta and endometrium between normal and intrauterine growth restricted pig fetuses. PLoS One. 2015;**10**:e0142396

[65] Cucurull E, Gharavi AE, Menon Y, Wilson WA. Antiphospholipid antibody syndrome. Current Treatment Options in Cardiovascular Medicine. 2003;**5**:127-136

[66] Härtel C, von Otte S, Koch J, Ahrens P, Kattner E, Segerer H, Möller J, Diedrich K, Göpel W. Polymorphisms of haemostasis genes as risk factors for preterm delivery. Thrombosis and Haemostasis. 2005;**94**(1):88-92

[67] Reinl EL, England SK. Fetal-to-maternal signaling to initiate parturition. The Journal of Clinical Investigation. 2015;**125**:2569

[68] Geach T. Pregnancy: Fetal signalling initiates parturition. Nature Reviews Endocrinology. 2015;**11**:505

Chapter 2

The Role of One- and Two-Dimensional Electrophoretic Techniques in Proteomics of the Lung

Simona Viglio, Maddalena Cagnone,
Laurent Chiarelli, Roberta Salvini and Paolo Iadarola

Additional information is available at the end of the chapter

http://dx.doi.org/10.5772/intechopen.75042

Abstract

The current chapter was designed to keep the reader informed about the present status of pulmonary proteome. Taken together, the results documented here demonstrate that, after a decade of activity, proteomics of pulmonary diseases is catching up with its promise. The constantly growing number of reports in this area supports the view of this approach as one of the decisive methodological tools for the identification/characterization of disease-associated proteins. In terms of experimental procedures, the basic options available for proteomic investigations consist in the identification of proteins through the use of gel-based or gel-free techniques followed by MS. Obviously, the question arises of whether sophisticated technologies (such as the non-gel-based proteomic procedures) may currently be more fruitful, in terms of candidate protein marker identification, than "conventional" (read electrokinetic) approaches. In light of the versatility and high degree of reproducibility shown by these new potent strategies, a positive answer is perhaps not surprising. Nevertheless, as documented in this chapter, despite being less sophisticated than competing ones, gel-based techniques still represent a widely used procedure able to generate a reliable protein "fingerprint" and to produce qualitative and quantitative information on the protein patterns of a variety of human fluids.

Keywords: proteomics, lung diseases, 1-DE, 2-DE, 2D-DIGE, CE, MS

1. Introduction

The changes of the research strategy in the biochemical field driven by technological advancements occurred in these years allowed proteomics to progress and become one of the most captivating

branches of biochemistry. It is no exaggeration to say that, thanks to the significant step forward in the sensitivity and specificity of analytical methods, (almost) all proteins expressed by an organism can be detected/quantified even in extremely complex biological matrices. The monitoring of protein expression patterns in clinical specimens may indeed offer great opportunities to establish sets of biomarkers potentially associated with a specific disease status [1–8]. Despite these advantages, the question arises whether the application of these sophisticated proteomic procedures have profoundly affected the study of human diseases. If the number of publications in this field counts for something, the answer is undoubtedly positive. Through its ability to provide insights into both specific and system-level changes in cell, tissue and human physiology, proteomics has driven the progress observed in the last years in the elucidation of a variety of multifactorial pathological conditions, including less commonly diagnosed disorders [9–13]. In clinical proteomics several tissues and/or biological fluids are routinely analyzed for expressed proteins. Obviously, to make these analyses quantitative and reproducible, reliable profiling procedures should be established. Such procedures must rely on efficient and robust separation systems whose pivotal role is to make the complexity of mixtures simpler. Electrophoretic separations, both in-gel (1-DE and 2-DE) and in-solution (capillary electrophoresis (CE) and liquid chromatography (LC) approaches, both coupled to mass spectrometry (MS)), are currently the most attractive strategies toward the separation of hundreds/thousands of proteins. While acknowledging a remarkable success of electrophoretic approaches over the years, their intrinsic limitations cannot be hushed up. For example, the poor (if any) resolution of hydrophobic membrane proteins or of proteins that are too basic/acidic or too large/small is a well-known limit of 2-DE. The high protein amount required, the long time needed to run the samples, and the difficulty in automating the whole system are additional potential drawbacks of these techniques. The advent of LC-based procedures, characterized by unquestionable advantages, seemed to mark the fate of electrokinetic methods in the proteomic area. Being a bit of years elapsed, it can be argued that, despite the strong competition with LC, gel-based techniques do not appear to have lost this "struggle" yet [14–17]. Electrokinetic approaches, in fact, not only maintain their position but also still possess numerous characteristics currently unmatched by other proteomic methodologies. 2-DE approaches in fact remain the conventional procedure applied to the differential (control *vs.* diseased case) analysis of biological samples [18–24].

2. Outline of the chapter

The aim of this chapter is to illustrate the potential of electrokinetic procedures to the investigation of a variety of acute and chronic lung disorders. Why focus on pulmonary disorders? First, because lung diseases, which involve tens of million people, are some of the most common medical conditions in the world. Second, while few proteomic studies had been specifically designed to address this topic in the past, the depth of analysis ultimately reached by current procedures provides a new and larger context for future studies on the biology of these pathologies. This has allowed for the generation of protein profiles that are useful for exploring protein-based pathological mechanisms and/or discovering new potential therapeutic targets for a variety of pulmonary disorders.

Each paragraph of this chapter will address the proteomic data relative to a specific lung disease. Given that proteomic studies on pulmonary disorders have been carried out mostly on biofluids, the chapter will focus on the protein profiles obtained from serum/plasma, bronchoalveolar

lavage fluid, exhaled breath condensate, sputum and urine of individuals with asthma, interstitial lung disease (ILD), cystic fibrosis (CF), chronic obstructive pulmonary disease (COPD), and other "minor" pathologies. Since different fluids may serve as a rich source of information for the same disorder, specific subsections inside each paragraph have been dedicated to the presentation of the proteomic results relative to a peculiar fluid.

Given the hugeness of the subject, proteomics of lung cancer has thoroughly been investigated and greatly acknowledged elsewhere. In keeping with this large deal of literature, this topic would require a chapter dedicated, and it was intentionally left out of this chapter.

3. Principles of electrokinetic procedures

Since electrokinetic approaches play a pivotal role throughout the whole chapter, a few details about the principles of techniques cited in the following paragraphs will be given here. The term "electrokinetics" refers to the motion of charged particles by an applied electrical field. The standard laboratory technique by which charged molecules migrate through a porous matrix which

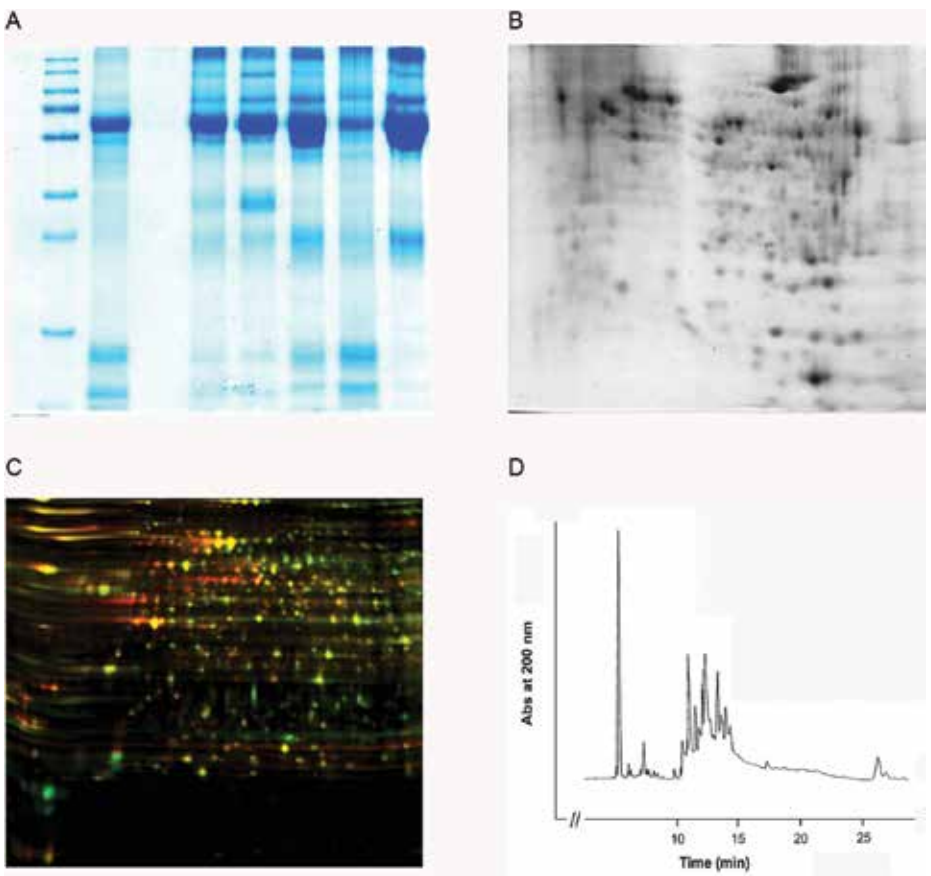

Figure 1. Representative examples of 1-DE, 2-DE, 2D-DIGE, and CE: panels A, B, C, and D, respectively (unpublished results from our laboratory).

behaves like a molecular sieve is electrophoresis. Polyacrylamide is an ideal support for separating most proteins; under denaturing/reducing conditions and with a discontinuous buffer system, one-dimensional sodium dodecyl sulfate polyacrylamide gel electrophoresis (SDS-PAGE) or 1-DE is the most widely used electrophoretic technique separating proteins primarily by mass. When the ionic detergent SDS binds to proteins, they assume a uniform negative charge. Upon application of a current, all SDS-bound proteins in the sample will migrate toward the positive electrode, and, because of the sieving effect of the gel matrix, proteins with less mass split from those with greater mass because they travel more quickly. When the mixture of proteins is very complex, higher resolution may be obtained by applying a two-dimensional (2-DE) procedure which separates proteins according to their isoelectric point in the first dimension followed by an orthogonal separation via SDS-PAGE in the second one. Similar to 2-DE is two-dimensional difference gel electrophoresis (2D-DIGE) in which, however, two or more samples are labeled with different fluorescent dyes and separated on the same gel, thus eliminating gel-to-gel variability. An instrumental evolution of the abovementioned electrophoretic techniques is capillary electrophoresis (CE) in which separation occurs in fused-silica capillaries and separation of proteins involves application of high voltages across buffer-filled capillaries. Once separated by electrophoresis, gel bands/spots are excised and proteins extracted for analysis by mass spectrometry.

Representative examples of 1-DE, 2-DE, 2D-DIGE, and CE are shown in **Figure 1** (panels A, B, C, and D, respectively).

4. Asthma

Asthma is an airway disease originating from complex interactions between genetic factors and environmental agents. It affects over 300 million people around the world and is characterized by airflow limitation resulting in shortness of breath. Bronchial obstruction is extremely variable and often reversible in asthma. Being a global health problem, tools which allow its early diagnosis, monitoring, and follow-up would offer great advantages for a better insight into its physiopathology. The articles discussed in the following sections prove that the proteomic content of sputum/induced sputum and BALf may allow for the identification of specific biomarkers in asthma.

4.1. Sputum/induced sputum

2-DE coupled to MALDI/TOF allowed Lee et al. [25] to compare the proteomic profiles of sputum from patients with neutrophilic-type uncontrolled asthma (UA) and from patients with neutrophilic controlled asthma (CA). It could be observed that, while a few proteins (including calgranulin S100A9) were overexpressed in sputum of UA patients, others, associated with inflammation, anti-inflammation, enzymatic activity, and immunity signaling, were downregulated. Differences in protein abundance and composition between asthma and rhinitis were revealed by the proteomic approach (2D-DIGE and MS) applied by Suojalehto et al. [26] to induced sputum (IS) and nasal lavage fluid (NLF) of patients. Their findings showed that (i) fatty acid-binding protein 5 (FABP5) was upregulated in IS of asthmatics, (ii) vascular endothelial growth factor (VEGF) was increased in NLF of asthmatics, and (iii) in NLF of these subjects,

FABP5 and VEGF were positively correlated with cysteinyl leukotriene (CysLT). Based on their results, the authors hypothesized that, in asthma, FABP5 may contribute to the airway remodeling and inflammation by regulating the levels of CysLTs which, in turn, induce VEGF production.

4.2. Bronchoalveolar lavage fluid

A differential study on BALf of asthmatic individuals was performed by Wu et al. [27] who produced the first comprehensive database of BALf proteins. Abundant proteins were depleted by immunoaffinity chromatography, and all others were separated by 1-DE and identified by nano-LC-MS/MS. Chemokines and cytokines and a variety of matrix metalloproteases (MMPs) were upregulated in subjects after segmental allergen challenge. Other highly overexpressed proteins included pulmonary surfactants and LPLUNC1.

5. Interstitial lung disease

Interstitial lung disease (ILD) describes a collection of more than 200 lung disorders that involve inflammation and fibrosis of the alveoli, distal airways, and septal interstitium of the lungs. Typically, ILD presents with progressive breathlessness, lung crackles, and a diffusely abnormal chest radiograph. This disorder can be caused by long-term exposure to hazardous materials or by some types of autoimmune diseases, such as rheumatoid arthritis. In some cases, however, the etiology remains unknown. The following sections summarize the latest proteomic studies aimed at clarifying the pathophysiological mechanisms involved in the development and progression of ILD. All recent proteomic studies in this area based on electrokinetic approaches have been performed on BALf.

5.1. Idiopathic pulmonary fibrosis

Idiopathic pulmonary fibrosis (IPF) is a progressive fibroproliferative disorder characterized by continuous production of extracellular matrix that alters parenchymal lung structure and effective gas exchange. Cigarette smoking, exposure to agriculture and farming, livestock, wood and metal dust, stone, and silica have been associated with significantly increased risk of IPF. The etiopathogenesis of the disease is not completely understood, and the prognosis is very poor. In light of this, proteomic studies aimed at the discovery of molecules involved in triggering and progression of this disorder could help to a better understanding of its physiopathology. As expected, all proteomic approaches to study this disorder which involved the use of an electrokinetic procedure have been performed on BALf.

Kim et al. [28] compared by 2-DE and nano-LC-MS/MS the proteomes of BALf from patients affected by IPF and healthy subjects. An increase of haptoglobin and a decrease of α1-antitrypsin, α1-antichymotrypsin, macrophage capping protein, angiotensinogen, hemoglobin chain B, apolipoprotein (Apo A-I), clusterin, protein disulfide isomerase A3, immunoglobulin, and complement C4A were observed in IPF subjects. That a local treatment with Apo A-I could be effective against the development of experimental lung fibrosis was shown in mice. The main goal of the study performed by Ishikawa and colleagues [29] was to discover

new markers for both IPF and chronic obstructive pulmonary disease (COPD). By comparing the 1-DE and 2-DE profiles of BALf and IS of IPF and COPD patients with those of controls, they showed a reduction in the levels of hemoglobin α (Hbα) and hemoglobin β (Hbβ) monomers and complexes only in IPF patients. Furthermore, MS analyses revealed that a modification at Cys 105 (most likely the site involved in complex formation) of Hbα was responsible for the lack of the Hbα complexes formation in IPF patients. 2-DE, MS, Western blotting, and ELISA were applied by Ohlmeier et al. [30] to lung tissues and BALf of IPF, COPD, and alpha-1 antitrypsin-deficient (AATD) patients with the aim to investigate the different receptors for advanced glycation end product (RAGE) isoforms. Their analyses revealed a decrease of the full-length RAGE (FL-RAGE) and its C-terminal processed variant (cRAGE) in the lung tissues of IPF and COPD patients but not in AATD. The endogenous secretory RAGE (esRAGE) level was reduced in IPF but remained unchanged in COPD. The 2-DE proteomic study by Hara et al. [31] aimed at searching for BALf biomarkers allowing to distinguish IPF from other fibrotic interstitial pneumonias. Their study showed that S100A9 protein (or calgranulin B, a member of the calcium-binding S100 protein family) was upregulated in IPF patients compared to patients with other fibrotic interstitial diseases and healthy controls. Based on these findings, S100A9 was thought to be a good candidate biomarker to discriminate IPF from other fibrotic interstitial pneumonias. The research group by Landi et al. [32] used the electrokinetic approach to compare the proteome of BALf from patients affected by four interstitial lung diseases (sarcoidosis, idiopathic pulmonary fibrosis, pulmonary Langerhans cell histiocytosis, fibrosis associated to systemic sclerosis) with that of controls (smokers and nonsmokers). The proteins they identified (i.e., plastin 2, annexin A3, 14-3-3ε, and S10A6) could be directly or indirectly related to the pathophysiology of the different interstitial lung diseases. The same research group compared the profile of BALf proteins from IPF patients, never-smokers, and smokers to understand which protein(s) could be potentially related to disease progression and pathogenesis. Their findings showed that angiotensin system maturation, renin angiotensin-aldosterone system, heme metabolism, coagulation system, response to hypoxia, oxidative stress, and iron transport were the metabolic pathways involved in disorder [33]. The same group also investigated the molecular patterns and their variability in familial and sporadic IPF patients through a differential proteomic analysis based on 2-DE and MS [34]. It was observed that, while in familial IPF, the upregulated proteins were those involved in wounding and immune responses, coagulation system, and ion homeostasis, and those involved in the oxidative stress response were upregulated in sporadic IPF.

5.2. Sarcoidosis

Sarcoidosis is a multisystem disorder characterized by the formation of epithelioid cell granulomas. Even though lungs, lymph nodes, and eyes are most commonly involved, any organ or system of the body can be affected. Patients with genetic susceptibility undergoing persistent exposure to unknown inhaled antigens may develop an excessive immune response mediated by antigen-presenting cells (APC) that can trigger the pathological mechanisms of the disease. However, its etiology still remains an enigma and a challenge for researchers and clinicians due to its unknown, variegated, and unpredictable presentation. The recent state of the art relative to the application of proteomic studies aimed at gaining insights into the mechanisms of the disease is reported in this section.

Silva et al. [35] have used a 2D-based proteomic approach to analyze BALf of patients affected by sarcoidosis and chronic beryllium disease (CBD) with the aim of comparing the protein profiles at the site of active inflammation. Briefly, the differentially expressed proteins were highlighted by 2D-DIGE and identified by MALDI-TOF. In accordance with the ongoing chronic inflammation response in lungs of these patients, most of these proteins were immune-related proteins.

While being a well-known risk factor for the development of various interstitial lung diseases, smoking is generally not related to the occurrence of sarcoidosis. To evaluate better the influence of cigarette smoking on the proteome of BALf from sarcoidosis patients and to study the pathogenetic mechanism of the disease, Landi et al. [36] investigated by 2-DE the protein profile and network of BALf from sarcoidosis patients, smokers (SC), and nonsmokers (NSC) used as controls. MALDI-TOF MS revealed that 34 spots contained unique proteins involved in lipid, mineral, and vitamin D metabolism and immune regulation of macrophage function. These findings confirmed that, differently from other ILDs, the expression profile of proteins from sarcoidosis patients was more comparable to that of NSC than of SC.

5.3. Lung fibrosis associated with systemic sclerosis

Systemic sclerosis (SSc) is a disease of unknown origin characterized by increased deposition of collagen and other extracellular matrix proteins in skin and multiple internal organs. About 70% of SSc patients develop a severe and progressive lung fibrosis, ILD being the main cause of mortality. Nevertheless, the mechanisms involved in the onset and progression of fibrosis remains unknown. To clarify the causative role of ILD in SSc, Shirahama et al. [37] analyzed the protein profiles of BALf from patients affected by SSc with and without pulmonary fibrosis (SSc-fib+ and SSc-fib−). 2-DE combined with MALDI-TOF MS was the method of choice. The authors showed that, among other proteins identified, α2-macroglobulin, α1-antitrypsin, and pulmonary surfactant protein A were upregulated in SSc-fib+ patients, while α2 heat shock protein (HSP) and glutathione S-transferase (GST) were downregulated in the same patients compared to SSc-fib ones. These results suggested that these proteins could be potentially involved in the development of ILD in SSc patients.

5.4. Rheumatoid arthritis-associated lung disease

Rheumatoid arthritis (RA) is a systemic autoimmune disease affecting 0.5–1.0% of the adult population worldwide. Rheumatoid arthritis-associated interstitial lung disease (RA-ILD) occurs in 10–30% of RA patients and is associated with increased mortality in up to 10% of RA patients. The pathogenetic mechanisms of RA-ILD are still unknown. The most common pulmonary patterns in RA-ILD are usual interstitial pneumonia (UIP) and nonspecific interstitial pneumonia (NSIP). Nevertheless, the less common organizing pneumonia (OP) and lymphocytic interstitial pneumonia are not as rare as hypothesized. The proteomic profiles of UIP and OP were compared by Suhara et al. [38] by analyzing BALf of patients with 2-DE and nano-LC-ESI-MS/MS. The levels of the fragmented proteins gelsolin and Ig kappa chain C region were found to be significantly higher in UIP patients compared to those with an OP pattern. Conversely, the levels of α1-antitrypsin, C-reactive protein (CRP), haptoglobin β, and surfactant protein A (isoform 5) were significantly higher in the OP than in the UIP patterns.

Based on these considerations, the hypotheses were made that (i) identified proteins may play a role in the onset and progression of UIP and OP and (ii) fragmented gelsolins may contribute to the development of pulmonary fibrosis.

5.5. Pulmonary Langerhans cell histiocytosis

Pulmonary Langerhans cell histiocytosis (PLCH) is a rare interstitial lung disease associated with the exposure to tobacco smoke. To provide new insights into its pathogenesis and to compare this disorder with COPD, Ghafouri et al. [39] analyzed BALf from a biopsy-proven case of PLCH, a COPD patient, and a healthy control. Proteins were separated by 2-DE, and their patterns were analyzed with a computerized 2-DE imaging system. If compared with the profiles of the COPD patient and the healthy control, that of PLHC patient lacked significant amounts of protective and anti-inflammatory proteins. These findings opened a new route for a better understanding of the pathophysiology of PLCH.

6. Cystic fibrosis

Cystic fibrosis (CF) is an autosomal recessive monogenic disease caused by mutations in the gene coding for the CF transmembrane conductance regulator (CFTR) protein. The main clinical features of this disorder are progressive bronchiectasis and pancreatic exocrine insufficiency. Since airway inflammation and recurrent infections leading to respiratory failure represent the major causes of morbidity and mortality among CF patients, clinical research is mainly focused on these topics. The characterization of proteins from different sources and the study of their interactions within the lung microenvironment may be useful tools toward the identification of biomarkers for the diagnosis/prognosis of this disorder. The following subsections show recent reports on proteomic research in this field.

6.1. Induced sputum

The proteomic approach based on 1-DE, MALDI-TOF-MS, and LC-ESI-MS/MS allowed Schulz et al. [40] to analyze high molecular mass proteins in induced sputum from (i) CF adults with and without acute exacerbation, (ii) CF children with stable disease and preserved lung function, and (iii) healthy adults and children (controls). The main high molecular mass proteins in sputum from all subjects investigated were MUC5B and MUC5AC, two mucins that, in exacerbated CF adults, seemed degraded and also showed increased sialylation and reduced sulfation/fucosylation. In addition, while two CF children showed mucin profiles similar to those of exacerbated CF adults, the remaining CF children had profiles comparable to those of healthy controls. Based on these observations, the authors suggested that the processes of mucin glycosylation and degradation may be considered as predictive biomarkers of lung condition in CF patients.

6.2. Serum

Charro et al. [41] worked on immunodepleted sera of CF patients and of healthy CF and non-CF carriers. The combination of 2D-PAGE and shotgun LC-MS/MS showed that members of the apolipoproteins family were deregulated in CF patients, while heat shock 70 kDa protein 5

and the multifunctional enzyme NDKB (an ion sensor in epithelial cells, pancreatic secretion, neutrophil-mediated inflammation, and energy production) were identified exclusively in the CF group. This interesting comparative study allowed the authors to identify deregulated proteins involved in tissue remodeling, complement system dysfunction with consequent impairment on defense mechanisms and chronic inflammation, nutritional imbalance, and colonization by *P. aeruginosa*.

7. Chronic obstructive pulmonary disease

Chronic obstructive pulmonary disease (COPD) is an "umbrella" term that combines different pathological conditions such as emphysema, chronic bronchitis, nonreversible asthma, and some types of bronchiectasis characterized by irreversible airflow limitations. Its clinical features are a general progressive airflow limitation, destruction of the lung parenchyma, and/or local fibrosis. Even though the main cause of the disorder is cigarette smoking, continuous inhalation of toxic gases and particles which promotes chronic airway inflammation may contribute to its development. COPD can also be determined by genetic factors, i.e., the deficiency of α-1 antitrypsin (AATD).

The following subsections describe electrokinetic-based proteomic studies aimed at elucidating the mechanism underlying the pathobiology of the disease.

7.1. Plasma

To shed new light on the molecular mechanisms of COPD, Merali et al. [42] investigated the plasma proteome of 10 COPD patients and 10 healthy controls. Briefly, abundant proteins in pooled plasma from each group were immunodepleted; samples were then fractionated by 1-DE prior to ESI-MS/MS. A few proteins including acute-phase response proteins, CRP, fibrinogen, coagulation factors, and adhesion molecules were upregulated in COPD patients compared to controls. By contrast, molecules involved in protease-induced lung tissue injury and repair were downregulated.

7.2. Induced sputum

In a proteomic study aimed at identifying proteins involved in COPD pathogenesis, Ohlmeier et al. [43] analyzed induced sputum of nonsmokers, smokers, and smokers with moderate COPD by cysteine-specific 2D-DIGE coupled with MS. Among other candidates, polymeric immunoglobulin receptor (PIGR), a protein involved in specific immune defense and inflammation, appeared upregulated in smokers and subjects with COPD, thus suggesting its possible role in the regulation of inflammation during COPD pathogenesis.

7.3. Bronchoalveolar lavage fluid

The application of 2-DE followed by LC-MS/MS allowed Plymoth et al. [44] to investigate the global proteome of BALf from 29 light and heavy smokers and 18 never-smokers in 6–7 years of follow-up study. During this study 7 of the 29 smokers developed moderate COPD.

The authors observed that, although protein components were variably expressed in individuals, inflammatory and redox proteins were unambiguously upregulated in smokers compared to never-smokers.

To elucidate putative molecular mechanisms underlying gender-based differences in the pathophysiology of COPD, Kohler et al. [45] applied 2D-DIGE coupled to nano-LC-MS to investigate the proteome of non-symptomatic smokers and smokers with COPD. The authors observed significant gender differences with a subset of 19 proteins providing a highly predictive model for classification of female non-symptomatic smokers from female smokers with COPD. Subsequent pathway analyses correlated the observed alterations to downregulation of the lysosomal pathway and upregulation of the oxidative phosphorylation pathway. No altered proteins were found in the corresponding male classification model.

An interesting research (based on 2-DE and MALDI-TOF/TOF) by Pastor et al. [46, 47] evidenced a distinct proteomic reactive oxygen species (ROS) protein signature in BALf from COPD and lung cancer patients. Their findings highlight the role of ROS proteins in the pathogenic pathways of both diseases and provide new candidate biomarkers and predictive tools for lung cancer and COPD diagnosis.

8. Other pulmonary disorders

8.1. Idiopathic pulmonary arterial hypertension

Idiopathic pulmonary arterial hypertension (IPAH) is a rare, life-threatening disorder clinically characterized by sustained elevations of pulmonary artery pressure (PAP). Together with intimal proliferation, in situ thrombi, deposition of extracellular matrix, and inflammation, the remodeling of the pulmonary arterial vasculature with medial and adventitial thickening of the arteries and arterioles is the main feature of IPAH. This leads to increased pulmonary vascular resistance, right heart failure, and death. The latest proteomic studies aimed at providing insights into the molecular mechanisms underlying IPAH are presented in this section. All recent proteomic studies based on the use of an electrokinetic approach have been performed on serum/plasma.

The first proteomic approach aimed at identifying protein changes in serum from IPAH patients was performed by Yu et al. [48] by using a combination of 2-DE and MS. The attention of the authors was focused on α-1 antitrypsin and vitronectin that, being downregulated in IPAH patients, were indicated as proteins involved in the development of the disorder. In fact, while the decrease of plasma vitronectin might favor platelet aggregation and thrombus formation, the decrease of α-1 antitrypsin might induce apoptosis of endothelial cells resulting in proliferation of apoptosis-resistant endothelial cell arteriolar occlusion. 2-DE and immunoblotting were the combination applied by Terrier et al. [49] to identify the target antigens of antifibroblast antibodies (AFAs) in patients affected by IPAH. Among the 21 protein spots specifically recognized by serum IgG antibodies from IPAH patients, 16 proteins involved in (i) regulation of cytoskeletal function, (ii) cell contraction, (iii) oxidative stress, (iv) cell energy metabolism, and (v) other key cellular pathways were identified.

The comparative proteomic analysis based on 2-DE and MALDI-TOF performed by Zhang et al. [50] on serum of IPAH patients and controls identified, among other proteins showing significant changes, leucine-rich α-2-glycoprotein (LRG) as a possible specific prognostic biomarker of IPAH. 2D-DIGE coupled to MALDI-TOF-MS was used by Yeager et al. [51] to investigate the plasma proteome of IPAH children with good and poor outcome to long-term vasodilator therapy. Before and after therapy, serum amyloid A (SAA-4) was found to be fourfold lower in patients with good outcome compared to those with poor outcome, while serum amyloid P (SAP) was 1.3-fold lower prior to therapy in patients with good outcome. Since these proteins regulate circulating mononuclear phagocytes, they may contribute to the differential response to chronic vasodilator therapy.

8.2. Pulmonary embolism

Pulmonary emboli usually arise from thrombi originating in the deep venous system of the lower extremities that travel to the lung and can lodge at the bifurcation of the main pulmonary artery or the lobar causing hemodynamic compromise. Mortality rates in patients with acute pulmonary embolism (PE) vary from 1.4 to 17.4% during the first 3 months of treatment. The causes of most early deaths are complications such as acute pulmonary arterial hypertension and right heart failure, whereas medical problems underlying PE are responsible for most late deaths. The subsections reported below describe the recent advances in PE proteomics.

8.2.1. Plasma

To identify biomarkers useful for the risk stratification in patients with acute symptomatic PE, Insenser et al. [52] studied the plasma proteome of PE patients with low, intermediate, and high risk. 2D-DIGE was used to compare the abundance of plasma proteins in the three cohorts, and candidate protein markers were identified by MALDI-TOF. Differences among patients with different PE severities were observed in a panel of four biomarkers (haptoglobin, hemopexin, α2-macroglobulin, and Ig α-1-chain C region) involved in iron metabolism pathways and acute-phase response. Among them, the reduced concentrations of haptoglobin could be considered an accurate signal for the biochemical detection of high-risk PE.

8.2.2. Urine

A proteomic approach based on capillary electrophoresis coupled to mass spectrometry (CE-MS) was applied by von zur Mühlen et al. [53] for noninvasive identification of PE specific urinary markers of pathophysiological relevance. The analysis of urine from patients with symptoms associated with deep vein thrombosis and pulmonary embolism (DVT + PE) allowed the authors to identify 62 urinary peptides, i.e., fragments of type I collagen and a fragment of fibrinogen β-chain, whose presence in organized and acute thrombus has been demonstrated by the authors using immunohistochemistry.

Compared to asthma, interstitial lung disease, cystic fibrosis, and COPD, fewer articles have been published for "minor" diseases including acute respiratory distress syndrome (ARDS), high-altitude pulmonary edema (HAPE), and invasive pulmonary aspergillosis (IPA). This is, in large part, due to the lower prevalence of these disorders which results in difficulties

recruiting cohorts of patients whose size allows detection of statistically significant data. Nevertheless, Chang et al. [54] and Sixt et al. [55] investigated the proteomics of ARDS; proteomic data on HAPE have been published by Ahmad et al. [56, 57] and by Yang et al. [58], and preliminary data on IPA have been produced by Brasier et al. [59].

9. Tuberculosis

With more than 10.4 million new cases and about 1.8 million deaths each year, tuberculosis (TB) still remains an urgent global health problem. Being all deaths mainly due to the increasing spread of *Mycobacterium tuberculosis* drug-resistant strains, early diagnosis and treatment of infection would be essential for the prevention. However, routine laboratory tests for drug-resistant TB with sufficient sensitivity and specificity are still not available. This is the rationale for the development of electrophoretic-based proteomic approaches aimed at identifying host TB-associated proteins or antigens useful for the serodiagnosis of drug-resistant *M. tuberculosis* strains. To better understand and monitor the disease process, Tanaka et al. [60] analyzed whole blood supernatants from TB patients by 2D-DIGE followed by MS. Among others, the authors observed that retinol-binding protein 4 (RBP4) and fetuin-A were significantly lowered in patients with active TB compared to controls, thus suggesting that they could be considered potential biomarkers for monitoring the course of the disease during clinical treatment.

Method	Advantages/disadvantages	Lung disease	Matrix	Ref. no.
1-DE	—Allows separation of all types of proteins, even those insoluble in water	Asthma	BALf	[27]
	—Overlapping of closely spaced bands leading to limited resolution	IPF	BALf/IS	[29]
	—Often needs the coupling of another detection technique, i.e., immunoblotting or MS	CF	IS	[40]
		COPD	Plasma	[29, 42]
2-DE	—Good resolution of protein mixtures	Asthma	IS	[25]
	—Allows discernment of posttranslational modifications	IPF	BALf	[29–34]
	—Comparison of multiple gels facilitated by image analysis software	Sarcoidosis	BALf	[32, 35–36]
	—Unable to resolve low molecular weight proteins (<10 kDa)	Lung fibrosis associated to SSc	BALf	[32, 37]
	—Presence of high-abundance protein (i.e., albumin, immunoglobulin) hiding low-abundance proteins	RA-ILD	BALf	[38]
		PLCH	BALf	[32, 39]
	—Final identification requires spot removal from gels, digestion, and peptide analysis by MS	CF	Serum	[41]
	—Low throughput	COPD	BALf	[29, 30, 44, 46, 47]
		IPAH	Serum	[48–50]
		TB	Serum	[61]

Method	Advantages/disadvantages	Lung disease	Matrix	Ref. no.
2D-DIGE	—Very sensitive	Asthma	Sputum/NLF	[26]
	—Ratio of protein expression can be obtained in a single gel	COPD	IS	[43]
			BALf	[45]
	—An internal standard can be introduced in each gel reducing gel-to-gel variation	IPAH	Serum	[51]
	—Presence of high-abundance protein (i.e., albumin, immunoglobulin) hiding low-abundance proteins	PE	Plasma	[52]
	—Unable to resolve low molecular weight proteins (<10 kDa)	TB	Serum	[60]
	—Low throughput			
	—Final identification requires spot removal from gels, digestion, and peptide analysis by MS			
CE	—Less expensive than LC-MS	PE	Urine	[53]
	—Very small volumes of samples injected (nL)			
	—Detection of basic and hydrophilic peptides			
	—Fast separation			
	—Limited loading capacity			
	—Unavailability of an integrated system as a marketed solution			

Table 1. List of proteomic approaches considered in this report together with their advantages/disadvantages, the type of pulmonary disorder, the matrix considered, and the original article of reference.

Using an immune-proteomic approach based on 2-DE coupled to MALDI-TOF/TOF, Zhang et al. [61] analyzed serum from healthy controls and patients infected with drug-resistant or drug-susceptible *M. tuberculosis* strains. By comparing the immune-reactive proteins, the authors identified antigens present only in drug-resistant strains. Among the identified immune-reactive proteins, Rv2031c, Rv3692, and Rv0444c had the greater antigenic activity. This feature made them possible candidate biomarkers for the serum diagnosis of drug-resistant TB.

The list of proteomic approaches considered in this report, together with their advantages/disadvantages, the type of pulmonary disorder, the matrix considered, and the original article of reference, is shown in **Table 1**.

10. General considerations

Although the characterization of the full proteome is still challenging, the recent technological innovations have improved our ability to obtain cross-sectional time and space snapshots of protein levels that reflect observed phenotypes more closely than those of genomic techniques. The current successes in the use of proteomic approaches to understand disease and enable drug development resulted in optimism that many more effective diagnostic tests

and treatments tailored to genetic, environmental, and lifestyle factors of individuals will be developed. Showing a great ability in providing reference data for the identification of groups of individuals who share various attributes, these approaches have opened new opportunities for the discovery of potential diagnostic/prognostic protein biomarkers in several pulmonary disorders. By helping researchers in understanding the pathogenesis of respiratory diseases and improve patient care, the recent findings have indeed progressively increased the interest for the application of proteomics in clinical practice. The current chapter was designed to keep the reader informed about the present status of pulmonary proteome. Taken together, the results documented here demonstrate that, after a decade of activity, proteomics of pulmonary diseases is catching up with its promise. The constantly growing number of reports in this area supports the view of this approach as one of the decisive methodological tools for the identification/characterization of disease-associated proteins. In terms of experimental procedures, the basic options available for proteomic investigations consist in the identification of proteins through the use of gel-based or gel-free techniques followed by MS. Undoubtedly, the striking improvement in technologies related to accuracy, when coupled to quantitative approaches, has a great impact on the quality of the results. Obviously, the question arises of whether sophisticated technologies (such as the non-gel-based proteomic procedures) may actually be more fruitful, in terms of candidate protein marker identification, than "conventional" (read electrokinetic) approaches. In light of the versatility and high degree of reproducibility shown by these new potent strategies, a positive answer is perhaps not surprising, at least for one reason. The very high number of peptides identified and quantified results in a higher accuracy, which translates into improved alignment and quantification across spectra. Nevertheless, as documented in this chapter, despite being less sophisticated than competing ones, gel-based techniques still represent a widely used procedure able to generate a reliable protein "fingerprint." Though it may seem nonsense, it is precisely the "limited" amount of information produced by electrokinetic approaches that may result in an easy interpretation of data. The possibility to compare a sample in physiological and pathological conditions allows, in fact, immediate detection of possible relevant changes in protein expression which differentiate the two conditions. These changes are essential in demonstrating progression from health to disease and understanding the relationship between function and modification. The wide spectrum of examples presented in this chapter confirms that the application of 1-DE/2-DE/2-DIGE/CE (followed by MS) to a variety of biological fluids from individuals with different respiratory diseases may result in the production of data with clinical relevance which allow a better understanding of the molecular basis of the disorder investigated. However, as it can be observed from the data presented in this chapter, while peculiar proteins are pointed out as potential biomarkers of specific disorders, a good number of proteins is implicated across a variety of different diseases. This makes the notion of a single biomarker to indicate a specific disease more difficult. For example, while α2-macroglobulin and surfactant protein A have been indicated as candidate biomarkers of both lung fibrosis associated with systemic sclerosis and asthma [27, 37], the former protein (together with other proteins) was suggested to be also a potential biomarker of pulmonary embolism [52]. Indeed, for greater confidence in disease diagnosis or prognosis, a suite of biomarkers would provide more specificity than a single one. In other words, should the identification of hundreds of candidate biomarkers come at the

price of sacrificing their specificity? This discrepancy, however, is only apparent and may be reconciled with a harmonization of results. In fact, given that a single molecule can hardly discriminate complex processes without context, the finding of common signatures for several pulmonary disorders contributes to drawing intriguing parallels among them. This obviously results in a better understanding of the disease mechanism. On the other hand, the fact that several proteins found (e.g., in COPD) have not been reported in other chronic lung diseases suggests that the merits of proteomics in hunting down biomarkers with high specificity cannot be under-evaluated. In this context, the finding of significantly altered levels of cathepsin B, ATP synthase, and chaperonin in the BALf of female COPD patients, but not in that of males, while supporting the hypothesis that these proteins were the most prominent marker candidates for this gender only, confirmed the abovementioned merits of proteomics [45]. Proteomic studies have also discovered panels/clusters of oxidant/antioxidant enzymes that may be utilized for the assessment of disease severity [44]. Overproduction of ROS can also cause oxidative modifications of several important antioxidant/defense enzymes, which may be associated with alterations in enzyme conformation, and thus they can function as markers of the degree of oxidative stress present in the airways [46, 47]. The huge amount of experimental data generated in some cases (i.e., COPD and asthma) represent the first attempts to identify the principal pathways involved in the pathogenesis and already allow interesting candidate biomarkers to emerge [26, 43].

As the goal of the authors is to offer a broad picture of the subject, readers interested in learning more about specific techniques or their application to pulmonary diseases are encouraged to refer to excellent review articles in this field which show the merits of proteomic techniques in producing qualitative and quantitative information on the protein patterns of a variety of human fluids/tissues [62–65]. Taken together, these articles represent a good resource which describes in depth the status of electrokinetic (and chromatographic) proteomic methods and provide a comprehensive picture of proteomics of pulmonary disorders to date.

11. Conclusions

Aside from the interest in deciphering the function of individual proteins, the set of data produced by proteomic methods represent the starting point for studying large-scale interactions that serve to discover general important properties for interaction participation. The fact that highly interactive proteins are often well conserved and/or essential or that homologous proteins, and, in particular, proteins with domains from the same family, tend to interact more frequently than others will likely improve the knowledge of their intrinsic properties. Thus, the understanding of the role these proteins play in the pathogenesis of respiratory diseases, while opening the door to much more powerful protein diagnostics, reinforces the linkage between basic medical research and clinical laboratory medicine. Addressing these concerns is obviously a top priority for the field, the ultimate goal of researchers being to understand the biology of disease and to translate this knowledge into the clinic.

There is no doubt that this branch of respiratory proteomics will have substantial improvement in the future.

Acknowledgements

The authors would like to acknowledge Maurizio Luisetti, MD, a dear friend who was a medical director at the Clinic of Respiratory Diseases, IRCCS Policlinico San Matteo (Pavia, Italy) for 20 years. He passed away on Monday, Oct. 20, 2014 at age 61. Besides his outstanding competence, Maurizio was a person with extraordinary humanity and commitment toward his patients and coworkers with whom he was always friendly and ready to help and cooperate. Thank you, Maurizio, for all you have done and all you have given us in these years. You are still sadly missed.

Conflict of interest

The authors declare no conflict of interest.

Author details

Simona Viglio[1], Maddalena Cagnone[1], Laurent Chiarelli[2], Roberta Salvini[1] and Paolo Iadarola[2]*

*Address all correspondence to: piadarol@unipv.it

1 Department of Molecular Medicine, Biochemistry Unit, University of Pavia, Pavia, Italy

2 Department of Biology and Biotechnologies "L.Spallanzani," University of Pavia, Pavia, Italy

References

[1] Drake RR, Cazare LH, Semmes OJ, Wadsworth JT. Serum, salivary and tissue proteomics for discovery of biomarkers for head and neck cancers. Expert Review of Molecular Diagnostics. 2005;**5**:93-100. DOI: 10.1586/14737159.5.1.93

[2] Morita A, Miyagi E, Yasumitsu H, Kawasaki H, Hirano H, Hirahara F. Proteomic search for potential diagnostic markers and therapeutic targets for ovarian clear cell adenocarcinoma. Proteomics. 2006;**6**:5880-5890. DOI: 10.1002/pmic.200500708

[3] Casado B, Iadarola P, Pannell LK, Luisetti M, Corsico A, Ansaldo E, Ferrarotti I, Boschetto P, Baraniuk JN. Protein expression in sputum of smokers and chronic obstructive pulmonary disease patients: A pilot study by CapLC-ESI-Q-TOF. Journal of Proteome Research. 2007;**6**:4615-4623. DOI: 10.1021/pr070440q

[4] Zhou JY, Hanfelt J, Peng J. Clinical proteomics in neurodegenerative diseases. Proteomics Clinical Applications. 2007;**1**:1342-1350. DOI: 10.1002/prca.200700378

[5] Kentsis A, Monigatti F, Dorff K, Campagne F, Bachur R, Steen H. Urine proteomics for profiling of human disease using high accuracy mass spectrometry. Proteomics Clinical Applications. 2009;**3**:1052-1061. DOI: 10.1002/prca.200900008

[6] Bloemen K, van den Heuvel R, Govarts E, Hooyberghs J, Nelen V, Witters E, Desager K, Schoeters G. A new approach to study exhaled proteins as potential biomarkers for asthma. Clinical and Experimental Allergy. 2011;**41**:346-356. DOI: 10.1111/j.1365-2222.2010.03638.x

[7] Whelan SA, He J, Lu M, Souda P, Saxton RE, Faull KF, Whitelegge JP, Chang HR. Mass spectrometry (LC-MS/MS) identified proteomic biosignatures of breast cancer in proximal fluid. Journal of Proteome Research. 2012;**11**:5034-5045. DOI: 10.1021/pr300606e

[8] Fumagalli M, Ferrari F, Luisetti M, Stolk J, Hiemstra PS, Capuano D, Viglio S, Fregonese L, Cerveri I, Corana F, Tinelli C, Iadarola P. Profiling the proteome of exhaled breath condensate in healthy smokers and COPD patients by LC-MS/MS. International Journal of Molecular Sciences. 2012;**13**:13894-13910. DOI: 10.3390/ijms131113894

[9] Dias GS, Oliveira JL, Vicente J, Martin-Sanchez F. Integrating medical and genomic data: A successful example for rare diseases. Studies in Health Technology and Informatics. 2006;**124**:125-130

[10] Vilasi A, Capasso G. Proteomics and tubulopathies. Journal of Nephrology. 2010;**23**:221-227

[11] Qualtieri A, Urso E, Le Pera M, Sprovieri T, Bossio S, Gambardella A, Quattrone A. Proteomic profiling of cerebrospinal fluid in Creutzfeldt-Jakob disease. Expert Review of Proteomics. 2010;**7**:907-917. DOI: 10.1586/epr.10.80

[12] Caubet C, Lacroix C, Decramer S, Drube J, Ehrich JH, Mischak H, Bascands JL, Schanstra JP. Advances in urinary proteome analysis and biomarker discovery in pediatric renal disease. Pediatric Nephrology. 2010;**25**:27-35. DOI: 10.1007/s00467-009-1251-5

[13] Füvesi J, Hanrieder J, Bencsik K, Rajda C, Kovács SK, Kaizer L, Beniczky S, Vécsei L, Bergquist J. Proteomic analysis of cerebrospinal fluid in a fulminant case of multiple sclerosis. International Journal of Molecular Sciences. 2012;**13**:7676-7693. DOI: 10.3390/ijms13067676

[14] Wright EP, Prasad KAG, Padula MP, Coorssen JR. Deep imaging: How much of the proteome does current top-down technology already resolve? PloS One. 2014;**9**:e86058. DOI: 10.1371/journal.pone.0086058

[15] Rogowska-Wrzesinska A, Le Bihan MC, Thaysen-Andersen M, Roepstorff P. 2D gels still have a niche in proteomics. Journal of Proteomics. 2013;**88**:4-13. DOI: 10.1016/j.jprot.2013.01.010

[16] Oliveira BM, Coorssen JR, Martins-de-Souza D. 2DE: The phoenix of proteomics. Journal of Proteomics. 2014;**104**:140-150. DOI: 10.1016/j.jprot.2014.03.035

[17] Weiss W, Görg A. High-resolution two-dimensional electrophoresis. Methods in Molecular Biology. 2009;**564**:13-32. DOI: 10.1007/978-1-60761-157-8_2

[18] Rabilloud T. Two-dimensional gel electrophoresis in proteomics: Old, old fashioned, but it still climbs up the mountains. Proteomics. 2002;**2**:3-10. DOI: 10.1002/1615-9861 (200201)2:1<3::AID-PROT3>3.0.CO;2-R

[19] Wong SC, Chan CM, Ma BB, Lam MY, Choi GC, Au TC, Chan AS, Chan AT. Advanced proteomic technologies for cancer biomarker discovery. Expert Review of Proteomics. 2009;**6**:123-134. DOI: 10.1586/epr.09.1

[20] Pérès S, Molina L, Salvetat N, Granier C, Molina F. A new method for 2D gel spot alignment: Application to the analysis of large sample sets in clinical proteomics. BMC Bioinformatics. 2008;**9**:460. DOI: 10.1186/1471-2105-9-460

[21] Rabilloud T, Chevallet M, Luche S, Lelong C. Two-dimensional gel electrophoresis in proteomics: Past, present and future. Journal of Proteomics. 2010;**73**:2064-2077. DOI: 10.1016/j.jprot.2010.05.016

[22] Yoshida K, Kuramitsu Y, Murakami K, Ryozawa S, Taba K, Kaino S, Zhang X, Sakaida I, Nakamura K. Proteomic differential display analysis for TS-1-resistant and -sensitive pancreatic cancer cells using two-dimensional gel electrophoresis and mass spectrometry. Anticancer Research. 2011;**31**:2103-2108

[23] Hosseinifar H, Gourabi H, Salekdeh GH, Alikhani M, Mirshahvaladi S, Sabbaghian M, Modarresi T, Gilani MA. Study of sperm protein profile in men with and without varicocele using two-dimensional gel electrophoresis. Urology. 2013;**81**:293-300. DOI: 10.1016/j.urology.2012.06.027

[24] Von Löhneysen K, Scott TM, Soldau K, Xu X, Friedman JS. Assessment of the red cell proteome of young patients with unexplained hemolytic anemia by two-dimensional differential in-gel electrophoresis (DIGE). PLoS One. 2012;**7**:e34237. DOI: 10.1371/journal.pone.0034237

[25] Lee TH, Jang AS, Park JS, Kim TH, Choi YS, Shin HR, Park SW, Uh ST, Choi JS, Kim YH, Kim Y, Kim S, Chung IY, Jeong SH, Park CS. Elevation of S100 calcium binding protein A9 in sputum of neutrophilic inflammation in severe uncontrolled asthma. Annals of Allergy, Asthma & Immunology. 2013;**111**:268-275. DOI: 10.1016/j.anai.2013.06.028

[26] Suojalehto H, Kinaret P, Kilpeläinen M, Toskala E, Ahonen N, Wolff H, Alenius H, Puustinen A. Level of fatty acid binding protein 5 (FABP5) is increased in sputum of allergic asthmatics and links to airway Remodeling and inflammation. PLoS One. 2015;**10**:e0127003. DOI: 10.1371/journal.pone.0127003

[27] Wu J, Kobayashi M, Sousa EA, Liu W, Cai J, Goldman SJ, Dorner AJ, Projan SJ, Kavuru MS, Qiu Y, Thomassen MJ. Differential proteomic analysis of bronchoalveolar lavage fluid in asthmatics following segmental antigen challenge. Molecular & Cellular Proteomics. 2005;**4**:1251-1264. DOI: 10.1074/mcp M 500041-MCP 200

[28] Kim TH, Lee YH, Kim KH, Lee SH, Cha JY, Shin EK, Jung S, Jang AS, Park SW, Uh ST, Kim YH, Park JS, Sin HG, Youm W, Koh ES, Cho SY, Paik YK, Rhim TY, Park CS. Role of lung apolipoprotein A-I in idiopathic pulmonary fibrosis: Anti-inflammatory and anti-fibrotic effect on experimental lung injury and fibrosis. American Journal of Respiratory and Critical Care Medicine. 2010;**182**:633-642. DOI: 10.1164/rccm.200905-0659OC

[29] Ishikawa N, Ohlmeier S, Salmenkivi K, Myllärniemi M, Rahman I, Mazur W, Kinnula VL. Hemoglobin α and β are ubiquitous in the human lung, decline in idiopathic pulmonary fibrosis but not in COPD. Respiratory Research. 2010;**11**:123. DOI: 10.1186/1465-9921-11-123

[30] Ohlmeier S, Mazur W, Salmenkivi K, Myllärniemi M, Bergmann U, Kinnula VL. Proteomic studies on receptor for advanced glycation end product variants in idiopathic pulmonary fibrosis and chronic obstructive pulmonary disease. Proteomics Clinical Applications. 2010;**4**:97-105. DOI: 10.1002/prca.200900128

[31] Hara A, Sakamoto N, Ishimatsu Y, Kakugawa T, Nakashima S, Hara S, Adachi M, Fujita H, Mukae H, Kohno S. S100A9 in BALF is a candidate biomarker of idiopathic pulmonary fibrosis. Respiratory Medicine. 2012;**106**:571-580. DOI: 10.1016/j.rmed.2011.12.010

[32] Landi C, Bargagli E, Bianchi L, Gagliardi A, Carleo A, Bennett D, Perari MG, Armini A, Prasse A, Rottoli P, Bini L. Towards a functional proteomics approach to the comprehension of idiopathic pulmonary fibrosis, sarcoidosis, systemic sclerosis and pulmonary Langerhans cell histiocytosis. Journal of Proteomics. 2013;**83**:60-75. DOI: 10.1016/j.jprot.2013.03.006

[33] Landi C, Bargagli E, Carleo A, Bianchi L, Gagliardi A, Prasse A, Perari MG, Refini RM, Bini L, Rottoli P. A system biology study of BALF from patients affected by idiopathic pulmonary fibrosis (IPF) and healthy controls. Proteomics Clinical Applications. 2014;**8**:932-950. DOI: 10.1002/prca.201400001

[34] Carleo A, Bargagli E, Landi C, Bennett D, Bianchi L, Gagliardi A, Carnemolla C, Perari MG, Cillis G, Armini A, Bini L, Rottoli P. Comparative proteomic analysis of bronchoalveolar lavage of familial and sporadic cases of idiopathic pulmonary fibrosis. Journal of Breath Research. 2016;**10**:026007. DOI: 10.1088/1752-7155/10/2/026007

[35] Silva E, Bourin S, Sabounchi-Schütt F, Laurin Y, Barker E, Newman L, Eriksson H, Eklund A, Grunewald J. A quantitative proteomic analysis of soluble bronchoalveolar fluid proteins from patients with sarcoidosis and chronic beryllium disease. Sarcoidosis, Vasculitis, and Diffuse Lung Diseases. 2007;**24**:24-32

[36] Landi C, Bargagli E, Carleo A, Bianchi L, Gagliardi A, Cillis G, Perari MG, Refini RM, Prasse A, Bini L, Rottoli P. A functional proteomics approach to the comprehension of sarcoidosis. Journal of Proteomics. 2015;**128**:375-387. DOI: 10.1016/j.jprot.2015.08.012

[37] Shirahama R, Miyazaki Y, Okamoto T, Inase N, Yoshizawa Y. Proteome analysis of bronchoalveolar lavage fluid in lung fibrosis associated with systemic sclerosis. Allergology International. 2010;**59**:409-415. DOI: 10.2332/allergolint.10-OA-0176

[38] Suhara K, Miyazaki Y, Okamoto T, Ishizuka M, Tsuchiya K, Inase N. Fragmented gelsolins are increased in rheumatoid arthritis-associated interstitial lung disease with usual interstitial pneumonia pattern. Allergology International. 2016;**65**:88-95. DOI: 10.1016/j.alit.2015.08.002

[39] Ghafouri B, Persson HL, Tagesson C. Intriguing bronchoalveolar lavage proteome in a case of pulmonary Langerhans cell histiocytosis. American Journal of Case Reports. 2013;**14**:129-133. DOI: 10.12659/AJCR.889037

[40] Schulz BL, Sloane AJ, Robinson LJ, Prasad SS, Lindner RA, Robinson M, Bye PT, Nielson DW, Harry JL, Packer NH, Karlsson NG. Glycosylation of sputum mucins is altered in cystic fibrosis patients. Glycobiology. 2007;**17**:698-712. DOI: 10.1093/glycob/cwm036

[41] Charro N, Hood BL, Faria D, Pacheco P, Azevedo P, Lopes C, de Almeida AB, Couto FM, Conrads TP, Penque D. Serum proteomics signature of cystic fibrosis patients: A complementary 2-DE and LC-MS/MS approach. Journal of Proteomics. 2011;**74**:110-126. DOI: 10.1016/j.jprot.2010.10.001

[42] Merali S, Barrero CA, Bowler RP, Chen DE, Criner G, Braverman A, Litwin S, Yeung A, Kelsen SG. Analysis of the plasma proteome in COPD: Novel low abundance proteins reflect the severity of lung remodeling. COPD. 2014;**11**:177-189. DOI: 10.3109/15412555.2013.831063

[43] Ohlmeier S, Mazur W, Linja-Aho A, Louhelainen N, Rönty M, Toljamo T, Bergmann U, Kinnula VL. Sputum proteomics identifies elevated PIGR levels in smokers and mild-to-moderate COPD. Journal of Proteome Research. 2012;**11**:599-608. DOI: 10.1021/pr2006395

[44] Plymoth A, Löfdahl CG, Ekberg-Jansson A, Dahlbäck M, Broberg P, Foster M, Fehniger TE, Marko-Varga G. Protein expression patterns associated with progression of chronic obstructive pulmonary disease in bronchoalveolar lavage of smokers. Clinical Chemistry. 2007;**53**:636-644. DOI: 10.1373/clinchem.2006.076075

[45] Kohler M, Sandberg A, Kjellqvist S, Thomas A, Karimi R, Nyrén S, Eklund A, Thevis M, Sköld CM, Wheelock ÅM. Gender differences in the bronchoalveolar lavage cell proteome of patients with chronic obstructive pulmonary disease. The Journal of Allergy and Clinical Immunology. 2013;**131**:743-751. DOI: 10.1016/j.jaci.2012.09.024

[46] Pastor MD, Nogal A, Molina-Pinelo S, Meléndez R, Salinas A, González De la Peña M, Martín-Juan J, Corral J, García-Carbonero R, Carnero A, Paz-Ares L. Identification of proteomic signatures associated with lung cancer and COPD. Journal of Proteomics. 2013;**89**:227-237. DOI: 10.1016/j.jprot.2013.04.037

[47] Pastor MD, Nogal A, Molina-Pinelo S, Meléndez R, Romero-Romero B, Mediano MD, López-Campos JL, García-Carbonero R, Sanchez-Gastaldo A, Carnero A, Paz-Ares L. Identification of oxidative stress related proteins as biomarkers for lung cancer and chronic obstructive pulmonary disease in bronchoalveolar lavage. International Journal of Molecular Sciences. 2013;**14**:3440-3455. DOI: 10.3390/ijms14023440

[48] Yu M, Wang XX, Zhang FR, Shang YP, Du YX, Chen HJ, Chen JZ. Proteomic analysis of the serum in patients with idiopathic pulmonary arterial hypertension. Journal of Zhejiang University. Science. B. 2007;**8**:221-227. DOI: 10.1631/jzus.2007.B0221

[49] Terrier B, Tamby MC, Camoin L, Guilpain P, Broussard C, Bussone G, Yaïci A, Hotellier F, Simonneau G, Guillevin L, Humbert M, Mouthon L. Identification of target antigens of antifibroblast antibodies in pulmonary arterial hypertension. American Journal of Respiratory and Critical Care Medicine. 2008;**177**:1128-1134. DOI: 10.1164/rccm.200707-1015OC

[50] Zhang J, Zhang Y, Li N, Liu Z, Xiong C, Ni X, Pu Y, Hui R, He J, Pu J. Potential diagnostic biomarkers in serum of idiopathic pulmonary arterial hypertension. Respiratory Medicine. 2009;**103**:1801-1806. DOI: 10.1016/j.rmed.2009.07.017

[51] Yeager ME, Colvin KL, Everett AD, Stenmark KR, Ivy DD. Plasma proteomics of differential outcome to long-term therapy in children with idiopathic pulmonary arterial hypertension. Proteomics Clinical Applications. 2012;**6**:257-267. DOI: 10.1002/prca.201100078

[52] Insenser M, Montes-Nieto R, Martínez-García MÁ, Durán EF, Santiuste C, Gómez V, Kline JA, Escobar-Morreale HF, Jiménez D. Identification of reduced circulating haptoglobin concentration as a biomarker of the severity of pulmonary embolism: A nontargeted proteomic study. PLoS One. 2014;**9**:e100902. DOI: 10.1371/journal.pone.0100902

[53] von Zur Mühlen C, Koeck T, Schiffer E, Sackmann C, Zürbig P, Hilgendorf I, Reinöhl J, Rivera J, Zirlik A, Hehrlein C, Mischak H, Bode C, Peter K. Urine proteome analysis as a discovery tool in patients with deep vein thrombosis and pulmonary embolism. Proteomics Clinical Applications. 2016;**10**:574-584. DOI: 10.1002/prca.201500105

[54] Chang DW, Hayashi S, Gharib SA, Vaisar T, King ST, Tsuchiya M, Ruzinski JT, Park DR, Matute-Bello G, Wurfel MM, Bumgarner R, Heinecke JW, Martin TR. Proteomic and computational analysis of bronchoalveolar proteins during the course of the acute respiratory distress syndrome. American Journal of Respiratory and Critical Care Medicine. 2008;**178**:701-709. DOI: 10.1164/rccm.200712-1895OC

[55] Sixt SU, Alami R, Hakenbeck J, Adamzik M, Kloss A, Costabel U, Jungblut PR, Dahlmann B, Peters J. Distinct proteasome subpopulations in the alveolar space of patients with the acute respiratory distress syndrome. Mediators of Inflammation. 2012;**2012**:204250. DOI: 10.1155/2012/204250

[56] Ahmad Y, Shukla D, Garg I, Sharma NK, Saxena S, Malhotra VK, Bhargava K. Identification of haptoglobin and apolipoprotein A-I as biomarkers for high altitude pulmonary edema. Functional & Integrative Genomics. 2011;**11**:407-417. DOI: 10.1007/s10142-011-0234-3

[57] Ahmad Y, Sharma NK, Ahmad MF, Sharma M, Garg I, Srivastava M, Bhargava K. The proteome of hypobaric induced hypoxic lung: Insights from temporal proteomic profiling for biomarker discovery. Scientific Reports. 2015;**5**:10681. DOI: 10.1038/srep10681

[58] Yang Y, Ma L, Guan W, Wang Y, DU Y, Ga Q, Ge RL. Differential plasma proteome analysis in patients with high-altitude pulmonary edema at the acute and recovery phases. Experimental and Therapeutic Medicine. 2014;**7**:1160-1166. DOI: 10.3892/etm.2014.1548

[59] Brasier AR, Zhao Y, Spratt HM, Wiktorowicz JE, Ju H, Wheat LJ, Baden L, Stafford S, Wu Z, Issa N, Caliendo AM, Denning DW, Soman K, Clancy CJ, Nguyen MH, Sugrue MW, Alexander BD, Wingard JR. Improved detection of invasive pulmonary aspergillosis arising during leukemia treatment using a panel of host response proteins and fungal antigens. PLoS One. 2015;**10**:e0143165. DOI: 10.1371/journal.pone.0143165

[60] Tanaka T, Sakurada S, Kano K, Takahashi E, Yasuda K, Hirano H, Kaburagi Y, Kobayashi N, Hang NTL, Lien LT, Matsushita I, Hijikata M, Uchida T, Keicho N. Identification of tuberculosis-associated proteins in whole blood supernatant. BMC Infectious Diseases. 2011;**11**:71. DOI: 10.1186/1471-2334-11-71

[61] Zhang L, Wang Q, Wang W, Liu Y, Wang J, Yue J, Xu Y, Xu W, Cui ZL, Zhang X, Wang H. Identification of putative biomarkers for the serodiagnosis of drug-resistant *Mycobacterium tuberculosis*. Proteome Science. 2012;**10**:12. DOI: 10.1186/1477-5956-10-12

[62] Rossi R, De Palma A, Benazzi L, Riccio AM, Canonica GW, Mauri P. Biomarker discovery in asthma and COPD by proteomic approaches. Proteomics Clinical Applications. 2014;**8**:901-915. DOI: 10.1002/prca.201300108

[63] Viglio S, Stolk J, Iadarola P, Giuliano S, Luisetti M, Salvini R, Fumagalli M, Bardoni A. Respiratory proteomics today: Are technological advances for the identification of biomarker signatures catching up with their promise? A critical review of the literature in the decade 2004-2013. Proteomes. 2014;**2**:18-52. DOI: 10.3390/proteomes2010018

[64] Terracciano R, Pelaia G, Preianò M, Savino R. Asthma and COPD proteomics: Current approaches and future directions. Proteomics Clinical Applications. 2015;**9**:203-220. DOI: 10.1002/prca.201400099

[65] Kan M, Shumyatcher M, Himes BE. Using omics approaches to understand pulmonary diseases. Respiratory Research. 2017;**18**:149. DOI: 10.1186/s12931-017-0631-9

Chapter 3

Peculiarities of SDS-PAGE of Titin/Connectin

Ivan M. Vikhlyantsev and Zoya A. Podlubnaya

Additional information is available at the end of the chapter

http://dx.doi.org/10.5772/intechopen.75902

Abstract

Titin (also known as connectin) is a giant elastic protein of striated and smooth muscles of vertebrates. The molecular weight of its isoforms is 3.0–3.7 MDa in striated muscles and 0.5–2.0 MDa in smooth muscles. Titin was discovered 40 years ago using the sodium dodecyl sulfate-polyacrylamide gel electrophoresis (SDS-PAGE). At the present time, this method has not lost its relevance but has undergone a number of modifications that improve visualization of giant titin isoforms in the gel. This chapter provides historical insights into the technical aspects of the electrophoresis methods used to identify titin and its isoforms. We focus on the peculiarities of the technique because of which titin molecules remain intact and its high molecular weight isoforms can be visualized. Electrophoretic testing of changes in titin content in muscles can be used in medical practice to diagnose pathological processes and evaluate effective approaches to their correction.

Keywords: striated muscles, titin (connectin), titin isoforms, SDS-PAGE, agarose-strengthened macroporous polyacrylamide gel

1. Introduction

Titin (also known as connectin) is a giant elastic protein of striated [1–6] and smooth [7] muscles of vertebrates. The molecular weight of its isoforms is 3.0–3.7 MDa in striated muscles and 0.5–2.0 MDa in smooth muscles [7]. Titin is the third protein in quantity (after actin and myosin) in the sarcomeres of cardiac and skeletal muscles (**Figure 1**). Titin molecules of about 1 μm in length and 3–4 nm in diameter [8, 9] overlap the half of the sarcomere from the M-line to the Z-line, forming a third filamentous system in myofibrils [10]. In the A-zone of the sarcomere, titin is connected with myosin filaments [11]. In the I-band of the sarcomere, some regions of the titin molecule may interact with actin filaments [12, 13], but most of the titin molecule in this zone passes freely, connecting the ends of myosin filaments with the Z-disc

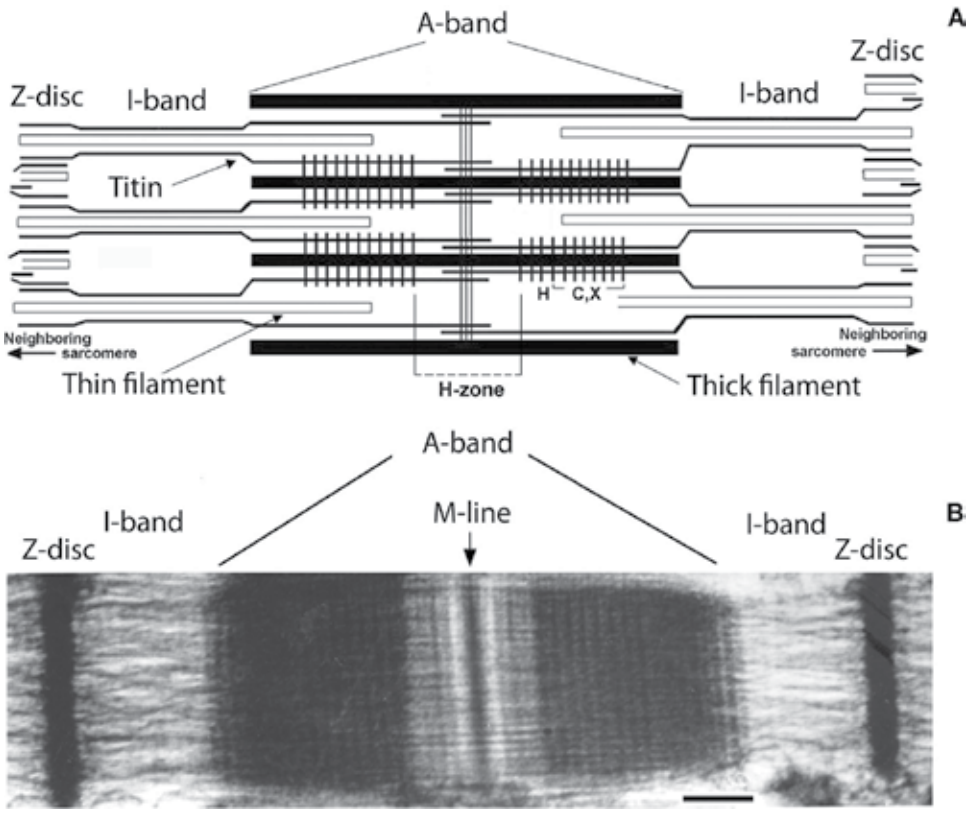

Figure 1. Sarcomere structure of vertebrate striated muscles. (A) Scheme of sarcomeric structure. Thick filaments consisting mainly of myosin are located in the A-band. Thin filaments consisting mainly of actin are located in the I-band of the sarcomere and in the A-band, where they overlap with thick filaments. The H-zone is the central part of the A-band free from thin filaments. Titin molecules are arranged from the M-line to the Z-disc of the sarcomere. Transversal bands of myosin-binding proteins (H, C, X) in the A-band of the sarcomere are indicated. (B) Microphotograph of sarcomere of demembranized rabbit lumbar muscle. Scale bar: 200 nm.

(**Figure 1**). Each half of myosin filament in sarcomere includes six titin molecules [14] with N- and C-ends overlapping in the Z- and M-line of the sarcomere, respectively [15].

Titin molecule consists of repeating immunoglobulin-like (IgC2) and fibronectin-like (FnIII) domains. Titin also contains a kinase domain in M-line, unique sequences N2A, N2B, and PEVK in I-zone and phosphorylation sites in Z-disc, M-band, and I-band of sarcomere [15].

The giant size of titin molecule and its location in all zones of sarcomere provide a basis for polyfunctionality of this protein. It has been shown that titin is a framework for the assembly of thick filaments and the sarcomere [16, 17]; is involved in maintenance of the highly ordered sarcomere structure [18, 19]; contributes to the passive tension developed by the muscle during stretching and develops the restoring force during sarcomere shortening [20–22]; is involved in the regulation of actin-myosin interaction [2, 4, 13, 23–31]. The results of recent studies suggest that the elastic protein titin, as a mechanosensor (strain sensor and stress sensor), plays a key role in intracellular signaling processes and in particular, participates in the regulation of muscle gene expression and protein turnover in sarcomere [2, 6, 32–37]. These

conclusions are based on the results of investigations showing the presence in the sarcomere of mechanosensory "hotspots": complexes of signal proteins joined by titin into a single network, the activity of which varies during muscle stretching or variations in its mechanical loading [32–34, 38]. Titin is supposed to "…sense the mechanical stimuli and transform them into biochemical signals…" [34]. Great attention is now focused on the study of titin role in cardiomyopathies and skeletal muscle diseases [2, 39–47].

This paper provides historical insights into the technical aspects of electrophoresis methods used to identify titin and its isoforms. We focus on the peculiarities of the technique because of which titin molecules remain intact and its high molecular weight isoforms can be visualized.

2. History of the discovery and study of titin/connectin by SDS gel electrophoresis technique

Titin was discovered in 1979 by Kuan Wang and his coauthors [48] using gel electrophoresis. In macroporous polyacrylamide gel prepared according to Etlinger et al. [49] and containing 3.2% acrylamide, three new bands were found above the myosin heavy chain: a closely spaced doublet and a singlet band with faster mobility [48]. Using crosslinked myosin heavy chains (MHC, 205 kDa) as standards, the authors were able to estimate that each of these doublet bands (1 and 2) has a Mr. $\sim 1 \times 10^6$. Proteins 1 and 2 appeared to be immunologically identical and were named titin 1 (T1) and titin 2 (T2). The third protein had Mr. $\sim 5 \times 10^5$ and was thereafter named nebulin [50].

Another group of investigators headed by Maruyama studied the properties of connectin – the protein they discovered [51]. The properties of connectin as a protein candidate for the elastic filaments in sarcomeres of striated muscles of vertebrate animals were intensively explored by this group of authors in the late 1970s [52–54]. In 1981, having conducted a comparative study of electrophoretic mobility, amino acid composition, and localization in myofibrils of titin and connectin, Maruyama and coauthors showed that the major high molecular weight component of connectin was identical with that of titin [55]. Using 1.8–3.0% polyacrylamide tube gels prepared according to Weber and Osborn [56], and crosslinked MHC as standards, the authors showed that the molecular weights of α-connectin (corresponding to intact molecules of titin-1) and β-connectin (corresponding to proteolytic fragments of T1–T2) of breast muscle of the chicken were 2.8×10^6 and 2.1×10^6, respectively [57].

Further electrophoretic studies of titin (connectin) using different types of gels (1.8% or 2.3–4% polyacrylamide tube gels, 2–12% gradient polyacrylamide slab gel) [58–63]) revealed differences in electrophoretic mobility of T1 (α-connectin) in cardiac and skeletal muscles of vertebrates animals (fishes, amphibians, reptiles, birds, mammals). In particular, plots of molecular mass versus mobility, assuming 2.8 and 2.4 MDa for T1 and T2 of the rabbit psoas, respectively, yielded the following set of values for T1: 2.8 MDa (adductor magnus), 2.88 MDa (longissimus dorsi, sartorius), 2.94 MDa (soleus, semitendinosus) [60]. Cardiac muscle displayed the smallest titin. Similar data were obtained by us using 2.5–9% gradient polyacrylamide slab gel (**Figure 2**). Based on data obtained the assumption on the existence of isoforms of T1 was made [60, 61].

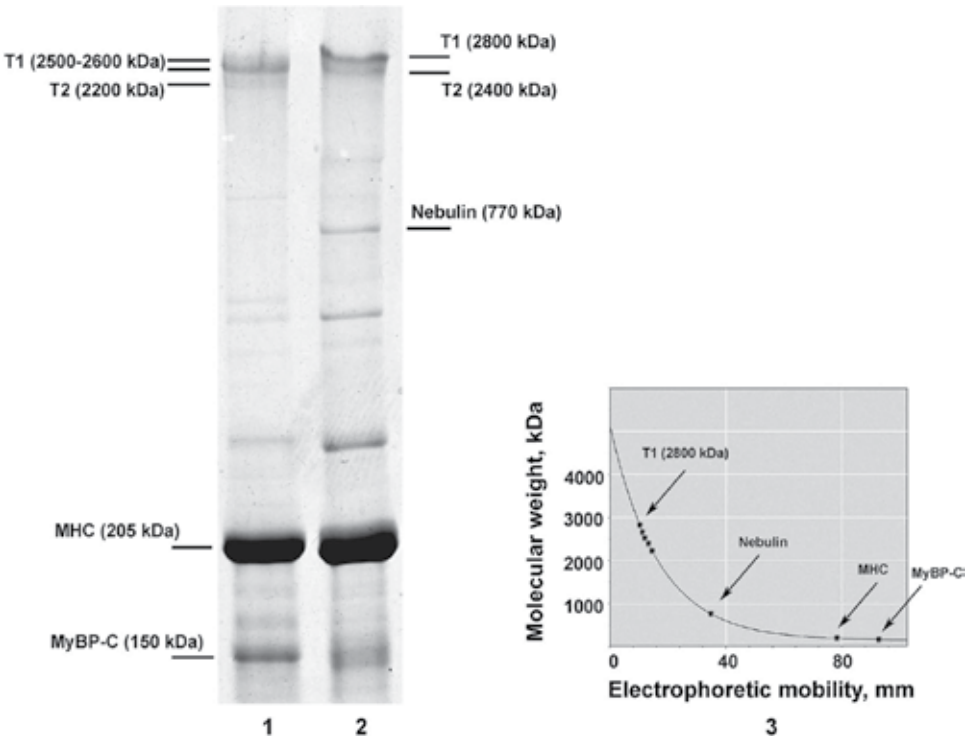

Figure 2. Molecular weights of T1 isoforms from rabbit striated muscles. Electrophoresis was performed in a gradient 2.5–9.0% polyacrylamide vertical gel (8 × 10 × 0.1 cm). (1) myocardium (left ventricle); (2) m. soleus; (3) logarithmic dependence of molecular weight on protein electrophoretic mobility in gel. T1 molecular weight was assessed by the following standards: Cardiac MyBP-C (150 kDa), as well as myosin heavy chains (MHC, 205 kDa), nebulin (770 kDa), and T2-fragment (2400 kDa) of rabbit skeletal muscles [60, 87, 88].

In 1995, the complete complementary DNA sequence of human cardiac titin was determined [64]. Further studies showed that the titin gene (TTN) consists of 363 coding exons, which can be differentially spliced and theoretically could generate more than one million splice variants in striated and smooth muscles of mammals [7, 65–68]. Adult striated muscles express three major titin isoforms: N2A in skeletal muscles (3.35–3.7 MDa), N2B, and N2BA in cardiac muscle (2.97–3.3 MDa, respectively) [65].

2.1. Electrophoretic detection of titin isoforms

To confirm that muscles contain N2A, N2B, and N2BA isoforms of titin, different macroporous gels (2–9.5% gradient polyacrylamide slab gel, 1% agarose slab gel, agarose-strengthened 2% polyacrylamide slab gel, horizontal 1.3% polyacrylamide gel strengthened with 0.5% agarose) were used [69–73]. It was shown that the T1 mobility varied greatly between skeletal and cardiac muscles from different mammals. The major T1 bands were ascribed to the titin isoforms N2B and N2BA in cardiac muscle and the titin isoform N2A in skeletal muscles. According to Western blot data with using antibodies against the N-terminal and the C-terminal ends of titin, it was revealed that the N2A, N2B, and N2BA bands represent full-length titin molecules (titin 1 – T1) [69, 74].

Titin isoform analyses for 37 adult rabbit skeletal muscles showed sizes between 3.3 and 3.7 MDa [75]. N2BA titin isoforms in cardiac muscle of different mammals had sizes between 3.25 and 3.4 MDa [72].

Using 1% vertical agarose gel [70] at least four classes of cardiac N2BA titin isoforms were observed, of which two rat embryonic/neonatal forms (N2BA-N1, N2BA-N2) had sizes of 3710 and 3590 kDa. These isoforms were found during late embryonic and immediately post-natal period [76]. These were gradually replaced by adult forms (N2BA-A1, N2BA-A2) with sizes of 3390 and 3220 kDa, respectively [76]. Similar titin isoform transformations were observed in embryonic/neonatal hearts of rat and other mammals and reported by the researchers [74, 77–80].

Giant titin isoforms expressed in rat striated muscles with an RBM20 autosomal dominant mutation were reported [81–83]. The molecular masses of these isoforms were estimated from their electrophoretic mobility in 1% vertical agarose gel to be 3750 and 3830 kDa [83].

2.2. New high molecular weight forms of titin in striated muscles of mammals: aggregates or intact isoforms?

Our group headed by Zoya Podlubnaya conducts a comparative study of titin isoform composition in mammalian striated muscles under conditions of hibernation, microgravity, and during the development of pathological processes [84]. Vertical agarose-strengthened 2.2% polyacrylamide gel prepared according to Tatsumi and Hattori [85] was used to separate titin isoforms and their fragments.

Our first experiments, conducted more than 10 years ago, showed that, in addition to N2A, N2BA, N2B and T2 bands, there exist one or two more high Mr. bands (named NT) [84, 86]. Staining the gels with ethidium bromide revealed no nucleic acids in the bands, although western blots with 9D10 antibodies revealed titin bands. The bands were visualized in the electropherograms of striated muscles of mammals, but in the electropherograms of striated muscles in other groups of vertebrates (amphibians and birds) revealed no NT bands [84].

The content of NT titins in muscles of animals and humans was as follows: Mongolian gerbil (8–14%), mouse (13–18%), rat (9–26%), rabbit (13–30%), ground squirrel (24–33%), and human (29–41%) [73, 84]. Using human and animal skeletal muscle myosin heavy chain (205 kDa) and nebulin (770–890 kDa), as well as the N2A titin isoform (~3600 and 3700 kDa) of rabbit and human soleus as standards [60, 75, 87, 88], we estimated that the NT has a Mr. of ~3.8–3.9 × 10^6 [73]. Expression of titin isoforms with these molecular weights is not excluded [66, 67, 82, 83], but titin aggregates in gels could not be excluded either [69, 88]. Data published in 2003 demonstrated in electropherograms of the dog heart left ventricle, together with the known N2BA and N2B isoforms and T2-fragments of titin, the presence of higher molecular weight double protein bands that were named titin aggregates [70].

We were also not absolutely sure that titin NT bands were not aggregates of its lower molecular weight isoforms and their fragments. If this were so, then the proteolytic cleavage of titin accompanied by an increase in the content of its fragments must result in the higher content of aggregates. Experiments on proteolytic cleavage of titin in muscle tissue under the influence of endogenous proteases were performed to test this assumption [84] (**Figure 3**).

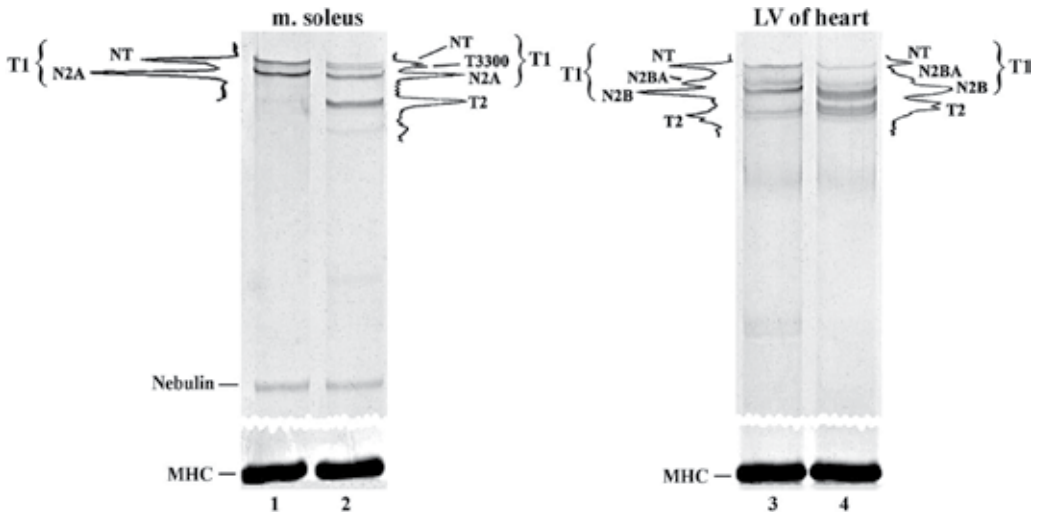

Figure 3. Proteolytic changes in titin in ground squirrel muscles. Electrophoresis was performed in vertical agarose-strengthened 2.1% polyacrylamide gel (8 × 10 × 0.1 cm). (1) m. soleus (control); (2) m. soleus (proteolysis, 1 h); (3) left ventricle of heart (control); (4) left ventricle of heart (proteolysis, 30 min). Proteolytic cleavage of titin was performed under the influence of endogenous muscular proteases. To this end, small pieces of muscle tissue (20–30 mg) were held for 30–60 min at 25–30°C. Then, 2–3 mg pieces were taken from the muscle sample and placed into solubilizing solution (10 mM Tris–HCl, 1.2% SDS, 10% glycerol, 2% β-mercaptoethanol or 75 mM DTT, 8–10 μg/ml of leupeptin or E64, pH 7.0) for the extraction and further electrophoretic testing of the proteins. T3300 is probably the proteolytic fragment of NT titin with molecular weight of ~3300 kDa.

It was found that proteolysis of titin in m. soleus for 30–60 min resulted in a reduction (six-fold to sevenfold) of the content of NT titin and twofold reduction of the content of N2A titin (**Figure 3**, lanes 1 and 2). At the same time, a considerable increase in the content of T2 and appearance of a band with a molecular weight of ~3200–3300 kDa (T3300) were detected, which is probably a product of NT titin degradation.

Proteolysis of titin in cardiac muscle for 30–60 min resulted in a 2–3-fold decrease in the content of NT and N2BA (**Figure 3**, lanes 3 and 4). At the same time, the increase in the content of not only T2-fragments but also N2B isoform of titin was observed, which could be explained by the presence of fragments of NT and N2BA titins in this protein band. Densitometry data showed that the total titin content (relative to MHC content) in muscles as a result of 30–60 min proteolysis has not changed.

Thus, the results did not confirm our assumption that NT bands are aggregates of lower molecular weight titin isoforms and their fragments. However, these data did not exclude the aggregative origin of NT bands. Assuming that molecular masses of titin aggregates should considerably exceed 3800–3900 kDa, we decided to find out more about the differences in electrophoretic mobility of the observed bands. We developed a horizontal agarose-strengthened gel system using 1.3% polyacrylamide and 0.5% agarose [73].The gels showed that mobility of the NT bands, as well as other titin bands, varied greatly in different muscles.

Using human and animal skeletal muscle nebulin (770–890 kDa) as well as MHC (205 kDa) as standards the molecular masses of N2A, N2BA, N2B, T2, and NT titin bands were estimated. The results obtained were unexpected for us. The NT bands had sizes between 3230 and 3730 kDa,

whereas the N2A, N2BA, N2B, and T2 bands had sizes between 2100 and 2800 kDa [73, 84]. The last values corresponded to a set of values for T1 (α-connectin) and T2 (β-connectin) [57, 60, 88]. Similar data were obtained for vertical agarose-strengthened 1.9% polyacrylamide gels (**Figure 4**). The gel resolved a doublet NT band at 3300–3400 kDa for cardiac muscle and a singlet band of 3600–3700 kDa for skeletal muscles of mammals.

Results from western blots with Z1/Z2 antibodies against the N-terminal end and AB5 antibodies against the C-terminal end of titin revealed the NT bands were full-length titin molecules [89] (**Figure 5**). We, therefore, hypothesized that the NT bands are intact N2A, N2BA, N2B titin isoforms [89]. Although this requires further research, we cannot exclude the possibility that the NT bands are the other protein immunologically identical to titin, for example, a protein whose long thin filaments were revealed in the "shades" of rabbit psoas myofibrils remaining after sequential removal of myosin, actin, tropomyosin, troponins, and the minor M-band proteins [90] (**Figure 6**).

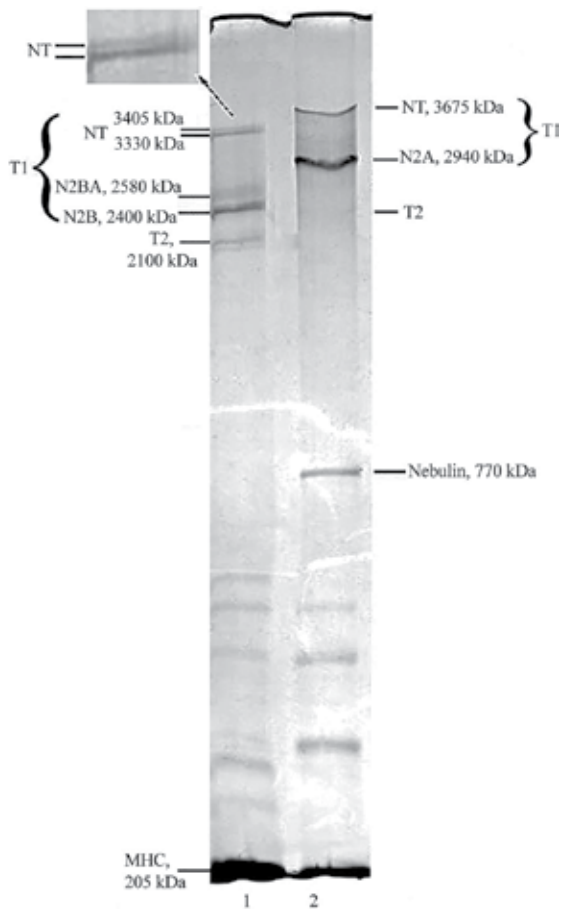

Figure 4. SDS-PAGE analysis of titin isoforms in striated muscles of ground squirrel (*Spermophilus undulatus*); a modified view from [89]. Vertical agarose-strengthened 1.9% polyacrylamide gel (14.5 × 16.0 × 0.15 cm) was used to separate the titin isoforms. (1) Myocardium (left ventricle); (2) m. soleus. T1 molecular weight was assessed by the following standards: MHC (205 kDa), nebulin (770–890 kDa), titin-2 (2100–2400 kDa) of rabbit and human striated muscles [60, 87, 88].

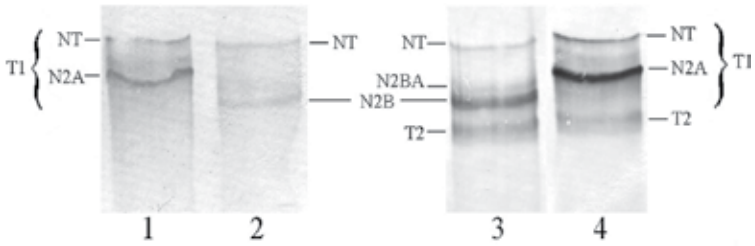

Figure 5. Western blotting of titin in striated muscles of ground squirrel; a modified view from [89]. As primary antibodies, the following were used: Z1/Z2 to N-end of titin molecule located in Z-disc of sarcomere (1, 2); AB5 to the part of titin molecule in A-disk located near the M-line of sarcomere (3,4); (1,4) m. soleus; (2,3) myocardium (left ventricle).

2.3. Nuances of sample preparation of titin

In the paper of Granzier and Wang [88], particular attention was paid to sample preparation of titin. The authors pointed to the fact that titin is extraordinarily sensitive to proteolysis in situ by endogenous proteases and by exogenous proteases such as those found in buffers that are contaminated with bacteria and fungi. According to these and other authors, even in SDS-solubilized myofibril samples, appreciable degradation of titin by residual protease activity can occur in a few days at room temperature [50, 88, 91].

To limit proteolysis, a number of authors suggested the inclusion of protease inhibitors in SDS samples prior to electrophoresis. Leupeptin, E-64, and a protease inhibitor cocktail have been used to inhibit proteolytic degradation of titin [21, 70, 72, 73, 85, 92]. In order to attain better solubilization of titin, it has been proposed to use urea-thiourea SDS DTT sample buffer [70, 93].

Another crucial methodical nuance that should be taken into account during sample`s preparation of titin is heat treatment of the samples. SDS samples are usually prepared by heating them in boiling water for several minutes. This process promotes denaturation of proteins and facilitates disulfide reduction. However, different authors have shown that boiling degrades titin [70, 88, 94, 95]. Samples heated at 100°C had less intact titin and more breakdown products

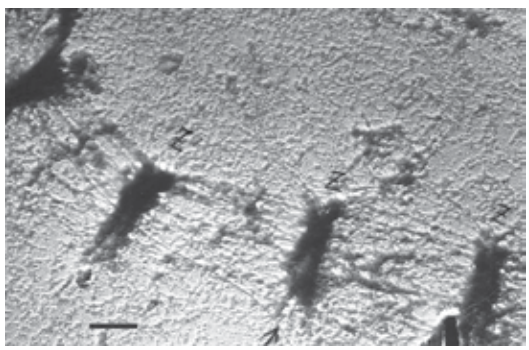

Figure 6. Microphotograph of isolated negatively stained myofibril of rabbit lumbar muscle after the extraction of myosin and actin filaments. The remaining "Z-discs" are kept in the register by longitudinal filaments continually passing through the entire myofibril (indicated by the arrow). Scale bar: 100 nm.

(smears migrating near the bottom of the gel) than those at 60°C [70]. A temperature of 50–60°C for 10–20 min has been considered optimal for the extraction and preservation of intact titin [70, 88, 95]. Results of our studies demonstrated that heating of SDS sample at the said temperature may lead to artifacts in the content of titin. SDS samples of mammalian cardiac muscle heated at 60–65°C for 20 min had another N2BA/N2B ratio than those at 30–40°C [96]. We recommended heating titin in SDS at 35–40°C for 30–40 min [73, 84].

2.4. Other details of the electrophoretic study of titin

It is suggested that titin has a tendency to aggregate during electrophoresis, especially in gel systems that use a stacking gel or discontinuous buffers [88]. Fritz et al. [93], as well as Greaser and Warren [97, 98], recommended the inclusion of β-mercaptoethanol in the top anodic buffer to prevent disulfide crosslinking.

There is some peculiarity that should be noted with regard to the preparation of agarose-strengthened 2% polyacrylamide gel. Tatsumi and Hattori [85] to prevent polyacrylamide polymerizing before agarose is polymerized, cooled the glass cell with agarose solution (40°C) for 5 min in ice water. Similarly, we added the agarose solution to glass cells that were pre-cooled to 8–10°C and left the gel for 10 min in the refrigerator at 5°C. Then, we kept the gel for 30 min at 20°C and then for 2–2.5 h at 27°C.

It is recommended to perform electrophoresis using macroporous, agarose-strengthened polyacrylamide gels at low currents. Neagoe (of Wolfgang Linke's group) noted that the best separation of the high molecular weight proteins was obtained by running the electrophoresis overnight at 2 mA per 8.6 × 7.7 cm gel [99]. In our studies with the use of similar gels (8.0 × 10.0 × 0.10 cm), we perform electrophoresis at 3 mA for 40 min, then increasing the current strength up to 7–8 mA [96].

Granzier and Wang recommended to refresh the tank buffer once at 2.5 h to limit pH changes caused by electrolysis during electrophoresis [88].

3. Conclusion

In summary, it should be noted that SDS-PAGE of titin is quite difficult and not a routine procedure. Giant molecular mass and the susceptibility of titin to degrade during preparation significantly complicate the study of this protein by electrophoresis. It is necessary to know the three main rules for a successful study of titin by electrophoresis: (1) use protease inhibitors (leupeptin, E-64, protease inhibitor cocktail); (2) do not heat SDS samples higher than 40–60°C; and (3) judiciously select the type of the gel. Currently, the most suitable gels for analyzing titin are the following: (1) vertical agarose-strengthened 2% polyacrylamide gel [85]; (2) vertical 1% agarose gel [70]; and (3) horizontal agarose-strengthened 1.3% polyacrylamide gel [73].

It should be noted that we have obtained experimental evidence of existence in mammalian striated muscles of higher molecular weight isoforms of titin, named NT. According to our data, the development of pathological processes leads to the destruction of NT titins (**Figure 7**),

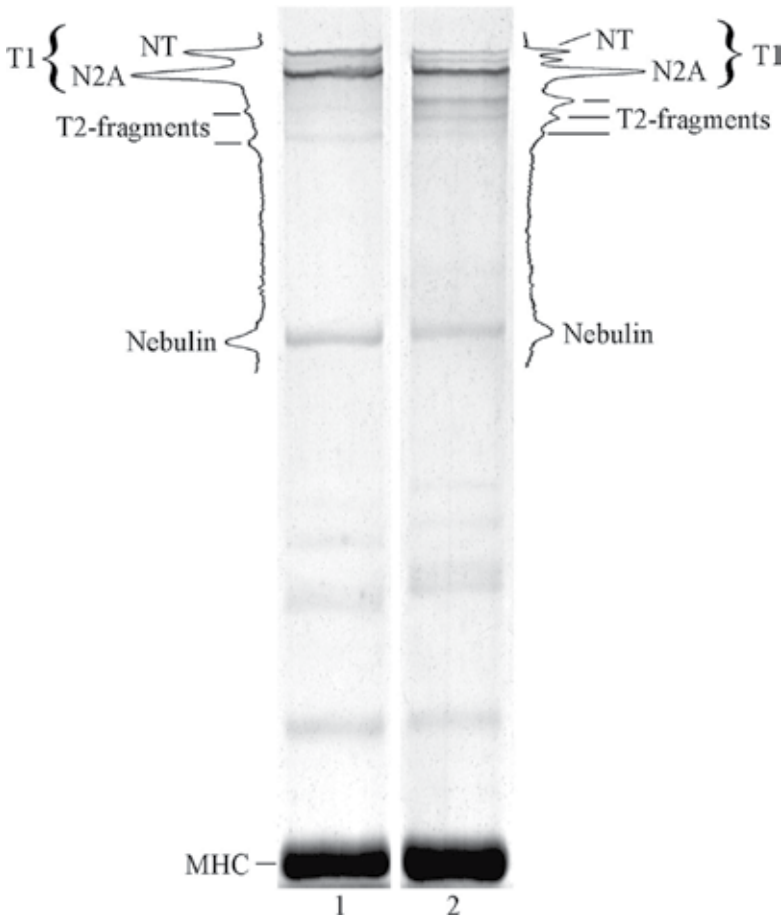

Figure 7. Increased proteolysis of titin and reduction of T1 content in m. Soleus of post-apoplectic patient. Vertical agarose-strengthened 2.3% polyacrylamide gel (8.0 × 10.0 × 0.10 cm) was used to separate titin isoforms. (1) Human m. soleus (control); (2) m. soleus of post-apoplectic patient.

which is accompanied by disorders of sarcomeric structure and impairment of the contractile ability of muscles [84]. In addition to fundamental value, these findings are of great practical value, because the testing of changes in titin content in muscles can be used in medical practice to diagnose pathological processes and evaluate effective approaches to their correction.

Acknowledgements

The authors are grateful to Drs. L. A. Tskhovrebova and J. Trinick for kindly providing the antibodies against titin. The authors also thank Sergey Udaltsov for helpful discussions on electrophoretic techniques. This work was financially supported by the Russian Foundation for Basic Research (project No. 17-04-00326) and by the Russian Science Foundation (project No. 18-15-00062).

† In memoriam to Dr. Zoya Podlubnaya.

Conflict of interest

Ivan M. Vikhlyantsev and Zoya A. Podlubnaya declare that there is no conflicts of interest.

Author details

Ivan M. Vikhlyantsev[1,2]* and Zoya A. Podlubnaya[1†]

*Address all correspondence to: ivanvikhlyantsev@gmail.com

1 Institute of Theoretical and Experimental Biophysics, Russian Academy of Sciences, Pushchino, Russia

2 Pushchino State Institute of Natural Science, Pushchino, Russia

† Zoya Podlubnaya died on March 26, 2018

References

[1] Tskhovrebova L, Trinick J. Titin and Nebulin in thick and thin filament length regulation. Sub-Cellular Biochemistry. 2017;**82**:285-318. DOI: 10.1007/978-3-319-49674-0_10

[2] Linke WA. Titin gene and protein functions in passive and active muscle. Annual Review of Physiology. 2018;**80**:389-411. DOI: 10.1146/annurev-physiol-021317-121234

[3] Tonino P, Kiss B, Strom J, Methawasin M, Smith JE 3rd, Kolb J, Labeit S, Granzier H. The giant protein titin regulates the length of the striated muscle thick filament. Nature Communications. 2017;**8**(1):1041. DOI: 10.1038/s41467-017-01144-9

[4] Herzog W. The multiple roles of titin in muscle contraction and force production. Biophysical Reviews. 2018. DOI: 10.1007/s12551-017-0395-y. [Epub ahead of print]

[5] Gautel M, Djinović-Carugo K. The sarcomeric cytoskeleton: From molecules to motion. The Journal of Experimental Biology. 2016;**219**(Pt 2):135-145. DOI: 10.1242/jeb.124941

[6] LeWinter MM, Granzier HL. Cardiac titin and heart disease. Journal of Cardiovascular Pharmacology. 2014;**63**(3):207-212. DOI: 10.1097/FJC.0000000000000007

[7] Labeit S, Lahmers S, Burkart C, Fong C, McNabb M, Witt S, Witt C, Labeit D, Granzier H. Expression of distinct classes of titin isoforms in striated and smooth muscles by alternative splicing, and their conserved interaction with filamins. Journal of Molecular Biology. 2006;**362**(4):664-681

[8] Suzuki J, Kimura S, Maruyama K. Electron microscopic filament lengths of connection and its fragments. Journal of Biochemistry. 1994;**116**(2):406-410

[9] Tskhovrebova L, Trinick J. Direct visualization of extensibility in isolated titin molecules. Journal of Molecular Biology. 1997;**265**(2):100-106

[10] Fürst DO, Nave R, Osborn M, Weber K. Repetitive titin epitopes with a 42 nm spacing coincide in relative position with known a band striations also identified by major myosin-associated proteins. An immunoelectron-microscopical study on myofibrils. Journal of Cell Science. 1989;**94**(Pt 1):119-125

[11] Houmeida A, Holt J, Tskhovrebova L, Trinick J. Studies of the interaction between titin and myosin. The Journal of Cell Biology. 1995;**131**(6 Pt 1):1471-1481

[12] Trombitás K, Pollack GH. Elastic properties of the titin filament in the Z-line region of vertebrate striated muscle. Journal of Muscle Research and Cell Motility. 1993;**14**(4):416-422

[13] Kulke M, Fujita-Becker S, Rostkova E, Neagoe C, Labeit D, Manstein DJ, Gautel M, Linke WA. Interaction between PEVK-titin and actin filaments: Origin of a viscous force component in cardiac myofibrils. Circulation Research. 2001;**89**(10):874-881

[14] Liversage AD, Holmes D, Knight PJ, Tskhovrebova L, Trinick J. Titin and the sarcomere symmetry paradox. Journal of Molecular Biology. 2001;**305**(3):401-409

[15] Gregorio CC, Granzier H, Sorimachi H, Labeit S. Muscle assembly: A titanic achievement? Current Opinion in Cell Biology. 1999;**11**(1):18-25

[16] Peckham M, Young P, Gautel M. Constitutive and variable regions of Z-disk titin/connectin in myofibril formation: A dominant-negative screen. Cell Structure and Function. 1997;**22**(1):95-101

[17] van der Ven PF, Bartsch JW, Gautel M, Jockusch H, Fürst DO. A functional knock-out of titin results in defective myofibril assembly. Journal of Cell Science. 2000;**113**(Pt 8): 1405-1414

[18] Horowits R, Kempner ES, Bisher ME, Podolsky RJ. A physiological role for titin and nebulin in skeletal muscle. Nature. 1986;**323**(6084):160-164

[19] Higuchi H. Changes in contractile properties with selective digestion of connectin (titin) in skinned fibers of frog skeletal muscle. Journal of Biochemistry. 1992;**111**(3):291-295

[20] Linke WA, Popov V, Pollack GH. Passive and active tension in single cardiac myofibrils. Biophysical Journal. 1994;**67**(2):782-792

[21] Granzier HL, Irving TC. Passive tension in cardiac muscle: Contribution of collagen, titin, microtubules, and intermediate filaments. Biophysical Journal. 1995;**68**(3):1027-1044

[22] Helmes M, Trombitás K, Granzier H. Titin develops restoring force in rat cardiac myocytes. Circulation Research. 1996;**79**(3):619-626

[23] Kimura S, Maruyama K, Huang YP. Interactions of muscle beta-connectin with myosin, actin, and actomyosin at low ionic strengths. Journal of Biochemistry. 1984;**96**(2):499-506

[24] Cazorla O, Vassort G, Garnier D, Le Guennec JY. Length modulation of active force in rat cardiac myocytes: Is titin the sensor? Journal of Molecular and Cellular Cardiology. 1999;**31**(6):1215-1227

[25] Podlubnaya ZA, Shpagina MD, Vikhlyantsev IM, Malyshev SL, Udaltsov SN, Ziegler C, Beinbrech G. Comparative electron microscopic study on projectin and titin binding to F-actin. Insect Biochemistry and Molecular Biology. 2003;**33**(8):789-793

[26] Vikhlyantsev IM, Podlubnaya ZA. Phosphorylation of sarcomere cytoskeletal proteins as an adaptive factor of inhibiting the contractile activity of muscle in hibernation. Biophysics. 2003;**48**(3):471-476

[27] Niederländer N, Raynaud F, Astier C, Chaussepied P. Regulation of the actin-myosin interaction by titin. European Journal of Biochemistry. 2004;**271**(22):4572-4581

[28] Bianco P, Nagy A, Kengyel A, Szatmári D, Mártonfalvi Z, Huber T, Kellermayer MS. Interaction forces between F-actin and titin PEVK domain measured with optical tweezers. Biophysical Journal. 2007;**93**(6):2102-2109

[29] Fukushima H, Chung CS, Granzier H. Titin-isoform dependence of titin-actin interaction and its regulation by S100A1/Ca2+ in skinned myocardium. Journal of Biomedicine & Biotechnology. 2010;**2010**:727239. DOI: 10.1155/2010/727239

[30] Vikhlyantsev IM, Okuneva AD, Shpagina MD, Shumilina YV, Molochkov NV, Salmov NN, Podlubnaya ZA. Changes in isoform composition, structure, and functional properties of titin from Mongolian gerbil (Meriones unguiculatus) cardiac muscle after space flight. Biochemistry (Mosc). 2011;**76**(12):1312-1320. DOI: 10.1134/S0006297911120042

[31] Li Y, Lang P, Linke WA. Titin stiffness modifies the force-generating region of muscle sarcomeres. Scientific Reports. 2016;**6**:24492. DOI: 10.1038/srep24492

[32] Tskhovrebova L, Trinick J. Muscle disease: A giant feels the strain. Nature Medicine. 2005; **11**(5):478-479

[33] Lange S, Xiang F, Yakovenko A, Vihola A, Hackman P, Rostkova E, Kristensen J, Brandmeier B, Franzen G, Hedberg B, Gunnarsson LG, Hughes SM, Marchand S, Sejersen T, Richard I, Edström L, Ehler E, Udd B, Gautel M. The kinase domain of titin controls muscle gene expression and protein turnover. Science. 2005;**308**(5728):1599-1603

[34] Voelkel T, Linke WA. Conformation-regulated mechanosensory control via titin domains in cardiac muscle. Pflügers Archiv. 2011;**462**(1):143-154. DOI: 10.1007/s00424-011-0938-1

[35] Gautel M. The sarcomeric cytoskeleton: Who picks up the strain? Current Opinion in Cell Biology. 2011;**23**(1):39-46. DOI: 10.1016/j.ceb.2010.12.001

[36] Gautel M. Cytoskeletal protein kinases: Titin and its relations in mechanosensing. Pflügers Archiv. 2011;**462**(1):119-134. DOI: 10.1007/s00424-011-0946-1

[37] Krysiak J, Unger A, Beckendorf L, Hamdani N, von Frieling-Salewsky M, Redfield MM, Dos Remedios CG, Sheikh F, Gergs U, Boknik P, Linke WA. Protein phosphatase 5 regulates titin phosphorylation and function at a sarcomere-associated mechanosensor complex in cardiomyocytes. Nature Communications. 2018;**9**(1):262. DOI: 10.1038/s41467-017-02483-3

[38] Linke WA, Krüger M. The giant protein titin as an integrator of myocyte signaling pathways. Physiology (Bethesda). 2010;**25**(3):186-198. DOI: 10.1152/physiol.00005.2010

[39] Gerull B. Between disease-causing and an innocent bystander: The role of titin as a modifier in hypertrophic cardiomyopathy. The Canadian Journal of Cardiology. 2017; **33**(10):1217-1220. DOI: 10.1016/j.cjca.2017.07.010

[40] Hessel AL, Nishikawa KC. Effects of a titin mutation on negative work during stretch-shortening cycles in skeletal muscles. Experimental Biology. 2017;**220**(Pt22):4177-4185. DOI: 10.1242/jeb.163204

[41] Tayal U, Newsome S, Buchan R, Whiffin N, Halliday B, Lota A, Roberts A, Baksi AJ, Voges I, Midwinter W, Wilk A, Govind R, Walsh R, Daubeney P, Jarman JWE, Baruah R, Frenneaux M, Barton PJ, Pennell D, Ware JS, Prasad SK, Cook SA. Phenotype and clinical outcomes of titin cardiomyopathy. Journal of the American College of Cardiology. 2017;**70**(18):2264-2274. DOI: 10.1016/j.jacc.2017.08.063

[42] Vikhorev PG, Smoktunowicz N, Munster AB, Copeland O, Kostin S, Montgiraud C, Messer AE, Toliat MR, Li A, Dos Remedios CG, Lal S, Blair CA, Campbell KS, Guglin M, Knoll R, Marston SB. Abnormal contractility in human heart myofibrils from patients with dilated cardiomyopathy due to mutations in TTN and contractile protein genes. Scientific Reports. 2017;**7**(1):14829. DOI: 10.1038/s41598-017-13675-8

[43] Gritsyna YV, Salmov NN, Bobylev AG, Ulanova AD, Kukushkin NI, Podlubnaya ZA, Vikhlyantsev IM. Increased autolysis of μ-Calpain in skeletal muscles of chronic alcohol-fed rats. Alcoholism, Clinical and Experimental Research. 2017;**41**(10):1686-1694. DOI: 10.1111/acer.13476

[44] Ehsan M, Jiang H, L Thomson K, Gehmlich K. When signalling goes wrong: Pathogenic variants in structural and signalling proteins causing cardiomyopathies. Journal of Muscle Research and Cell Motility. 2017;**38**(3-4):303-316. DOI: 10.1007/s10974-017-9487-3

[45] Ware JS, Cook SA. Role of titin in cardiomyopathy: From DNA variants to patient stratification. Nature Reviews Cardiology. 2017;**14**. DOI: 10.1038/nrcardio.2017.190

[46] Tasca G, Udd B. Hereditary myopathy with early respiratory failure (HMERF): Still rare, but common enough. Neuromuscular Disorders. 2017;**12**. pii: S0960-8966(17)31223-3. DOI: 10.1016/j.nmd.2017.12.002

[47] Rexiati M, Sun M, Guo W. Muscle-specific Mis-splicing and heart disease exemplified by RBM20. Genes (Basel). 2018;**9**(1):1-13. pii: E18. DOI: 10.3390/genes9010018

[48] Wang K, McClure J, Tu A. Titin: Major myofibrillar components of striated muscle. Proceedings of the National Academy of Sciences of the United States of America. 1979; **76**(8):3698-3702

[49] Etlinger JD, Zak R, Fischman DA. Compositional studies of myofibrils from rabbit striated muscle. The Journal of Cell Biology. 1976;**68**(1):123-141

[50] Wang K. Purification of titin and nebulin. Methods Enzymol. 1982;**85 Pt B**:264-274

[51] Maruyama K, Natori R, Nonomura Y. New elastic protein from muscle. Nature. 1976;**262**(5563):58-60

[52] Maruyama K, Matsubara S, Natori R, Nonomura Y, Kimura S. Connectin, an elastic protein of muscle. Characterization and function. Journal of Biochemistry. 1977;**82**(2):317-337

[53] Matsubara S, Maruyama K. Role of connectin in the length-tension relation of skeletal and cardiac muscles. The Japanese Journal of Physiology. 1977;**27**(5):589-600

[54] Toyoda N, Maruyama K. Fine structure of connectin nets in cardiac myofibrils. Journal of Biochemistry. 1978;**84**(1):239-241

[55] Maruyama K, Kimura S, Ohashi K, Kuwano Y. Connectin, an elastic protein of muscle. Identification of "titin" with connectin. Journal of Biochemistry. 1981;**89**(3):701-709

[56] Weber K, Osborn M. The reliability of molecular weight determinations by dodecyl sulfate-polyacrylamide gel electrophoresis. The Journal of Biological Chemistry. 1969; **244**(16):4406-4412

[57] Maruyama K, Kimura S, Yoshidomi H, Sawada H, Kikuchi M. Molecular size and shape of beta-connectin, an elastic protein of striated muscle. Journal of Biochemistry. 1984 May;**95**(5):1423-1433

[58] Hu DH, Kimura S, Maruyama K. Sodium dodecyl sulfate gel electrophoresis studies of connectin-like high molecular weight proteins of various types of vertebrate and invertebrate muscles. Journal of Biochemistry. 1986 May;**99**(5):1485-1492

[59] Wang K, Wright J. Architecture of the sarcomere matrix of skeletal muscle: Immunoelectron microscopic evidence that suggests a set of parallel inextensible nebulin filaments anchored at the Z line. The Journal of Cell Biology. 1988;**107**(6 Pt 1):2199-2212

[60] Wang K, McCarter R, Wright J, Beverly J, Ramirez-Mitchell R. Regulation of skeletal muscle stiffness and elasticity by titin isoforms: A test of the segmental extension model of resting tension. Proceedings of the National Academy of Sciences of the United States of America. 1991;**88**(16):7101-7105

[61] Horowits R. Passive force generation and titin isoforms in mammalian skeletal muscle. Biophysical Journal. 1992 Feb;**61**(2):392-398

[62] Kawamura Y, Ohtani Y, Maruyama K. Biodiversity of the localization of the epitopes to connectin antibodies in the sarcomeres of lamprey, electric ray, and horse mackerel skeletal muscles. Tissue & Cell. 1994;**26**(5):677-685

[63] Spierts IL, Akster HA, Granzier HL. Expression of titin isoforms in red and white muscle fibres of carp (Cyprinus carpio L.) exposed to different sarcomere strains during swimming. Journal of Comparative Physiology B. 1997;**167**(8):543-551

[64] Labeit S, Kolmerer B. Titins: Giant proteins in charge of muscle ultrastructure and elasticity. Science. 1995;**270**(5234):293-296

[65] Freiburg A, Trombitas K, Hell W, Cazorla O, Fougerousse F, Centner T, Kolmerer B, Witt C, Beckmann JS, Gregorio CC, Granzier H, Labeit S. Series of exon-skipping events in the elastic spring region of titin as the structural basis for myofibrillar elastic diversity. Circulation Research. 2000;**86**(11):1114-1121

[66] Bang ML, Centner T, Fornoff F, Geach AJ, Gotthardt M, McNabb M, Witt CC, Labeit D, Gregorio CC, Granzier H, Labeit S. The complete gene sequence of titin, expression of an unusual approximately 700-kDa titin isoform, and its interaction with obscurin identify a novel Z-line to I-band linking system. Circulation Research. 2001;**89**(11):1065-1072

[67] Guo W, Bharmal SJ, Esbona K, Greaser ML. Titin diversity–alternative splicing gone wild. Journal of Biomedicine & Biotechnology. 2010;**2010**:753675. DOI: 10.1155/2010/753675

[68] Gerull B. The rapidly evolving role of titin in cardiac physiology and cardiomyopathy. The Canadian Journal of Cardiology. 2015;**31**(11):1351-1359. DOI: 10.1016/j.cjca.2015.08.016

[69] Cazorla O, Freiburg A, Helmes M, Centner T, McNabb M, Wu Y, Trombitás K, Labeit S, Granzier H. Differential expression of cardiac titin isoforms and modulation of cellular stiffness. Circulation Research. 2000;**86**(1):59-67

[70] Warren CM, Krzesinski PR, Greaser ML. Vertical agarose gel electrophoresis and electroblotting of high-molecular-weight proteins. Electrophoresis. 2003;**24**(11):1695-1702

[71] Warren CM, Jordan MC, Roos KP, Krzesinski PR, Greaser ML. Titin isoform expression in normal and hypertensive myocardium. Cardiovascular Research. 2003;**59**(1):86-94

[72] Neagoe C, Opitz CA, Makarenko I, Linke WA. Gigantic variety: Expression patterns of titin isoforms in striated muscles and consequences for myofibrillar passive stiffness. Journal of Muscle Research and Cell Motility. 2003;**24**(2-3):175-189

[73] Vikhlyantsev IM, Podlubnaya ZA. On the titin isoforms. Biophysics. 2006;**51**(5):842-848

[74] Lahmers S, Wu Y, Call DR, Labeit S, Granzier H. Developmental control of titin isoform expression and passive stiffness in fetal and neonatal myocardium. Circulation Research. 2004;**94**(4):505-513

[75] Prado LG, Makarenko I, Andresen C, Krüger M, Opitz CA, Linke WA. Isoform diversity of giant proteins in relation to passive and active contractile properties of rabbit skeletal muscles. The Journal of General Physiology. 2005;**126**(5):461-480

[76] Warren CM, Krzesinski PR, Campbell KS, Moss RL, Greaser ML. Titin isoform changes in rat myocardium during development. Mechanisms of Development. 2004;**121**(11):1301-1312

[77] Opitz CA, Leake MC, Makarenko I, Benes V, Linke WA. Developmentally regulated switching of titin size alters myofibrillar stiffness in the perinatal heart. Circulation Research. 2004;**94**(7):967-975. Epub 26 February 2004

[78] Greaser ML, Krzesinski PR, Warren CM, Kirkpatrick B, Campbell KS, Moss RL. Developmental changes in rat cardiac titin/connectin: Transitions in normal animals and in mutants with a delayed pattern of isoform transition. Journal of Muscle Research and Cell Motility. 2005;**26**(6-8):325-332

[79] Krüger M, Kohl T, Linke WA. Developmental changes in passive stiffness and myofilament Ca2+ sensitivity due to titin and troponin-I isoform switching are not critically triggered by birth. American Journal of Physiology. Heart and Circulatory Physiology. 2006;**291**(2):H496-H506

[80] Vikhlyantsev IM, Podlubnaya ZA. Nuances of electrophoresis study of titin/connectin. Biophysical Reviews. 2017;**9**(3):189-199. DOI: 10.1007/s12551-017-0266-6

[81] Greaser ML, Warren CM, Esbona K, Guo W, Duan Y, Parrish AM, Krzesinski PR, Norman HS, Dunning S, Fitzsimons DP, Moss RL. Mutation that dramatically alters rat

titin isoform expression and cardiomyocyte passive tension. Journal of Molecular and Cellular Cardiology. 2008;**44**(6):983-991. DOI: 10.1016/j.yjmcc.2008.02.272

[82] Guo W, Schafer S, Greaser ML, Radke MH, Liss M, Govindarajan T, Maatz H, Schulz H, Li S, Parrish AM, Dauksaite V, Vakeel P, Klaassen S, Gerull B, Thierfelder L, Regitz-Zagrosek V, Hacker TA, Saupe KW, Dec GW, Ellinor PT, MacRae CA, Spallek B, Fischer R, Perrot A, Özcelik C, Saar K, Hubner N, Gotthardt M. RBM20, a gene for hereditary cardiomyopathy, regulates titin splicing. Nature Medicine. 2012;**18**(5):766-773. DOI: 10.1038/nm.2693

[83] Li S, Guo W, Schmitt BM, Greaser ML. Comprehensive analysis of titin protein isoform and alternative splicing in normal and mutant rats. Journal of Cellular Biochemistry. 2012;**113**(4):1265-1273. DOI: 10.1002/jcb.23459

[84] Vikhlyantsev IM, Podlubnaya ZA. New titin (connectin) isoforms and their functional role in striated muscles of mammals: Facts and suppositions. Biochemistry (Mosc). 2012;**77**(13):1515-1535. DOI: 10.1134/S0006297912130093

[85] Tatsumi R, Hattori A. Detection of giant myofibrillar proteins connectin and nebulin by electrophoresis in 2% polyacrylamide slab gels strengthened with agarose. Analytical Biochemistry. 1995;**224**(1):28-31

[86] Vikhlyantsev IM, Malyshev SL, Shenkman BS, Podlubnaya ZA. Composition of the titin family proteins in skeletal muscle of ground squirrel during hibernation and rats in simulated microgravity. Biophysics. 2004;**49**(6):895-900

[87] Kruger M, Wright J, Wang K. Nebulin as a length regulator of thin filaments of vertebrate skeletal muscles: Correlation of thin filament length, nebulin size, and epitope profile. The Journal of Cell Biology. 1991;**115**(1):97-107

[88] Granzier HL, Wang K. Gel electrophoresis of giant proteins: Solubilization and silver-staining of titin and nebulin from single muscle fiber segments. Electrophoresis. 1993; **14**(1-2):56-64

[89] Vikhlyantsev IM, Podlubnaya ZA. Composition of titin isoforms of skeletal and cardiac muscles in pathologies. Biophysics. 2008;**53**(6):592-597

[90] Latsabidze IL. Electron microscopic study of the structure of myosin containing filaments as part of anisotropic discs of vertebrate striated muscles: Candidate's dissertation [in Russian]. Pushchino: Erevan State University; 1985. p. 153

[91] Wang K. Sarcomere-associated cytoskeletal lattices in striated muscle. Review and hypothesis. Cell and Muscle Motility. 1985;**6**:315-369

[92] Linke WA, Ivemeyer M, Labeit S, Hinssen H, Rüegg JC, Gautel M. Actin-titin interaction in cardiac myofibrils: Probing a physiological role. Biophysical Journal. 1997;**73**(2):905-919

[93] Fritz JD, Swartz DR, Greaser ML. Factors affecting polyacrylamide gel electrophoresis and electroblotting of high-molecular-weight myofibrillar proteins. Analytical Biochemistry. 1989;**180**(2):205-210

[94] King NL, Kurth L. SDS gel electrophoresis studies of connectin. In: Parry D, Creamer LK, editors. Fibrous Proteins: Scientific, Industrial and Medical Aspects. Vol. 2. New York: Academic; 1980. pp. 57-66

[95] Mitsuhashi T, Kasai M, Hatae K. Detection of giant myofibrillar proteins connectin and nebulin in fish meat by electrophoresis in 3-5 gradient sodium dodecyl sulfate polyacrylamide slab gels. Journal of Agricultural and Food Chemistry. 2002;**50**(26):7499-7503

[96] Vikhlyantsev IM. Polymorphism of titin of striated muscles under normal conditions, during adaptation and pathology: Doctoral's dissertation [in Russian]. Institute of Theoretical and Experimental Biophysics, Russian Academy of Sciences, Pushchino; 2011. p. 235

[97] Greaser ML, Warren CM. Efficient electroblotting of very large proteins using a vertical agarose electrophoresis system. Methods in Molecular Biology. 2009;**536**:221-227. DOI: 10.1007/978-1-59745-542-8_24

[98] Greaser ML, Warren CM. Protein electrophoresis in agarose gels for separating high molecular weight proteins. Methods in Molecular Biology. 2012;**869**:111-118. DOI: 10.1007/978-1-61779-821-4_10

[99] Neagoe C. Biochemical and mechanical investigation of cardiac titin isoforms. Doctor scientiarum humanarum (Dr. sc. hum.). Heidelberg: Ruprecht-Karls-Universität; 2008

Chapter 4

Electrophoresis in the Comet Assay

Gunnar Brunborg, Linn Rolstadaas and
Kristine B. Gutzkow

Additional information is available at the end of the chapter

http://dx.doi.org/10.5772/intechopen.76880

Abstract

The comet assay is a sensitive technique to measure lesions in DNA, based on electrophoretic separation of DNA from cells embedded in agarose. Movement of DNA fragments is determined by the potential (V/cm), the time, and the viscosity of the medium (agarose). There is historically considerable confusion as to other factors, that is, current, liquid depths, circulation of the liquid, and temperature. Lack of standardization of electrophoresis including suboptimal power supplies and electrophoresis tanks causes considerable variations within and between laboratories. Ring trials have not been able to clearly identify the cause(s) of variation. Comparison of comet data from cohorts of human blood lymphocytes is used in the COST project hCOMET to identify early biomarkers of the disease. This calls for standardization of analysis. We performed measurements of electric potentials in a tank using multiple electrodes. Variations (time/position) were reduced by circulating electrophoresis liquid at 10% (volume) per min; this also stabilized the temperature. Circulation was accompanied by only slightly reduced variation in DNA damage among 384 irradiated cell samples electrophoresed concomitantly. In conclusion, comparing data between laboratories and cohorts must give emphasis to electrophoresis conditions. Results should be specified with respect to voltage (V/cm), time, and agarose concentration. We expect that suitable correction factors for these parameters may reduce inter-laboratory variations in comet data, allowing more precise comparison of results from different human cohorts.

Keywords: comet assay, electrophoresis, electric potential, agarose, power supply

1. Introduction

Efficient methods for quantifying DNA damage in cells of various types have been available for more than 30 years. Methods have suffered from low sensitivity, complicated protocols, or

they were used only for a limited spectrum of cell types. The assay mostly used during the last three decades was first published by the Swedes Östling and Johanson in 1984 [1]; other versions followed, from N.P. Singh and R. Tice in 1988 [2], and Peggy Olive and co-workers [3]. These protocols are in principle quite similar but vary in their use of neutral or alkaline electrophoresis conditions and also in some other steps of the procedures, such as lysis cell conditions. The methods were initially given different names: microelectrophoresis [1], single cell gel electrophoresis [2], and Comet Assay [3]. The latter name—which we will mostly use in this chapter—stems from the comet-like image seen in micrographs of damaged cellular DNA as it stretches out after electrophoresis.

In the comet assay, cellular DNA embedded in thin layers of agarose (researchers choose different concentrations) are electrophoresed while placed in a horizontal electrophoresis tank. At this stage the cells are dead and devoid of most of their proteins—whether they originate from a live organism: human blood or a specific organ, an animal, a fish or a sea star, or a plant (there is in fact hardly no limitation)—or from cells or organ cultures treated with radiation, or chemicals in vitro.

The comet assay has often been used simply to show the formation or presence of DNA damage in cells in a relative scale, without any reference to a standardized output or a calibration. However, in various applications, there is a need for standardization and calibration of comet assay data. Examples are when results from different experiments, cell types, and laboratories are to be compared, or when different human cohorts are combined in international collaborative studies. In the EU COST action hCOMET, the main aims are to create a unified database of comet assay data relating to human health and disease that will be the base for pooled analysis on DNA damage and repair in humans; the ultimate purpose is to investigate the significance of comet assay results as prognostic markers of disease. Such comparisons do not make sense if the sensitivity of the assays used is very different.

Attempts have indeed been made to establish standardized protocols, and/or identifying the experimental steps that are most significant in determining the sensitivity and reproducibility of the comet assay. Validation studies and ring trials of various types have been described [4–9], involving, for example, distribution of treated cells to different laboratories followed by local comet assay analysis, or local treatment, and analysis of cells with chemical mutagens according to specific protocols. In spite of these attempts, no key factor explaining the observed rather large inter-laboratory differences has yet been identified [8]. It is concluded that there is hence still a need for further validation of the assay [5].

The separation of DNA fragments according to their size and structure—either single- or double-stranded—is in all versions of the comet assay based on electrophoresis at low-voltage (across the tank approximately 25 V) and short duration (20–30 mins). Cell isolation and manipulation, including long-time storage through freezing, are of uttermost importance for the final output measured by the assay; this concerns, in particular, the background level of DNA damage in "untreated" cells. We shall not deal with such issues here, but rather focus on technical aspects of the electrophoresis, including some of its physics and chemistry.

http://dx.doi.org/10.5772/intechopen.76880

2. Comet assay electrophoresis in principle

Analysis of charged molecules by means of an electric potential (or electric field) is a technique that has been known, understood and applied in experimental biology and biochemistry for decades. Electrophoresis separates charged molecules according to their mobility. The driving force is the electric potential; the mobility depends on the charge, size and shape of the molecules, and the movement is inhibited by viscous forces (depending on the medium including its pore size). Cellular DNA (in a diploid human cell) has a total size of approximately 2 $*10^{12}$ Da, which in an intact cell is organized in 23 pairs of chromosomes. Under alkaline conditions, DNA from a lysed cell exists in stretches of single helixes, which may be of all sizes, either linear and free or more or less entangled with each other. When these negatively charged molecules are broken—either into discrete fragments or into a distribution of differently sized molecules—they are separated in size when subjected to an electric potential in a medium through which they have some freedom to move.

The charge per unit length of DNA is determined by its base composition, which is quite constant on a large scale. The movement (velocity per time) may be adjusted via the electric potential (V/cm) and the viscosity (related, primarily, to the agarose concentration), so that the separation of a distribution of differently sized DNA molecules may be optimized. This optimization may vary depending on the specific application of the assay. For most purposes, however, molecular sizes expected to be measurable in the comet assay would be in the range $2*10^8$–10^{10} Da (i.e., from a few hundred to ten thousand breaks per cell). The DNA distribution after electrophoresis is determined with fluorescent micrographic imaging. Using various algorithms, characteristic parameters have been worked out to characterize the population of differently sized molecules, to give the medium, the average and the distribution of the molecular weight or size (denoted scoring).

3. Early protocols for electrophoresis in the comet assay

Publications during the last 30 years specify experimental protocols often by referring to the early comet assay protocols. Quite often, however, the conditions are still undefined or confusing. This relates, in particular, to a lack of precise definition of the local electric potential; at the same time, there is a frequent—and surprising—specification of the current used (mostly 300 mA). We have attempted to understand the basis for the apparent misconceptions; it seems to reflect history rather than science. The electrophoresis step was described and specified somewhat differently in the three early publications [1–3]. Östling and Johanson [1] separated cellular DNA under neutral (non-alkaline) conditions, "… and electric potential of about 5 V/cm is applied for 5 minutes …". The tank size, the current or the volume of liquid are not specified, which is in fact quite OK since the magnitude of the local electric potential is defined. Singh and

co-workers, the first to describe an alkaline version of the assay, specify that electrophoresis is carried out for 20 mins at 25 V, at 300 mA, and a depth of liquid of 0.25 cm [2]. Since the tank dimensions are not known, the local electric potential is undefined. In a follow-up review paper, the electrophoresis is at 12 V and 100 mA, with the circulation of the electrophoresis solution at 100 ml/min of a total volume of 1 liter [10]; again, this implies an undefined electric potential. In a later publication [11], the same group describes electrophoresis at 12 V (0.4 V/cm), 250 mA, and a duration of 20 mins.

In guidelines from 2000 [12], R.T. Tice (who was also co-author of the 1988 protocol with N. P. Singh [2]) states that "… due to the large variability in the size of commercially available electrophoresis units, it is more accurate and useful to present the voltage in V/cm". Concerning voltage, 0.7–1.0 V/cm and a duration of 5–40 mins are specified, and circulation (whereas current, liquid volume, and depth are not mentioned in these guidelines) [12]. In the comet assay later described by Peggy Olive [3, 13], electrophoresis was run at 1 V/cm for 20 min (nothing said about volume and current). In a follow-up protocol by Peggy Olive in 2006 [14], electrophoresis is conducted at 0.6 V/cm for 25 min; "The current should be about 40 mA if using 20 V. The distance in centimeters is measured between the negative and positive electrophoresis in the electrophoresis chamber." There is a problem associated with this approach, which we will discuss later.

Among the early comet assay protocols, the most cited ones (by March 2018) are [2] (6522 citations) and [12] (2906 citations); citations for Östling & Johansson [1] are not available. Judging from these bibliographic data, and since the electrophoresis conditions in [2] are undefined with respect to electric potential but recommending a specific current (300 mA), it seems that much of the confusion in the literature stems from the uncritical reference to [2]. A more frequent use of the guidelines [12] might have avoided some of the unexpected comet assay results published during the last 20–30 years.

The current plays no direct role in electrophoretic mobility, but may indirectly affect the local distribution of the electric potential in a tank. The organisation for economic co-operation and development (OECD) In vivo comet assay Test Guidelines protocol 489 [15] from 2014, correctly states that the "… level of DNA migration is linearly associated with the duration of electrophoresis, and also with the electric potential (V/cm)." However, there is still the recommendation of a "starting current of 300 mA (—), the depth should be adjusted to achieve these conditions, and the current at the start and the end of the electrophoresis should be recorded". It is worth noticing, however, that attempts to control the current often lead to very shallow liquid levels. In [16] the level of the buffer is described as "… about 2–3 mm above the agarose on the slide"; in [2] the depth was 0.25 cm. It is often underlined in the protocols that the electrophoresis tank must be in the level, so that the depth above the gels is equal over the platform surface. However, keeping a large tank level in each run, within an error of, for example, 1 mm is hardly achievable. The implication is that the resistance of the liquid on the platform will vary relatively much, leading to potentially large differences in local electric potential. Specifying a much higher depth, for example, 6–10 mm solves this problem, although a larger current would put demands on the power supply. We will get back to this problem in the recommendations at the end of this text.

4. Results

4.1. Electrophoresis conditions and DNA damage levels

We have previously studied experimentally [17] the conditions which determine the level of migration measured in the comet assay. Cell cultures of two types were treated with genotoxicants and then assayed for DNA damage using different physical conditions during electrophoresis. Linear regression of the experimental data in [17] shows highly linear relationships for V/cm and time (**Table 1**) and an inverse relationship for agarose. Fitting straight lines to the figures in [17] results in the regression data (for human blood mononuclear cells) in **Table 1**.

There was no effect of altering the electrophoresis current (between 210 and 400 mA), except for a slight downward trend which is explained as an indirect effect on the electric potential [17].

4.2. Position- and time-dependent variations in local electric potential

Since the local electric potential determines the mobility of DNA fragments in the comet assay, it is essential that the electric potential is defined at all positions of the electrophoresis platform. This may be particularly important if the comet gels are small in the surface. We have described a high-throughput comet assay with 96 minigels, each of 4 μl, placed in an array of Gelbond plastic membranes as substrate [18, 19]. The minigels give results which are highly similar to results obtained with standard glass slides. We also evaluated this revised comet assay with respect to variation in DNA damage levels measured within one electrphoresis. Based on preliminary studies [18], DNA damage measured in parallel samples depended significantly on the circulation of the liquid during electrophoresis. We now report on a series of measurements of local electric potentials, with the purpose of identifying possible time-dependent differences in electrophoresis between neighboring samples. A multi-electrode gauge was made (**Figure 1**) consisting of 20 evenly spaced (5 mm) platinum electrodes, each covered with a thin plastic tube except for 1 mm protruding free end.

This multi-electrode gauge was placed in an electrophoresis tank with the free electrode ends immersed in a thin layer of agarose of the same concentration (0.675%) as used to embed cells in the comet assay (**Figure 2**) [20]. The electrode ends were a fraction of a millimeter above the

Factor and unit (and range)	*Linear regression parameters*	*Goodness-of-fit (R^2)*	*Comment*
Voltage (V/cm) (0.16–1.48)	34.1 (*V/cm)	0.964	Linear, through zero
Time (min) (5–40)	1.42 (*min)	0.950	Linear, through zero
Agarose (%) (0.4–0.95)	−30.29 (*% + 52.7)	0.955	Inverse

Table 1. Linear regression of data from [17], with goodness-of-fit. The regression curves for electric potential (V/cm) and time (min) were both forced through zero.

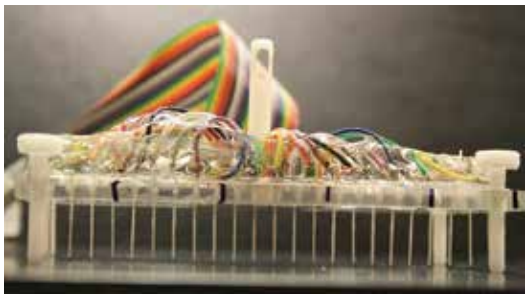

Figure 1. Multi-electrode gauge connected to a multiplexing digital voltmeter (Agilent 34972A with Multiplexer 34901A) allowing the potential at up to 20 electrodes to be sequentially scanned at intervals.

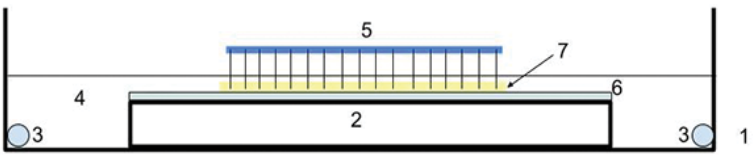

Figure 2. A schematic diagram illustrating the electrophoresis tank (1) with the platform (2) and the electrodes (3). During electrophoresis the tank was filled with liquid (4) and an electrode gauge (5) was connected to an electrode plate (6) and placed across the center of the platform with its electrodes covered in agarose (7) when performing the measurements of the electric potentials.

GelBond films. The dimensions of the tank are listed in **Table 2**. The electric potential of each minielectrode could be scanned and recorded automatically during 1 s, for every 10 s, using a multiplexer and a digital voltmeter with input resistance in the mega-ohm range. This also allowed continuous measurements of the temperature in the solution.

Systematic studies of the role of circulation were carried out, using external circulation at 21, 58, 109, 201, and 285 ml/min. With a total volume of 1640 ml, this compares to 1, 4, 7, 12, and 17% exchange of volume per min, respectively. Apparently, there were significant differences in electrode potentials at neighboring positions and also time-dependent changes (**Figures 3** and **4**, upper panels). With circulation, however, these variations were much reduced (**Figures 3** and **4**, lower panels; figures show graphs for 109 ml/min circulation). In **Figure 4**, the data from **Figure 3** have been converted into local electric potentials.

Description	*Length (mm)*	*Width (mm)*	*Height (mm)*
Tank	290	262	70
Platform	180	262	26
Side wells × 2	110	262	26
Electrode plate	180	262	9

Table 2. Physical dimensions of the electrophoresis tank and the electrode plate.

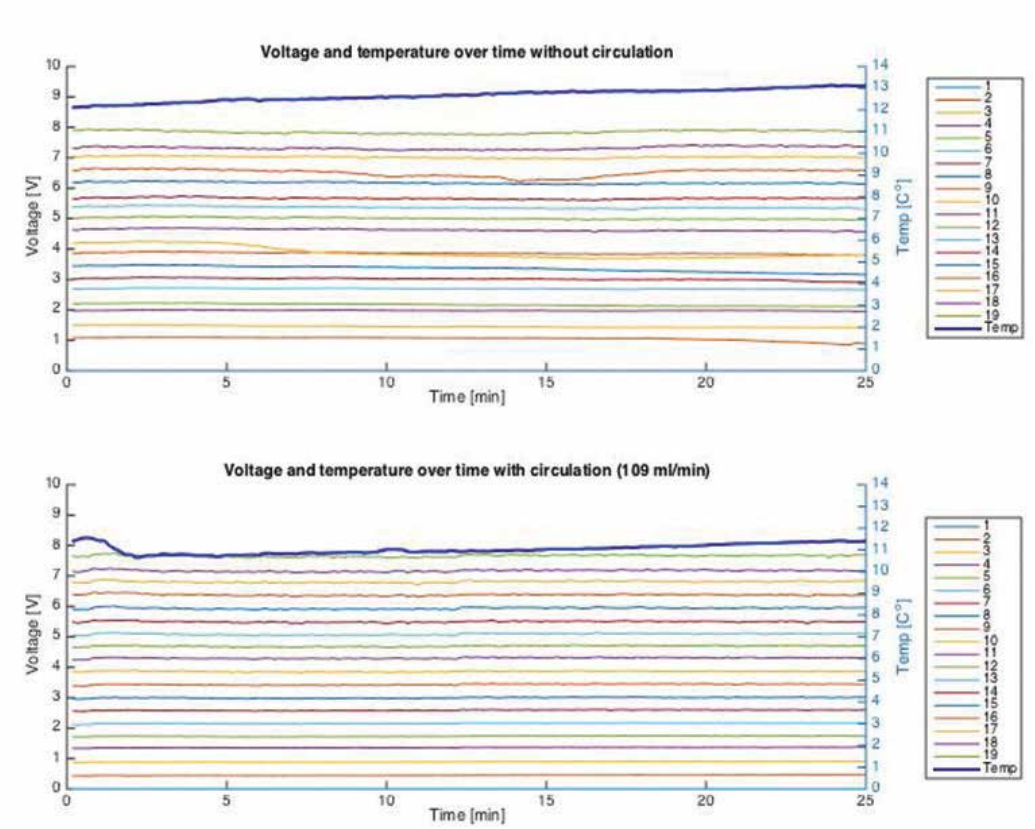

Figure 3. Measured voltage across the platform during electrophoresis. The relative voltage at each electrode and temperature over time during an electrophoresis time of 25 mins from one representative experiment with (109 ml/min) and without circulation. The number of each electrode and the temperature are indicated to the right of the figure. The blue thick lines in both plots represent the temperature. The figures are from one representative experiment [20].

The calculated total migration of DNA in each electrophoresis is derived from the time-integrated electric potential (dimension V/cm*min). **Figure 5** presents these data for electrophoresis during 25 min, with and without circulation. Corrections due to some differences in the spacing between the electrodes were included in the calculations.

These experiments were repeated several times; data averaged for all electrodes are presented in **Figure 6**. In total, there was a consistent and clearly reduced inter-experimental variation, when circulation was used (109 ml/min).

4.3. Position-dependent variations in DNA damage measured in samples exposed to irradiation

The electric potential measurements were paralleled by analysis of DNA damage in cell samples from a batch of human blood mononuclear cells exposed to a fixed dose of ionizing radiation (X-rays) on ice. This dose (8 Gy) was established from a dose-response curve (**Figure 7**). Materials

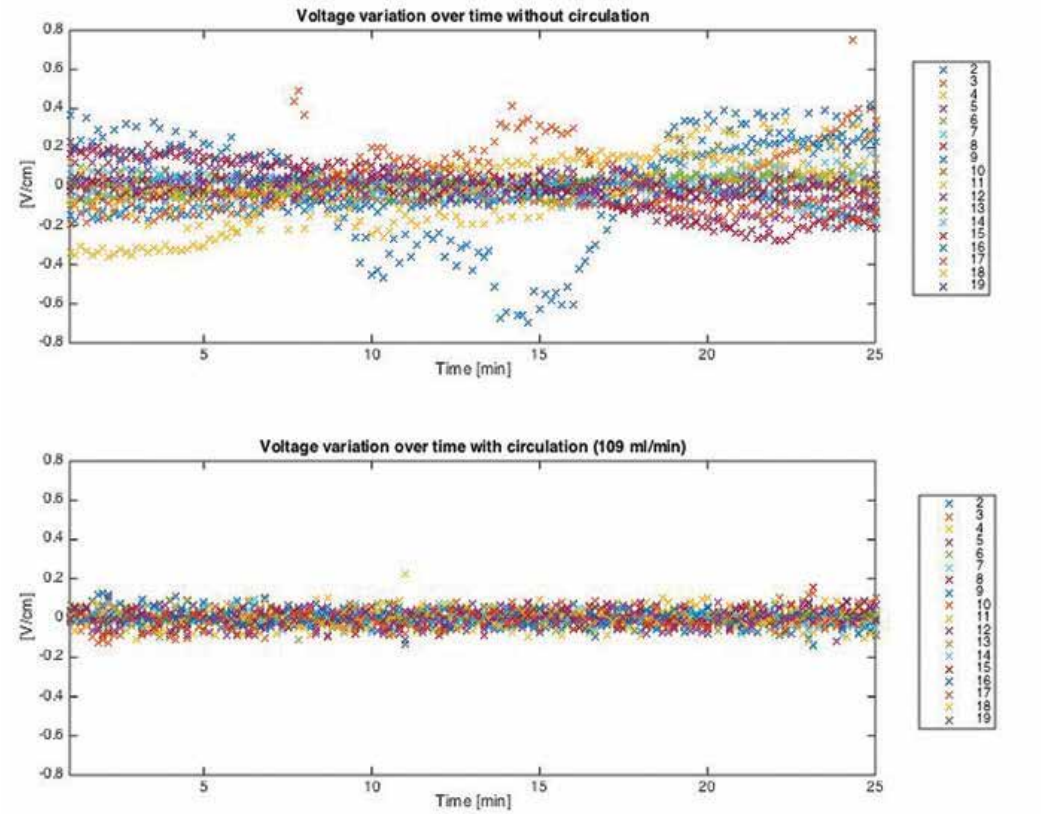

Figure 4. Stabilization of the voltage at each electrode position with circulation. Corrected voltage variations per cm (calculated from **Figure 3**) during the electrophoresis time of 25 mins for each of the electrodes, with 109 ml/min or without circulation (Figure from [20]). One representative experiment. The number of each electrode is indicated to the right of the figure. In this specific experiment, electrode #16 showed particularly large variations without circulation, whereas other electrodes were affected in other experiments.

and methods used in the experiments were the same as in [18], based on our system of 96 minigels on GelBond films. For scoring of comets, a fully automated system (Imstar Pathfinder™, Paris, France) was used, for two reasons; (1) unsupervised scoring avoids errors introduced by operator interactions; (2) there were very large numbers of samples to be scored (384 samples per electrophoresis). To ensure that automated scoring gives comet results comparable to the standard semi-automated scoring (Comet IV, Perceptive Instruments Ltd., Bury St Edmunds, UK) we used both systems to generate the data in **Figure 7**; they gave highly similar rates of median DNA damage (denoted as Tail%DNA, i.e. the fluorescence of the comet tail divided by the total fluorescence of the comet), versus the dose of radiation. At 15 Gy the Tail%DNA is saturated and the dose response is no longer linear; this data was therefore omitted in the linear regression analysis. The dose 8 Gy which was used in cell exposures is in the linear part of the curve and is well below saturation.

A large number of comet electrophoresis experiments was carried out with irradiated (8 Gy) mononuclear cells. We studied differences in means between experiments, with and without

http://dx.doi.org/10.5772/intechopen.76880

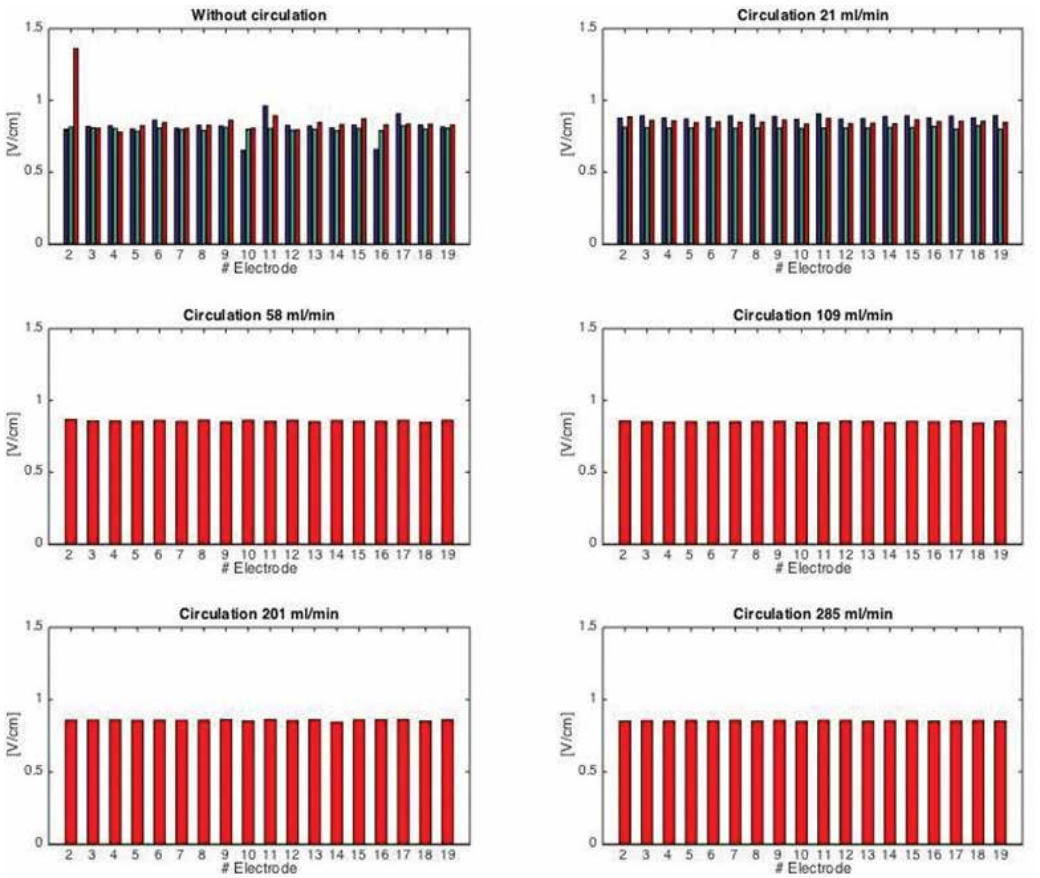

Figure 5. Voltage gradient at each electrode position during electrophoresis with circulation at different flow rates. The corrected electric potentials were time-integrated during an electrophoresis time of 25 mins, and are presented (V/cm) during one (average) mins. Data are from three experiments without circulation or with circulation at 21 ml/min (upper panel); the blue, green, and red bars correspond to each of the three experiments. For higher flow rates (58, 109, 201, and 285 ml/min), the data (lower panels) represent one representative experiment. Figure from [20].

circulation, and differences between samples belonging to different rows or columns in the array (8 columns × 12 rows) on each of four films in one electrophoresis.

The experiments included electrophoresis of either one film placed in the center of the platform, or 4 films totaling 384 samples covering the whole platform [18] (**Figure 8**).

The median (Tail%DNA) of all scored comets in each sample was used as the basis for further statistical analyses. In some calculations, the values were weighted, based on the number of comets scored in each sample. Normality of distribution of DNA damage in each cell sample was tested using a Lilliefors test, in MATLAB R2014b (significance level 5%). Differences between groups (rates of circulation, sample positions in rows and columns) were tested with one-way ANOVA. A structure of statistics obtained from the one-way ANOVA was used to perform the multiple comparison tests, which determined whether any group mean was significantly different; two group means were significantly different if their intervals were disjoint. A Wilcoxon

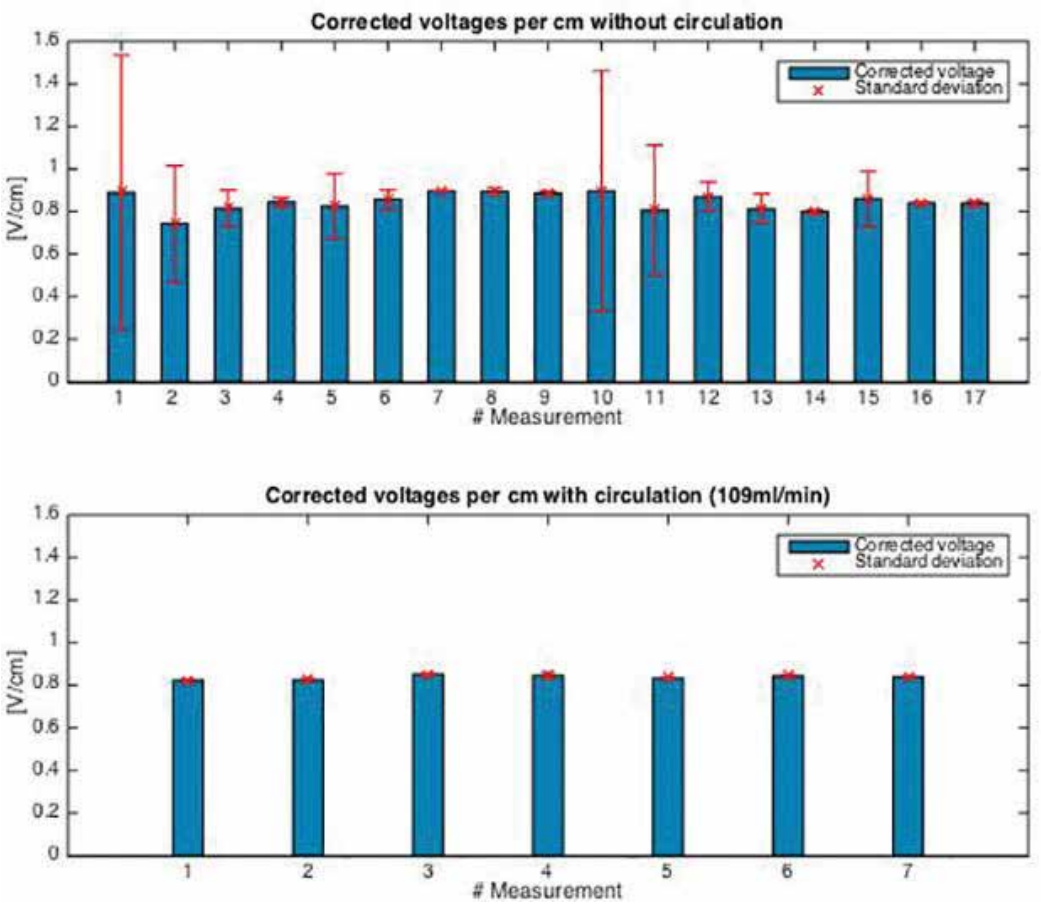

Figure 6. Average electric potentials measured in several experiments. Time-integrated corrected voltage per cm averaged for all electrodes during an electrophoresis time of 25 mins for each measurement with (109 ml/min, lower panel) and without (upper panel) circulation. The standard deviations are shown as red error bars and illustrate the degree of variation in voltage per cm for each measurement. Figure from [20].

rank sum test—not requiring the normal distribution of samples—was used when the Tail% DNA values were shown not to be normally distributed by the Lilliefors test.

We observed small differences in Tail%DNA levels in experiments using different rates of circulation. This is illustrated in **Table 3** and in **Figure 9**, both based on weighted data (to avoid that low numbers of scored comets should be given too much weight).

5. Discussion and conclusions

The ultimate aim of this study [20] was to establish electrophoresis conditions that are optimal for the comet assay, hopefully contributing to reducing the unexplainable variations, which are often found both within and between experiments. A further aim is to establish correction

http://dx.doi.org/10.5772/intechopen.76880

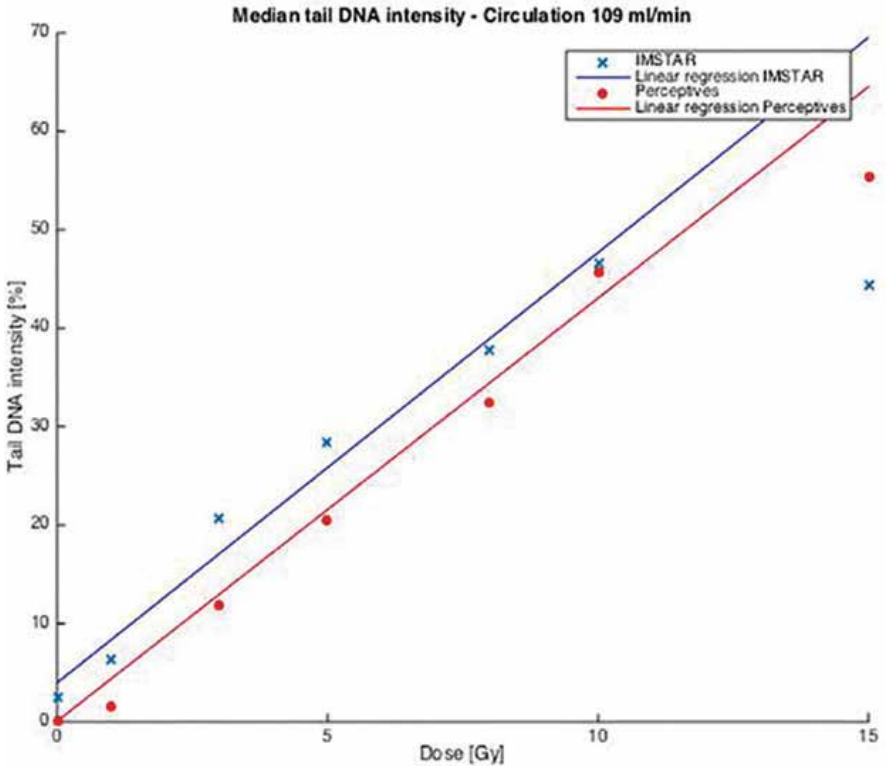

Figure 7. Dose-response curves showing DNA damage versus radiation dose. One experiment; scoring of DNA damage in 96 samples with the semi-automated (Perceptives) and the automated scoring (IMSTAR Pathfinder) systems. Irradiation with X-rays (0–15 Gy) and circulation (109 ml/min) during electrophoresis. The Tail%DNA relative to the head is given as the median value of at least 50 comets in each sample. Linear regression lines are shown, with linear relations $y = 3.99 + 4.37x$ and $y = 0.1 + 4.30x$, and coefficients of variation (CV) $R^2 = 0.72$ and $R^2 = 0.96$, for IMSTAR and Perceptives, respectively. The experimental points at dose 15 Gy were omitted from the linear regression.

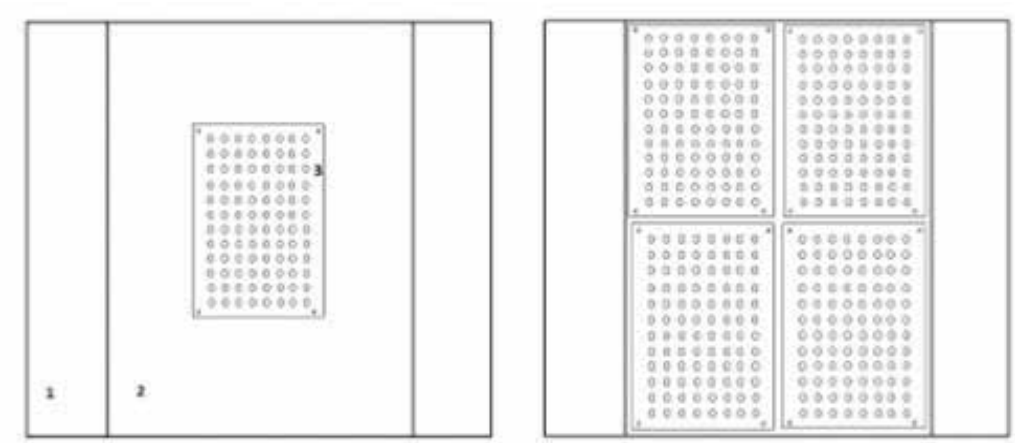

Figure 8. Illustration of positioning of Gelbond films with one film (left; 96 minigels), or four films (right; 384 minigels) on a platform in an electrophoresis tank. Figure from [20].

Flow rate (ml/min)	Mean tail DNA intensity (%)	Mean STD (%)	Mean CV (%)
0	39.53	4.15	10.50
21	42.75	4.31	10.07
58	34.83	3.89	11.18
109	34.75	3.28	9.44
153	36.27	2.28	8.14

Table 3. Mean Tail%DNA in electrophoresed samples of cells irradiated with X-rays (8 Gy). Standard deviations of parallel samples and coefficients of variation are also listed. Data are from three experiments with or without circulation at different flow rates during electrophoresis. Data are weighted on the basis of the number of comets scored in each sample.

factors, which may be used to translate data from laboratories using different electrophoresis conditions.

A systematic investigation of comet assay electrophoresis had not previously been carried out. Since the electric potential is known to be the major physical force causing charged molecules to move during electrophoresis, we recorded the electric potential at multiple sites on the platform of a standard horizontal tank used for comet assay electrophoresis. In a previous study, we had observed that variations in DNA damage levels among parallel samples were considerably reduced when the liquid was circulated during electrophoresis [18].

We made detailed measurements of electric potentials using a gauge containing 20 platinum electrodes coupled to a voltage recording device with input resistance in the mega-ohm range. Using this setup we could confirm that the measured local electric potential was highly affected by circulating the electrophoresis liquid; that is, time- and position- dependent variations seemed to be reduced by circulation. For a standard electrophoresis time of 25 mins, the time-integrated variation (Coefficient of Variation, CV) of the electric potential at electrode positions was more than 8% without circulation; this was reduced to less than 1% with circulation at more than 58 ml/min, i.e. 5% volume change per min (**Table 4**). We initially hypothesized this reduction to

Flow rate	Mean corrected electrode voltage	Mean CV
ml/min	V/cm	%
0	0.82	8.28
21	0.85	1.17
58	0.86	0.53
109	0.83	0.65
201	0.84	0.70
285	0.83	0.50

Table 4. Electric potentials and their variation at electrode positions as a function of circulation flow rate. The corrected electrode voltage per cm averaged over 25 mins is shown, with CV averaged for all electrodes. Data from three experiments with and without circulation at different flow rates.

be due to a better stabilization of local temperature that could alter the conductivity; a further mechanism could be a build-up of local concentration gradients of electrophoresis liquid, which are likely to be reduced by an increased flow. A positive feedback loop could then possibly take place in the absence of circulation.

The logical extension of these observations was that the variations should be paralleled by variations in the level of DNA damage. We therefore examined populations of cells exposed to a genotoxic treatment (X-rays) under different electrophoresis conditions. The mean Tail% DNA of all samples in our minigel 4 × 96 array was remarkably constant, as concluded from three independent experiments (**Figure 9**). There was, however, a slight—but statistically not significant—tendency to a lower CV at the two highest rates of circulation (**Table 3**). This was unexpected in view of the markedly reduced variations in local electric potential with circulation. This is also unlike our preliminary findings [18].

A statistical analysis of Tail%DNA of samples in the row and column positions in the 4 × 96 array also did not reveal systematic differences that could be attributed to electric potential variations. However, for each film, there were clear indications of lower levels of median DNA damage in samples, which were applied late in each pipetting (data not shown). We interpret this as due to some rapid repair of radiation damage, during the short period when cell samples are heated to 37°C for mixing with agarose.

It is possible that variations in electric potentials are related to properties of the measuring gauge. The electric potential is dependent on the concentration gradient in a solution. Small differences in the concentration of reactants and products involved in the redox reaction

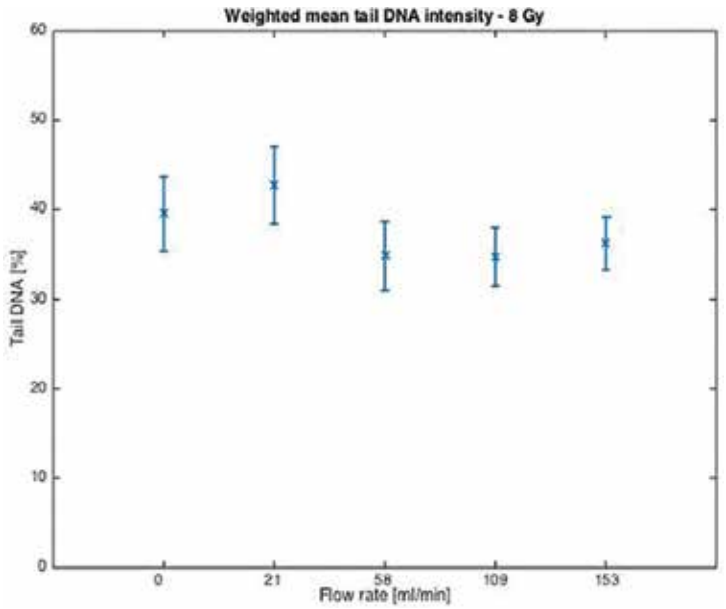

Figure 9. Mean Tail%DNA in electrophoresed samples of cells irradiated with X-rays (8 Gy). DNA damage levels of data from three experiments are shown (+/− STD; error bars) as a function of circulation flow rate. Figure from [20].

occurring at each electrode surface during measurements may cause variation in the recorded electric potential. Circulating the electrophoresis solution may contribute to reducing the build-up of concentration differences, resulting in turn in less variation in the measured electric potential. A reference electrode should be used in order to determine the potential differences across the platform with higher precision. The reference electrode must have a well-defined and reproducible potential, that is, both reactants and products must be present with the kinetics of the reactions sufficiently fast for the species to be present at their equilibrium concentrations. Taken together, the measurements using the multi-electrode gauge were probably more representative for the local electric potential in the presence of circulation. Without circulation, however, these measurements are less reliable.

In conclusion, it seems that circulation of the liquid during electrophoresis has minor effects on the recorded level DNA damage. Even so, there are several arguments for using circulation in comet assay electrophoresis. Uncontrolled changes in temperature, not analyzed in this project but studied by Sirota and co-workers [21], may lead to heterogeneities in DNA damage expression. External peristaltic pumps combined with a spiral of stainless steel tubing placed in ice/water represent an efficient method to stabilize the temperature during electrophoresis, which also becomes more important with higher currents (more heat dissipation). Furthermore, standardization of data relies on the accurate determination of the electric potential. This should be determined using a suitable gauge; from our experiments, it appears that circulation stabilizes the measurement of the potential. It is stated in [16] that "A

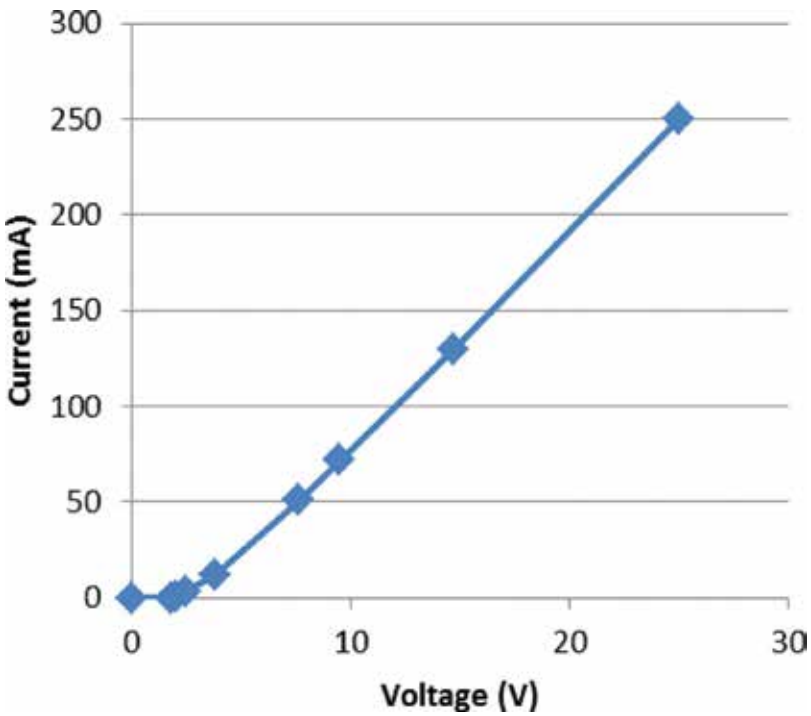

Figure 10. Current in an electrophoresis tank measured as a function of the applied voltage.

typical voltage for an electrophoresis chamber is determined by measuring the perpendicular distance in cm between the positive and negative electrodes in the electrophoresis chamber, and multiplying this distance by 0.6." This simplified method to determine the electric potential (V/cm) may introduce errors and should not be used. Firstly, there is a voltage drop at each electrode (the electrode potential at standard state for platinum equals 1.18 V [22]). This electrode potential is evident from the measurement of the current at increasing electrode voltage (from the power supply) in a tank; see **Figure 10**. There is no current at voltages lower than 2.5 V; the curve extrapolates at zero current to 2.7 V, which is close to the electrode potentials at both electrodes (2.38 V). Furthermore, the side wells have higher conductivity (per length) than the platform. In a small tank, the electrode potential may introduce serious errors.

Care should also be taken concerning the resistance of the cathode and anode electrodes. There is a voltage drop along these electrodes, even with platinum (specific resistance $1.05 * 10^{-7}$ohm *m (at 20°C)). Depending on the electrode cross-section and the current, this could result in as much as 5–10% lower voltage at the far end of the tank (i.e. opposite to where the connecting leads are). This error can be reduced by using thicker (very expensive) platinum, but a cheaper solution is to connect both ends of each electrode to the power supply (4 leads). An alternative approach is to measure and/or calculate the electric potential (V/cm) along both sides of the platform and introduce correction factors to account for the difference in each position.

In summary, based on our experiments and the evaluations above, we suggest a number of simple recommendations:

6. Recommendations for comet assay electrophoresis

- When introducing a new tank: measure and record the voltage and the current of the electrophoresis tank, when containing different volumes of liquid.
- Circulate the electrophoresis liquid during electrophoresis using an external pump (e.g., there are cheap peristaltic pumps made for aquariums). The advantages are (1) stable conditions allowing more precise measurement of the electric potential; (2) more stable temperature during electrophoresis; and (3) (probably) reduced variations in the local electric potential.
- Use sufficient volume of electrophoresis liquid to cover the agarose samples with at least 5 mm.
- Ensure that a power supply is used which can supply the output current at the constant voltage and with sufficient volume of liquid (two car batteries are a very cheap and useful alternative).
- Use electrodes of sufficient size (cross section), to avoid a voltage drop due to high ohmic resistance. The overall resistance is reduced if both ends of each electrode are connected to the output cable from the power supply.

- Measure the local potential on the platform, preferably using a gauge with platinum electrodes at defined positions. Measure in the presence of circulation.
- Take great care in preparing the agarose used for embedding gel samples (avoid evaporation during heating).
- Calculate the Electric Potential * Time (EPT) value (dimension: V/cm*min) for your setup. Use the EPT value in your publications and when comparing your results with those from other experiments and laboratories.

Acknowledgements

The authors are grateful to the COST Action CA15132, "hCOMET," for support. This work was financed by the Research Council of Norway through its Centers of Excellence funding scheme, project number 223268/F50 CERAD Centre for Environmental Radioactivity (CoE CERAD).

Author details

Gunnar Brunborg[1]*, Linn Rolstadaas[1,2] and Kristine B. Gutzkow[1]

*Address all correspondence to: gunnar.brunborg@fhi.no

1 Norwegian Institute of Public Health, Oslo, Norway

2 St. Olavs Hospital, Trondheim, Norway

References

[1] Ostling O, Johanson KJ. Microelectrophoretic study of radiation-induced DNA damages in individual mammalian cells. Biochemical and Biophysical Research Communications. 1984;**123**(1):291-298

[2] Singh NP, McCoy MT, Tice RR, Schneider EL. A simple technique for quantitation of low levels of DNA damage in individual cells. Experimental Cell Research. 1988;**175**(1):184-191

[3] Olive PL, Johnston PJ, Banath JP, Durand RE. The comet assay: A new method to examine heterogeneity associated with solid tumors. Nature Medicine. 1998;**4**(1):103-105

[4] Zainol M, Stoute J, Almeida GM, Rapp A, Bowman KJ, Jones GD. Introducing a true internal standard for the comet assay to minimize intra- and inter-experiment variability in measures of DNA damage and repair. Nucleic Acids Research. 2009;**37**(22):e150

[5] Forchhammer L, Johansson C, Loft S, Moller L, Godschalk RW, Langie SA, et al. Variation in the measurement of DNA damage by comet assay measured by the ECVAG inter-laboratory validation trial. Mutagenesis. 2010;**25**(2):113-123

[6] Johansson C, Moller P, Forchhammer L, Loft S, Godschalk RW, Langie SA, et al. An ECVAG trial on assessment of oxidative damage to DNA measured by the comet assay. Mutagenesis. 2010;**25**(2):125-132

[7] Godschalk RW, Ersson C, Riso P, Porrini M, Langie SA, van Schooten FJ, et al. DNA-repair measurements by use of the modified comet assay: An inter-laboratory comparison within the European comet assay validation group (ECVAG). Mutation Research. 2013; **757**(1):60-67

[8] Ersson C, Moller P, Forchhammer L, Loft S, Azqueta A, Godschalk RW, et al. An ECVAG inter-laboratory validation study of the comet assay: Inter-laboratory and intra-laboratory variations of DNA strand breaks and FPG-sensitive sites in human mononuclear cells. Mutagenesis. 2013;**28**(3):279-286

[9] Moller P, Loft S, Ersson C, Koppen G, Dusinska M, Collins A. On the search for an intelligible comet assay descriptor. Frontiers in Genetics. 2014;**5**:217

[10] Singh NP. Microgels for estimation of DNA strand breaks, DNA protein crosslinks and apoptosis. Mutation Research. 2000;**455**(1–2):111-127

[11] Singh NP, Penn PE, Pendergrass WR, Wolf NS. White light-mediated DNA strand breaks in lens epithelial cells. Experimental Eye Research. 2002;**75**(5):555-560

[12] Tice RR, Agurell E, Anderson D, Burlinson B, Hartmann A, Kobayashi H, et al. Single cell gel/comet assay: Guidelines for in vitro and in vivo genetic toxicology testing. Environmental and Molecular Mutagenesis. 2000;**35**(3):206-221

[13] Olive PL, Wlodek D, Durand RE, Banath JP. Factors influencing DNA migration from individual cells subjected to gel electrophoresis. Experimental Cell Research. 1992;**198**(2): 259-267

[14] Olive PL, Banath JP. The comet assay: A method to measure DNA damage in individual cells. Nature Protocols. 2006;**1**(1):23-29

[15] OECD. Test No. 488: Transgenic Rodent Somatic and Germ Cell Gene Mutation Assays. Paris: OECD Publishing; 2014

[16] Olive PL. The comet assay. An overview of techniques. Methods in Molecular Biology (Clifton, NJ). 2002;**203**:179-194

[17] Azqueta A, Gutzkow KB, Brunborg G, Collins AR. Towards a more reliable comet assay: Optimising agarose concentration, unwinding time and electrophoresis conditions. Mutation Research, Genetic Toxicology and Environmental Mutagenesis. 2011;**724**(1–2):41-45

[18] Gutzkow KB, Langleite TM, Meier S, Graupner A, Collins AR, Brunborg G. High-throughput comet assay using 96 minigels. Mutagenesis. 2013;**28**(3):333-340

[19] Brunborg G, Jackson P, Shaposhnikov S, Dahl H, Azqueta A, Collins AR, et al. High throughput sample processing and automated scoring. Frontiers in Genetics. 2014;**5**:373

[20] Rolstadaas L. Towards minimizing variations in the comet assay: The electric potential during electrophoresis and implications of circulating the electrophoresis solution [Master's thesis]. Trondheim: Norwegian University of Science and Technology; 2016

[21] Sirota NP, Zhanataev AK, Kuznetsova EA, Khizhnyak EP, Anisina EA, Durnev AD. Some causes of inter-laboratory variation in the results of comet assay. Mutation Research, Genetic Toxicology and Environmental Mutagenesis. 2014;**770**:16-22

[22] Aylward GH, Findlay TJV. SI Chemical Data. Sidney, Australia: John Wiley and Sons Ltd; 2007

Chapter 5

Lactate Dehydrogenase Isoenzyme Electrophoretic Pattern in Serum and Tissues of Mammalian and Bird Origin

Dagmar Heinová, Zuzana Kostecká and
Eva Petrovová

Additional information is available at the end of the chapter

http://dx.doi.org/10.5772/intechopen.76322

Abstract

Lactate dehydrogenase (LDH) is a tetrameric enzyme that in vertebrates exists in five electrophoretically distinguishable forms known as isoenzymes. According to their different mobility to anode, they are denoted LDH_1 (H_4), LDH_2 (H_3M), LDH_3 (H_2M_2), LDH_4 (HM_3), and LDH_5 (M_4). A buffer system of the pH values 8.6–8.8 is commonly used for the separation of these isoenzymes in mammals. In the case of bird LDHs, the observation of five fractions is very difficult under this condition as they usually produce a pattern of one diffuse zone. Isoelectric focusing technique (IEF) in the pH range of 3–9 enabled a good and clear resolution of all five bird LDHs. Using this technique, it was also possible to observe the pattern in some tissues of chicken embryo.

Keywords: lactate dehydrogenase isoenzymes, isoelectric focusing technique, birds, mammals, embryo

1. Introduction

Lactate dehydrogenase (EC 1.1.1.27, LDH) is an enzyme ubiquitary distributed in cells of living systems. It catalyzes an interconversion of lactate and pyruvate with nicotinamide adenine dinucleotide (NAD^+) as coenzyme both in cytoplasm and in mitochondria [1, 2]. This enzyme is also present in the sera of animals and humans where its changed pattern serves as a valuable adjunct indicator in the diagnostics of heart, skeletal muscle, and liver disorders [3]. In tissues of vertebrates, LDH exists in several electrophoretically distinguishable forms known

as isoenzymes. They catalyze the same biochemical reaction but differ from each other in their kinetic characteristics (K_m, k_{cat}), physicochemical properties (different net charge), response to the inhibition by substrate (pyruvate) [4–6], and immunological response. Despite a profound understanding of LDHs, there was a lack of data concerning their relative distribution and pattern in bird tissues and sera. This gap in our knowledge of these enzymes was probably due to the fact that electrophoretic techniques routinely used in separating mammalian LDH isoenzymes did not produce a satisfactory separation of all bird isoenzymes [7, 8]. Thus, their application in research as well as in diagnostic practice remained in birds limited to the determination of the total LDH activity without the possibility for the correct interpretation of data in relation to their quantitative patterns in respective tissues/organs. The aim of our work was to separate lactate dehydrogenase isoenzymes of bird origin and to characterize the pattern of their relative distribution in tissues and sera using a suitable electrophoretic technique.

2. Isoenzymes of lactate dehydrogenase and their electrophoretic separation

LDH is a tetrameric enzyme that exists in three basic homotetrameric forms in vertebrates: H_4 (LDH_1), M_4 (LDH_5), and C_4 (LDH-X) [9–16]. Three structurally different polypeptide chains of homotetrameric LDH molecules are encoded by three different genes [13, 17–19]. Lactate dehydrogenase H_4 and M_4 forms, also called somatic LDH [20], are present in tissues of all studied vertebrates, while the tissue distribution of LDH-C_4 isoenzyme varies from organism to organism. In mammals and columbid birds, this isoenzyme is expressed only in mature testes [19, 21, 22]. Except H_4 and M_4 homotetramers, somatic LDH also exists in three hybrid forms, thus being present in five structural entities in cells of most tissues. According to their different motility to the anode, somatic LDHs are denoted LDH_1 (H_4), LDH_2 (H_3M), LDH_3 (H_2M_2), LDH_4 (HM_3), and LDH_5 (M_4) with LDH_1 having the highest and LDH_5 the lowest migration rate to the anode. Three hybrid forms (LDH_2, LDH_3, and LDH_4) are relatively equally spread between LDH_1 and LDH_5 on the electrophoreogram. Protomers of the somatic LDH isoenzymes are, in general, designated H (heart) or B, and M (muscle) or A according to the domination of homotetrameric molecules in the cells of respective organs of adult vertebrates. Hybrid forms of LDH are present in various levels in the individual organs of an animal/human.

Although catalyzing the same overall reaction, LDH isoenzymes differ in their kinetic characteristics (K_m, k_{cat}) as documented in **Table 1** [4–6, 23–25].

As seen, H_4 homotetramers have a lower value of Michaelis constant K_m for pyruvate as substrate. Moreover, H_4 is more sensitive to inhibition by high pyruvate concentration than M_4 isoenzyme, which is relatively indifferent to substrate concentration [3].

Different structures of lactate dehydrogenase isoenzyme molecules predetermine their different net charge and, consequently, different migration rate in electric field. It is known that the charge of a protein and, therefore, its motility in the electric field vary with the pH of its environment. Maximum resolution is achieved when the proteins of interest have

		Chicken	Rabbit	Cattle
K_m (mol.l^{-1})	H_4	8.9×10^{-5}	6.7×10^{-5}	7.1×10^{-5}
	M_4	3.2×10^{-3}	3.5×10^{-4}	1.0×10^{-4}
k_{cat} (s^{-1})	H_4	45,000	41,000	49,400
	M_4	93,400	not determined	80,200

Table 1. Kinetic constants determined for the catalytic action of H_4 and M_4 homotetramers of lactate dehydrogenase.

widely varying electrical charges. Conversely, no or poor separation of proteins is achieved when there are only small differences in the electrical charges of molecules at a given pH values. Changing the pH of the electrophoresis media may alter the charges on respective proteins, thus producing a better separation. Generally, a buffer system of pH 8.6 is chosen for the separation of the five lactate dehydrogenase isoenzymes. At pH 8.6, their electrophoretic migration depends on the two pure types, that is, the H_4 and M_4 forms [9]. The more widely the two homotetramers differ in charge (the case of mammalian lactate dehydrogenases), the more separable are the hybrids by electrophoresis. In the case of bird lactate dehydrogenases, the two pure types migrate relatively close together toward the negative pole at pH 8.6, and the observation of the hybrid forms under these conditions is very difficult [9]. To overcome this difficulty, we chose a gradient of pH 3–9 for the electrophoretic separation of bird lactate dehydrogenase isoenzymes (isoelectric focusing technique, IEF) [8]. By this technique, we achieved a good and clear resolution of all five forms of the enzyme in serum and tissues of chicken (adult as well as in embryonic), turkey, pheasant, and pigeon. We also compared patterns in bird tissues and sera with those of mammalian origin.

3. Preparation of the samples for electrophoresis

Sera from various animal species were obtained from rested and clinically healthy animals. The blood collection for the serum samples was performed by standard procedures, and no hemolyzed sera were used for the examination. The determination of total lactate dehydrogenase activity as well as separation of the isoenzymes was performed on the same day as the blood collection.

Tissue samples were taken from birds after decapitation and immediately put into ice-cold buffer saline. The tissues were cut into small pieces and washed in buffered saline to remove excess blood and connective tissue. Two grams of tissue were homogenized in 10 volumes of cold buffer (0.05 mol/L Tris-HCl buffer, pH 7.3 with 0.01% EDTA). The homogenate was centrifuged at 19,000 × *g* for 60 min at 4°C, and the supernatant was used for enzyme assay and electrophoretic separation.

Blood for erythrocytes LDH pattern was collected in test tubes containing sodium heparin and centrifuged at 450 × *g* for 10 min at 4°C. Plasma was discarded and erythrocytes washed

thoroughly three times in twice their volume, and the supernatant discarded. The cells were then lysed with the addition of three volumes of cold distilled water and centrifuged at 19,000 × *g* for 60 min at 4°C.

Chicken embryonic organs/tissues were taken from 9-day-old chicken embryo (n = 6), washed in buffer saline, and homogenated in 50 mM Tris-HCl, pH 7.5, with the content of 0.01% EDTA using Precellys 24—Dual homogenizer (Bertin Technologies, France). The homogenates were centrifuged at 25,000 × *g* for 30 min at 4°C, and the supernatants served as the source of the enzyme.

Catalytic activity of LDH was assayed colorimetrically at 37°C using lactate as the substrate with NAD^+ as the coenzyme and brownish-red pyruvate hydrazone as the measured product (A_{505}). Protein concentration for the calculation of specific enzyme activity (U/g) was determined using Bradford method [26]. The activity of LDH in erythrocytes was expressed in enzyme units per gram of hemoglobin (U/g of hemoglobin).

4. Electrophoretic techniques used for separation of LDH isoenzymes

Lactate dehydrogenase isoenzymes can be separated using various supporting media such as starch, agarose, cellulose acetate, and polyacrylamide gel. The separations should be carried out with cooling to 4°C in order to prevent the possibility of enzyme inactivation, particularly heat-sensitive slow-moving isoenzymes (LDH_4 and LDH_5) [3].

Two types of polyacrylamide gel electrophoresis for the separation of lactate dehydrogenase isoenzymes of mammalian and bird origin were used in our laboratory (PhastSystem, Pharmacia LKB, Sweden):

1. Gradient polyacrylamide gel electrophoresis with continuous 10–15% gradient gel zone and 2% cross-linking (PAGE 10–15) as well as with continuous 8–25% gradient gel zone (PAGE 8–25). Separation conditions: 400 V, 10.0 mA, 45 min separation time at 4°C and with a buffer system of 0.88 mol/L L-alanine/0.25 mol/L Tris pH 8.8.
2. Isoelectric focusing technique with a pH range of 3–9 in homogeneous 5% polyacrylamide gel containing Pharmalyte carrier ampholytes (IEF 3–9). Separation conditions: 2000 V, 2.5 mA, 15°C, 20 min separation time.

5. Detection and quantification of lactate dehydrogenase isoenzymes

As many proteins were separated by electrophoresis, lactate dehydrogenase isoenzymes were detected (stained) specifically using a colorimetric method with an assay system in 0.1 M Gly-NaCl-NaOH, pH 8.3: 1.0 mol/l sodium lactate (1.0 ml), 10 mg/ml NAD^+ (1.5 ml), 1.0 mg/ml nitro blue tetrazolium (NBT) (6.0 ml), and 2.0 mg/ml phenasine methosulfate (PSM) (0.6 ml)

up to 30 ml with 0.1 M Gly-NaCl-NaOH, pH 8.3. In this reaction mixture, the gels were incubated at 37°C for 20–30 min. Then, they were immersed into 7.5% (v/v) acetic acid to stop the reaction. To detect lactate dehydrogenase isoenzyme zones on the electrophoreogram, we avoid using Tris-HCl buffer as it produced quite an intensive background on the gel. PhastImage system (Pharmacia LKB, Sweden) served for densitometric scanning (613 nm) of the pattern, and for the determination of relative distribution (%) of the isoenzyme fractions, GEL LOGIC 100 IMAGING SYSTEM with Kodak 1D Image Analysis Software (Japan) was used as well. To identify individual bird LDH isoenzymes on the electrophoreogram, a principle commonly used for the identification of mammalian LDH isoenzymes was applied: the fraction nearest to the anode was designated LDH_1 and that nearest to the cathode LDH_5.

6. Patterns of LDH isoenzymes and their interpretation

Four to five isoenzymes of LDH are usually present in normal sera of animal and human beings as a result of natural degradation of cells of various tissues/organs. Their quantitative distribution in the serum is different and relatively characteristic for a particular biological species (**Figure 1**) [8]. After their separation in a concentration gradient of polyacrylamide (10–15%) and at pH 8.8, mammalian lactate dehydrogenases were separated with a good resolution, whereas bird serum (chicken) produced only one, somewhat diffuse enzymatic zone [8].

A good and clear resolution of bird LDH (chicken and pheasant) isoenzymes with all five isoenzymes zones was achieved using isoelectric focusing technique in a pH range of 3–9 [8]. A similar pattern was also produced by turkey isoenzymes [27]. A comparison of LDH catalytic activity and relative distribution (%) of its isoenzymes in the sera of the investigated animals (**Figure 1**) revealed that the predominant portion of chicken serum LDH activity was concentrated in the muscle form of the enzyme (LDH_5) (66%), followed by LDH_4 (23%). LDH_1 to

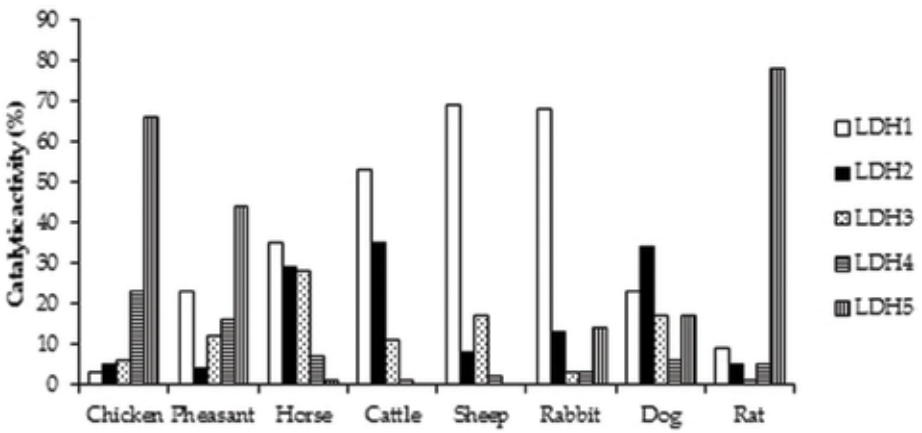

Figure 1. Lactate dehydrogenase isoenzyme patterns in the serum of some birds and mammals.

LDH_3 occurred in low amounts with fairly similar proportions (3–6%). The muscle isoenzyme was also the main fraction in pheasant and turkey serum [8, 27] (44 and 50%, respectively). Heart homotetramer as well as hybrid forms were present in smaller amounts. Most mammals showed a reverse pattern: the main portion of serum lactate dehydrogenase activity migrated in the first three anodic fractions, while LDH_4 and LDH_5 made only minor contributions (**Figure 1**). The serum pattern of LDH isoenzymes probably reflects the pattern of the main LDH organ donors (heart, skeletal muscle, and liver) and differs from animal to animal species. As an example, the quantitative analysis can serve organ/tissue pattern and relative distribution of LDH isoenzymes in chicken (**Figure 2**) [28]. The patterns of lactate dehydrogenase isoenzymes in various chicken tissues, erythrocytes, and serum can be divided into three groups: (1) those with cathodic domination, (2) those with anodic domination, and (3)

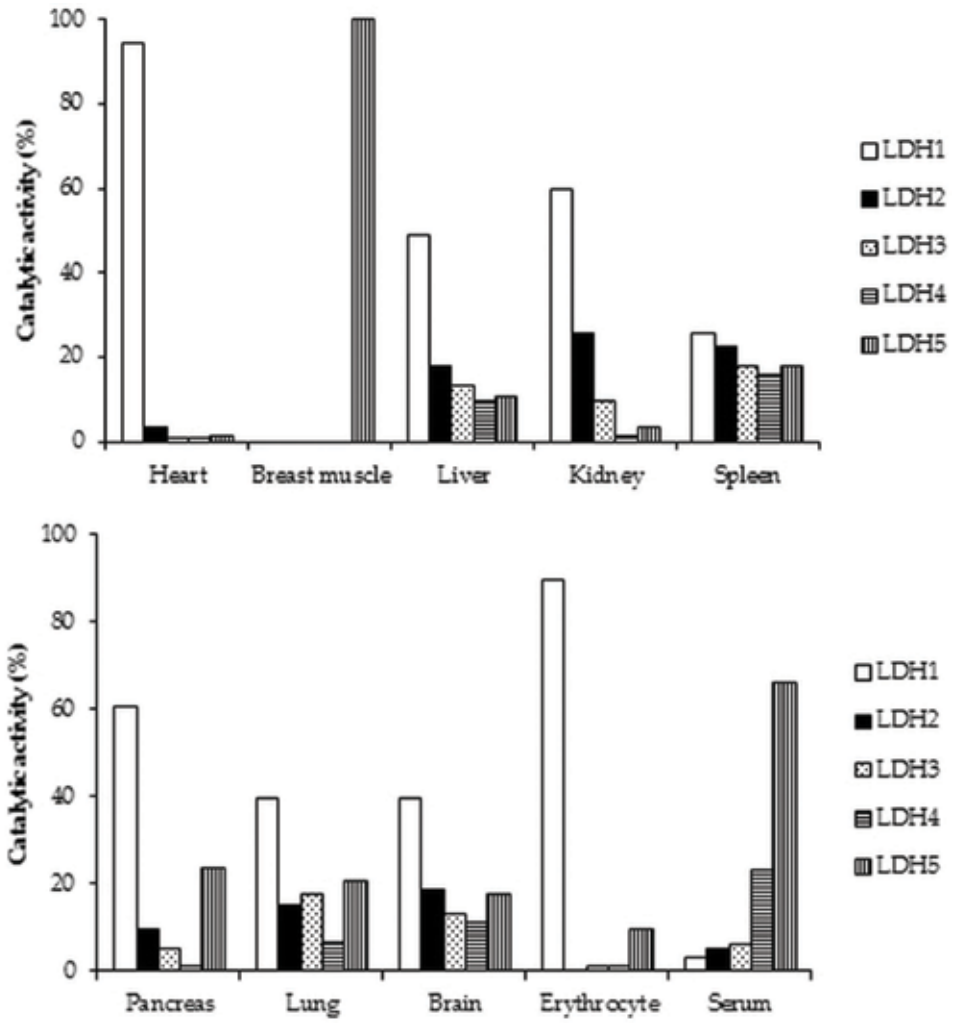

Figure 2. Lactate dehydrogenase isoenzymes pattern in chicken tissues and blood.

those distributed in the entire electrophoreogram. The anodic domination (LDH_1) is seen in the cardiac muscle and erythrocytes, while the cathodic domination (LDH_5) is seen in the breast muscle. Other tissues and serum exhibit a more spread pattern with some anodic tendency (kidney, liver), cathodic tendency (skeletal muscle, serum), and more even distribution (spleen, pancreas, lung, and brain). Similar distribution and pattern of LDH isoenzymes were described in turkey [27].

Comparing the isoenzyme patterns of birds (chicken, turkey) [27, 28] to human and other mammals reveals some differences. While the heart and skeletal muscle patterns are similar in birds and mammalians, it differs in other tissues, especially in the liver. While in most mammals, the liver pattern is quantitatively dominated by the slower moving cathodic isoenzymes similar to skeletal muscle (LDH_4, LDH_5; rabbit, horse, lamb, dog, humans) [29], in chicken and turkey, the patterns are opposite, with the prevalence of anodic isoenzymes similar to the aerobic heart muscle isoenzyme [27, 28]. The reason for these differences is not clear but it may suggest that the bird internal organs are geared to function better under aerobic metabolism.

Besides the serum and tissue LDH isoenzymes of adult birds, we also succeeded in separating lactate dehydrogenases originated from selected chicken embryo tissues using IEF technique in the pH range of 3–9 (**Table 2**).

An interesting pattern was found in the muscle of chicken embryo where all five isoforms were present (**Table 2**), while in adult animal tissue, only one, LDH_5 isoenzyme, was detected (**Figure 2**). This difference can be related to the developmental changes of LDH isoenzymes, similar to heart chicken embryonic lactate dehydrogenases. They were also relatively equally distributed on the electrophoreogram producing a pattern different from adult chicken heart where anodic LDH_1 isoform prevails over cathodic ones that are either absent or present only in a trace amount.

Tissue	Lactate dehydrogenase (%)				
	1	**2**	**3**	**4**	**5**
Skeletal muscle	18	21	21	20	20
Heart	12	21	23	21	18

Table 2. Relative distribution (%) of lactate dehydrogenase isoenzymes in skeletal muscle and heart of chicken embryo (n = 6).

7. Conclusion

A suitable method for electrophoretic separation of bird lactate dehydrogenase isoenzymes is isoelectric focusing technique in a pH range of 3–9. It enabled to determine patterns and relative distribution (%) of LDH isoforms in bird sera and tissues (chicken adult and embryonic, as well as turkey). They were characterized by a prevalence of slow moving LDH_5 in sera in both species probably originated from breast muscle that distinguish them from mammalian

pattern where anodic LDH_1-LDH_3 dominate over cathodic form/s. Mammalian tissues pattern of lactate dehydrogenase isoenzymes differs from species to species with the highest enzyme activity in the skeletal muscle followed by heart and liver. Chicken adult and embryonic lactate dehydrogenases differ each other especially in the pattern of breast muscle with all five isoenzymes being present in the tissue of embryonic origin.

Acknowledgements

This work was supported by a research grant from Scientific Grant Agency VEGA No. 1/0046/16.

Conflict of interest

The authors have declared no conflict of interest.

Author details

Dagmar Heinová, Zuzana Kostecká* and Eva Petrovová

*Address all correspondence to: zuzana.kostecka@uvlf.sk

University of Veterinary Medicine and Pharmacy in Košice, Košice, Slovak Republic

References

[1] Brooks GA, Dubouchaud H, Brown M, Sicurello JP, Butz CE. Role of mitochondrial lactate dehydrogenase and lactate oxidation in the intracellular lactate shuttle. Proceedings of the National Academy of Sciences of the United States of America. 1999;**96**:1129-1134

[2] Elustondo PA, White AE, Hughes ME, Brebner K, Pavlov E, Kane DA. Physical and functional association of lactate dehydrogenase (LDH) with skeletal muscle mitochondria. Journal of Biological Chemistry. 2013;**288**:25309-25317. DOI: 10.1074/jbc.M113.476648

[3] Maekawa M. Lactate dehydrogenase isoenzymes. A review. Journal of Chromatography. 1988;**429**:373-398

[4] Plagemann PGW, Gregory KF, Wróblewski F. The electrophoretically distinct forms of mammalian lactic dehydrogenase. II. Properties and interrelationships of rabbit and human lactic dehydrogenase isoenzymes. Journal of Biological Chemistry. 1960;**8**: 2288-2293

[5] Dawson DM, Goodfriend TL, Kaplan NO. Lactic dehydrogenases: Function of the two types. Science. 1964;**143**:929-933

[6] Fondy TP, Kaplan NO. Structural and functional properties of the H and M subunits of lactic dehydrogenases. Annals of the New York Academy of Sciences. 1965;**119**:888-903

[7] Heinová D, Blahovec J. Lactate dehydrogenase isoenzymes in mammalian and fowl sera (in Slovak). Veterinary Medicine—Czech. 1994;**39**:75-84

[8] Heinová D, Blahovec J, Rosival I. Lactate dehydrogenase isoenzyme pattern in bird, carp and mammalian sera. European Journal of Clinical Chemistry and Clinical Biochemistry. 1996;**34**:91-95

[9] Cahn RD, Kaplan NO, Levine L, Zwilling E. Nature and development of lactic dehydrogenases. The two major types of this enzyme form molecular hybrids which change in makeup during development. Science. 1962;**136**:962-969

[10] Wilson AC, Cahn RD, Kaplan NO. Functions of the two forms of lactic dehydrogenase in the breast muscle of birds. Nature. 1963;**197**:331-334

[11] Roussel JD, Stallcup OT. Distribution of lactic dehydrogenase and transaminase in the genital tissues of Holstein-Friesian bulls. Journal of Dairy Science. 1967;**50**:1306-1309

[12] Holmes RS. Evolution of lactate dehydrogenase genes. FEBS Letters. 1972;**28**:51-55

[13] Wu KC, Chan K, Lee CY, Lau YF. Molecular isolation and sequence determination of the cDNA for the mouse sperm-specific lactate dehydrogenase—X gene. Biochemical and Biophysical Research Communications. 1987;**146**:964-970

[14] Li SSL, Fitch WM, Pan YCE, Sharief FS. Evolutionary relationship of vertebrate lactate dehydrogenase genes A (muscle), B (heart) and C (testis). Journal of Biological Chemistry. 1983;**258**:7029-7032

[15] Quattro JM, Woods HA, Powers DA. Sequence analysis of teleost retina specific lactate dehydrogenase C: Evolutionary implications for the vertebrate lactate dehydrogenase gene family. Proceedings of the National Academy of Sciences of the United States of America. 1993;**90**:242-246

[16] Goldberg E, Eddy EM, Duan C, Odet F. LDHC the ultimate testis specific gene. Journal of Andrology. 2010;**31**:86-94. DOI: 10.2164/jandrol.109.008367

[17] Zinkham WH, Isensee H. Genetic control of lactate dehydrogenase synthesis in the somatic and gametic tissues of pigeon. Johns Hopkins Medical Journal. 1972;**130**:11-25

[18] Salehi-Ashtiani K, Goldberg E. Differences in regulation of testis specific lactate dehydrogenase in rat and mouse occur at multiple levels. Molecular Reproduction and Development. 1993;**35**:1-7

[19] Tsoi SCM, Li SSL. The nucleotide and deduced amino-acid sequences of a cDNA encoding lactate dehydrogenase from *Caenorhabditis elegans*: The evolutionary relationship of lactate dehydrogenases from mammals, birds, amphibian, fish, nematode,

plants, bacteria, mycoplasm, and plasmodium. Biochemical and Biophysical Research Communications. 1994;**205**:558-564

[20] Bonny C, Cooker LD, Goldberg E. Deoxyribonucleic acid-protein interactions and expression of the human testis-specific lactate dehydrogenase protomer: Transcription factor Sp1 plays a major role. Biology of Reproduction. 1988;**58**:754-759

[21] Tsuji S, Quereshi MA, Hou EW, Fitch WM, Li SSL. Evolutionary relationships of lactate dehydrogenases (LDHs) from mammals, birds, an amphibian, fish, barley, and bacteria: LDH cDNA sequences from xenopus, pig, and rat. Proceedings of the National Academy of Sciences of the United States of America. 1994;**91**:9392-9396

[22] Mannen H, Tsoi SC, Krushkal JS, Li WH, Li SS. The cDNA cloning and molecular evolution of reptile and pigeon lactate dehydrogenase isoenzymes. Molecular Biology and Evolution. 1997;**14**(11):1081-1087

[23] Battelino LJ, Blanco A. Catalytic properties of the lactate dehydrogenase isoenzyme "X" from mouse testis. Journal of Experimental Zoology. 1970;**174**:173-186

[24] Kopperschlager G, Kirchberger J. Methods for the separation of lactate dehydrogenases and clinical significance of the enzyme. Journal of Chromatography. B, Biomedical Applications. 1996;**684**:25-49

[25] Holland LZ, McFall-Ngai M, Somers GN. Evolution of lactate dehydrogenase-A homologs of barracuda fishes (genus Sphyranea) from different thermal environments: Differences in kinetic properties and thermal stability are due to amino-acid substitutions outside the active site. Biochemistry. 1997;**36**:3207-3215

[26] Bradford MM. A rapid and sensitive method for the quantification of microgram quantities of protein utilizing the principle of protein-dye binding. Analytical Biochemistry. 1976;**72**:248-254

[27] Heinová D, Kostecká Z, Csank T. Separation of turkey lactate dehydrogenase isoenzymes using isoelectric focusing technique. Electrophoresis. 2016;**37**:335-338. DOI: 10.1002/elps.201500407

[28] Heinová D, Rosival I, Avidar Y, Bogin E. Lactate dehydrogenase isoenzyme distribution and patterns in chicken organs. Research in Veterinary Science. 1999;**67**:309-312

[29] Heinová D, Kostecká Z, Nagy O. Lactate dehydrogenase of bird and mammalian origin. In: Collins M, editor. Dehydrogenases. Biochemistry, Functions and Role in Disease. 1st ed. New York: Nova Science Publishers Inc; 2017. pp. 1-22

Chapter 6

Two-Dimensional Gel Electrophoresis as an Information Base for Human Proteome

Stanislav Naryzhny

Additional information is available at the end of the chapter

http://dx.doi.org/10.5772/intechopen.75125

Abstract

The main intricacy in the human proteome is that it is tremendously complex and composed of diverse and heterogeneous gene products. These products are called protein species or proteoforms and are the smallest units of the proteome. In pursuit of the comprehensive profiling of the human proteome, significant advances should be performed. The approaches that allow disclosing and keeping the information about human proteome using two-dimensional gel electrophoresis (2DE) are described. Experimental identification methods such as mass spectrometry of high resolution and sensitivity (MALDI-TOF MS and ESI LC-MS/MS) or immunodetection in combination with bioinformatics and 2DE can be used for the development of a comprehensive knowledge base of the human proteome.

Keywords: two-dimensional gel electrophoresis, proteome, proteoforms, mass spectrometry, bioinformatics

1. Introduction

The first aim in human proteomics, as it was proposed by the Human Proteome Organization (HUPO), is a complete catalog of all human proteins. Due to collaborative efforts inside the Chromosome-based Human Proteome Project (C-HPP), this task is close to completion now [1, 2]. According to NextProt release from Aug 1, 2017, 17,168 from 20,199 predicted proteins have already been found. Still, ~3000 proteins are in the list of so-called "missing proteins." But even after completion of this task, only representative proteins will be identified in most cases [3, 4]. The situation here is much more complicated, as proteins can exist as different proteoforms (protein species) [5–7]. Proteoforms, as the smallest units of the proteome, are molecules (polypeptides) arising from all combinatorial sources of variation after

expression of a single gene. Each proteoform is a chemically clearly defined molecule. These molecules are different due to genetic variation, alternatively spliced RNA, transcripts and posttranslational modifications [5, 7]. Accordingly, the term protein refers to its coding gene and, therefore, becomes as the umbrella term for all developing proteoforms/protein species [6]. Sometimes the term "proteoform" is used for the description of structural variants of proteins as well [8]. But it will make the issue of terminology in proteomics more complicated and confused, as even inside the abovementioned definition, a proteomics field of proteoforms is very broad and could encompass many billions of components [9–12]. For instance, all combinations of 30 known modifications of histone H3 alone can theoretically produce more than 1 billion of proteoforms [10, 13]. Because of such a variety, huge range of concentration (7–8 orders of magnitude in blood plasma), and dynamic changes during life cycle, their identification, quantitation and database organization is a serious challenge. Nevertheless, there is evident progress in this area. So far, the main workhorse in proteomics was bottom-up mass spectrometry, but the top-down approach is becoming pre-eminent today [14]. Top-down proteomics implies that mass spectrometry is applied at the proteoform level, allowing the acquisition of information about all intramolecular complexity preserved during analysis, that might be overlooked in bottom-up shotgun workflows [14, 15]. But top-down proteomics cannot be just a one-step procedure. There are also several approaches based on protein separation that are involved in proteoform analysis. Among these methods, two-dimensional gel electrophoresis (2DE) occupies the special place. Accordingly, different schemes could be used to establish a basis for a comprehensive knowledge base for protein/proteoform inventory.

2. The principles of protein separation by 2DE

Application of different electrophoretic separation methods in two-dimensional combinations has a long history [16–23]. Continuous development on improvement of electrophoretic techniques and working out new support media for separation of proteins allowed to achieve better and better resolution. Finally, the best combination was chosen and optimized by O'Farrell in 1975 [24]. The method is based on separations in completely denaturing conditions according to two independent parameters (pI and Mw). Isoelectric focusing (IEF) that separates proteins due to difference in their isoelectric points (pI) is used as a first direction. High resolution according to protein size or weight (Mw) in the second direction is achieved by SDS polyacrylamide gel electrophoresis (SDS-PAGE) [23]. Quickly, the method was accepted by scientific community as the most powerful approach for separation of complex protein samples [25, 26]. Besides the high resolution, an important part of this method is that all stages of separation are performed in denaturing conditions, so in case of complex mixtures like cell extracts, all proteins or proteoforms are separated according to their basic parameters (pI and Mw) of their primary chemical structure (**Figure 1**). This is very important, as it allows not only to separate proteoforms but **also to** experimentally determine their pI and Mw. Also, these parameters can be calculated based on information about the chemical structure of the

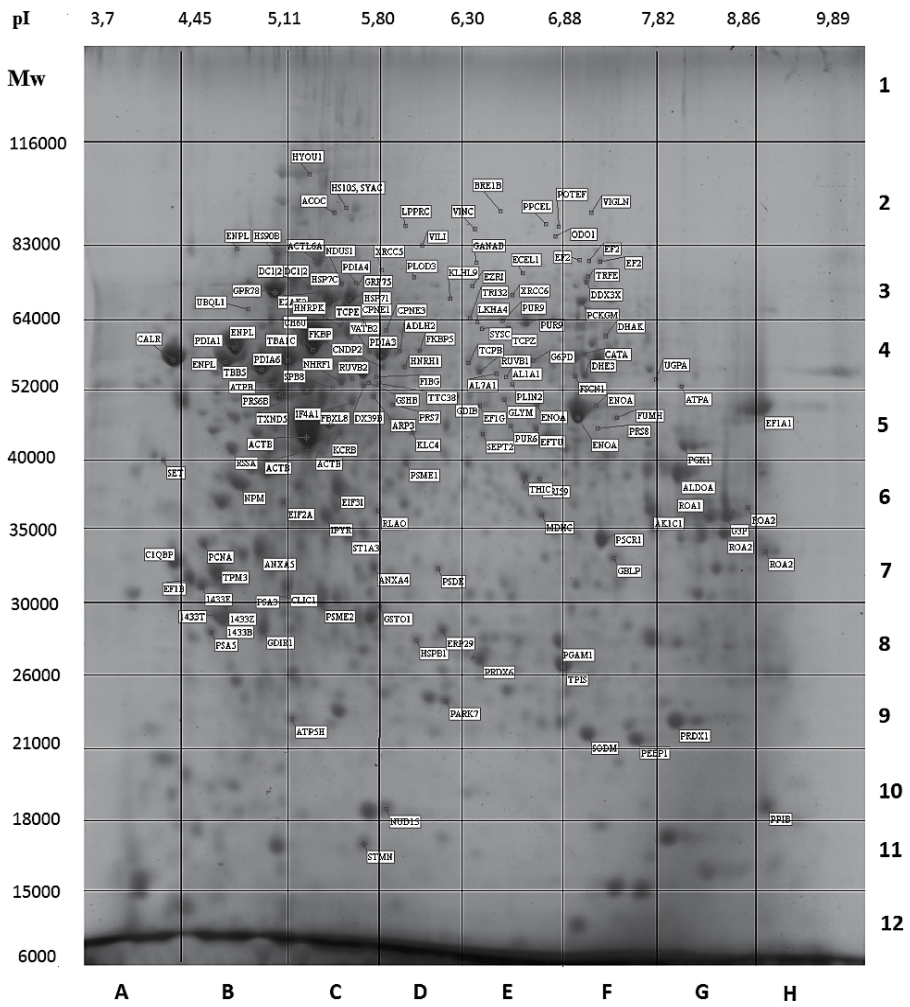

Figure 1. 2DE map of HepG2 proteins. Spots with proteins identified by MALDI TOF-MS are annotated. Sections in 2D gel selected for following LC ESI-MS/MS analysis are shown. Adapted from Naryzhny et al. [28].

proteoforms. Accordingly, two-dimensional separation of proteoforms can be performed not only experimentally but virtually as well [27–29] (**Figure 2**).

3. Information produced by 2DE gels

Separation with high resolution of proteoforms is the main function of 2DE, but extra steps should be done toward obtaining necessary information. Protein identification is the next very important step. Immunological methods as most specific approaches were mainly used for this

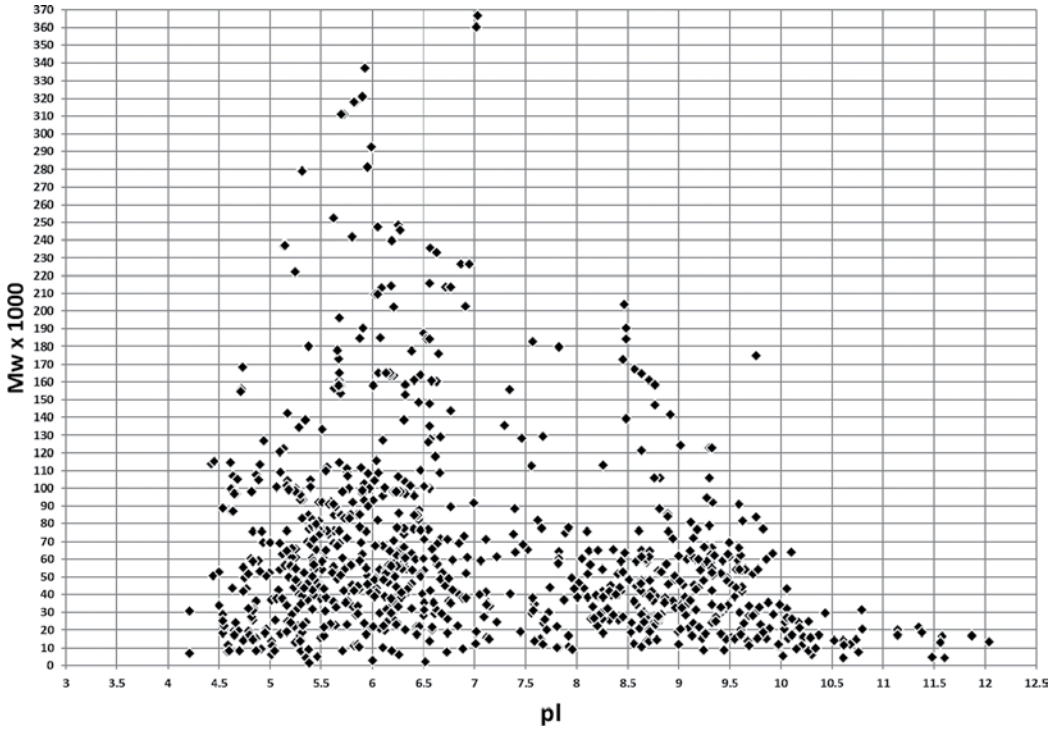

Figure 2. A virtual 2DE map of proteins coded by human chromosome 18.

purpose. They are still successfully used in 2DE-based proteomics for protein identification (Western blot) (**Figure 3**).

To study protein-protein interactions, so-called Far-Western blot is used (**Figure 4**) [32, 33]. In this case, the proteins after 2DE separation are transferred to a membrane and then treated with a set of buffers, which apply washes that allow "prey" proteins to denature and renature [32–34]. The membrane is then blocked and probed with a purified "bait" protein (the protein, which binding partners ("preys") need to be detected). The bait protein is detected on spots where the prey protein is located if the bait proteins and the prey protein bind together. For detection of bait proteins, they can be labeled, or antibodies can be used [32, 33]. This technique is not only very informative but also laborious and not convenient for a large-scale analysis. The situation was radically improved when mass spectrometry became a central element for proteomics analysis [35, 36].

The MS approach for protein identification by searching for the best match between peptide masses produced by specific hydrolysis and peptide masses calculated from theoretical cleavage of proteins was developed simultaneously by different groups [37–41]. In this case, the peptide mass sets are acquired by matrix-assisted laser desorption/ionization time-of-flight mass spectrometry (MALDI-TOF MS). This approach was named peptide mass fingerprinting (PMF). For a long time, PMF has been the most powerful technique for high-throughput

http://dx.doi.org/10.5772/intechopen.75125

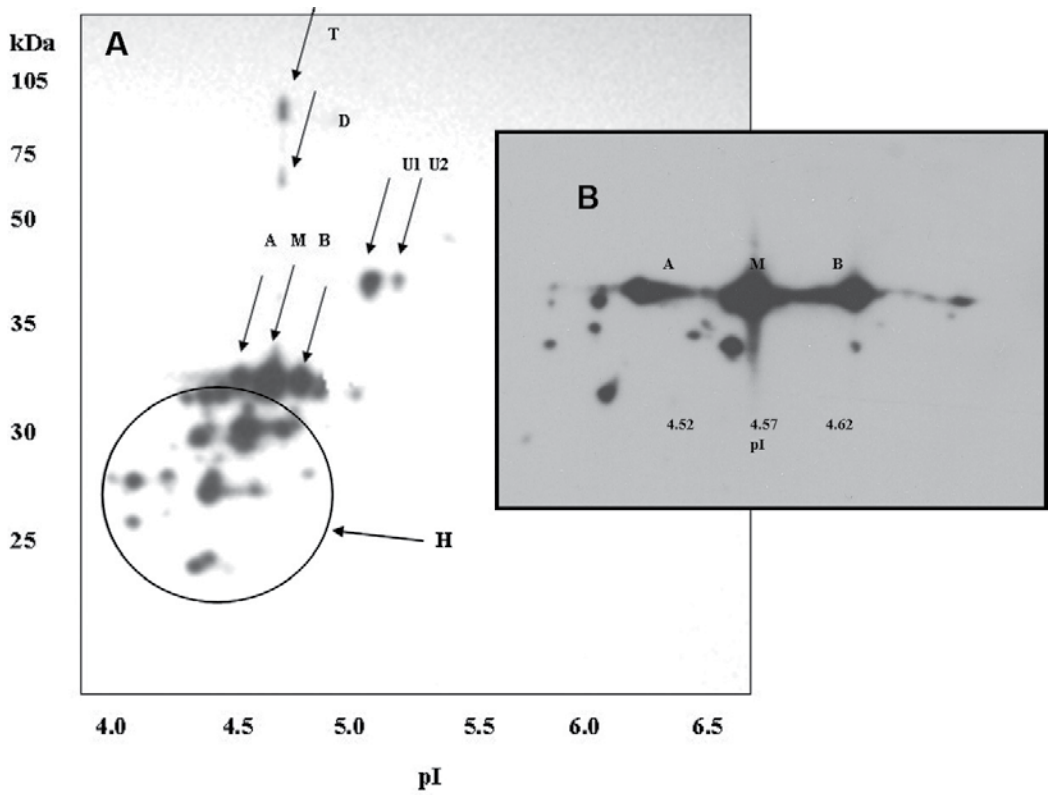

Figure 3. Multiple spots of PCNA (proteoforms) can be detected by 2DE. After 2DE separation and transfer to Immobilon-P membrane, immunostaining was performed using PCNA-specific antibody PC10. A, M, B, T and D denote acidic, main, basic, probable trimer and probable dimer forms of PCNA, respectively. U1 and U2 are ubiquitinated forms of PCNA monomer. H is a cluster of PCNA hydrolysis products, which is produced by proteasome action [30]. (A) 2DE (pH 4–7, 13 cm – first dimension, 10% SDS-PAGE, 13 cm – second dimension). (B) 2DE (pH 4–5, 18 cm – first dimension, 10% SDS-PAGE, 13 cm – second dimension). Adapted from Naryzhny [31].

protein identification. Using more sophisticated MS instruments (especially ESI LC–MS/MS), it was revealed that, depending on the gel resolution, the 2DE spots often contain more than a single protein, especially in the case of mammalian cells [29, 42]. Accordingly, the quantitation of proteins became an ambiguous task, as the densitometry of spots cannot be used for accurate proteoform quantitation. Fortunately, the special MS-based quantitative approaches can be applied in this case. In addition, as only the proteins detected as stained spots are analyzed, a lot of information is missing. This problem can be solved only by analyzing all parts of the gel [28, 43]. The general view of this method is shown in **Figure 1**. The main steps are as follows:

1. 2DE separation.
2. Staining the gel with Coomassie R350.
3. Scanning the image produced (2DE map).

4. Analyzes and calibration of the 2DE map by Image Master 2DE Platinum (GE Healthcare, Pittsburgh, PA, USA). Calibration was performed according to the position of several major protein spots that had been previously identified: actin cytoplasmic (ACTB_HUMAN, pI 5.29/Mw 42,052), 78 kDa glucose-regulated protein (GRP78_HUMAN, pI 5.07/Mw 72,333), tropomyosin alpha-3 chain (TPM3_HUMAN, pI 4.68/Mw 32,950), stathmin 1 (STMN_HUMAN, pI 5.76/Mw 17,292) and alpha-enolase (ENOA_HUMAN, pI 7.01/Mw 47,481).

5. The separation of the gel into 96 sections (identified as 1–12 along the Mw dimension and A–H along the pI dimension). According to the calibration, each section is given pI/Mw coordinates.

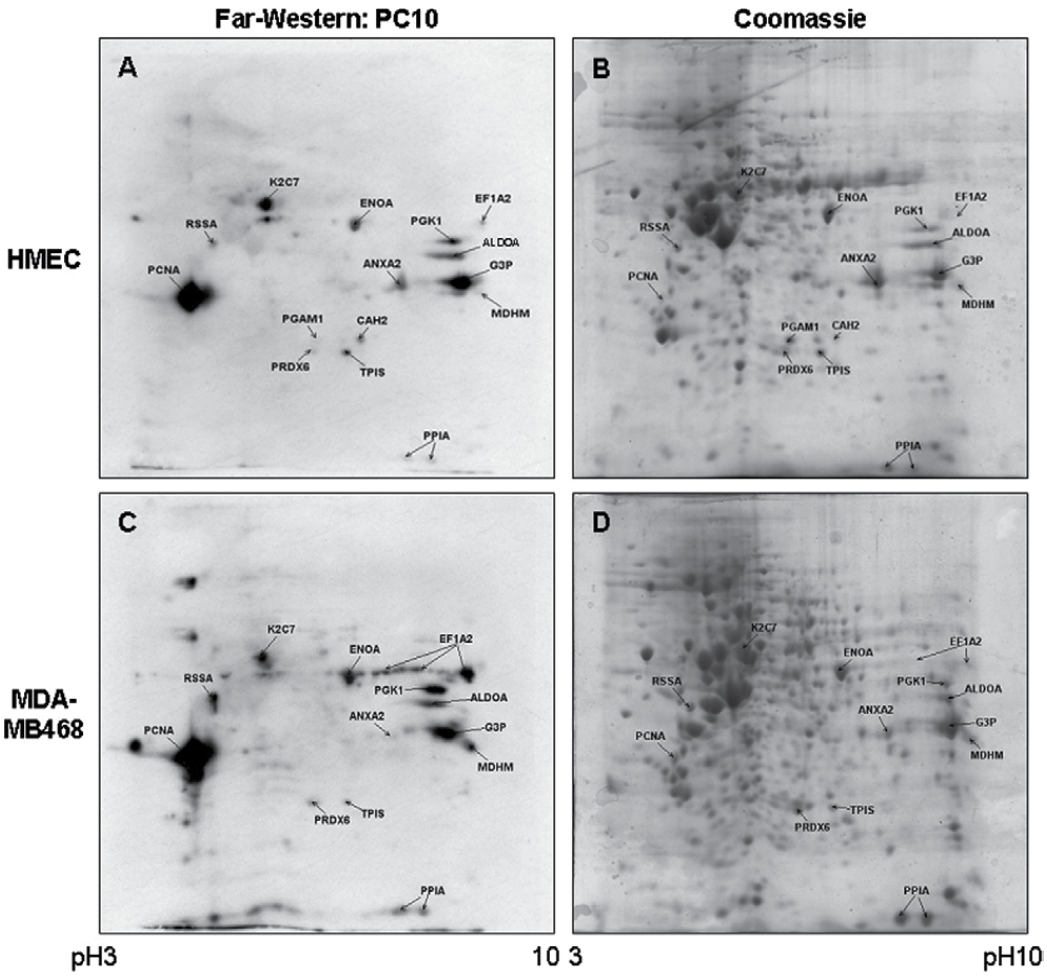

Figure 4. Identification of PCNA-binding proteins in normal and cancer cells by 2DE-Far-Western blotting. Protein extracts from HMEC (A and B) or MDA-MB468 (C and D) were separated by 2DE, transferred onto a membrane, renatured and incubated with PCNA. PCNA-binding proteins were then detected with the PC10 monoclonal anti-PCNA antibody. (B and D) Proteins separated by 2DE were stained with Coomassie R350, protein spots corresponding to signals on the membrane (A and C) were identified, cut out, and the identity of the proteins was determined by mass spectrometry. Adapted from Naryzhny et al. [32].

6. The treatment of each section with trypsin according to the protocol for mass-spectrometry by ESI LC–MS/MS.
7. Analysis of the tryptic peptides obtained from each 2DE section by Orbitrap Q-Exactive mass spectrometer.
8. Protein identification and relative quantification are performed using Mascot "2.4.1" and exponentially modified form of protein abundance index (emPAI).

In total, up to 500 unique proteins were identified in each section of 2DE gel after separation of proteins from glioblastoma cell extract (**Figure 1**). All proteins detected in the same section were given the pI/Mw parameters of this section.

Respectively, the same proteins detected in different sections were considered as different proteoforms. About 20,000 proteoforms coded by ~4000 genes were identified using this approach [28, 43]. Additionally, 3D graphs represented gene centric expression of proteoforms can be generated (**Figure 5**). Here, the proteoform profiles for each gene can

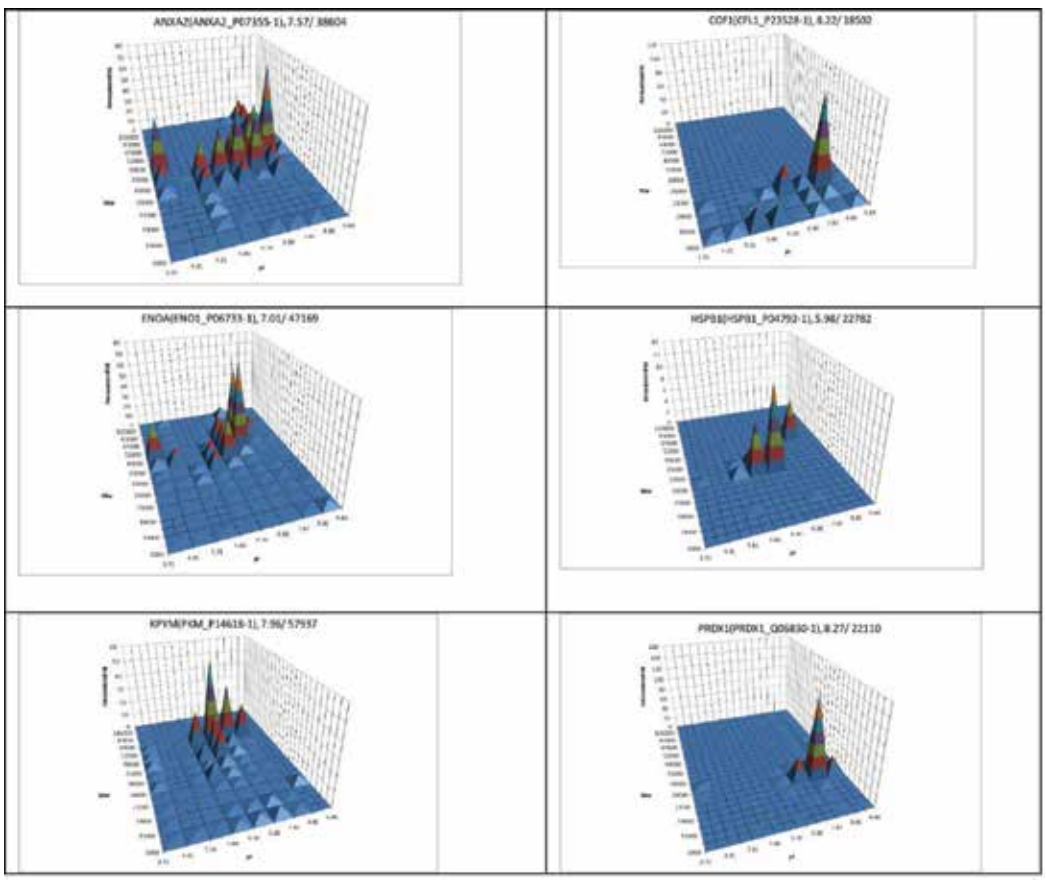

Figure 5. The examples of 3D graphs showing distribution of proteoforms between different sections of the 2DE map. A semiquantitative (estimated by emPAI) distribution of the same protein (gene) around the different gel sections was plotted. Proteins, the potential biomarkers, are shown. Reproduced with permission from Naryzhny et al. [43].

be observed. Considering that only 96 sections from a small gel (8 cm × 8 cm) were taken for analysis, the situation can be improved significantly by increasing the gel size, the sampleloading and the number of sections. This approach also solves the problem with a sensitivity of the staining. However, there are still some issues that need to be tackled. One of them is a resolution, which drops largely if we cut the gel into big sections. Ideally, the size of these sections should be close to the size of the smallest spots. But in this case, we are facing a dramatically increased amount of samples (around 1000). As there is a limitation in the processing time of each sample by ESI LC–MS/MS (usually at least 0.5 h per sample), we will need about 1 month of continuous work on the Orbitrap to analyze these samples from a single 2DE gel. Another issue is proteoform quantitation. There are several options available. The exponentially modified form of protein abundance index (emPAI) [28, 43, 44] is not ideal, since it gives only a relative and not very accurate estimation of the protein content. Another option is MaxQuant that recently became possibly the most frequently used platforms for mass-spectrometry (MS)-based proteomics data analysis [45]. Since its release in 2008, it has been improved substantially [45, 46]. Selected reaction monitoring (SRM) and isotope-coded affinity tag (ICAT) are other excellent examples of the power of MS technology in protein quantitation [47–49]. There are also more approaches that are described and reviewed [50, 51].

4. Databases based on 2DE gels

The overall approach has been used to generate annotated 2DE gel databases for many cell types. The first 2DE database, SWISS-2DPAGE database has been launched in 1993 and is maintained by the Central Clinical Chemistry Laboratory of the Geneva University Hospital and the Swiss Institute of Bioinformatics (SIB). Now this database is a part of the World-2DPAGE (http://world-2dpage.expasy.org/list/), a dynamic portal to query simultaneously world-wide gel-based proteomics databases. These databases put together over 250 maps for 23 species, totalizing nearly 40,000 identified spots, making it the biggest gel-based proteomics dataset accessible from a single interface. Here, we can select a 2DE map which will be displayed for inspection. The database can be queried by keywords (protein description, protein name, gene name, species, author, full text, protein spot serial number) or graphically by clicking on a spot. Each spot is linked to a page containing the corresponding gene (protein) information and identification details. Also, information is displayed about other spots in different maps, where product of the same gene is detected. All these spots are highlighted in the maps and the calculated parameters [isoelectric point (pI) and molecular weight (Mw)] are displayed. There is a possibility for cross-references and obtaining more information from different 2DE databases and from UniProtKB. UniProtKB, a comprehensive protein sequence knowledge base has two sections: UniProtKB/Swiss-Prot, which is manually curated and UniProtKB/TrEMBL that contains computer-annotated entries. UniProtKB/Swiss-Prot entries provide users with cross-links to about 100 external databases and with access to additional information or tools [52].

http://dx.doi.org/10.5772/intechopen.75125

5. Collection of experimental and theoretical data on the platform of 2DE gel

The proteomes can be retrieved from experimental data or generated by available programs, which calculate theoretical protein parameters [27, 53, 54]. According to their basic parameters (pI/Mw), the unique principles of separation of polypeptides allow to organize the crosstalk between experimental and theoretical data. In a simple way, this approach was realized in abovementioned 2DE databases. The main idea behind the approach, where each spot is considered as containing only one protein, works well only with simple proteomes (for instance, mycoplasm), where the number of proteoforms are not so big as in mammalian cells [11, 12, 55, 56]. A European pathogenic microorganism proteome database focused on pathogenic microorganisms was launched. Now, under the name "The Proteome 2D-PAGE Database," this database currently contains 13,893 identified spots and 3245 mass peak lists in 57 reference maps representing experiments from 26 different organisms and strains. The database provides protein information such as ORF name, predicted isoelectric point (pI) and molecular weight (Mw), several protein identifiers, identification method, sequence coverage, and so on. [57]. This database contains information about mammalian cells as well. Therefore, multiple proteins can be attributed to the same spot in case of these cells.

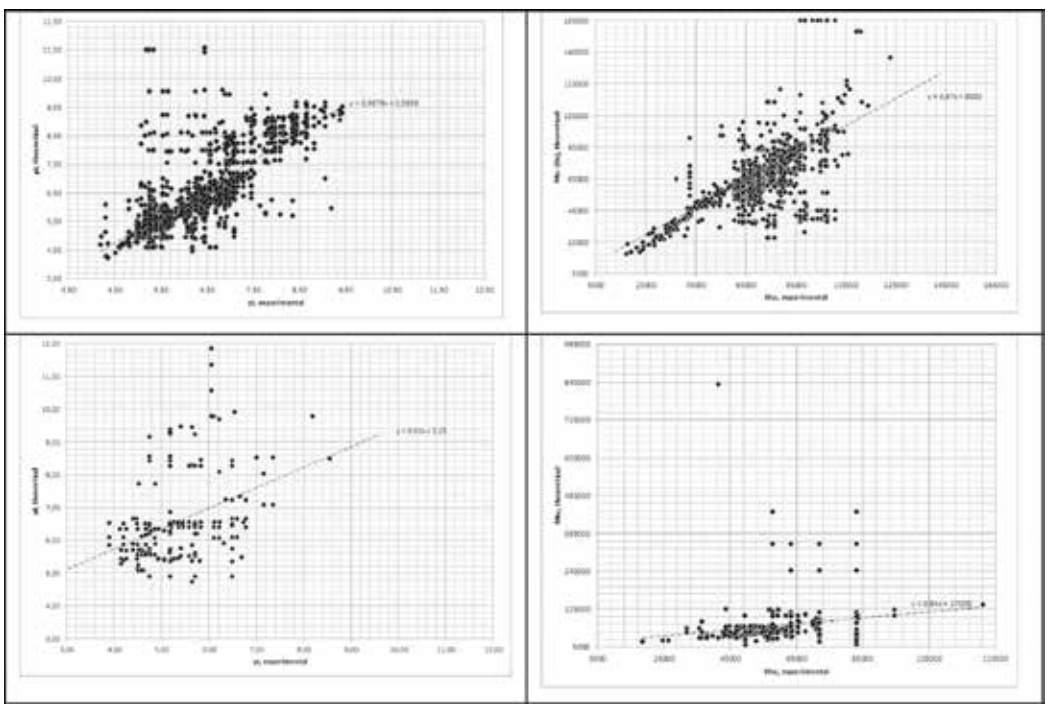

Figure 6. Relationship between theoretically (in silico) determined pI (left) or mw (right) of proteins (canonical forms) and experimentally detected pI/mw of proteoforms. Top – HepG2 cells, bottom – human depleted plasma. Adapted from Naryzhny et al. [29].

The idea to manage the theoretical proteomes and link them with experimental, 2DE-based data has been tried to realize in another online database, DynaProt 2D [58]. It was developed for dynamic access to proteomes and 2DE gels. Here, a 2DE gel could serve as a reference map and as a tool for navigation of the database [58]. Integrated into 2DE database a complete theoretical proteome could provide a powerful tool allowing simply linking newly identified spots to the already available appropriate theoretical data [58]. But this idea was tried for one organism only, Lactococcus lactis, and stopped in realization.

If we plot experimentally measured physicochemical parameters of proteoforms (pI or Mw) against the theoretical ones, the general view of the proteome according to the diversity of proteoforms is revealed (**Figure 6**). Here, the dots are distributed along the diagonal in the graph, if experimentally detected parameters match or are close to the theoretical values. Otherwise, dots are distributed above or below the diagonal, and the bigger the difference between theoretical and experimental parameters, the bigger the deviation of the dot position from the diagonal. In particular, in case of pI, the location of proteoform dots above the diagonal shows that the experimental pIs of this proteoform is smaller than the theoretical

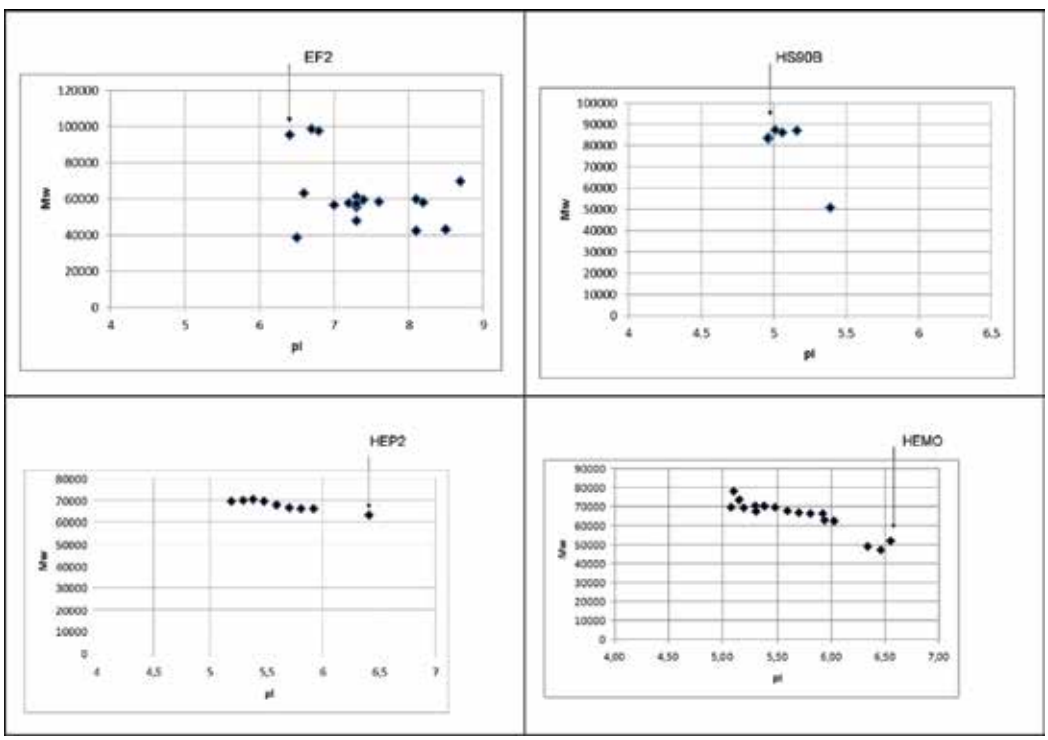

Figure 7. The examples of variety of proteoforms in HepG2 cells (top) and human plasma (bottom). The arrow shows the predicted location of the master polypeptide (polypeptide coded by the canonical sequence). Adapted from Naryzhny et al. [29].

one. It can be usually because of adding negative charges (phosphorylation) or removing positive charges (acetylation). An opposite situation with increased pI (the dots are under the diagonal) is observed; then, PTMs are removing negative charges from proteins (esterification). In case of Mw, location of a dot above the diagonal means that theoretical mass (weight) of this polypeptide is bigger than the experimentally observed one. It could be if the polypeptide is truncated or proteolytically processed. If the dots are observed below the diagonal, it can be because of several reasons. It can happen because of technical issues of 2DE procedure (protein polymerization, aggregation or precipitation). Glycosylation also can strongly increase a polypeptide mass. This situation can be analyzed in more detail by representation of all proteoforms corresponding to the same gene on the separate chart (**Figure 7**).

6. Conclusion

The continuing evolution of the detection technique (mostly mass spectrometry) and usage of it in combination with optimum protein separation techniques will finally allow us to reach the main aim of the HUPO—image of the whole human proteome. A union of such a classic proteomics method for separation of proteins as 2DE with bottom-up mass spectrometry (shot-gun analysis of peptides by ESI LC-MS/MS) is an efficient approach for increasing the productivity of tandem mass-spectrometry. Additionally, this union of top-down and bottom-up approaches allows very convenient visual representation (profiling) of information about diverse proteoforms. As 2DE maps are a convenient and effective way to represent information about proteomes and navigate around all its proteoforms, it will allow the construction of a knowledge base for an inventory of all human protein species/proteoforms, that is, visually attractive, clear, easy to search and perceptive.

Particularly, the development of chromosome-centric interactive virtual 2DE maps of proteins coded by specific genes in combination with experimental 2DE protein maps will allow executing more effectively C-HPP, to estimate more accurately the number of proteoforms and could be a basis for the knowledge base of human proteins. The development of such inventory will be based on existing databases like http://world-2dpage.expasy.org/, https://www.nextprot.org/, http://www.uniprot.org/ and http://atlas.topdownproteomics.org.

Acknowledgements

The study was performed in frames of Program of Fundamental Research of State Academies of Sciences for 2013-2020. Mass spectrometry measurements were performed using the equipment of "Human Proteome" Core Facilities of the Institute of Biomedical Chemistry (Russia) which is supported by Ministry of Education and Science of the Russian Federation (agreement 14.621.21.0017, unique project ID RFMEFI62117X0017).

Author details

Stanislav Naryzhny[1,2]

Address all correspondence to: snaryzhny@mail.ru

1 Institute of Biomedical Chemistry, Moscow, Russia

2 Petersburg Nuclear Physics Institute, National Research Center "Kurchatov Institute", Leningrad Region, Russia

References

[1] Kim MS, Pinto SM, Getnet D, Nirujogi RS, Manda SS, Chaerkady R, et al. A draft map of the human proteome. Nature [Internet]. 2014;**509**(7502):575-581. Available from: http://www.ncbi.nlm.nih.gov/pubmed/24870542

[2] Wilhelm M, Schlegl J, Hahne H, Gholami AM, Lieberenz M, Savitski MM, et al. Mass-spectrometry-based draft of the human proteome. Nature. 2014;**509**(7502):582-587

[3] Aebersold R, Mann M. Mass spectrometry based proteomics. Nature [Internet]. 2003;**422**: 198-207. Available from: http://www.ncbi.nlm.nih.gov/pubmed/12634793

[4] de Godoy LMF, Olsen J V., Cox J, Nielsen ML, Hubner NC, Fröhlich F, et al. Comprehensive mass-spectrometry-based proteome quantification of haploid versus diploid yeast. Nature [Internet]. 2008;**455**(7217):1251-1254. Available from: http://www.nature.com/doifinder/10.1038/nature07341

[5] Schlüter H, Apweiler R, Holzhütter H-G, Jungblut PR. Finding one's way in proteomics: a protein species nomenclature. Chemistry Central Journal [Internet]. 2009;**3**:11. Available from: http://www.pubmedcentral.nih.gov/articlerender.fcgi?artid=2758878&tool=pmcentrez&rendertype=abstract

[6] Jungblut P, Thiede B, Zimny-Arndt U, Müller EC, Scheler C, Wittmann-Liebold B, et al. Resolution power of two-dimensional electrophoresis and identification of proteins from gels. Electrophoresis. 1996;**17**(5):839-847

[7] Smith LM, Kelleher NL. Proteoform: A single term describing protein complexity. Nature Methods. 2013;**10**:186-187

[8] Uversky VN. p53 Proteoforms and intrinsic disorder: An illustration of the protein structure-function continuum concept. International Journal of Molecular Sciences. 2016;**17**(11):1874

[9] Kelleher NL. A cell-based approach to the human proteome project. Journal of the American Society for Mass Spectrometry. 2012;**23**(10):1617-1624

[10] Jungblut PR. The proteomics quantification dilemma. Journal of Proteomics [Internet]. 2014;**107**:98-102 Available from: http://dx.doi.org/10.1016/j.jprot.2014.03.015

[11] Naryzhny SN, Lisitsa AV, Zgoda VG, Ponomarenko EA, Archakov AI. 2DE-based approach for estimation of number of protein species in a cell. Electrophoresis. 2014; **35**(6):895-900

[12] Naryzhny SN, Zgoda VG, Maynskova MA, Ronzhina NL, Belyakova N V, Legina OK, et al. Experimental estimation of proteome size for cells and human plasma. Biomeditsinskaia Khimiia [Internet]. 2015;**61**(2):279-285. Available from: http://www.ncbi.nlm.nih.gov/pubmed/25978394

[13] Garcia BA, Pesavento JJ, Mizzen CA, Kelleher NL. Pervasive combinatorial modification of histone H3 in human cells. Nature Methods [Internet]. 2007;**4**(6):487-489 Available from: http://www.nature.com/doifinder/10.1038/nmeth1052

[14] Toby TK, Fornelli L, Kelleher NL. Progress in top-down proteomics and the analysis of Proteoforms. Annual Review of Analytical Chemistry [Internet]. 2016;**9**(1):499-519 Available from: http://www.annualreviews.org/doi/10.1146/annurev-anchem-071015-041550

[15] Durbin KR, Fornelli L, Fellers RT, Doubleday PF, Narita M, Kelleher NL. Quantitation and identification of thousands of human proteoforms below 30 kDa. Journal of Proteome Research. 2016;**15**(3):976-982

[16] Bussard A, Huet JM. Description of a technic simultaneously combining electrophoresis and immunological precipitation in gel: Electrosyneresis. Biochimica et Biophysica Acta. 1959;**34**:258-260

[17] Laurell CB. Electroimmuno assay. Scandinavian Journal of Clinical and Laboratory Investigation [Internet]. 1972;**29**(s124):21-37 Available from: http://www.tandfonline.com/doi/full/10.3109/00365517209102748

[18] Laurell C-B. Quantitative estimation of proteins by electrophoresis in agarose gel containing antibodies. Analytical Biochemistry [Internet]. 1966;**15**(1):45-52 Available from: http://www.sciencedirect.com/science/article/pii/0003269766902466

[19] Awdeh ZL, Williamson AR, Askonas BA. Isoelectric focusing in polyacrylamide gels. Nature. 1968;**219**:66-67

[20] Righetti PG, Drysdale JW. Isoelectric focusing in gels. Journal of Chromatography. A. 1974;**98**(2):271-321

[21] Dale G, Latner AL. Isoelectric focusing in polyacrylamide gels. Lancet. 1968;**1**:847-848

[22] Fawcett JS. Isoelectric fractionation of proteins on polyacrylamide gels. FEBS Letters. 1968;**1**:81-82

[23] Laemmli UK. Cleavage of structural proteins during the assembly of the head of bacteriophage T4. Nature. 1970;**227**(5259):680-685

[24] O'Farrell PH. High resolution two-dimensional electrophoresis of proteins. Journal of Biological Chemistry [Internet]. 1975;**250**(10):4007-4021 Available from: http://www.pubmedcentral.nih.gov/articlerender.fcgi?artid=2874754&tool=pmcentrez&rendertype=abstract

[25] Anderson NGAN. The human protein index. Clinical Chemistry [Internet]. 1982;**28**(4): 739-748 Available from: http://clinchem.aaccjnls.org/content/28/4/739.long

[26] Anderson NG, Matheson A, Anderson NL. Back to the future: The human protein index (HPI) and the agenda for post-proteomic biology. Proteomics [Internet]. 2001;**1**(1):3-12 Available from: http://onlinelibrary.wiley.com/doi/10.1002/1615-9861(200101)1:1%3C3::AID-PROT3%3E3.0.CO;2-T/abstract

[27] Hiller K, Schobert M, Hundertmark C, Jahn D, Münch R. JVirGel: Calculation of virtual two-dimensional protein gels. Nucleic Acids Research. 2003;**31**(13):3862-3865

[28] Naryzhny SN, Maynskova MA, Zgoda VG, Ronzhina NL, Kleyst OA, Vakhrushev IV, et al. Virtual-experimental 2DE approach in chromosome-centric human proteome project. Journal of Proteome Research. 2016

[29] Naryzhny SN, Zgoda VG, Maynskova MA, Novikova SE, Ronzhina NL, Vakhrushev IV, et al. Combination of virtual and experimental 2DE together with ESI LC-MS/MS gives a clearer view about proteomes of human cells and plasma. Electrophoresis. 2016;**37**(2):302-309

[30] Naryzhny SN, Lee H. Observation of multiple isoforms and specific proteolysis patterns of proliferating cell nuclear antigen in the context of cell cycle compartments and sample preparations. Proteomics. 2003;(6):930

[31] Naryzhny SN. Proliferating cell nuclear antigen: A proteomics view. Cellular and Molecular Life Sciences C [Internet]. 2008;**65**(23):3789-3808. Available from: http://www.ncbi.nlm.nih.gov/pubmed/18726183

[32] Naryzhny SN, Lee H. Proliferating cell nuclear antigen in the cytoplasm interacts with components of glycolysis and cancer. FEBS Letters. 2010;**584**(20):4292-4298

[33] Wu Y, Li Q, Chen X-Z. Detecting protein-protein interactions by far western blotting. Nature Protocols. 2007;**2**(12):3278-3284

[34] Guichet A, Copeland JW, Erdélyi M, Hlousek D, Závorszky P, Ho J, et al. The nuclear receptor homologue Ftz-F1 and the homeodomain protein Ftz are mutually dependent cofactors. Nature [Internet]. 1997;**385**(6616):548-552. Available from: http://www.ncbi.nlm.nih.gov/pubmed/9020363

[35] Perkins DN, Pappin DJ, Creasy DM, Cottrell JS. Probability-based protein identification by searching sequence databases using mass spectrometry data. Electrophoresis [Internet]. 1999;**20**(18):3551-3567. Available from: http://www.ncbi.nlm.nih.gov/pubmed/16638152

[36] Webster J, Oxley D. Protein identification by MALDI-TOF mass spectrometry. Methods in Molecular BiologyMethods in Molecular Biology [Internet]. 2012;**800**:227-240. Available from: http://www.ncbi.nlm.nih.gov/pubmed/21964792

[37] Pappin DJC, Hojrup P, Bleasby AJ. Rapid identification of proteins by peptide-mass fingerprinting. Current Biology. 1993;**3**(6):327-332

[38] Henzel WJ, Billeci TM, Stults JT, Wong SC, Grimley C, Watanabe C. Identifying proteins from two-dimensional gels by molecular mass searching of peptide fragments in protein

sequence databases. Proceedings of the National Academy of Sciences of the United States of America [Internet]. 1993;**90**(11):5011-5015 Available from: http://www.pubmedcentral.nih.gov/articlerender.fcgi?artid=46643&tool=pmcentrez&rendertype=abstract

[39] Mann M, Hojrup P, Roepstorff P. Use of mass spectrometric molecular weight information to identify proteins in sequence databases. Biological Mass Spectrometry. 1993;**22**(6): 338-345

[40] James P, Quadroni M, Carafoli E, Gonnet G. Protein identification by mass profile fingerprinting, Biochemical and Biophysical Research Communications [Internet]. 1993;**195**:58-64. Available from: http://www.ncbi.nlm.nih.gov/pubmed/8363627

[41] Yates JR, Speicher S, Griffin PR, Hunkapiller T. Peptide mass maps: A highly informative approach to protein identification. Analytical Biochemistry [Internet]. 1993;**214**(2):397-408 Available from: http://www.sciencedirect.com/science/article/pii/S0003269783715149

[42] Thiede B, Koehler CJ, Strozynski M, Treumann A, Stein R, Zimny-Arndt U, et al. Protein species high resolution quantitative proteomics of HeLa cells using SILAC-2-DE-nanoLC/-LTQ-Orbitrap mass spectrometry. Molecular & Cellular Proteomics [Internet]. 2012;**12**(2):529-538. Available from: http://www.pubmedcentral.nih.gov/articlerender.fcgi?artid=3567871&tool=pmcentrez&rendertype=abstract

[43] Naryzhny SN, Maynskova MA, Zgoda VG, Ronzhina NL, Novikova SE, Belyakova NV, Kleyst OA, Legina OK, Pantina RAFM. Proteomic profiling of high-grade glioblastoma using virtual-experimental 2DE. Journal of Proteomics and Bioinformatics. 2016;**9**(6):158-165

[44] Ishihama Y, Oda Y, Tabata T, Sato T, Nagasu T, Rappsilber J, et al. Exponentially Modified Protein Abundance Index (emPAI) for estimation of absolute protein amount in proteomics by the number of sequenced peptides per protein. Molecular & Cellular Proteomics [Internet]. 2005;**4**(9):1265-1272. Available from: http://www.mcponline.org/content/4/9/1265.abstract

[45] Tyanova S, Temu T, Cox J. The MaxQuant computational platform for mass spectrometry-based shotgun proteomics. Nature Protocols. 2016;**11**(12):2301-2319

[46] Cox J, Mann M. MaxQuant enables high peptide identification rates, individualized p.p. b.-range mass accuracies and proteome-wide protein quantification. Nature Biotechnology. 2008;**26**(12):1367-1372

[47] Lange V, Picotti P, Domon B, Aebersold R. Selected reaction monitoring for quantitative proteomics: A tutorial. Molecular Systems Biology. 2008;**4**(222):222

[48] Gygi SP, Rist B, Gerber SA, Turecek F, Gelb MH, Aebersold R. Quantitative analysis of complex protein mixtures using isotope-coded affinity tags. Nature Biotechnology [Internet]. 1999;**17**(10):994-999 Available from: http://dx.doi.org/10.1038/13690

[49] Kusebauch U, Campbell DS, Deutsch EW, Chu CS, Spicer DA, Brusniak MY, Slagel J, Sun Z, Stevens J, Grimes B, Shteynberg D, Hoopmann MR, Blattmann P, Ratushny AV, Rinner O, Picotti P, Carapito C, Huang CY, Kapousouz M, Lam H, Tran T, Demir E, Aitchison JD, Human MR. SRMAtlas: A resource of targeted assays to quantify the complete human proteome. Cell. 2016;**166**(3):766-778

[50] Cox J, Hein MY, Luber CA, Paron I, Nagaraj N, Mann M. Accurate proteome-wide label-free quantification by delayed normalization and maximal peptide ratio extraction, termed MaxLFQ. Molecular & Cellular Proteomics [Internet]. 2014;**13**(9):2513-2526 Available from: http://www.mcponline.org/lookup/doi/10.1074/mcp.M113.031591

[51] Blein-Nicolas M, Zivy M. Thousand and one ways to quantify and compare protein abundances in label-free bottom-up proteomics. Biochimica et Biophysica Acta – Proteins and Proteomics. 2015

[52] Boutet E, Lieberherr D, Tognolli M, Schneider M, Bairoch A. UniProtKB/Swiss-Prot. Methods in Molecular Biology [Internet]. 2007;**406**:89-112. Available from: http://www.ncbi.nlm.nih.gov/pubmed/18287689

[53] Perez-Riverol Y, Vizcaíno JA. Synthetic human proteomes for accelerating protein research. Nature Methods. 2017;**14**:240-242

[54] Pruess M, Fleischmann W, Kanapin A, Karavidopoulou Y, Kersey P, Kriventseva E, et al. The proteome analysis database: A tool for the in silico analysis of whole proteomes. Nucleic Acids Research. 2003;**31**:414-417

[55] Ueberle B, Frank R, Herrmann R. The proteome of the bacterium mycoplasma pneumoniae: Comparing predicted open reading frames to identified gene products. Proteomics. 2002;**2**: 754-764

[56] Jungblut PR, Hecker M, editors. Proteomics of microbial pathogens. Wiley-VCH Verlag Weinheim; 2007. 326 p. DOI: 10.1002/9783527610099.ch6

[57] Pleißner KP, Eifert T, Jungblut PR. A European pathogenic microorganism proteome database: Construction and maintenance. Comparative and Functional Genomics. 2002; **3**(2):97-100

[58] Drews O, Görg A. DynaProt 2D: An advanced proteomic database for dynamic online access to proteomes and two-dimensional electrophoresis gels. Nucleic Acids Research. 2005;**33**(Database Issue):D583-D587

Chapter 7

The Use of Gel Electrophoresis and Mass Spectrometry to Identify Nitroproteins in Nervous System Tumors

Xianquan Zhan and Na Li

Additional information is available at the end of the chapter

http://dx.doi.org/10.5772/intechopen.76889

Abstract

Protein tyrosine nitration is an important molecular event in nervous system tumor such as glioma and pituitary adenomas. It is the essential step to identify the protein targets and exact modified sites of tyrosine nitration for addressing the biological roles of protein tyrosine nitration in nervous system tumors and discovering effective biomarkers to understand in-depth molecular mechanisms and determine new diagnosis strategy and novel therapeutic targets. One/two-dimensional gel electrophoresis (1DGE, 2DGE), or nitrotyrosine affinity column (NTAC), coupled with tandem mass spectrometry (MS/MS) have been successfully applied in the analysis of nitroproteins in nervous system tumors. This article address the basic concept of protein tyrosine nitration, nitroproteomics methodology based on gel electrophoresis/immunoaffinity enrichment and tandem mass spectrometry, and the current status of nitroprotein study in nervous system tumors. The established nitroproteomics approach is easily translated to study other diseases.

Keywords: two-dimensional gel electrophoresis, one-dimensional gel electrophoresis, tandem mass spectrometry, tyrosine nitration, nitroprotein, nitroproteomics, nervous system tumors

1. Introduction

The incidence of central nervous system (CNS) has been increasing over the last 30 years, and unfortunately, become younger and younger [1]. More remarkable, patients (20–40%) with systemic cancer will occur metastatic disease to the CNS [2]. Primary malignant brain tumors and other metastatic disease to the CNS threaten human health. Astrocytoma is a type of primary malignant brain tumor that range from 20 to 40% of glioma, which is the most common

primary brain tumor in adults [3]. Here, we put research emphasis on two kinds of primary intracranial tumor, astrocytomas and pituitary adenomas. Astrocytomas cells possess the characteristic of high invasion to cause difficulty in therapy and high mortality (median survival = 9–12 months) [4]. A pituitary adenoma is quite common, and accounts for 10% of all primary intracranial neoplasias [5]. Even only a minority of pituitary adenomas (0.1–0.2%) develops into metastatic cancer, pituitary adenomas arise clinical problems: (a) Compress the adjacent brain organs appear symptoms including headache and visual failure. (b) An inappropriate hormone secretion led to hormone syndromes, including hypopituitarism, acromegaly, hyperprolactinemia and Cushing's syndrome [6]. The molecular mechanisms of those diseases remain unclear, and the traditional treatment models contain surgical excision, radiotherapy, and medical therapies [7]. Discovering in-depth molecular mechanisms, new diagnosis strategy, novel therapeutic targets are urgent.

Protein tyrosine nitration is an important posttranslational modification (PTM) in nervous system tumors that is related with multiple abnormal pathophysiological processes [8]. The process of protein tyrosine nitration is formed from 3-nitrotyrosine group to position 3 of the tyrosine residue phenolic ring [9], which alters the electron density and pKa value (from ~10 for tyrosine into ~7.1 for 3-nitrotyrosine) of the tyrosine phenolic ring [10]. Such changes affect biochemical characteristics of the tyrosine residue that will change interaction between enzyme-substrate, antigen–antibody or receptor-ligand, when interacting regions were in nitration. Reactive nitrogen species (RNS) act as an important mediated material for protein nitration, and our studies [11] consistent with others [12, 13] have indicated that nitric oxide and protein nitration may play important roles in the nervous system tumors. Previous studies reported that (1) the inflammatory reaction is involved in nervous system tumors [14]; (2) NO and RNS are important inflammatory mediators [15]; and (3) increased production of NO, peroxinitrite and superoxide, occurs in nervous system tumors [16]; (4) higher levels of nitrotyrosine are observed in nervous system tumors than normal tissues with biochemical approaches and immunohistochemical, and only protein nitrotubulin and protein nitro-p53 have been determined in human nervous system tumors [17]. Furthermore, the amino acid analog 3-nitrotyrosine due to functional and morphological injury of mouse-neuroblastoma cell lines and rat-glioma cell lines [18]. These studies demonstrated the importance of protein tyrosine nitration in the pathogenesis of nervous system tumors. Illustrating the functions of nitroproteins might reveal in-depth molecular mechanisms and biological function of tyrosine nitration in human nervous system tumors. Literature-based review and comprehensive annotation of proteins on the SwissProt website were used to expound the nitroprotein domains/motifs, location of nitrotyrosine sites and possible signaling pathways relevant to nervous system tumors. Nitroproteins took part in multiple biological processes in the development of tumors as follows: (a) tumor cell migration and invasion [19]; (b) cell proliferation and apoptosis [20]; (c) chemotherapy resistance [21]; (d) signal transduction [22]; (e) phenotypic dedifferentiation [23]; (f) microtubule dynamic stabilization [24]; (g) tumor recurrence; (h) others such as immunoreaction and post-transcriptional regulation. Moreover, the discovery of tyrosine nitration being a reversible reaction [25] and having a competition between phosphorylation motif [26], led us to speculate that dynamic process of protein nitration might also be regulated and controlled. However, no definite target of intervention is found for tyrosine nitration in human nervous system tumors. It takes long time to study tumor-related nitroproteins and to illustrate molecular mechanisms in tumor formation.

Nitroproteomics methods were based on sample enrichment and mass spectrometry analysis. Modern nitroproteomics applies protein-separation-enrichment techniques such as gel methods and non-gel methods, including immunoprecipitation [11], anti-nitrotyrosine antibody-based enzyme-linked immunosorbent assay (ELISA) [27], and one/two-dimensional gel electrophoresis (1DGE/2DGE)-based Western blot analyses [9]. 1DGE/2DGE-based Western blots analyses can separate and preferentially enrich endogenous nitroproteins and also preliminarily determine the quantitative information of nitrotyrosine. Studies showed that the same protein was detected at multiple gel-spots on 2D electrophoresis gels, and single 2D electrophoresis gel-spot usually contains several proteins [28]. Therefore, 2D electrophoresis gel has advantages in protein component visualization, detection of protein species that are mainly derived from alternative splicing or PTMs [9]. Protein isoforms or variants present dynamic biological processes in vivo, and different protein species associated with different conditions and pathophysiological status [29]. We adopted 1DGE/2DGE-based Western blots analyses method: the scanned images of the silver-stained 2D electrophoresis gels and the visualization of Western blot membranes were input to a PDQuest system (Bio-Rad, version 7.1, Hercules, CA) to composite image that contained the Gaussian spots [30]. MS/MS is the mainstream technique to identify protein species and PTMs products with verification of amino acid sequence, splicing sites, and modification site [31]. However, it is also pointed out that the challenges faced by low abundance of tyrosine nitration and the elusive mass spectrometry result of a nitro group are existed [32]. For example, matrix-assisted laser desorption ionization (MALDI) is quite different from electrospray ionization (ESI)-MS when study the MS behaviors of a nitropeptide [33]. Photochemical decompositions of the nitro group ($–NO_2$) induced by the high-energy laser decrease the precursor-ion intensity of a nitropeptide, making an MS spectrum much more complex in process of MALDI. However, the decomposition pattern of a nitropeptide was well clarified by the photochemical decomposition pattern ([M + H]+, [M + H – 16]+, [M + H –30]+, and [M + H – 32]+). Even ESI does not produce photochemical decompositions, scanning for the characteristic immonium ion (m/z 181.06) by the precursor ion could help accurately identify a nitropeptide or nitroprotein under ESI conditions [34]. Above key factors, including low abundance of nitroproteins, preferential enrichment methods, sensitivity of MS analysis, complicated MS behaviors of a nitro group, that all determine success or failure in the identity of in vivo nitroproteins. Thus, nitropeptide was detected by a vMALDI MS/MS method [9, 11]. Accumulation of MS/MS scans was used to increase the signal-to-noise ratio (S/N), which is needed for the detection of endogenous nitroproteins. A single MS/MS scan can determine an amino acid sequence to study proteome and phosphoproteome.

Protein tyrosine nitration is an (PTM) in nervous system tumor such as astrocytoma and pituitary adenomas, and participates in multiple complex biological processes [9, 11, 35, 36]. For human astrocytoma and pituitary adenomas nitroproteomics studies, 2DGE-based nitrotyrosine Western blot analysis with MALDI-TOF were used to identify endogenous nitroproteins and nitrotyrosine sites from human pituitary control and adenoma tissues, and 2DGE-based nitro-tyrosine Western blot analysis with liquid chromatography-electrospray ionization-quadrupole ion trap (LC-ESI-Q-IT) were used to identify endogenous nitroproteins and nitrotyrosine sites from human astrocytoma brain tissues. Bioinformatics and pathway analysis were used to determine domains/motifs in a nitroprotein, location of nitrotyrosine sites, and possible signaling pathways. A total of eight nitrotyrosine-containing proteins in human pituitary control tissues [9, 36], and nine nitroproteins and three nitroprotein-interacting

proteins in a human nonfunctional pituitary adenoma tissue [11], 18 nitroproteins and their 23 nitrotyrosine sites in human astrocytoma tissues [35], were identified with 2DE-MS/MS. The nitration site was located onto the corresponding functional domain, and each nitroprotein was carried out pathway analysis to speculate the possible biological function.

2. Materials and methods

2.1. Tissues and extraction of proteins

A clinically nonfunctional human pituitary adenoma tissue was obtained during surgery. The expression of FSH, LH, GH, prolactin, TSH, and ACTH were all negative in tumor cells [11]. A normal human pituitary tissue acted as control group was obtained from the post-mortem sample (a drowning male) [9, 36]. Human astrocytoma brain tissues (including different clinical staging-I/II/III/IV) were obtained from the Department of Neurosurgery of Xiangya Hospital, China [35]. The tissues were frozen in liquid nitrogen immediately, then stored at −80°C. According to the protein extraction manuals (Pierce, Rockford, IL, USA),supernatant of the tissue lysate was extracted for further analysis.

2.2. 2DGE-based western blot detection of nitroproteins

2DGE: The precast IPG strips (pH 3–10 NL; 180 × 3 × 0.5 mm) and 18-cm IPGstrip holder was used for 2DGE first dimension—isoelectic focusing (IEF) on an IPGphor instrument (GE Heathcare) to separate protein sample. After IEF, the IPG strip was processed for 2DGE second dimension—sodium dodecyl sulfate–polyacrylamide gel electrophoresis (SDS-PAGE), namely, the equilibrated proteins in the IPG strips were separated by molecular weight during electrophoresis on in 12% PAGE resolving gel (250 × 215 × 1.0 mm), and visualized with silver-staining [9, 36] or Coomassie brilliant blue G staining [35].

2DGE-based Western blotting: The 2DGE-separated proteins were transferred to a PVDF membrane, which were blocked by BSA, incubated with an anti-human nitrotyrosine antibody and secondary antibody, then visualized with 1-Step™ nitro blue tetrazolium/5-bromo-4-chloro-3-indolyl phosphate (NBT/BCIP) (Thermo Product No. 3404).

Image analysis of a 2D gel and of 2D-Western blotting: The scanned images of the 2D gels and the Western blot membranes were input to a PDQuest analysis system (Bio-Rad, version 7.1, Hercules, CA) to synthesize image. Gaussian spots were applied to all subsequent spot-matching and analyses. Each spot volume was normalized to the total optical density (OD) to minimize experimental factors on a spot volume [30].

2.3. MS/MS characterization of tryptic nitropeptides from nitroproteins

LC-ESI-MS/MS: The nitrotyrosine-positive gel-spots were excised, digested, purified, eluted, air-dried, redissolved. Then, the peptide mixture was subjected to LC-ESI-quadrupole-time of flight (LC-ESI-qTOF) or LTQ-OrbiTrap Velos MS/MS analyses. The detailed operation process and parameter settings have been described [35].

MALDI-MS/MS: The immunopositive 2D gel spots were excised, digested, purified, eluted, air-dried, redissolved, and were spots onto MALDI-plate, which were subjected to MALDI-MS/MS analysis [37]. The detailed procedure has been described [9, 11, 36].

2.4. Identification of nitroproteins with MS/MS

MS/MS data were used to identify the protein and nitrotyrosine sites by searching the SwissProt and NCBInr databases with SQUEST or Mascot software, with mass modifications of +45 Da (+NO_2 – H) at Tyr, +57 Da (+NH_2COCH_2 – H) at Cys, +16 Da (oxidation) at Met. Protein domains and motifs analyses were carried out with ScanProsite software (http://us.expasy.org/tools/scanprosite). Nitrotyrosine sites within a given domain or motif were determined with MotifScan software (http://myhits.isb-sib.ch/cgi-bin/motif_scan). The functions and experimental data-based model of nitroproteins was searched on the Swiss-Prot database annotation page and the related literature resources.

2.5. Annotation of functional characteristics of the nitroproteins

Literature-based bioinformatics and comprehensive annotation of protein in the SwissProt page were used to rationalize the functional characteristics of each nitroprotein, and to provide important clues to the biological significance of each nitroprotein relevant to tumors.

3. Results and discussions

3.1. The level of protein tyrosine nitration in nervous system tumors

One1D gel-based Western blotting in combination with anti-nitrotyrosine antibody analysis revealed that the overall level of protein tyrosine nitration in astrocytoma was significantly higher than the controls (**Figure 1**).

3.2. Enrichment of endogenous nitroproteins in nervous system tumors

The challenges faced by low abundance of tyrosine nitration and the elusive mass spectrometry result of a nitro group are existed. Modern nitroproteomics applies protein-separation-enrichment techniques such as gel methods and non-gel methods, including immunoprecipitation [11, 37], anti-nitrotyrosine antibody-based enzyme-linked immunosorbent assay (ELISA) [27], and one/two-dimensional gel electrophoresis (1DGE/2DGE)-based Western blot analyses [9, 35]. 1DGE/2DGE-based Western blots analyses can separate and preferentially enrich endogenous nitroproteins and also preliminarily determine the quantitative information of nitrotyrosine. It should not be neglected that limitations of 2DGE-based method including coverage of proteome, dynamic range, sensitivity and throughput, which always were restricted by the amount of samples. Also, the non-nitrated tryptic peptides are much more than nitrated tryptic peptides after a 2DGE-separated nitroprotein was digested, which will interrupt MS/MS signal of nitrated tryptic peptides [38]. However, for the proteome study, a 2DGE gel could detect more than 1000 spots [39]. Different proteins may be contained within the same spot [40].

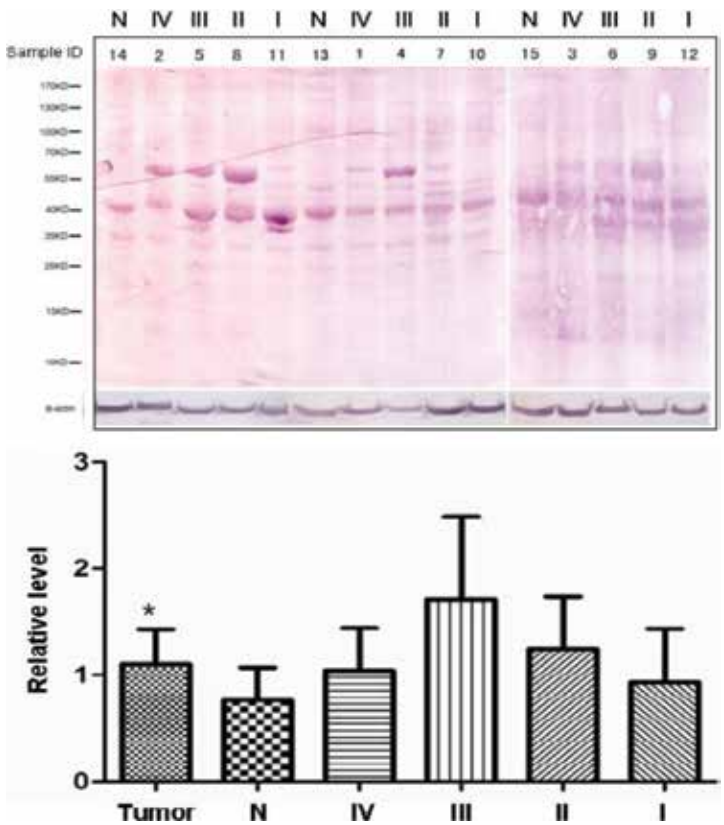

Figure 1. The nitrotyrosine immunoactivities in different grade (I, II, III, and IV) of astrocytoma tissues relative to normal controls (N), detected with nitrotyrosine immunoaffinty-based western blotting (n = 3). Tumor = sum of different grade (I, II, III, and IV) of astrocytomas. *p < 0.05. Reproduced from Peng and Zhan [35], with permission from Springer, copyright 2015.

Many proteins were detected in several analyzed spots showing 2DE-MS separate ability at the protein species level [43]. Indeed, higher sensitivity had been expected when 2DE coupled with high-sensitivity LC–MS, and will detect, identify and quantify human proteome nearly 500,000 (with an estimated resolution) protein species [28]. We adopted 2DGE-based Western blots analyses method to separate and detect nitroproteins in nervous system tumors. Our previous study obtained enrichment of endogenous nitroproteins in human pituitary [9, 36] and astrocytoma [35].

The 2DGE-based Western blot coupled with anti-nitrotyrosine antibody was used to analyze nitroproteins in human astrocytoma tissues (**Figure 2**) [17]. Nearly 1100 protein spots were detected in each Coomassie-stained 2D gel. Most proteins were distributed within a range of pI 4–8 and Mr. of 15–150 kDa. A total of 57 nitrotyrosine-immunopositive gel spots were detected, and each positive spot corresponded to a Coomassie-stained 2D gel spot. In order to show non-specific nitrotyrosine-immunopositive Western blot spots, we setup a control experiment without primary antibody to determine cross-reactivity of the secondary antibody.

http://dx.doi.org/10.5772/intechopen.76889

A similar 2DGE-based Western blot coupled with anti-nitrotyrosine antibody was used to analyze nitroproteins in human pituitary tissues [35, 38]. Each pituitary silver-stained 2D gel image (pI 3–10; Mr. 10–100 kDa) contained ca. 1000 protein spots, and a total of 32 nitrotyrosine immunopositive Western blot spots were detected in human pituitary tissues.

An immunoprecipitation, nitrotyrosine affinity column (NTAC)-based MS/MS approach was also used to enrich and identify nitroproteins from a pituitary adenoma tissue (**Figure 3**) [37]. Briefly, the NTAC was prepared with protein G beads cross-linked with anti-nitrotyrosine antibodies. A volume (600 μl) of protein extracts from 62 mg wet weight of a pituitary adenoma

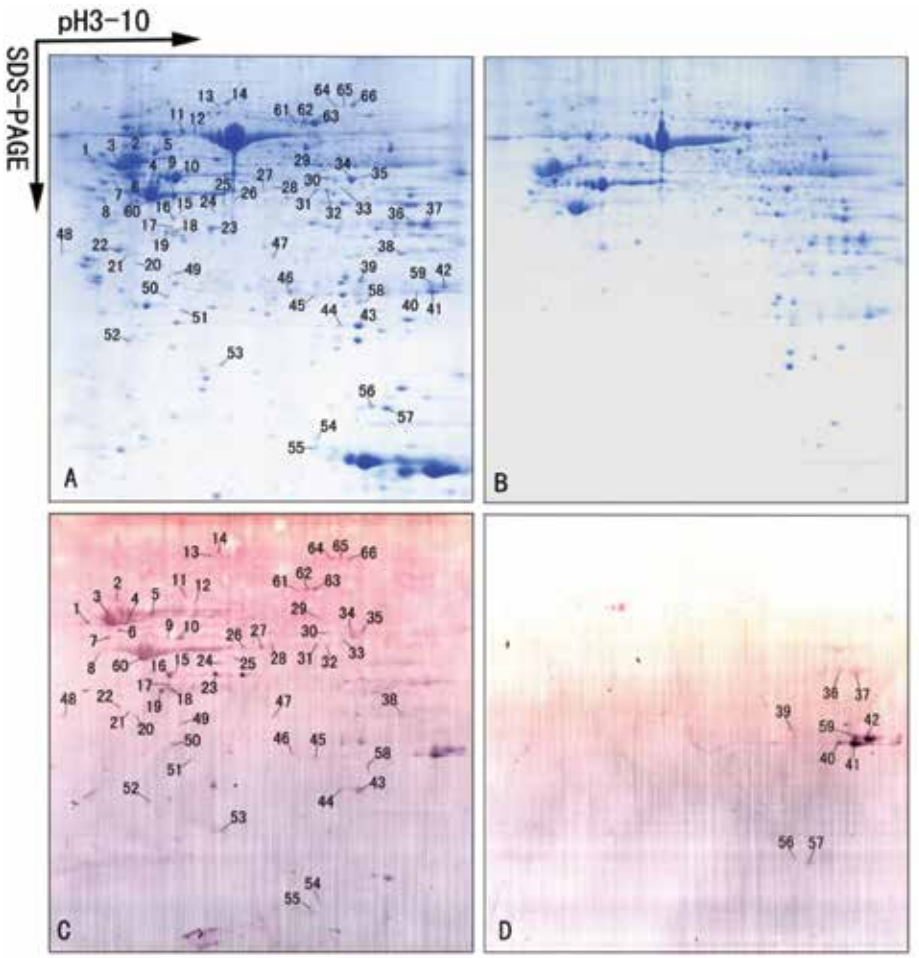

Figure 2. 2DGE-based Western blot analysis of nitroproteins in an IV-grade astrocytoma tissue (500 μg protein per 2D gel). (A) Coomassie blue-stained 2DGE image (before transfer of proteins). (B) Coomassie blue-stained 2DGE image (after transfer of proteins). (C) Western blotting image of nitroproteins (anti-nitrotyrosine antibodies + secondary antibodies). (D) Negative control of Western blotting to show the cross-reaction of the secondary antibody (only the secondary antibody; no anti-nitrotyrosine antibody). Reproduced from Peng and Zhan [35], with permission from Springer, copyright 2015.

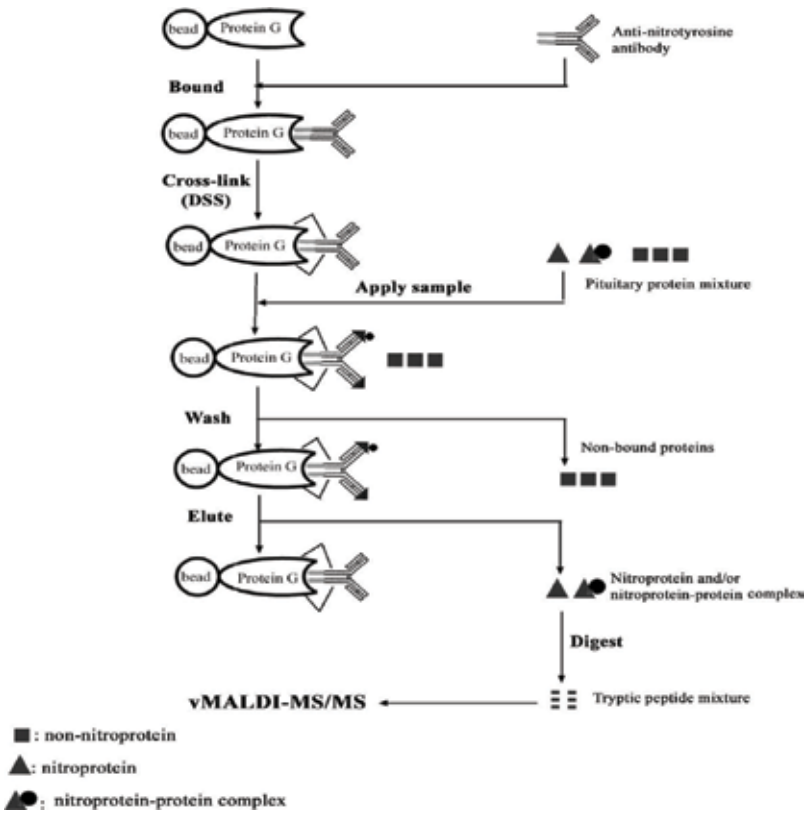

Figure 3. The use of NTAC to characterize nitroproteins and their complexes. A parallel control experiment was carried out without any anti-3-nitrotyrosine antibody. Reproduced from Zhan and Desiderio [11], with permission from Elsevier Science, copyright 2006.

tissue was diluted (1,1, v/v) with binding/washing buffer. Then, 500 μl diluted sample was incubated with the prepared NTAC to enrich and isolate nitroproteins and nitroprotein–protein complexes, followed by tripsin digestion and MS/MS identification.

3.3. MS/MS identification of nitroproteins and nitrated sites in nervous system tumors

MS/MS is the mainstream technique to identify protein species and PTMs products with verification of amino acid sequence, splicing sites, and modification site [31]. However, the very low abundance of tyrosine nitration in a proteome (one nitration in ~10^6 tyrosine residues) and the complicated mass spectrometry behaviors of a nitro group that we studied in nitroproteins complicate analyses [34, 38]. Different mass spectrometry has different advantages and complicated mass spectrometry behaviors, so choosing the proper method or combination with each other is necessary. For example, the MS behaviors of a nitropeptide differ significantly between matrix-assisted laser desorption ionization (MALDI)-and electrospray ionization (ESI)-MS on process of photochemical decompositions of the nitro group (–NO_2)

[33, 41]. Additionally, Specificity and sensitivity of the MALDI–LTQ MS/MS analytical system to characterize each nitroprotein and nitroprotein–protein complex should be considered. According to our previous experience [42], MALDI–LTQ has a number of advantages: (1) highly sensitive; (2) high accuracy measurement on amino acid sequence and nitration sites; (3) a prepared sample could be reanalyzed in several weeks.

For human astrocytoma and pituitary adenomas nitroproteomics studies, 2DGE-based nitrotyrosine Western blot analysis with MALDI-TOF were used to obtain endogenous nitroproteins from human pituitary control and adenoma tissues, and 2DGE-based nitrotyrosine Western blot analysis with liquid chromatography-electrospray ionization-quadrupole ion trap (LC-ESI-Q-IT) were used to obtain endogenous nitroproteins from human astrocytoma brain tissues, flowed by identification of nitroproteins, proteins interacted with nitroproteins and nitrotyrosine sites. A representative MS/MS spectrum was shown to identify nitropeptide (ITFDDnYIAC*C*VK) that is derived from sorcin (C9J0K6) in human astrocytoma tissue (**Figure 4**).

A total of eight nitroproteins was identified in human normal pituitary tissues with 2DGE-MS/MS [9, 36], and nine nitroproteins were identified in a human nonfunctional pituitary adenoma tissue with NTAC-MS/MS [11], and 18 nitroproteins and their 20 nitrotyrosine sites was identified in a human astrocytoma tissue with 2DGE-MS/MS [35] (**Table 1**). Three nitroprotein–protein complexes were also identified in a human nonfunctional pituitary adenoma tissue: the nitrated beta-subunit of cAMP-dependent protein kinase (PKA) complex, the nitrated proteasome–ubiquitin complex, and the nitrated interleukin 1 family member 6–interleukin 1 receptor–interleukin 1 receptor-associated kinase-like 2 (IL1-F6–IL1-R–IRAK-2) complex [37].

Furthermore, the 2DE-MS/MS-identified nitrosorcin in astrocytoma tissues was confirmed with immunoprecipitation coupled with 1D gel-Western blot experiments (**Figure 5**). The tyrosine nitration of sorcin was measured by immunoprecipitation coupled with Western blotting between IV-grade astrocytoma and normal control (N) tissues. Thus overall status of tyrosine nitration in the whole tissues could be displayed with anti-nitrotyrosine antibody. The results confirmed the tyrosine nitration of sorcin in astrocytoma, and the level of tyrosine nitration of sorcin in astrocytoma is obviously higher than the control tissues.

3.4. Functional characteristics of the nitroproteins

Comprehensive analysis of the functional characteristics of those nine nitroproteins and three nitroproten-protein complexes in a pituitary adenoma biological system revealed several important functional pathways involved in protein tyrosine nitration (**Figure 6**): Nitrated RHOGAP5 and nitrated rhophilin 2 are involved in the GTPase signal pathway. Nitrated CENT-beta 1 and nitrated PKAR1-beta are involved in the PKA signal pathway. IRAK-2 in the IL1-R complex and nitrated IL1-F6 are involved in the cytokine system. The nitrated proteasome–ubiquitin complex is an important enzymatic complex involved in the intracellular nonlysosomal proteolytic pathway. Nitrated LIRA4 might be involved in the immune system. Nitrated ZFP432 is involved in transcription regulatory systems. The nitrated S1P lyase 1 participates in sphingolipid metabolism to regulate cell proliferation, survival, and cell death as well as the immune system.

Comprehensive analysis of the functional characteristics of 18 astrocytoma nitroproteins revealed those nitroproteins participated in multiple cancer-related biological processes (**Figure 7**): (a) microtubule dynamic stabilization and cytoprotection, which mainly involvedβVIII-tubulin, and β-tubulin; (b) tumor migration and metastasis, which mainly

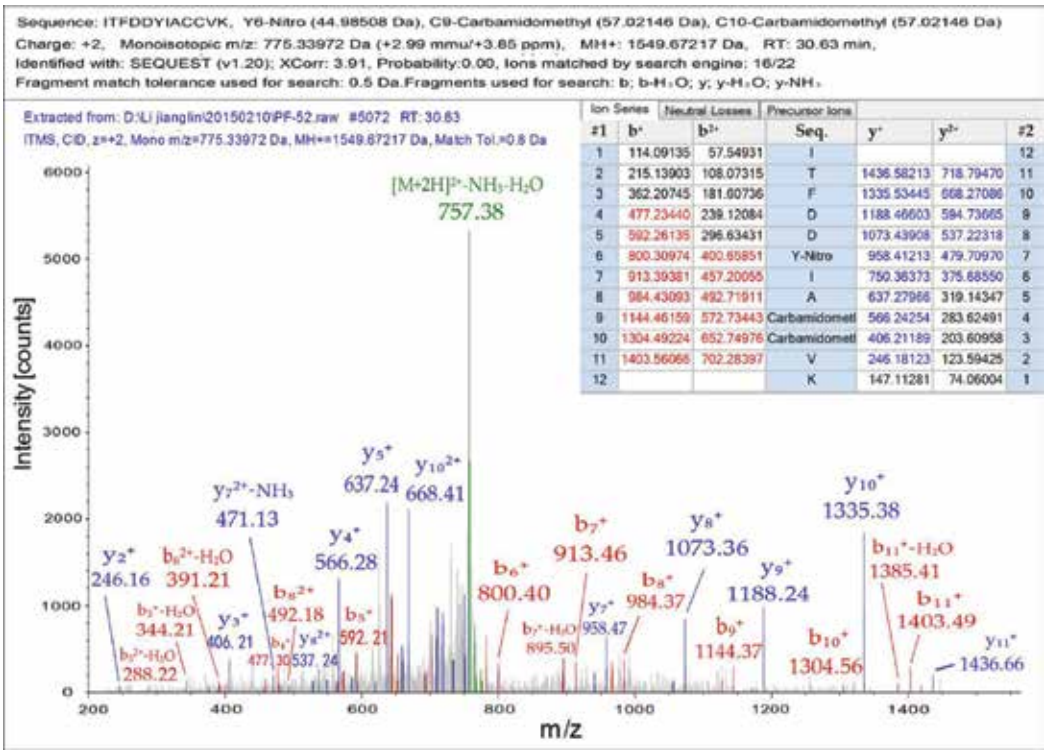

Figure 4. MS/MS spectrum of a nitropeptide (ITFDDnYIAC*C*VK) that is derived from sorcin (C9J0K6) in astrocytoma tissue. nY = nitrotyrosine residue. Reproduced from Peng and Zhan [35], with permission from Springer, copyright 2015.

Nervous system tumors/ control	Nitrated protein name	nY site
Pituitary adenoma	Rho-GTPase-activating 5 [Q13017] (ARHGAP5)	nY^{550}
	Leukocyte immunoglobulin-like receptor A4 [P59901]	nY^{404}
	Zinc finger protein 432 [O94892]	nY^{41}
	PKA beta regulatory subunit [P31321] (PRKAR1B)	nY^{20}
	Sphingosine-1-phosphate lyase 1 [O95470]	nY^{356}, Y^{366}
	Centaurin beta 1 [Q15027]	nY^{485}
	Proteasome subunit alpha type 2 [P25787] (PSMA2)	nY^{228}
	Interleukin 1 family member 6 [Q9UHA7] (IL1F6)	nY^{96}
	Rhophilin 2 [Q8IUC4] (RHPN2)	nY^{258}

Nervous system tumors/ control	Nitrated protein name	nY site
Pituitary control	Proteasome subunit alpha type 2 (PSMA2)	nY^{228}
	Mitochondrial co-chaperone protein HscB [Q8IWL3]	nY^{128}
	Actin [P03996] (ACTA2, ACTG2, ACTC1)	nY^{296}
	Synaptosomal-associated protein (SNAP91)	nY^{237}
	Ig alpha Fc receptor [P24071] (FCAR)	nY^{223}
	Progestin and adipoQ receptor family member III [Q6TCH7] (PAQR3)	nY^{33}
	PKG 2 [Q13237] (PRKG2)	nY^{354}
	Stanniocalcin 1[P52823] (STC1)	nY^{159}
Astrocytoma	Ras-related protein Rab-8B (H0YMN7)	nY^{77};nY^{78}
	Isoform 2 of Signal-induced proliferation-associated 1-like protein 2 (Q9P2F8–2)	nY^{1369}, nY^{1387}
	Regulating synaptic membrane exocytosis protein 1 (Q86UR5)	nY^{926}
	Isoform 2 of Grainyhead-like protein 1 homolog (Q9NZI5–2)	nY^{400}, nY^{402}
	Probable G-protein coupled receptor 52 (Q9Y2T5)	nY^{281}, nY^{284}
	Sorcin (C9J0K6)	nY^{116}
	Tubulin beta chain (P07437)	nY^{106}
	Tubulin beta-2A chain (Q13885)	nY^{106}, nY^{183}, nY^{200}
	Tubulin beta-2B chain (Q9BVA1)	nY^{106}
	Tubulin beta-3 chain (Q13509)	nY^{106}
	Ig kappa chain V-I region WAT (P80362)	nY^{49}
	Coiled-coil domain-containing protein 105 (Q8IYK2)	nY^{372}
	Helicase ARIP4 (E7EU19)	nY^{407}
	General transcription factor 3C polypeptide 3 (Fragment) (H7C0C0)	nY^{110}
	Isoform 2 of Arf-GAP with SH3 domain, ANK repeat and PH domain-containing protein 2 (O43150–2)	nY^{75}
	Isoform 2 of Toll-like receptor 9 (Q9NR96–2)	nY^{419}
	Transducin-like enhancer protein 2 (B4DE62)	nY^{369}

Note: nY = nitrotyrosine. Pituitary adenoma and control modified from Zhan and Desiderio [9, 11, 36], with permission from Elsevier Science, copyright 2004, 2006 and 2007. Astrocytoma modified from Peng and Zhan [35], with permission from Springer, copyright 2015.

Table 1. Nitroproteins and non-nitrated proteins identified from nervous system tumor.

involved sorcin, isoform 2 of Toll-like receptor 9, isoform 2 of Arf-GAP with SH3 domain/ ANK repeat and PH domain-containing protein 3, transducin-like enhancer protein 2, and GPR52; (c) chemotherapy resistance, which mainly involved Ras-related protein Rab 8,

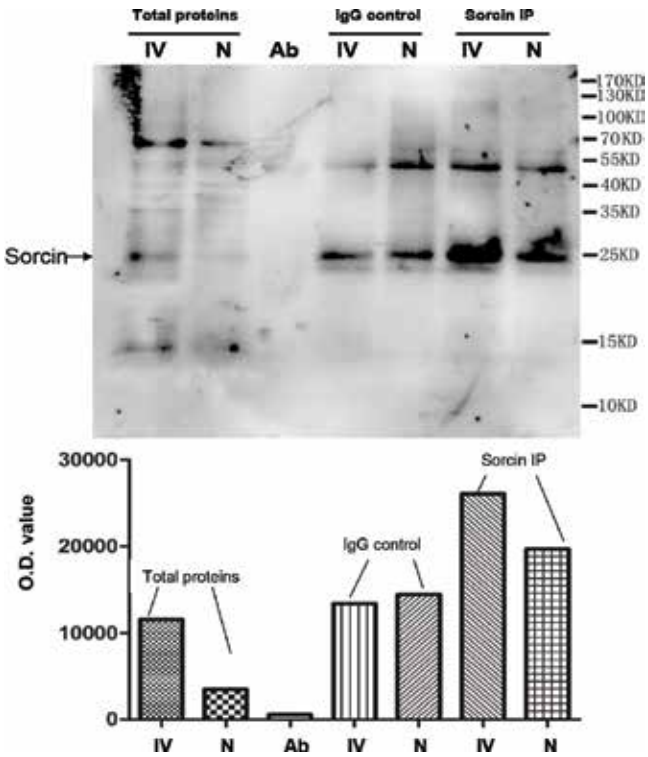

Figure 5. Nitrotyrosine immune activities in nitrosorcin-immunoprecipitated products from IV-astrocytoma and normal control (N) tissues. Reproduced from Peng and Zhan [35], with permission from springer, copyright 2015.

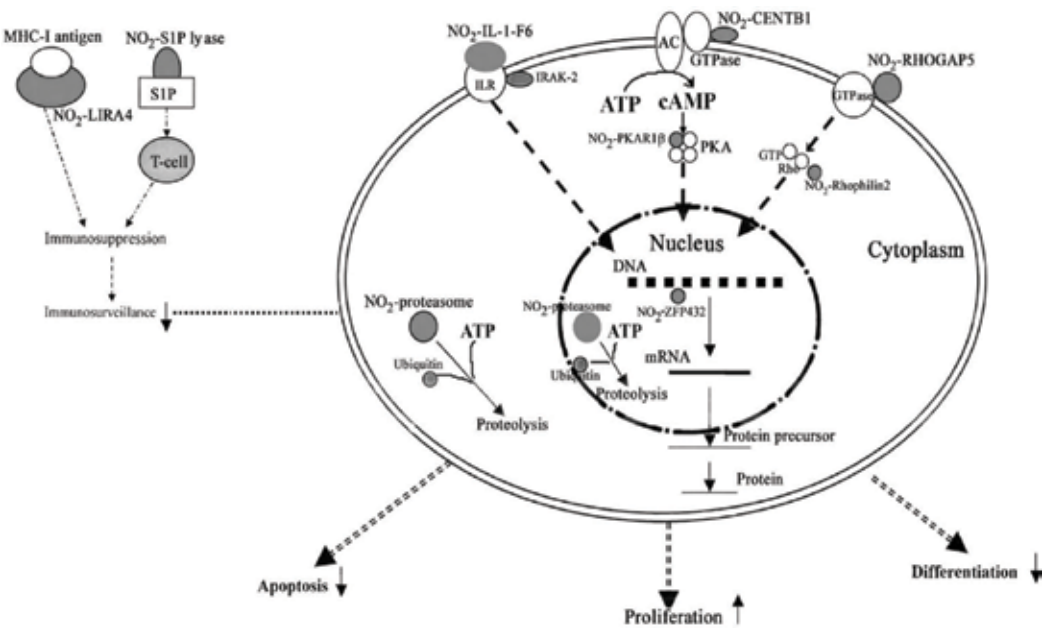

Figure 6. Experimental data-based model of nitroproteins and their functions in human nonfunctional pituitary adenomas. NO_2^-, nitroprotein. Reproduced from Zhan and Desiderio [11], with permission from Elsevier Science, copyright 2006.

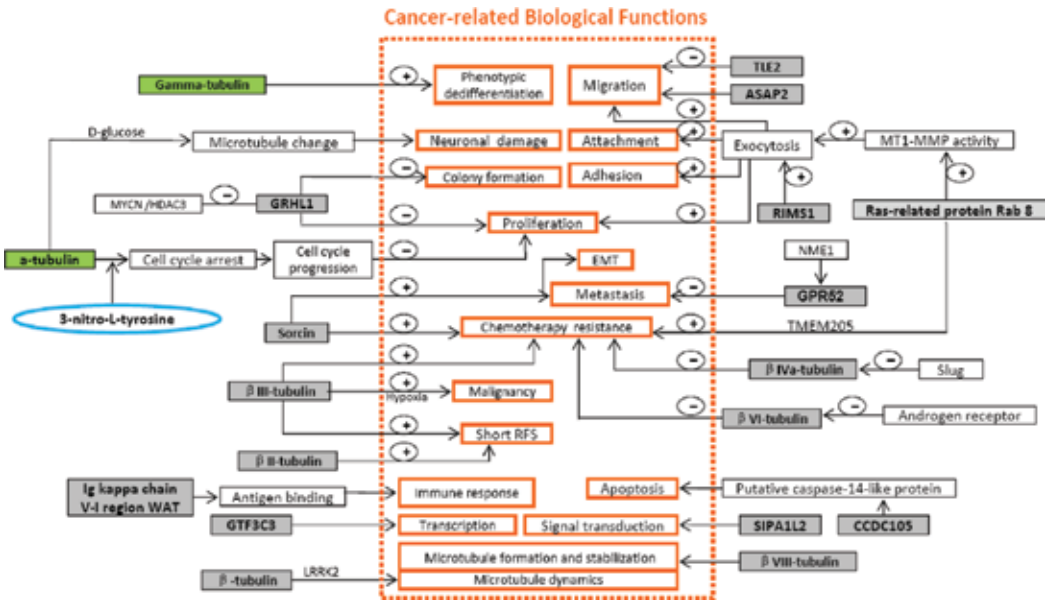

Figure 7. Experimental data-based diagram that rationalizes nitrotyrosine-containing proteins in the glioma biological system. Reproduced from Peng and Zhan [35], with permission from Springer, copyright 2015.

βIII-tubulin, βIVa-tubulin, βVI-tubulin, and sorcin; (d) cell proliferation and apoptosis, which mainly involved a-tubulin, isoform 2 of Grainyhead-like protein 1, Ras-related protein Rab 8, regulating synaptic membrane exocytosis protein 1, and coiled-coil domain-containing protein 105; (e) phenotypic dedifferentiation, which involved gamma-tubulin; (f) signal transduction, which mainly involved isoform 2 of signal-induced proliferation-associated 1-like protein 2; (g) others such as transcription, immune response, and transformation; (h) tumor malignancy and recurrence-free survival, which involvedβII-tubulin and βIII-tubulin.

4. Conclusion(s)

Protein tyrosine nitration, as one of an important PTMs generated in nervous system tumor, participates in multiple complex biological processes, including cell proliferation and apoptosis, metastasis, migration, drug-resistance, cytoskeleton, signal transduction, immune response and cellular differentiation [43]. What is the mechanism for protein tyrosine nitration in carcinogenesis and development of malignant tumors? How to identify the protein targets and exact modified sites of tyrosine nitration? One/two-dimensional gel electrophoresis-based nitrotyrosine Western blot analysis and tandem mass spectrometry have been successfully applied in the analysis of nitroproteins in nervous system tumors.

Further study is needed to solve those limits on protein nitration: (1) Protein tyrosine nitration and heterogeneity of neoplasm. (2) Three-dimensional spatial structure of a nervous system tumor-related nitroprotein. (3) Consistency issues between body fluid and tissue. With the clarification of those issues on nitroproteins, protein tyrosine nitration will have a significant impact on the field of nervous system tumors.

Acknowledgements

The authors acknowledge the financial supports from the National Natural Science Foundation of China (Grant No. 81572278 and 81272798 to X.Z.), China "863" Plan Project (Grant No. 2014AA020610-1 to X.Z.), the Hunan Provincial Natural Science Foundation of China (Grant No. 14JJ7008 to X.Z.), and the Xiangya Hospital Funds for Talent Introduction (to X.Z.). The scientific contributions of Dr. Dominic M. Desiderio and Fang Peng are also acknowledged.

Conflict of interest

We declare that we have no financial and personal relationships with other people or organizations.

Acronyms and abbreviations

CNS	central nervous system
ELISA	enzyme-linked immunosorbent assay
ESI	electrospray ionization
FDR	false discovery rates
IEF	isoelectic focusing
MALDI	matrix-assisted laser desorption ionization
MS/MS	tandem mass spectrometry
NTAC	nitrotyrosine affinity column
PAGE	polyacrylamide gel electrophoresis
PTM	posttranslational modification
Q-IT	quadrupole ion trap
RNS	reactive nitrogen species
SDS	sodium dodecyl sulfate
S/N	signal-to-noise ratio
TEMED	tetramethylethylenediamine
1DGE	one-dimensional gel electrophoresis
2DGE	two-dimensional gel electrophoresis

Author details

Xianquan Zhan* and Na Li

*Address all correspondence to: yjzhan2011@gmail.com

Key Laboratory of Cancer Proteomics of Chinese Ministry of Health, Xiangya Hospital, Central South University, Changsha, China

References

[1] Siegel R, Ma J, Zou Z, Jemal A. Cancer statistics, 2014. CA: A Cancer Journal for Clinicians. 2014;**64**:9-29. DOI: 10.3322/caac.21208

[2] Patchell RA. The management of brain metastases. Cancer Treatment Reviews. 2003; **29**:533-540

[3] Andersson U, Johansson D, Behnam-Motlagh P, Johansson M, Malmer B. Treatment schedule is of importance when gefitinib is combined with irradiation of glioma and endothelial cells in vitro. Acta Oncologica. 2007;**46**:951-960. DOI: 10.1080/02841860701253045

[4] Cobbs CS, Whisenhunt TR, Wesemann DR, Harkins LE, Van Meir EG, Samanta M. Inactivation of wild-type p53 protein function by reactive oxygen and nitrogen species in malignant glioma cells. Cancer Research 2003;**63**:8670-8673

[5] Wang F, Zhang J, Wang P, Zhou T, Meng X, Jiang J. Prediction of pituitary stalk position in pituitary adenomas by visualization of the hypothalamo-hypophyseal tract using diffusion tensor imaging tractography. Medicine (Baltimore). 2018;**97**:e0052. DOI: 10.1097/md.0000000000010052

[6] Vargas G, Balcazar-Hernandez LJ, Melgar V, Magrina-Mercado RM, Gonzalez B, Baquera J, Mercado M. An FSH and TSH pituitary adenoma, presenting with precocious puberty and central hyperthyroidism. Endocrinology, Diabetes & Metabolism Case Reports. 2017;**2017**:pii: 17-0057. DOI: 10.1530/edm-17-0057

[7] Jo J, Schiff D, Purow B. Angiogenic inhibition in high-grade gliomas: Past, present and future. Expert Review of Neurotherapeutics. 2012;**12**:733-747. DOI: 10.1586/ern.12.53

[8] Thomas LN, Chedrawe ER, Barnes PJ, Too CKL. Prolactin/androgen-inducible carboxypeptidase-D increases with nitrotyrosine and Ki67 for breast cancer progression in vivo, and upregulates progression markers VEGF-C and Runx2 in vitro. Breast Cancer Research and Treatment. 2017;**164**:27-40. DOI: 10.1007/s10549-017-4223-7

[9] Zhan X, Desiderio DM. The human pituitary nitroproteome: Detection of nitrotyrosylproteins with two-dimensional western blotting, and amino acid sequence determination with mass spectrometry. Biochemical and Biophysical Research Communications. 2004;**325**:1180-1186. DOI: 10.1016/j.bbrc.2004.10.169

[10] Yee CS, Seyedsayamdost MR, Chang MC, Nocera DG, Stubbe J. Generation of the R2 subunit of ribonucleotide reductase by intein chemistry: Insertion of 3-nitrotyrosine at residue 356 as a probe of the radical initiation process. Biochemistry. 2003;**42**:14541-14552. DOI: 10.1021/bi0352365

[11] Zhan X, Desiderio DM. Nitroproteins from a human pituitary adenoma tissue discovered with a nitrotyrosine affinity column and tandem mass spectrometry. Analytical Biochemistry. 2006;**354**:279-289. DOI: 10.1016/j.ab.2006.05.024

[12] McCann SM, Haens G, Mastronardi C, Walczewska A, Karanth S, Rettori V, Yu WH. The role of nitric oxide (NO) in control of LHRH release that mediates gonadotropin release and sexual behavior. Current Pharmaceutical Design. 2003;**9**:381-390

[13] McCann SM, Karanth S, Mastronardi CA, Dees WL, Childs G, Miller B, Sower S, Yu WH. Control of gonadotropin secretion by follicle-stimulating hormone-releasing factor, luteinizing hormone-releasing hormone, and leptin. Archives of Medical Research. 2001;**32**:476-485

[14] Xie T, Ma JW, Liu B, Dong J, Huang Q. Experimental study of glioma stem cell-mediated immune tolerance in tumor microenvironment. Zhonghua Zhong Liu Za Zhi. 2017;**39**:808-813. DOI: 10.3760/cma.j.issn.0253-3766.2017.11.002

[15] Sowers JL, Johnson KM, Conrad C, Patterson JT, Sowers LC. The role of inflammation in brain cancer. Advances in Experimental Medicine and Biology. 2014;**816**:75-105. DOI: 10.1007/978-3-0348-0837-8_4

[16] Tan KH, Harrington S, Purcell WM, Hurst RD. Peroxynitrite mediates nitric oxide-induced blood-brain barrier damage. Neurochemical Research. 2004;**29**:579-587

[17] Fiore G, Di Cristo C, Monti G, Amoresano A, Columbano L, Pucci P, Cioffi FA, Di Cosmo A, Palumbo A, d'Ischia M. Tubulin nitration in human gliomas. Neuroscience Letters. 2006;**394**:57-62. DOI: 10.1016/j.neulet.2005.10.011

[18] Zedda M, Lepore G, Gadau S, Manca P, Farina V. Morphological and functional changes induced by the amino acid analogue 3-nitrotyrosine in mouse neuroblastoma and rat glioma cell lines. Neuroscience Letters. 2004;**363**:190-193. DOI: 10.1016/j.neulet.2004.04.008

[19] Kauppila JH, Korvala J, Siirila K, Manni M, Makinen LK, Hagstrom J, Atula T, Haglund C, Selander KS, Saarnio J, Karttunen TJ, Lehenkari PP, Salo T. Toll-like receptor 9 mediates invasion and predicts prognosis in squamous cell carcinoma of the mobile tongue. Journal of Oral Pathology & Medicine. 2015;**44**:571-577. DOI: 10.1111/jop.12272

[20] Fabian J, Lodrini M, Oehme I, Schier MC, Thole TM, Hielscher T, Kopp-Schneider A, Opitz L, Capper D, von Deimling A, Wiegand I, Milde T, Mahlknecht U, Westermann F, Popanda O, Roels F, Hero B, Berthold F, Fischer M, Kulozik AE, Witt O, Deubzer HE. GRHL1 acts as tumor suppressor in neuroblastoma and is negatively regulated by MYCN and HDAC3. Cancer Research. 2014;**74**:2604-2616. DOI: 10.1158/0008-5472.can-13-1904

[21] Colotti G, Poser E, Fiorillo A, Genovese I, Chiarini V, Ilari A. Sorcin, a calcium binding protein involved in the multidrug resistance mechanisms in cancer cells. Molecules. 2014;**19**:13976-13989. DOI: 10.3390/molecules190913976

[22] Gualtieri M, Longhin E, Mattioli M, Mantecca P, Tinaglia V, Mangano E, Proverbio MC, Bestetti G, Camatini M, Battaglia C. Gene expression profiling of A549 cells exposed to Milan PM2.5. Toxicology Letters. 2012;**209**:136-145. DOI: 10.1016/j.toxlet.2011.11.015

[23] Caracciolo V, D'Agostino L, Draberova E, Sladkova V, Crozier-Fitzgerald C, Agamanolis DP, de Chadarevian JP, Legido A, Giordano A, Draber P, Katsetos CD. Differential expression and cellular distribution of gamma-tubulin and betaIII-tubulin in medulloblastomas and human medulloblastoma cell lines. Journal of Cellular Physiology 2010;**223**:519-529. DOI: 10.1002/jcp.22077

[24] Law BM, Spain VA, Leinster VH, Chia R, Beilina A, Cho HJ, Taymans JM, Urban MK, Sancho RM, Blanca Ramirez M, Biskup S, Baekelandt V, Cai H, Cookson MR, Berwick DC, Harvey K. A direct interaction between leucine-rich repeat kinase 2 and specific beta-tubulin isoforms regulates tubulin acetylation. The Journal of Biological Chemistry. 2014;**289**:895-908. DOI: 10.1074/jbc.M113.507913

[25] Irie Y, Saeki M, Kamisaki Y, Martin E, Murad F. Histone H1.2 is a substrate for denitrase, an activity that reduces nitrotyrosine immunoreactivity in proteins. Proceedings of the National Academy of Sciences of the United States of America. 2003;**100**:5634-5639. DOI: 10.1073/pnas.1131756100

[26] Zhan X, Desiderio DM. Nitroproteins identified in human ex-smoker bronchoalveolar lavage fluid. Aging and Disease. 2011;**2**:100-115

[27] Torreilles J, Romestand B. In vitro production of peroxynitrite by haemocytes from marine bivalves: C-ELISA determination of 3-nitrotyrosine level in plasma proteins from Mytilus galloprovincialis and Crassostrea gigas. BMC Immunology. 2001;**2**:1

[28] Zhan X, Yang H, Peng F, Li J, Mu Y, Long Y, Cheng T, Huang Y, Li Z, Lu M, Li N, Li M, Liu J, Jungblut PR. How many proteins can be identified in a 2DE gel spot within an analysis of a complex human cancer tissue proteome? Electrophoresis. 2018;**39**(7):965-980. DOI: 10.1002/elps.201700330

[29] Rogowska-Wrzesinska A, Le Bihan MC, Thaysen-Andersen M, Roepstorff P. 2D gels still have a niche in proteomics. Journal of Proteomics 2013;88:4-13. DOI: 10.1016/j.jprot.2013.01.010

[30] Zhan X, Desiderio DM. Spot volume vs. amount of protein loaded onto a gel: A detailed, statistical comparison of two gel electrophoresis systems. Electrophoresis. 2003;**24**:1818-1833. DOI: 10.1002/elps.200305375

[31] Guo T, Wang X, Li M, Yang H, Li L, Peng F, Zhan X. Identification of glioblastoma phosphotyrosine-containing proteins with two-dimensional western blotting and tandem mass spectrometry. BioMed Research International. 2015;**2015**:134050. DOI: 10.1155/2015/134050

[32] Zhan X, Wang X, Desiderio DM. Mass spectrometry analysis of nitrotyrosine-containing proteins. Mass Spectrometry Reviews. 2015;**34**:423-448. DOI: 10.1002/mas.21413

[33] Zhan X, Desiderio DM. MALDI-induced fragmentation of leucine enkephalin, nitro-Tyr leucine enkaphalin, and d(5)-Phe-nitro-Tyr leucine enkephalin. International Journal of Mass Spectrometry. 2009;**287**:77-86. DOI: 10.1016/j.ijms.2008.08.020

[34] Petersson AS, Steen H, Kalume DE, Caidahl K, Roepstorff P. Investigation of tyrosine nitration in proteins by mass spectrometry. Journal of Mass Spectrometry. 2001;**36**:616-625. DOI: 10.1002/jms.161

[35] Peng F, Li J, Guo T, Yang H, Li M, Sang S, Li X, Desiderio DM, Zhan X. Nitroproteins in human Astrocytomas discovered by gel electrophoresis and tandem mass spectrometry. Journal of the American Society for Mass Spectrometry. 2015;**26**:2062-2076. DOI: 10.1007/s13361-015-1270-3

[36] Zhan X, Desiderio DM. Linear ion-trap mass spectrometric characterization of human pituitary nitrotyrosine-containing proteins. International Journal of Mass Spectrometry. 2007;**259**:96-104. DOI: 10.1016/j.ijms.2006.06.009

[37] Shevchenko A, Jensen ON, Podtelejnikov AV, Sagliocco F, Wilm M, Vorm O, Mortensen P, Shevchenko A, Boucherie H, Mann M. Linking genome and proteome by mass spectrometry: Large-scale identification of yeast proteins from two dimensional gels. Proceedings of the National Academy of Sciences of the United States of America. 1996;**93**:14440-14445

[38] Zhan X, Desiderio DM. Comparative proteomics analysis of human pituitary adenomas: Current status and future perspectives. Mass Spectrometry Reviews. 2005;**24**:783-813. DOI: 10.1002/mas.20039

[39] Desiderio DM, Zhan X. The human pituitary proteome: The characterization of differentially expressed proteins in an adenoma compared to a control. Cellular and Molecular Biology (Noisy-le-Grand, France). 2003;**49**:689-712

[40] Peng J, Gygi SP. Proteomics: The move to mixtures. Journal of Mass Spectrometry. 2001;**36**:1083-1091. DOI: 10.1002/jms.229

[41] Sarver A, Scheffler NK, Shetlar MD, Gibson BW. Analysis of peptides and proteins containing nitrotyrosine by matrix-assisted laser desorption/ionization mass spectrometry. Journal of the American Society for Mass Spectrometry. 2001;**12**:439-448. DOI: 10.1016/s1044-0305(01)00213-6

[42] Zhan X, Desiderio DM. A reference map of a human pituitary adenoma proteome. Proteomics. 2003;**3**:699-713. DOI: 10.1002/pmic.200300408

[43] Zhan X, Desiderio DM. Signaling pathway networks mined from human pituitary adenoma proteomics data. BMC Medical Genomics. 2010;**3**:13. DOI: 10.1186/1755-8794-3-13

Chapter 8

Improving Tribological Behavior of Porous Anodic Film by Electrophoretic Impregnation by a Tio_2 Synthesized Nanoparticle

Koubaa Anouar and Bargui Mansour

Additional information is available at the end of the chapter

http://dx.doi.org/10.5772/intechopen.75782

Abstract

This chapter deals with the study of the elaboration of a stable suspension of TiO_2 nanoparticles and their incorporation by electrophoretic deposition into pores of anodized 5754 aluminum alloy. The as-synthesized TiO_2 nanopowder was characterized by X-ray diffraction, scanning and transmission electron microscopy (TEM), and infrared spectroscopy. During this work, transmission electronic microscopy (TEM) analysis showed that the resulting particles had a narrow size distribution with crystallite size of about 15 nm. The zeta potential and stability of TiO_2 nanoparticles dispersed with poly(acrylic acid) (PAA) in aqueous solution were also measured. Porous anodic film was elaborated in phosphoric acid electrolyte and then filled by TiO_2 particles using electrophoresis method. Furthermore, the effect of PAA content and pH on the suspension stability has been investigated. It was also demonstrated that buffered suspension by adding glycine avoids gelating phenomena which inhibits the insertion of nanoparticles inside the pores of anodic film. It was noted also that the electric field already applied greatly influences the electrophoretic deposition process (EPD). FEG-SEM observations showed that larger (125 nm diameter) and linear pores of 6 μm in length are successfully filled in 5 min. Finally, the composite anodic film tribological behavior was studied and the obtained results revealed that the insertion of the TiO_2 nanoparticles into the pores of the anodic film improves its tribological properties.

Keywords: electrophoretic impregnation, anodizing, TiO_2 nanoparticles, zeta potential, colloidal suspension

1. Introduction

Nanotechnology is based on the knowledge and mastery of the infinitely small. They constitute a multidisciplinary field of research and development involving the fabrication of new materials and devices from tools or techniques that can be used to structure matter at the atomic, molecular, or supramolecular level. The typical scales of nanotechnology range from 1 to 100 nm.

The nanomaterials thus derived from these nanotechnologies are materials composed or constituted for all or part of nano-objects which confer to them improved or specific properties of the nanometric dimension. In this context, we speak of nanocharged or nanoreinforced materials. These materials are developed by incorporating nano-objects in an organic or mineral matrix to provide new functionality or to modify mechanical, optical, magnetic, or thermal properties. Nanocomposites are one example. Nano-objects (**Figure 1**) that have two different forms, nanotubes (e.g., MWNT: multi wall carbon nanotubes) or spherical particles (e.g., alumina powder) are incorporated in the porous matrix by several techniques, among which and the most interesting is that of electrophoresis. In this chapter, we are interested in presenting a work whose main objectives consisted in developing a model anodizing layer on the 5754 aluminum alloy, then a stable suspension of nanometric titanium dioxide, then composite coatings based on TiO_2 nanoparticles by electrophoretic impregnation of the anodizing layer, and finally rigorously examine the impact of TiO_2 localization on the tribological behavior of the composite coating already developed.

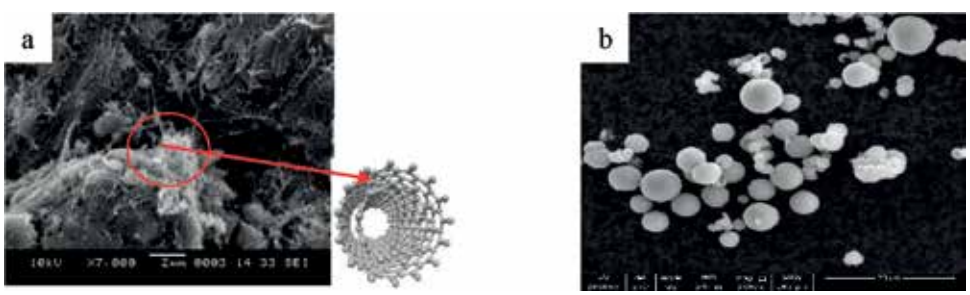

Figure 1. Different shapes of nano-objects (a) multi-wall carbon nanotubes and (b) spherical nanoparticles of alumina [1].

2. Protocol for incorporation of nanoparticles

The flowchart showed in **Figure 2** summarizes the range of the steps to be followed in order to prepare the model anodic film and fill its pores with nanoparticles of titanium dioxide.

2.1. Pretreatment: electropolishing

The electropolishing treatment was carried out in a bath already proposed by Sulka [2]. This pretreatment aims to reduce the roughness of the aluminum substrate. The results thus

http://dx.doi.org/10.5772/intechopen.75782

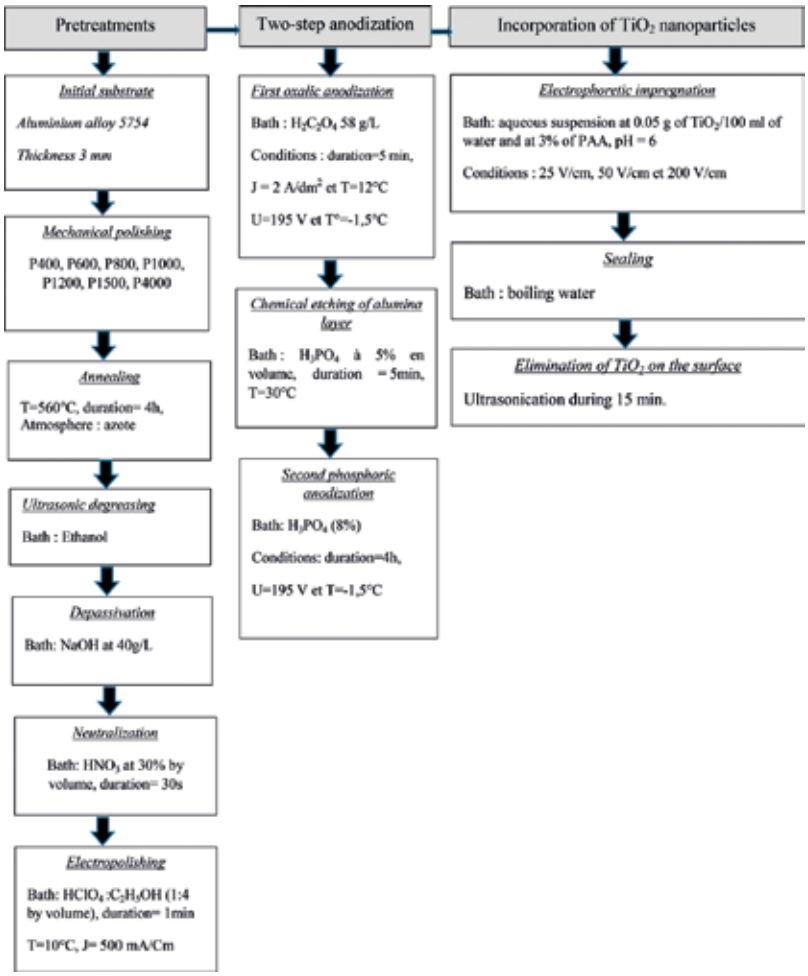

Figure 2. Incorporation flowchart of TiO_2 nanoparticles in the pores of anodic layer.

obtained are illustrated in **Figure 3**. Indeed the Al5754 aluminum substrate has an initial roughness (Ra = 740 nm and Rz = 7 μm) and a roughness after electrochemical polishing (Ra = 140 nm and Rz = 1.5 μm).

2.2. Two-step anodization

It should be noted that the anodization consists in carrying out the anodic polarization surface conversion of the base metal, immersed in a suitable electrolyte (generally an aqueous solution of a mineral acid). **Figure 4** shows an experimental setup of anodizing and the reactions that take place on the surfaces of the anode (Al5754) and the cathode.

Different kinds of electrolytes such as sulfuric acid, phosphoric acid, and oxalic acid can be used for anodization. Although sulfuric anodizing, which is nowadays the most commonly used process [3], phosphoric acid was used in the case of this study because it produces a

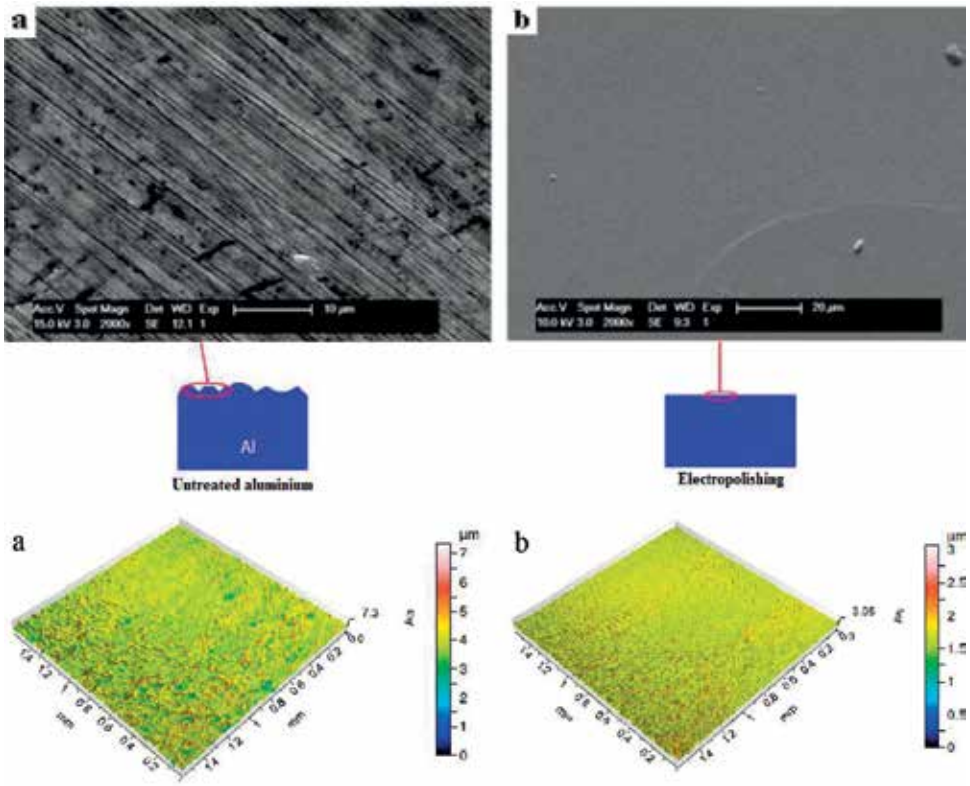

Figure 3. SEM observations associated with 3D roughness profiles: (a) sample after mechanical polishing and (b) after mechanical and electrochemical polishing.

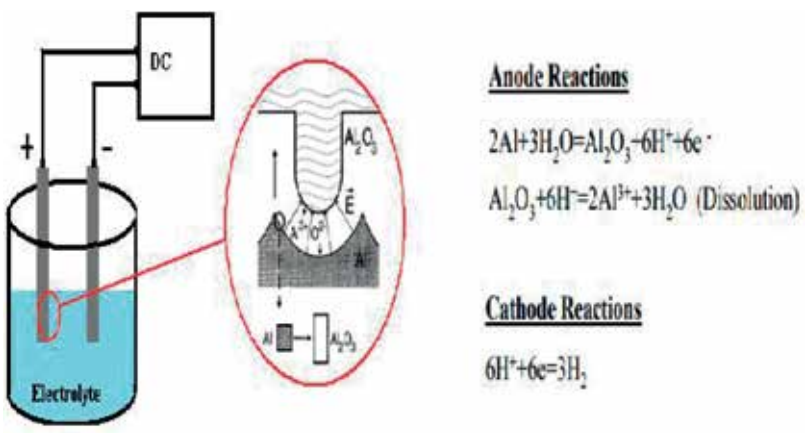

Figure 4. Experimental setup of anodizing.

porous anodic layer with the largest pore diameter. The anodizing of aluminum has to be done by preference on samples with a low surface roughness then anodized according to the **two-step anodization** to obtain an ordered porous anodic film [4] with a pore diameter greater than 100 nm. **Figure 5** reveals the approach for the conduct of the two-step anodization and **Figure 6** shows the scanning electronic microscopy (SEM) images of the obtained anodic layer that can be impregnated with 20 nm size TiO_2 nanoparticles using **electrophoretic method**.

2.3. Electrophoretic impregnation of porous anodizing layer by synthesized TiO_2 nanoparticles

2.3.1. Synthesis of TiO_2 nanoparticles

In order to prepare the TiO_2 nanopowder, 10 ml of ethanol (C_2H_5OH), 10 ml of acetic acid (CH_3COOH), 400 μL of hydrochloric acid (HCL) were used as catalysts, and 10 ml of titanium tetraisopropoxide precursor(Ti $(OCH(CH_3)_2)_4$) were mixed in the indicated order. The mixture was stirred for 30 min at a constant speed of 200 rpm to obtain the TiO_2 sol. Then the resulting sol was introduced into the autoclave (**Figure 7**) heated up to 243°C and pressurized to overcome the critical point of ethanol (T_c = 243°C, P_c = 63 bar). After maintaining temperature at 243°C for 1 h, the sol-gelation occurred. To evacuate the interstitial solvent, depressurization for 1 h down to room temperature was conducted with nitrogen gas. Finally, titanium aerogel was obtained.

Figure 8 indicates the sol-gel TiO_2 fabrication diagram.

2.3.2. Structural and morphological investigations of TiO_2 nanopowder

Fourier-transform infrared (FTIR) spectroscopy was used to identify the functional groups presented in the as-synthesized TiO_2 nanopowder. The FTIR absorbance spectra were given

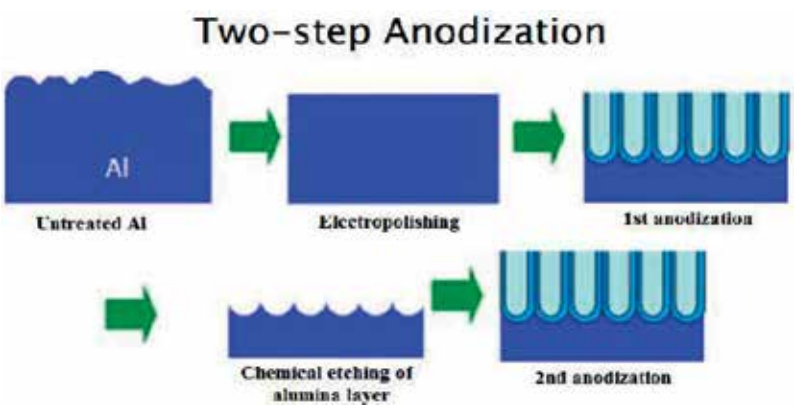

Figure 5. The approach for the conduct of the two-step anodization.

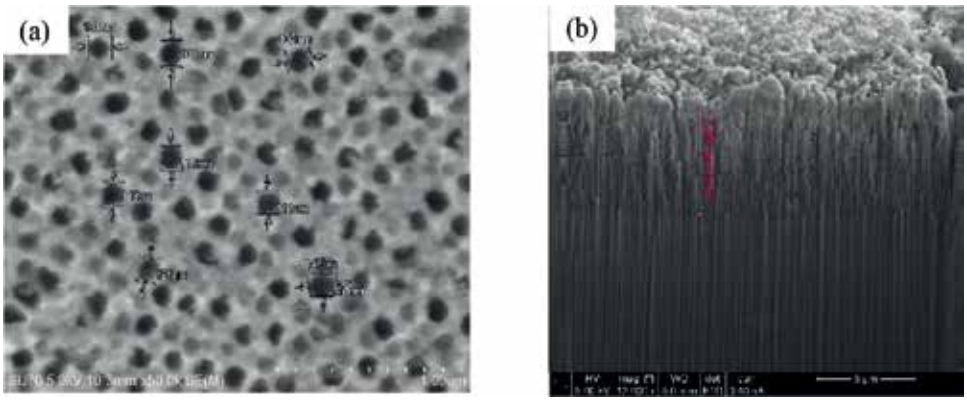

Figure 6. SEM images of anodic layer elaborated on th Al5754 aluminum alloy (a) in phosphoric bath (H_3PO_4 8%, U = 195 V, T = −1.5° C and t = 4 h) and (b) cross section of the anodizing layer [5].

Figure 7. PARR autoclave-type pressure reactor and solvent removal system.

in **Figure 9**. A wide band ranging between 400 and 900 cm^{-1} was attributed to Ti-O stretching vibrations [6]. In the medium wavenumber range, the bands at 1300–1800 cm^{-1} were attributed to ν[C=C, C=O] and δ CH_3 vibrations corresponding to the organic residues [7]. It was believed that a broad band at ds 3500 cm^{-1} corresponds to the surface-adsorbed water [8]. In fact, the energy dispersive X-ray (EDX) spectra shown in **Figure 11** indicates the presence of an oxygen excess which can be attributed to the adsorbed hydroxide groups on the surface of TiO_2 nanoparticles.

The XRD pattern of TiO_2 nanopowder is shown in **Figure 10**. The obvious diffraction peaks of anatase TiO_2 structure in the range of resolution of XRD were well defined which indicated the good crystallinity of the synthesized TiO_2 nanopowder. In fact, the diffraction peaks at

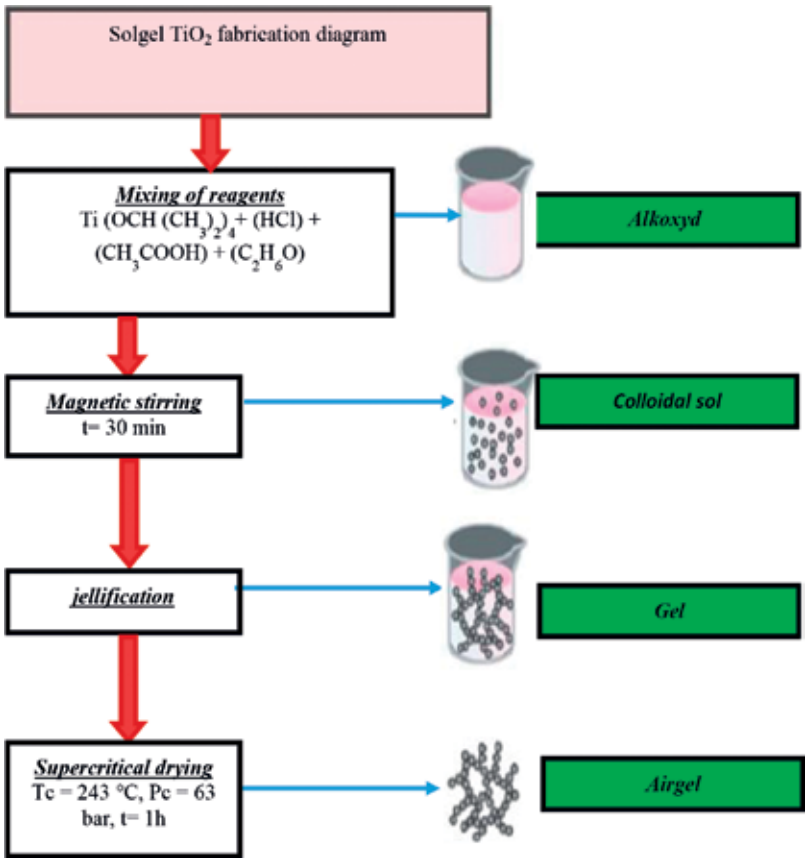

Figure 8. The sol-gel TiO_2 fabrication diagram.

2θ (degree) of 25.23, 37.81, and 48.14 degree were indexed as (101), (004), and (200) planes of anatase phase TiO_2 which matches well the reported data for TiO_2 ((PDF) # 00-021-1272).

The grain size of TiO_2 has been calculated using Scherer's equation [9].

With D as the crystallite size of TiO_2 thin films, k as a constant (=0.89), λ as the wavelength of X-ray (CuKα = 1.5406 Å), β as the true half-peak width, and θ as the half diffraction angle of the centroid of the peak in degree. Any contributions to broadening due to non-uniform stress were neglected and the instrumental line width in the XRD apparatus was subtracted. The calculated crystallite size of the anatase phase was about 20 nm.

2.3.3. Characterization of synthesized TiO_2 nanopowder by SEM and TEM

Figure 11 (a–b) shows the SEM micrographs that describe the morphology of the as-synthesized TiO_2 nanopowder. As it can be observed from the **Figure 11a**, the powder consists of spherical clusters. In addition, the expertise of **Figure 11b** suggested that the spherical-shaped

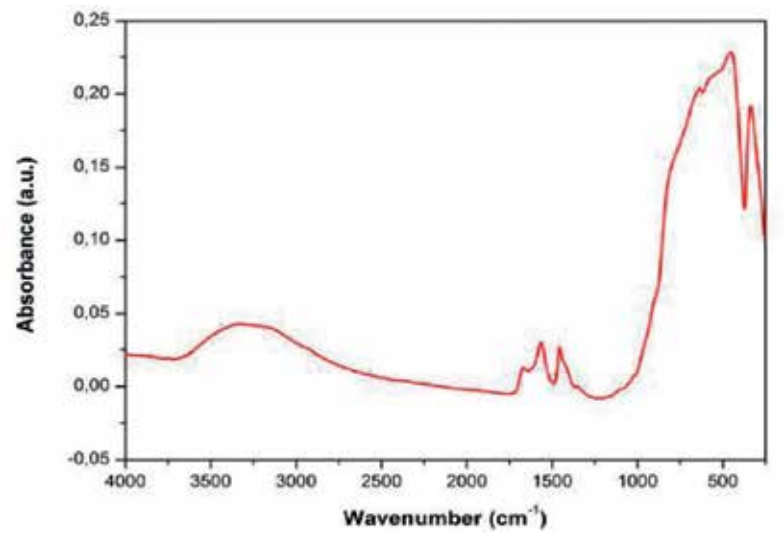

Figure 9. FTIR spectra of as-prepared TiO_2 nanopowder.

TiO_2 particles are hollow and composed of nanosized TiO_2 anatase. The TiO_2 nanoparticles show an even distribution with a mean size of about 20 nm.

Furthermore, the crystalline structure of TiO_2 nanopowder was investigated by transmission electronic microscopy (TEM) (**Figure 12**) observation in order to estimate the primary TiO_2 crystallite. The TEM images of TiO_2 nanopowder are shown in **Figure 12 (a–b)**. As shown

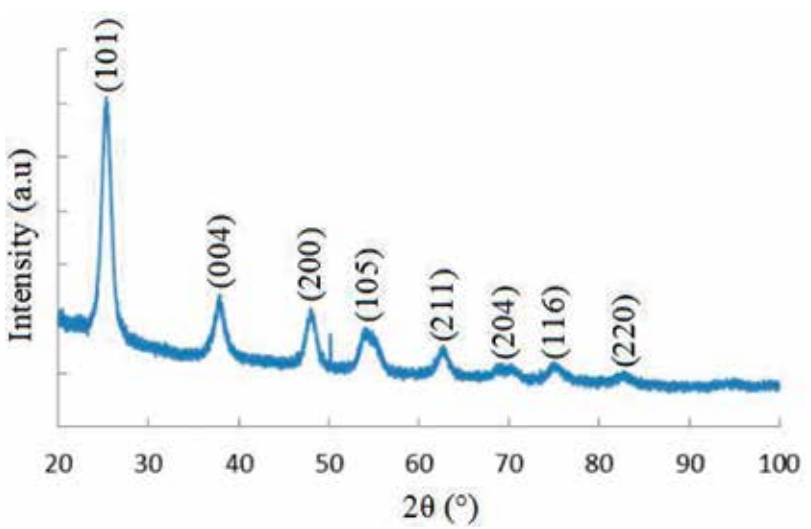

Figure 10. X-ray diffraction pattern of TiO_2 nanopowder synthesized by sol-gel process.

http://dx.doi.org/10.5772/intechopen.75782

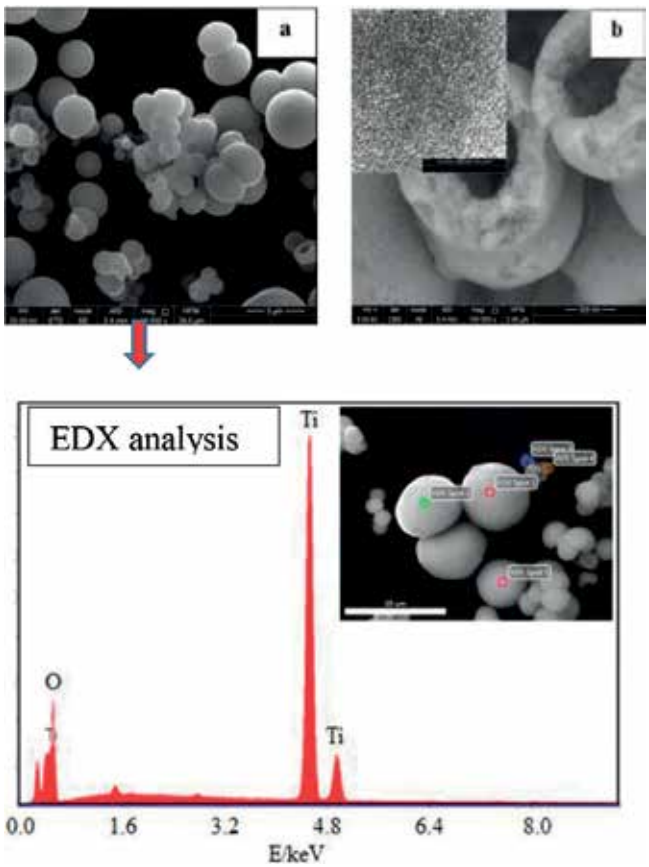

Figure 11. SEM images of synthesized TiO_2 nanopowder (a) Spherical clusters and (b) nanosized TiO_2 anatase.

in **Figure 12a**, the primary TiO_2 crystallite had a diameter of about 10–20 nm which was in a satisfactory agreement with the SEM results.

The local crystal structure of anatase was confirmed by selected area electron diffraction (SAED) technique. One SAED ring diffraction pattern with marked Miller indices of anatase TiO_2 nanopowder (JCPDS card no. 21-1272) is given in **Figure 12b**. The ring pattern confirmed that synthesized nanopowder is polycrystalline with constituent crystallites of about 10 nm or more. Thus from the morphological studies, we can say that the synthesized TiO_2 nanoparticles seemed adequate to be used for the pores filling using an adopted electrophoretic deposition process (EPD).

Energy dispersive X-ray (EDX) spectrometry analysis of the synthetized TiO_2 nanoparticles shows peaks for titanium (Ti) and oxygen (O) elements. There is no trace of any other impurities could be seen within the detection limit of the EDX as presented in **Figure 11**. This indicates that the synthesized TiO_2 nanopowder was qualified with a high purity.

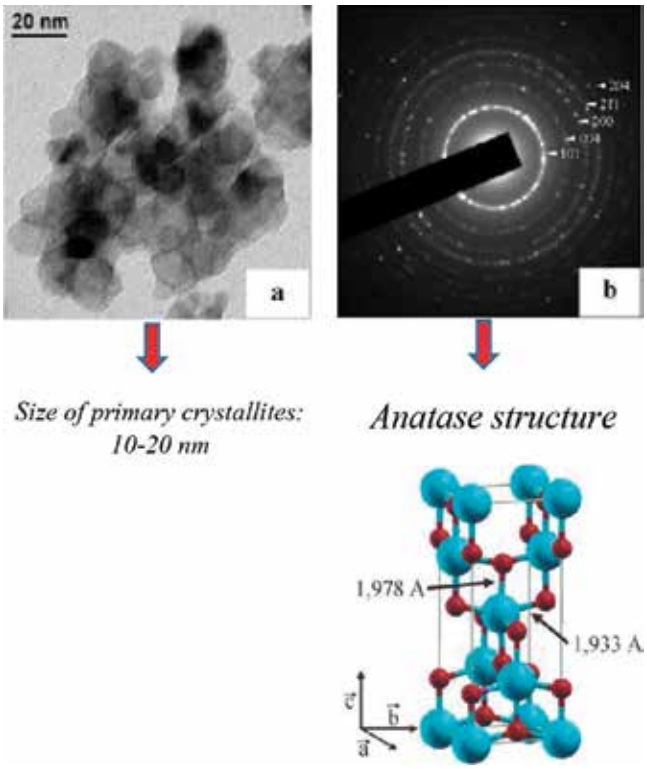

Figure 12. Characterization of synthesized nanopowder by SEM (a) Size of primary crystallites and (b) SAED ring diffraction pattern with marked Miller indices of anatase TiO_2 nanopowder.

2.3.4. Electrophoretic impregnation of anodizing layer by a synthesized TiO_2 nanoparticle

2.3.4.1. Preparation of the TiO_2 nanoparticles suspension

2.3.4.1.1. Effect of ultrasound on the dispersion of nanoparticles

According to preliminary studies, 0.05 g/100 ml of TiO_2 nanoparticles was chosen as the optimal concentration to achieve the EPD process. To do so, a stock solution (mother solution) that comprises mixing 0.05 g of TiO_2 with 100 ml of distilled water was prepared. The mixture was then magnetically stirred for 15 min. To investigate the effect of ultrasound on the dispersion of nanoparticles, the mother solution was subjected to ultrasonic various times (0, 5, 10, 20, 30, 60, and 90 min) (see **Figure 13**). According to the optical properties of the suspension, the absorbance increases with the increase of ultrasonic time. This indicates good dispersion of nanoparticles of TiO_2 in the aqueous suspension. Based on the findings shown in **Figure 14**, the use of ultrasound leads to the break of the clusters of TiO_2 into smaller agglomerates and aggregates. Agglomerated particles were thus eroded and divided by the collisions between particles [10–12]. A slight difference was observed between 60 and 90 min. So, 1 hour of ultrasonication seemed to be considered as an optimal setting for the preparation of a well-dispersed TiO_2 suspension.

http://dx.doi.org/10.5772/intechopen.75782

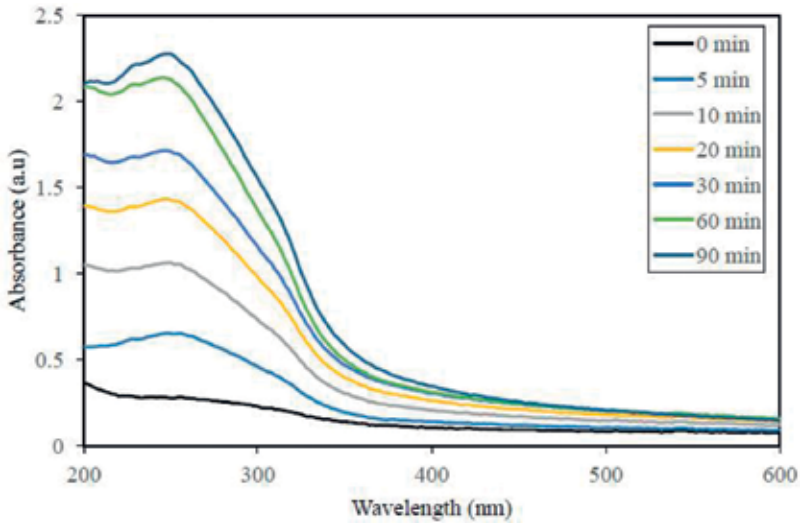

Figure 13. Absorbance spectra of the TiO_2 nanoparticles dispersed in water with and without ultrasound as a function of wavelength.

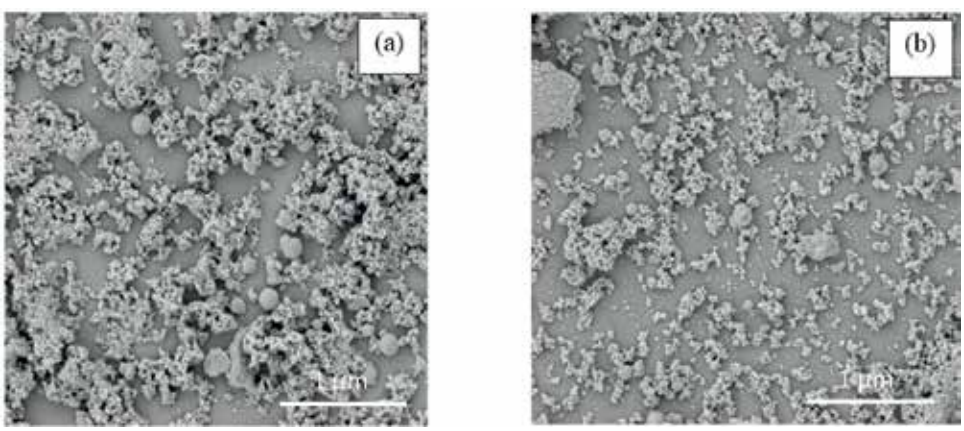

Figure 14. FEG-SEM images of TiO_2 nanoparticles: (a) without ultrasound and (b) after 90 min of ultrasound.

2.3.4.1.2. Effect of PAA amount on the zeta potential

Stability of TiO_2/poly(acrylic acid) (PAA) suspensions at different polymer content was measured on the basis of zeta potential measurements by means of the electrophoretic mobility. A zeta potential (ζ) of at least 30 mv (positive or negative) was normally required to achieve reasonably stable dispersion [13].

Figure 15 presents the effect of the polymer content on the stability of the suspensions at initial pH (6). According to **Figure 10**, the addition of PAA resulted in a good dispersion of the

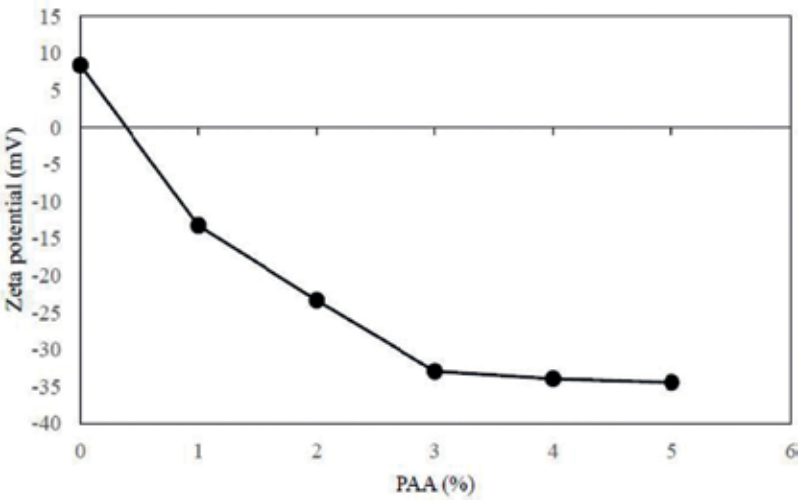

Figure 15. Effect of the amount of PAA on the stability of TiO_2 suspension.

suspensions with negative charge. The increase of negatively charged ▬COO▬ groups was assignable to the modification of the TiO_2 nanoparticles surface charge. The addition of 3% PAA was considered as the ideal condition to study and discuss the stability under various pH regions.

2.3.4.1.3. Effect of pH on the zeta potential of the TiO_2 suspension

Figure 16 shows the effect of pH on the zeta potential of the TiO_2/3% PAA suspension. As the pH increased, the number of negatively charged sites is continually increased until the zeta potential reaches a value over −35 mV at pH ranging between 6 and 8.

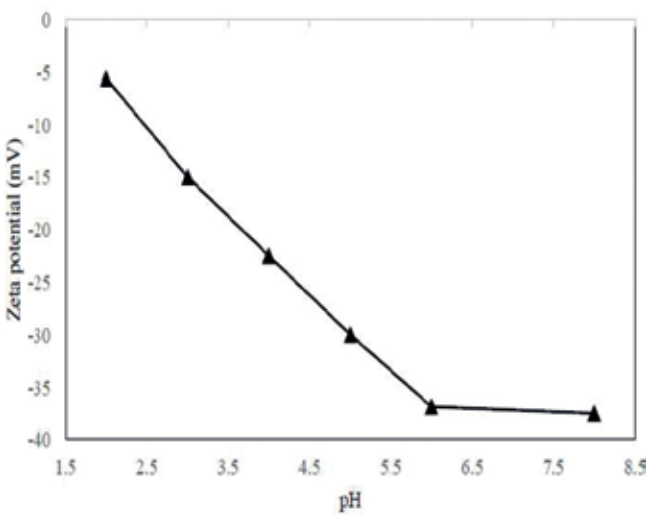

Figure 16. Variation of zeta potential as a function of pH of the TiO_2 suspension with 3% PAA.

According to the executed studies, the addition of 3% PAA was considered as the ideal condition and the pH is adjusted at 6.The as-prepared suspension has a zeta potential about −37 mV. So, it is considered a well-stable suspension to carry on electrophoretic process [14].

2.3.4.1.4. Stability of the TiO_2 suspension as a function of sedimentation time

Figure 17 shows the absorbance of titanium dioxide suspensions with and without PAA as a function of sedimentation time. In these tests, the PAA concentration was fixed at 3% and the pH is adjusted at 6. It is observed that the absorbance of titanium dioxide suspensions is lowering as the sedimentation proceeds. It is noteworthy that the absorbance of the suspension in the presence of PAA is stable for at least a week. This means that the adsorbed PAA was expected to provide a degree of electrosteric stabilization. Based on these results, the suspension (3% PAA at pH = 6) was suggested as an optimal standpoint stability to perform the incorporation of TiO_2 nanoparticles into the pores of the anodic oxide using EPD process.

2.3.4.1.5. Electrophoretic impregnation of anodic coating

Electrophoretic impregnation of porous anodizing layer elaborated in phosphoric acid was executed in aqueous TiO_2 nanoparticles suspension. It should be noted that impregnation process is conditioned by the applied electric field. Applying high electric field (200 V/cm) induce the jellification of TiO_2 sol because of the anodic electrolysis of water which decreases the pH near the electrode surface and then destabilize the suspension against coagulation at low pH. In order to avoid this phenomena and facilitate the insertion of titanium dioxide nanoparticles, the addition of the glycine to buffer the suspension is necessary. At the beginning of EPD, particles go to the bottom of pores which continue to fill progressively. These

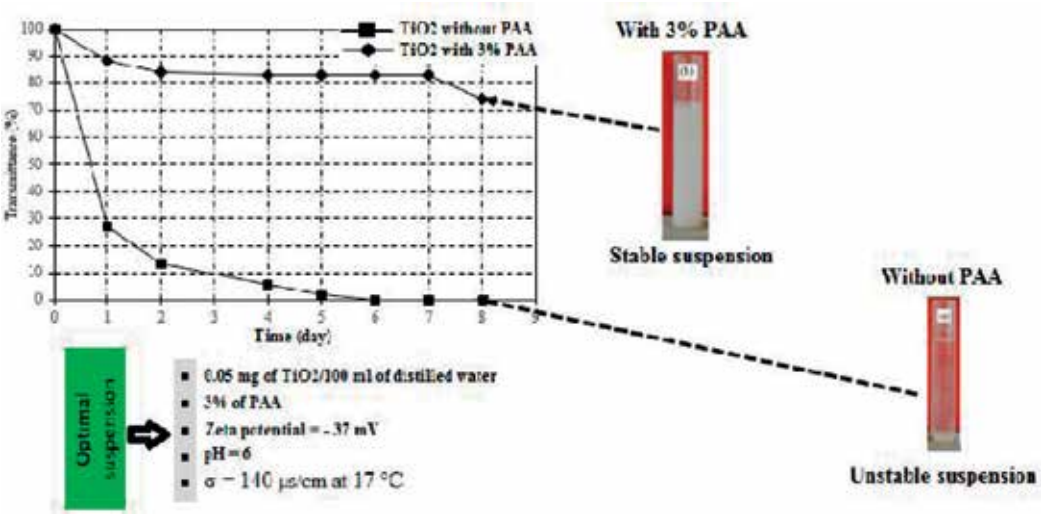

Figure 17. Variation of transmittance of the TiO_2 suspensions as a function of time.

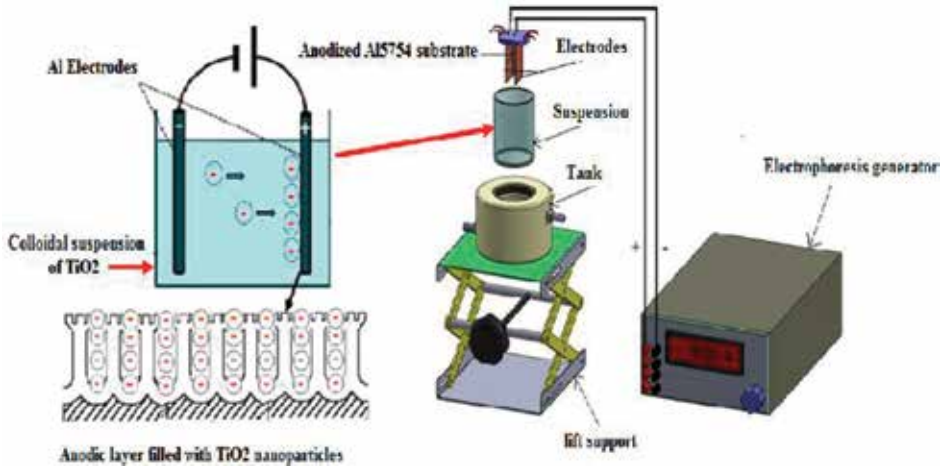

Figure 18. Experimental setup of electrophoretic impregnation of anodizing layer by a synthesized TiO_2 nanoparticle.

results attest that EPD can be used to fill successfully porous-anodizing layer despite the presence of the resistive barrier layer at the metal-oxide interface. **Figure 18** reveals experimental setup of electrophoretic impregnation of anodizing layer by a synthesized TiO_2 nanoparticle and the filled anodic layer is shown in **Figure 19**.

As shown in **Figure 19**, an increase of the electric field improves the impregnation depth of nanoparticles. Hence high electric field is necessary here to compensate the resistive

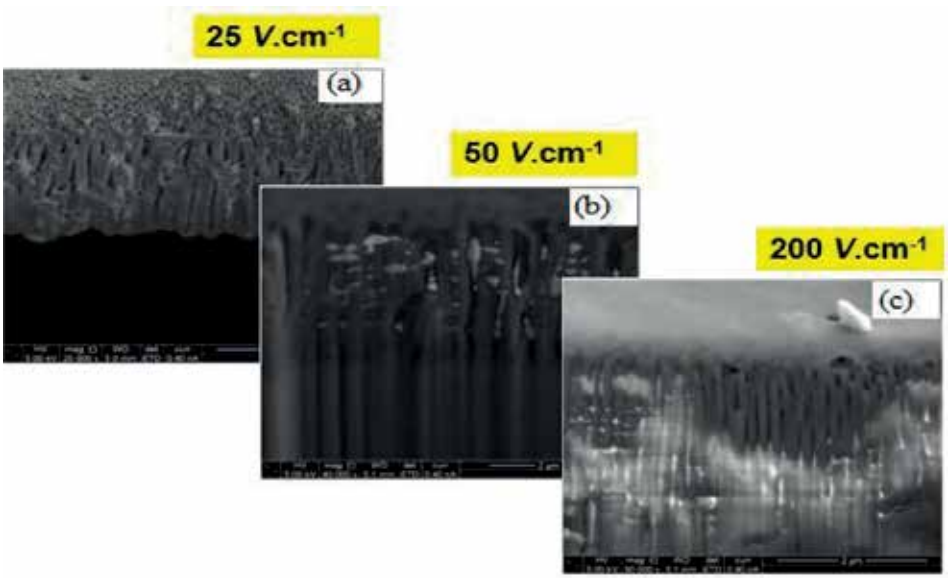

Figure 19. FEG-SEM cross sectional views of the porous anodic oxide: (a) after electrophoresis process using 25 V/cm, (b) after electrophoresis process using 50 V/cm, and (c) after electrophoresis process using 200 V/cm.

barrier layer at the metal-porous anodic film interface [15]. This finding is in satisfactory agreement with that of Fori et al. [15]. The following equation describes the migration speed of the nanoparticles:

$$\nu = \mu E \quad (1)$$

where ν as the speed of nanoparticles (m/s), μ as the electrophoretic mobility of nanoparticles (m^2/s.V), and E as the electric field (V/m). According to the this equation, an increase of the electric field promotes the driving forces of particles and then facilitates their incorporation inside pores of the anodizing layer.

3. Tribological behavior of Al_2O_3/TiO_2 composite coating

Tribological tests were carried out on a non-anodized aluminum substrate, an anodized coating alone, a composite coating of Al_2O_3 /TiO_2 and a TiO_2 massive produced by compression of a mass of a TiO_2 nanopowder already synthesized by a sol-gel process, in order to study the effect of the incorporation of TiO_2 nanoparticles. The results thus obtained bearing essentially on the quantification of friction coefficient and the wear volume are shown in **Figures 20** and **21**, respectively.

Examination of **Figure 20** reveals that the friction coefficient of the anodic coating alone has two periods: (1) a period of 250 seconds (approximately 414 cycles) during which the average friction coefficient fluctuates at about 0.8 and (2) a second period marked by a sharp drop in the friction coefficient until reaching a stable value almost equal to that of the non-anodized

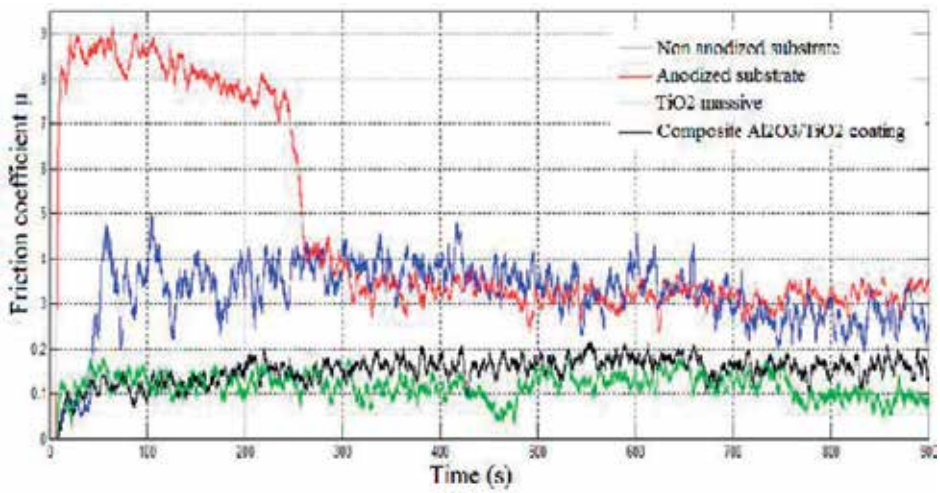

Figure 20. Variation of friction coefficient as a function of time (normal load Fn = 1 N, movement speed v = 0.052 $m.s^{-1}$, and time of friction t = 15 min).

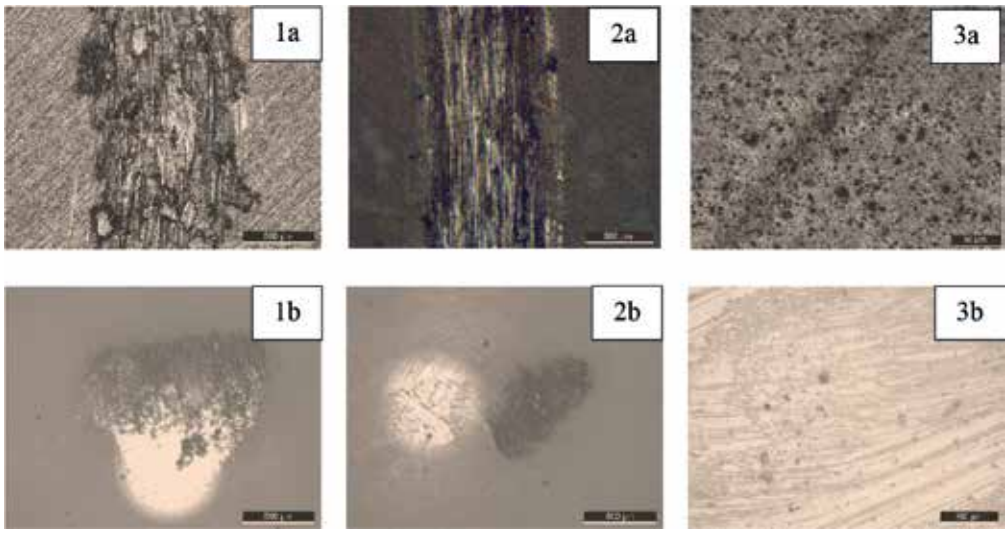

Figure 21. Optical micrographs of (a) the trace and (b) the alumina ball after friction test on (1) non-anodized aluminum, (2) anodic coating alone, and (3) composite coating Al_2O_3/TiO_2 (Fn = 1 N, v = 0,052 $ms^{-}1$ and t = 15 min).

substrate (μ = 0.3). This particular drop of the coefficient of friction indicates the total damage of the anodic coating alone and the alumina ball, constitutes our counterface, then becomes in direct contact with the exposed aluminum. This is confirmed by the optical micrographs of the traces of wear of the ball and the anodic coating alone (**Figure 21**). The anodic coating is totally worn out after 250 seconds (414 cycles) and its trace revealing the substrate and metal debris on the ball.

The TiO_2 massif has a friction coefficient (μ = 0.1) that is practically low throughout the tribological test compared to that of the substrate (μ = 0.30). Optical micrographs of the alumina ball show that TiO_2 arbed on their surfaces (**Figure 21 (2b)** and **Figure 16 (b)**).

At this level, we can partially conclude that after measuring the friction coefficient of the aluminum alloy (μ = 0.3), the anodic coating alone and the TiO_2 massif (μ = 0.1), it was therefore possible to evaluate the coefficient of friction and the lifetime of the anodic coating alone (μ = 0.8 and a lifetime = 414 cycles).

The curve reflecting the variation of the coefficient of friction of the composite anodic coating Al_2O_3/TiO_2 as a function of time evolves in two periods: (1) a first period (at approximately 100 seconds) during which the coefficient of friction is almost equal to that of the solid mass TiO_2 (μ = 0.1) and (2) a second period (the rest of the friction test) during which the coefficient of friction increases slightly until reaching an almost stable value (μ = 0.15). These two periods respectively correspond to the ball contacts of alumina/TiO_2 deposited on the surface of the anodic coating and ball of alumina/composite coating.

It should be noted that the composite anodic coating will end up with a mean friction coefficient μ = 0.15, intermediate between that of the TiO_2 massive (μ = 0.1) and that of the non-anodized

http://dx.doi.org/10.5772/intechopen.75782

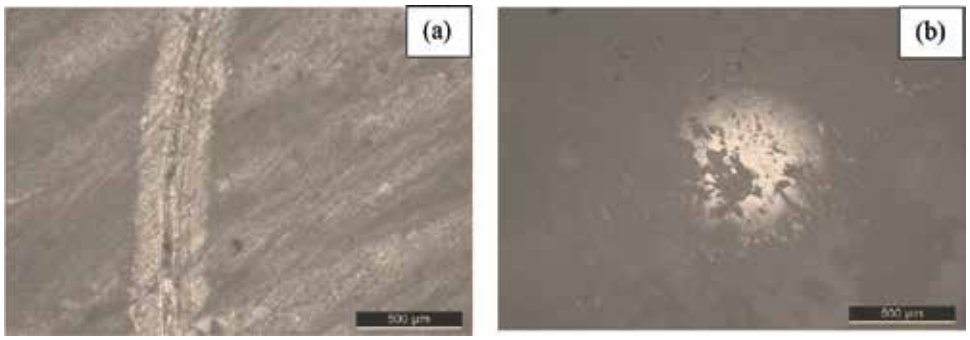

Figure 22. Optical micrographs (a) trace of wear of a TiO_2 solid and (b) trace of wear of the counterface (alumina ball) after friction test (Fn = 1 N, v = 0.052 m.s^{-1} and t = 15 min).

substrate (μ = 0.30) without causing a sudden variation. This reflects that this coating still persists in wear and has a lifetime greater than 900 seconds (1490 cycles). The optical image shown in **Figure 22 (3a)** shows that the composite coating has low wear free of microcracks. While, the counterface (**Figure 21 (3b)**) does not show either TiO_2 or oxide.

The characteristics of the wear traces of the various samples thus examined are measured and the volume of wear is calculated (**Figure 23**). The expertise of the latter figure shows that the TiO_2 massive has a low wear volume (29.6106 μm^3) intermediate between that of the substrate (461.4106 μm^3) and that of the anodic coating alone (373,106 μm^3). Such a coefficient of friction (μ = 0.1) and a low wear volume justify a credible choice of TiO_2 nanoparticles to be used

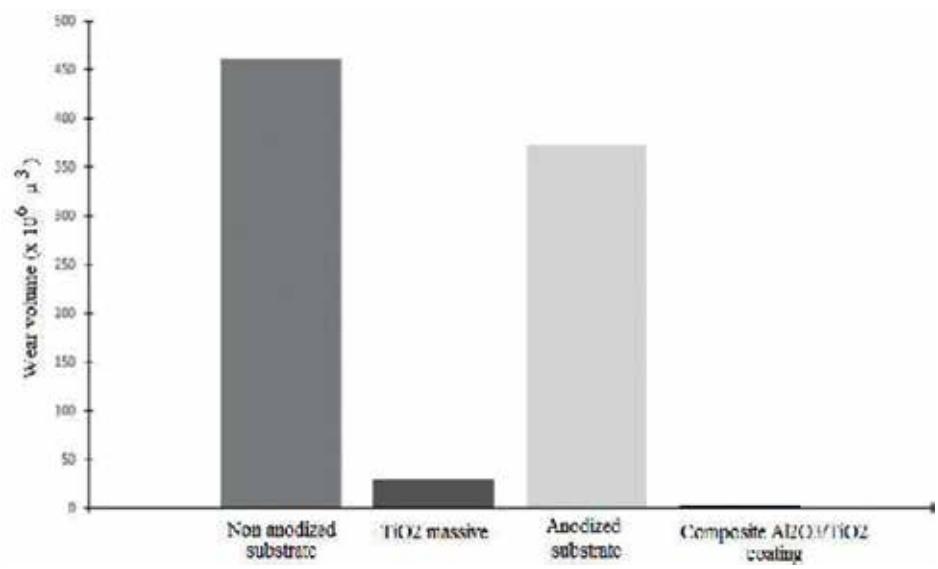

Figure 23. Variation of the wear volume of the worn samples after friction tests (Fn = 1 N, v = 0.052 m.s^{-1} and t = 15 min).

for the electrophoretic impregnation of the anodic coating developed in a phosphoric bath in order to reinforce its tribological behavior.

The composite anodic coating, as shown in **Figure 23**, has a wear volume (3.4106 μm^3) which has 0.73% of that of the substrate and about 0.91% of that of the anodic coating alone.

Finally, this panoply of the results confirms that the functionalization of the anodic coating by TiO_2 nanoparticles contributes to a significant improvement in its resistance to frictional wear.

These results are in satisfactory agreement with those found by Yugeswaram et al. [16] in the case of an Al_2O_3/13% TiO_2 composite coating developed by the Air Plasma Spray (APS) process.

4. Conclusion

Electrophoretic impregnation of porous anodizing layer elaborated in phosphoric acid was executed in aqueous TiO_2 nanoparticles suspension. It should be noted that impregnation process is conditioned by the applied electric field. Applying high electric field (200 V/cm) induces the jellification of TiO_2 sol because of the anodic electrolysis of water which decreases the pH near the electrode surface and then destabilizes the suspension against coagulation at low pH. In order to avoid this phenomenon and facilitate the insertion of titanium dioxide nanoparticles, the addition of the glycine to buffer the suspension is necessary. At the beginning of EPD, particles go to the bottom of pores which continue to fill progressively.

These results attest that EPD can be used to fill successfully porous anodizing layer despite the presence of the resistive barrier layer at the metal-oxide interface.

Author details

Koubaa Anouar* and Bargui Mansour

*Address all correspondence to: anouar.koubaa@gmail.com

High Institute of Technological Studies of Sfax, Tunisia

References

[1] Bal S, Samal SS, Mohanty UK. Mechanical and microstructural analysis of carbon nanotube composites pretreated at different temperatures. American Journal of Materials Science. 2011;**1**(1):5-11. DOI: 10. 5923/j.materials.20110101.02

[2] Sulka GD, Stroobants S, Moshchalkov V, Borghs G, Celis J-P. Synthesis of well-ordered nanopores by anodizing aluminium foils in sulfuric acid. Journal of the Elechtrochemical Society. 2002;**149**(7):D97-D103

[3] Seventy Years of Sulfuric Acid Anodizing-Brace-Trans MFI; 1997

[4] O'Sullivan JP, Wood GC. The morphology and mechanism of formation of porous anodic films on aluminium. The Royal Society's Physical Sciences Research Journal. 1970;**317** (1531). DOI: 10.1098/rspa.1970.0129

[5] Bargui M, Messaoud M, Elleuch K. Electrophoretic impregnation of porous anodizing layer by synthesized TiO_2 nanoparticles. Surface Engineering and Applied Electrochemistry. 2017;**53**(5):467-474. DOI: 10.3103/S1068375517050040

[6] Han LS, Rujkorakarn R, Sites JR, Ske CY. Thermally induced crystallization of amorphous-titania films. Journal of Applied Physics. 1986;**59**:3475. doi.org/10.1063/1.336817

[7] Fitzgibbons ET, Sladek KJ, Hartwig WH. TiO_2 film properties as a function of processing temperature. Journal of the Electrochemical Society. 1972;**119**:753. DOI: 10.1149/1.2404316735-739

[8] Cozzoli PD, Kornowski A, Weller H. Low-temperature synthesis of soluble and processable organic-capped anatase TiO_2 nanorods. The American Journal of Chemical Society. 2003;**125**:14539-14548. DOI: 10.1021/ja036505h

[9] Cullity BD. Elements of X-ray diffraction. Reading, Mass. Addison-Wesley; 1956. 514 p. (OCoLC)904102259

[10] Sato K, Li JG, Kamiya H, Ishigaki T. Ultrasonic Dispersion of TiO_2 Nanoparticles in Aqueous Suspension. American Journal of Ceramic Society. 2008;**91**(8):2481-2487. doi.org/10.1111/j.1551-2916.2008.02493.x

[11] Sato K et al. Ultrasonic dispersion of TiO_2 nanoparticles in aqueous suspension. Journal of the American Ceramic Society. 2008;**91**(8):2481-2487

[12] Escabor J, Arurault L, Turq V. Improvement of the tribological behavior of PTFE-anodic film composites prepared on 1050 aluminium substrate. Applied Surface Science. 2012;**258**:8199-8208. DOI: 10.1016/j.apsusc.2012.05.022

[13] Malvern Instrument – Zeta potential: An introduction in 30 minutes – Technicalnote MRK654-01

[14] Zeta Potential: An Introduction in 30 Minutes, Technical Note MRK654-01. Malvern Instrum: Malvern; 2017

[15] Fori B, Taberna PL, Arurault L, Bonino JP, Gazeau C, Bares P. Electrophoretic impregnation of porous anodic aluminum oxide film by silica nanoparticles. Colloids and Surfaces, A: Physicochemical and Engineering Aspects. 2012;**415**:187-194. DOI: 10.1016/j.colsurfa.2012.09.011

[16] Yugeswarana S, Selvarajana V, Vijaya M, Ananthapadmanabhanb PV, Sreekumarb KP. Influence of critical plasma spraying parameter (CPSP) on plasma sprayed alumina–titania composite coatings. Ceramics International. 2010;**36**:141-149. DOI: 10.1016/j.ceramint.2009.07.012

Edited by Oana-Maria Boldura and Cornel Baltă

Electrophoresis is a widely used method in the field of life sciences, having multiple practical applications in physical, chemical, biochemical, and molecular biology domains.

This book contains 8 chapters depicting various applications of this technique in biochemistry, molecular biology, and physical chemistry. This book presents the link between the exposed method and its applications in a very explicit manner and offers a wide range of practical examples. The book provides not only a vision of actual methods but also their necessary further improvements and suggested developments. Therefore, a particular attention was given to the described techniques as true guidelines in the fields where electrophoresis is recommended, being useful for not only the scientists but also the laboratory clinicians.

Published in London, UK

IntechOpen

ISBN 978-1-83881-596-7